THE STRUCTURE AND EVOLUTION OF PLANETARY NEBULAE WITH VERY HOT NUCLEI

by

Nicholas Andrew Walton BSc.

March 1987

A thesis submitted for the degree of Doctor of Philosophy of the University of London and for the Diploma of the Imperial College

Astrophysics Group,
Blackett Laboratory,
Imperial College,
London SW7 2BZ.

Abstract

The evolution of the central stars of Planetary Nebulae is reviewed. It is suggested that lack of observational measurements of those Planetary Nebulae having faint central stars may mean that very hot central stars have been systematically under represented in recent surveys.

New narrow band CCD images of 25 Planetary Nebulae, whose central stars had been previously undetected or poorly measured, are presented. Using this imaging technique it has been possible to determine visual magnitudes for these central stars.

The Zanstra method has been employed to determine the temperatures of these stars, several of which are found to have $T_{eff} > 2 \times 10^5$ K. Assuming a blackbody model, the luminosities and radii of the stars are determined. The central stars are positioned on the Hertzsprung-Russell diagram, this observational evidence being compared with theoretical evolutionary tracks. It is shown that a number of the central stars of this sample must have masses $> 1 M_{\odot}$.

The detection of the previously undetected star of NGC 2440 is reported, the star being found to have a temperature of 350,000 K, making it one of the hottest central stars observed. NGC 2440 has been observed in the near infra-red for emission from 'warm' molecular hydrogen. This has been found to exist in condensations within the HII region as well as in the transition between the HII and neutral HI regions. The molecular hydrogen excitation can be explained by mass loss from the central star in the form of a fast wind.

The unambiguous detection of the central star of NGC 7027 is reported. The star has a temperature of 250,000 K and a mass $> 0.8 M_{\odot}$.

Acknowledgements

First and foremost I would like to thank my supervisor Dr N.K. Reay who has been an invaluable source of help and advice over the last 3 years. I would like to thank Prof J. Ring who has given me much encouragement. I express my gratitude to Prof S.R. Pottasch for many helpful discussions. I would thank Mr. S. Hart for advice on computing techniques and guidance on the use of the STARLINK system. I am also extremely grateful for the assistance of many past and present members of the Astrophysics Group at Imperial College.

I would thank The Science and Engineering Research Council for supporting my studies with a research studentship during the period October 1983 to October 1986.

List of Figures and Plates

List of Tables

CHAPTER 1

Chapter 1

1 Planetary Nebula - Some Problems Concerning Their Evolution.

1.1 Introduction.

This work deals primarily with a number of observational tests which have been used to study a sample of Planetary Nebulae (P.N., plural: P.Ne.) with a view to better understanding their evolutionary processes.

I will give a brief outline of this thesis. In Chapter 1 a review of P.Ne. will be given and some of the more important points that this work sets out to address will be highlighted. Chapter 2 gives a detailed analysis of observations of a sample of central stars of P.Ne., these being chosen on the basis that they had faint or previously undetected central stars. Visual magnitudes are determined and from these various parameters concerning the central stars (eg Zanstra Temperatures) are derived. In Chapter 3 the well studied but peculiar P.N. NGC 7027 is reviewed. Observations of its central star are presented along with kinematical data. Additional molecular hydrogen detections are also reported. From this data, its evolutionary path is considered.

Chapter 4 deals briefly with the central star of NGC 2440, where evidence that it is one of the hottest central stars known is presented. Following on from this, Chapter 5 outlines observations made of molecular hydrogen emission in the near infrared from a number of P.Ne. The distribution of molecular hydrogen in NGC 2440 is presented in some detail and the importance of these results is discussed.

Finally in Chapter 6 the results of the observations detailed in the previous chapters are discussed. In particular estimates are made of the central star masses and the paradox between observed and expected evolutionary timescales are discussed. The importance of understanding the unionised material which surrounds a large number of observed P.Ne.

and how this relates to a better understanding of the central star's evolution is also emphasised. Suggestions for further observations are also made.

1.2 Planetary Nebulae and their Identifying Characteristics.

P.Ne. have long been known to astronomers, some of the first examples being noticed by Messier in 1771, who included them in his catalogue of nebulous objects because of their extended, non stellar, appearance. P.Ne. are HII regions excited by a hot star, with a temperature generally greater than 3×10^4 K. P.Ne. are usually identified from studying broadband photographs of the sky, for instance the Palomar Sky Survey, and looking for symetrical disk or shell structures. A second technique used, which is the main method for identifying small P.Ne ($<$ 15 arcsecs) is to look for charactaristic lines of Hα in emission and the forbidden transition lines of [OIII] in the candidate P.N's spectra. Confusion with Be shell stars can exist as these also show Hα in emission but typically the P.Ne. have a much reduced continuum compared to their line emission.

The ionised regions surrounding P.Ne are observed to be expanding with velocities typically of a few tens of kms^{-1}. This taken with measurements of their angular radii (and an estimate of their distances) means that observed P.Ne. have lifetimes of a few tens of thousands years. The maximum observed radius has given an age of $\approx$ 35,000 years. Consequently P.Ne. are short lived objects in terms of astronomical timescales. This means that the central stars must undergo a very rapid evolution in comparison with other stages in their lives, during which time their radii decrease from $\approx$ 1 $R_\odot$ down to that of a white dwarf of $\approx 10^{-2}$ $R_\odot$.

1.3 From Asymptotic Giant Branch to Planetary Nebula.

P.Ne. and their central stars are believed to be the chief transitional stage linking Red Giants with White Dwarfs. The approximate coincidence of the birth rates of P.Ne. with the death rates of main sequence stars suggests that most stars with masses between 1-5 $M_\odot$ go through the PN stage (Aller, 1983). Asymptotic Giant Branch evolution theory (Iben & Renzini, 1983) places an upper limit of 8-9 $M_\odot$ for progenitor stars of the central stars of P.Ne. Estimates of the birth rates of White Dwarfs have been made (Weidemann, 1977) and these also agree well with the birth rates of P.Ne. (Pottasch, 1984) being $\approx 2\times10^{-12}$ white dwarfs pc^{-3} $year^{-1}$.

It is generally accepted that P.Ne. evolve from the Asymptotic Giant Branch (AGB) stars. A recent review of AGB stars is given by Iben & Renzini (1983). Simplifying this it is thought that the nebula is the hydrogen rich envelope of the AGB star and the central star is the evolved core, now exposed.

During the course of the evolution of the AGB star it must loss a considerable amount of mass. For instance the progenitor of a core with mass 1.2 $M_\odot$ is thought to be about 8 $M_\odot$ and hence over 6 $M_\odot$ must be lost. AGB stars lose mass, typical mass loss rates for Mira's being 10^{-6} $M_\odot$ $year^{-1}$ (Zuckerman, 1980). However, these mass loss rates are too low to explain P.Ne. Typically P.Ne. have observed masses in the nebula of ≈ 0.2 $M_\odot$, which taken with lifetimes of $\approx 10^4$ years imply mass loss rates of 10^{-5} $M_\odot$ $year^{-1}$. Renzini (1981b has postulated that a 'superwind' may exist having the required mass loss rate. This wind may 'turn on' when the luminosity of the AGB star reaches some critical luminosity and then the remaining hydrogen envelope surrounding the core is ejected on a timescale which is short compared to that of the AGB stage of the stars evolution. However the physical nature of this wind is open to question, but it has been suggested that the Superwind may be caused be pulsational instabilities in the outer atmosphere (Tuchman et al, 1979).

The superwind removes the hydrogen rich envelope from the AGB star core until only a small remnant remains (<0.01 MG). At this point the AGB star rapidly evolves to the P.Ne. stage. The core consists mainly of Carbon and Oxgen, which is in the degenerate state. Surrounding this is the hydogen remnant and this burns in a shell. The star contracts and the superwind stops (Renzini, 1983). The hydrogen represents the bulk of the fuel available to the star. The luminosity of hydrogen burning around the inert C-O core depends only on the core mass. Hence as the hydrogen burns and is processed into the core the radius of the core decreases and hence, because the star is burning at a constant luminosity, the surface temperature of the star increases. When the surface temperature of the core reaches about 30,000 K the star produces enough ionising photons to ionise the nebula and a P.N. is formed.

1.4 The Evolutionary Paths of the Nuclei of P.Ne. in the H-R Diagram.

Models of the subsequent evolution of the central star were first developed by Paczynski (1971) then later by Schonberner (1979) and Iben (1984). Paczynski assumed that the envelope had been ejected leaving a C-O core surrounded by an inner helium burning shell and an outer hydrogen burning shell. The luminosity is fixed by the core mass eg Paczynski (1970a) giving:

$$L/L_{\odot} \approx 5.925\times10^{4} \, (M_c/M_{\odot} - 0.522)$$

The evolution is then calculated for a range of core masses. As the shell burning proceeds the envelope mass decreases as the burned matter is processed into the core. The radius decreases and the temperature increases. Eventually the shell fuel is exhausted and the burning ceases. The star cools down at a constant radius to become a white dwarf. The time for this evolution is critically dependent on the core mass going as $t \propto M_c^{-9.6}$ (Iben & Renzini, 1983).

There is some controversy at present over the mass range of the central stars of P.Ne. Schonberner (1981) came to the conclusion that the observed evolution of the central stars could be accounted for with post AGB stars having masses of 0.6 $M_\odot$ with their luminosity being supplied by quiescent hydrogen burning. The mass distribution function of the central stars was found to be sharply peaked at 0.58 $M_\odot$ hence stars with a wide range of progenitor mass would evolve to the same mass central star, following a single evolutionary track in the H-R diagram.

Kaler (1983) examined large, well evolved P.Ne. with lower luminosity stars. This showed a wider distribution of central star mass, with core masses upto 1 $M_\odot$ being found. This would support the view of Renzini (1979) that different parts of the observed central star sequence are populated with stars of different masses. It has been suggested by Pottasch (1981) that much hotter central stars exist and if found would point to the existence of more massive nuclei. These stars were not included in the analysis of Schonberner (1981) and hence the distribution that he finds may just be that due to the selection effects of chosing luminous, low temperature central stars which have well measured magnitudes.

To accurately position central stars in the H-R diagram accurate distance and magnitudes are needed. In the following Chapters new observational evidence will be presented showing the existence of a number of hot central stars for which a sensitive imaging technique has been employed to search for these faint objects.

CHAPTER 2

Chapter 2

2. Observations of the Central Stars of Selected Planetary Nebulae

2.1 Introduction

To accurately position the central stars of P.Ne. in the H-R diagram a knowledge of the distance to the P.Ne. is needed along with the magnitude of the central star.

The theory of stellar evolution of intermediate mass stars predicts the existence of very hot phases with $T>2\times10^5$ K when the post AGB star passes through the P.Ne. stage of its evolution before cooling to a white dwarf. These high temperatures are predicted for more massive central stars ($M > 0.7\ M_\odot$) with a small remnant hydrogen envelope ($<10^{-2}M_\odot$) (Iben, 1982). However Pottasch (1981) suggests that hot central stars have not been seriously studied, because temperature determinations (eg Harman & Seaton, 1966) rely on a knowledge of the central star visual magnitude. Brighter stars, which tend to be cooler, are more easily measured. Hot stars, which are intrinsically faint in th visual, may be systimatically overlooked.

This Chapter describes an imaging technique which has been employed, specifically to serch for the central stars of those P.Ne. which are known to have either no positively detected central star, or an extremley faint central star with an uncertain magnitude. With these magnitudes the Zanstra method is used to determine the temperatures of the central stars.

2.2 Methods Used In Determining Central Star Temperatures

Two of the main unknowns in trying to position central stars of P.N. on the evolutionary H-R diagram are the distance to the central star and its effective surface temperature. In this chapter I will discuss our approach to determining the second of these and present data for a number of central stars whose surface temperatures were previously rather poorly determined.

Before I go on to detail the observations I will first give a brief summary of some of the more commonly used techniques which have been used to obtain values of central star temperatures and then proceed to give a fuller account of the method that has been employed in this work.

2.2.1 Comparison with 'Normal' Spectra.

Perhaps the method giving the most certain estimates of central star temperatures is applicable to those central stars which have a normal O or Of type spectrum. For these stars model atmospheres can be computed and the predicted line shapes fitted against the observed line shapes. By obtaining the best fit the stellar effective temperature can be found. However this method has only been applied to a small number of central stars, these having spectra similar to normal O type stars, which tend to be the coolest of the central stars with $T < 50,000$ K.

2.2.2 Colour Temperatures from Direct Measurement of the Stellar Spectrum

Many P.Ne. are optically thin. In these cases the colour temperature of the central star is often determined by comparing the continuum emission and the UV emission from the central star with either a blackbody or a model atmosphere. Adjustment of these models with temperature to best fit the observed data leads to an estimate of the central star temperature being obtained.

Measurements of ultraviolet energy distributions have recently been made using satellite borne detectors, most importantly the Dutch ANS satellite (Pottasch et al, 1978) and more recently the more reliable measurements from the IUE satellite (e.g. Harrington et al, 1982 and

Grewing et al, 1986). These measurements have proved important as measuring the optical continuum from the central stars is complicated by the additional presence of nebula line and continuum emission. This effect is most pronounced for those small, dense nebula which tend to have hot, and hence faint in the visible, central stars associated with them. However in the UV the hot stars emit a much greater proportion of thier energy and hence are relatively easier to detect against the nebula emission (which tends to fall off towards shorter wavelengths). Also the UV measurements extend the wavelength range coverage. The main problem with the UV measurements though is that the effects of interstellar extinction become more pronounced at short wavelengths and hence a good knowledge of the extinction towards each individual P.N. is needed. Even so the corrections to the measured UV fluxes can be uncertain.

However, with the corrected visual and UV data, the fluxes can be compared with a blackbody (or model atmosphere) to give the colour temperature of the central star. This has been done for the central stars of several P.Ne (eg Pottasch et al, 1978) to give satifactory fits between the observed spectrum and the model curve. The temperatures of the stars studied using this technique are generally less than T=100,000 K. At temperatures greater than this the continuum from the central star becomes progressively more difficult to measure, especially in the visible.

2.2.3 The 'Stoy' or Energy Balance Method.

Another method originally formulated by Stoy (1933), known as the Energy Balance Method, does not rely on any knowledge of the actual central star to determine its temperature, but relies soley on nebula data. The excitation of forbidden lines (eg [OIII]) provides the main mechanism for cooling the nebula. Assuming that the nebula is in stable equilibrium the cooling rate must equal the heating rate. Measurement of the forbidden line flux gives the cooling flux, whilst measurement of the Hβ flux gives the stellar photon flux (if the nebula is optically thick). The ratio of the two fluxes, which gives a measure of the energy released from each photoionisation, is strongly dependent on temperature and allows the so called Stoy temperature to be deduced. This method has been examined and reformulated by Preite-Martinez and Pottasch (1983) who have obtained results on some 50 P.Ne.

The Stoy (ie the Energy Balance) method, however is considered to give seriously underestimated temperatures for those hot central stars of temperatures greater than 10^5 K. This is due to a number of factors, the most important of which is that a number of important collisionally excited lines, such as O VI at 1034Å, are at present unobservable. The importance of these lines in any particular P.N. is hard to estimate, for hotter stars though these lines would become progressively more important in cooling the nebula gas, and hence the energy balance method leads to underestimates of the stellar temperatures for these stars. A fuller analysis of this problem is given in Stasinska & Tylenda (1986).

Another factor that may be important is the effect of dust in the P.Ne. Peite-Martinez & Pottasch have not taken the effects of dust into account, citing Natta & Panagia (1981) who argue that the dust content in P.Ne. is relatively low, compared with say HII regions to which the Energy Balance method has also been applied (Maciel and Pottasch, 1981). However in small, dense nebula which may contain the hotter examples of central stars, dust may well play an important role, being a source of energy gain in the release of a photoelectron after having absorped a UV photon. Hence for these stars (eg NGC 7027 Helfer et al, 1981) the temperatures may be incorrectly determined.

2.2.4 Nebula Ionisation Models.

It is possible to use the abundances of pairs of ions of successive stages of ionisation of an element at any point in the nebula to fix the radiation field in the nebula, as the ratio depends on the radiation field at frequencies higher than that needed to ionise the lower ionisation state. If the optical depth between the star and the point at which the ratio is determined is known, then the stellar radiation field is related to the radiation field in the nebula by geometrical dilution. This description is rather simplified in that other effects have an important part to play.

Two possible methods are included under this heading. It is possible to construct a detailed model for a P.N. and in this way attempt to correct for other effects which can influence the nebula ionistaion equilibrium. Recently a number of detailed models have been computed for a number of well studied P.Ne. Bohlin et al (1982) have studied NGC 6853 and NGC 7293. Harrington et al (1982) have invesigated NGC 7662 whilst NGC 3918 has been comprehensively analysed by Clegg et al (1986). Additionally IC 3568 has been modelled by Harrington & Freibelman (1983).

In these models the electron density and electron temperature through the nebula are computed. To do this as a function of position requires that the geometry of the P.N. under consideration is known. It is freqently the case however that a spherical geometry is assumed. The nature of the radiation from the central star as a function of wavelength is also assumed as is the geometrical dilution within the nebula. Estimates of the chemical abundances in the P.N. are also needed and the effects of dust within the P.N. are sometimes considered. On making these assumptions the theoretical nebula spectrum can be modelled and this is then compared to the observed spectrum. The above parameters can be adjusted until the best fit with the observed spectrum is achieved. This then gives the stellar radiation field which in turn leads to a value of the central star effective temperature.

This method is the best method to use to study a particular P.N. but it requires a large amount of input data, hence can only be used for those nebula that have been well studied. Many problems also exist, is the geometry correct, this is difficult as the light received at the earth is integrated along the line of sight of the P.N. and hence kinematic studies such as those made of NGC 5189 (Reay et al, 1984) should be used to determine the geometry of each P.N. studied. Another problem regards the uniqueness of the final model fit. Harrington et al (1982) have shown how for the case of NGC 7662, a model assuming a blackbody flux distribution for the central star produces satisfactory fits to most spectral features. However this model was not able to reproduce the CIII λ2297 line nor the thermal IR emission. They went on to use a model atmosphere for the central star and also took account of dust within the nebula to give better agreement with observations. However it is not inconceivable that this model is not a unique solution.

For the more general case it is possible to use a considerably simplified version of the above technique. This version enables the frequency dependance of the stellar radiation field to be determined. The electron temperature and density for the P.Ne. are found from line ratios that are sensitive to them and these values are then assumed to be constant throughout the P.N. This method has been recently formalised by Natta et al (1980) who have been able to determine the radiation field as a function of frequency from about 100Å to 912Å for 10 P.Ne. One interesting conclusion of their study was that the 10 representive P.Ne. (with a variety of excitation class) investigated are optically thick or nearly so. This has important consequences for the Zanstra method which will be desribed next.

2.2.5 The Zanstra Method

The technique that has been chosen for this work is a method first suggested by Zanstra (1931). This method can be employed to obtain the temperature of any hot star which is surrounded by a nebula, for instance Population I stars in HII regions or in our case central stars of Planetary Nebulae. The basis of this technique is that for a nebula which is optically thick to the Lyman continuum, a knowledge of the flux from a hydrogen recombination line (usually Hβ) will enable the number of ionising photons from the exciting central star to be determined upon making certain assumptions. Then by comparing the ionising flux with the flux emitted in the visual (usually in the V band of the UBV system) a temperature for the exciting star can be found.

The formulation of this technique proceeds in the following manner. After Pottasch (1984) and Harman & Seaton (1966), a star radiating as a blackbody, having a radius, R_s, and temperature, T, can be written as:

$$L_\nu = 4\pi^2 R_s^2 B_\nu(T) \quad \text{ergs s}^{-1}\ \text{Hz}^{-1} \qquad (2.2.1)$$

where the Planck Function:

$$B_\nu(T) = 2h\nu^3 c^{-2}(e^{h\nu/kT} - 1)^{-1} \quad \text{ergs cm}^{-2}\ \text{s}^{-1}\ \text{Hz}^{-1}\ \text{ster}^{-1}$$

The total luminosity then is:

$$L = \int_0^\infty L_\nu \, d\nu \quad \text{ergs s}^{-1}$$

$$= \frac{8\pi^6 k^4}{15h^3c^2} R_s^2 T^4 \quad \text{ergs s}^{-1}$$

The luminosity can be written as:

$$L_\nu = 4\pi d^2 F_\nu \quad \text{ergs s}^{-1}\ \text{Hz}^{-1}$$

where F_n is the observed stellar flux at the surface of the earth corrected for extinction.

Rearranging 2.2.1 and substituting for L_ν gives:

$$R_s^2 = \frac{F_\nu d^2}{\pi B_\nu} \quad \text{cm}^2 \qquad (2.2.2)$$

Expressing L in terms of the solar luminosity gives:

$$\frac{L}{L_\odot} = \frac{R_s^2\ T^4}{R_\odot^2\ T_\odot^4}$$

where $L_\odot = 3.90\times10^{33}$ ergs s^{-1}, $R_\odot = 6.960\times10^{10}$ cm, $T_\odot = 5770$ K

Substituting for R_s^2:

$$\frac{L}{L_\odot} = \frac{d^2\ T^4\ F_\nu}{R_\odot^2 T_\odot^4 \pi B_\nu} \qquad (2.2.3)$$

The number of stellar quanta having freqency $\nu > \nu_i$ must be considered:

$$Q_i = \int_{\nu_i}^{\infty} \frac{L_\nu}{h_\nu}\, d\nu$$

which after Hummer & Seaton (1963)

$$= 8\pi^2 R_s^2 c^{-2}\ (kT/h)^3\ G_i(T) \quad \text{photons } s^{-1} \qquad (2.2.4)$$

$G_i(T)$ is an analytical function of the form

$$G_i(T) = \int_{h\nu_i/kT}^{\infty} x^2(e^x - 1)^{-1}\ dx$$

From equation 2.2.2

$$R_s^2 = \frac{15h^3c^2L}{8\pi^6k^4T^4} \quad cm^2$$

Combining this with equation 2.2.4

$$Q_i = \frac{15L}{\pi^4 kT} G_i(T) \quad \text{photons } s^{-1} \qquad (2.2.5)$$

The frequencies, ν_i, of interest are the HI lyman limit, ν_1; the HeI limit, $\nu_{1.807} = 1.807\nu_1$; and the HeII limit $\nu_4 = 4\nu_1$.

In the first instance the case for photons having energies above the HI Lyman limit will be considered. At the Lyman limit, $h\nu_1 = 13.6$eV, which is the energy required to ionise the hydrogen atom. This corresponds to λ=912Å, or $\nu=3.29\times10^{15}$ Hz^{-1}. This is used to determine what is known as the Hydrogen Zanstra temperature.

The assumption is made that the nebula surrounding the P.N. is optically thick to this ionising radiation. The validity, or otherwise, of this statement will be discussed in a later section. Each ionising photon, if the nebula is purely hydrogen, will be absorbed by the nebula gas. Hence, for a nebula in equilibrium the number of recombinations in the nebula per unit time equals the number of ionising photons emitted by the star per unit time. Hence the number of recombinations is:

$$Q_1 = \int n_e n(H^+)\alpha_B \, dV \quad \text{photons s}^{-1} \qquad (2.2.6)$$

where n_e and $n(H^+)$ are the electron and proton densities respectively, α_B is the recombination coefficient summed over all levels above the ground level and α_n is the recombination coefficient to level n :

$$\alpha_B = \sum_{n=2}^{\infty} \alpha_n$$

Q_1 also then is the number of ionising photons. Assuming that the filling factor for the nebula is unity this can be written:

$$Q_1 = \int_{\nu_1}^{\infty} \frac{L_\nu}{h\nu} d\nu \quad \text{photons s}^{-1}$$

Now the nebula emission in say the Hβ emission line depends on recombinations throughout the nebula. The flux in the Hβ line observed at the surface of the earth is:

$$4\pi d^2 F(H\beta) = h\nu(H\beta) \int n_e n(H^+)\alpha(H\beta)) \, dV \quad \text{ergs s}^{-1} \qquad (2.2.7)$$

with the integral being performed over the entire volume of the nebula.

By equating (2.2.5) and (2.2.6):

$$\int n_e n(H^+)\, dV = \frac{15\ G_1(T)L}{\pi^4 kT\ \alpha_B}$$

Substituting and rearranging in equation (2.2.7) the luminosity can be written as:

$$L = \frac{4\pi d^2 F(H\beta)\alpha_B \pi^4 kT}{15G_1(T)h\nu(H\beta)\alpha(H\beta)}$$

Substituting this into equation (2.2.3) one obtains the expression:

$$\frac{F(H\beta)}{F_\nu} = \frac{15h\nu(H\beta)}{4\pi^6 k} \cdot \frac{L_\odot}{R_\odot^2 T_\odot^4} \cdot \frac{\alpha(H\beta)}{\alpha_B} \cdot \frac{T^3 G_1(T)}{B_\nu} \quad \text{Hz} \qquad (2.2.8)$$

The number of Hβ photons that escape from the P.N., produced as a result of recombinations within the nebula, is related to the fraction of the recombination coefficients, $\alpha(H\beta)/\alpha_B$, and this ratio is nearly independent of density and temperature. Harrington et al, 1982, have given the approximate formula, with $N_e \approx 10^4\ cm^{-3}$, as:

$$\alpha_B(H^0)/\alpha(H\beta) = 8.49 \times (T_e/10^4)^{0.06}$$

The ratio of the recombination coefficients $\alpha(H\beta)/\alpha_B$ varies very weakly as a function of the nebula electron temperature. A plot of $\alpha(H\beta)/\alpha_B$ as a function of temperature is shown in Figure 2.1b. For those P.Ne. for which data on the electron temperature were not available the ratio of $\alpha(H\beta)/\alpha_B$ was taken assuming a value of the electron temperature of $T_e=10^4$ K. The values of $\alpha(H\beta)$ and α_B used, along with the corresponding values for the Helium case. $\alpha(4686)$ and He^+ α_B are tabulated in Table 2.1.

Equation (2.2.8) then is an expression which leads to a value of the temperature of the exciting star on measurement of the Hβ line flux from the entire nebula and the flux from the exciting star at some continuum

Figure 2.1

(a) Graph of $\alpha(4686)/\alpha_B(He^+)$ shown as a function of temp.

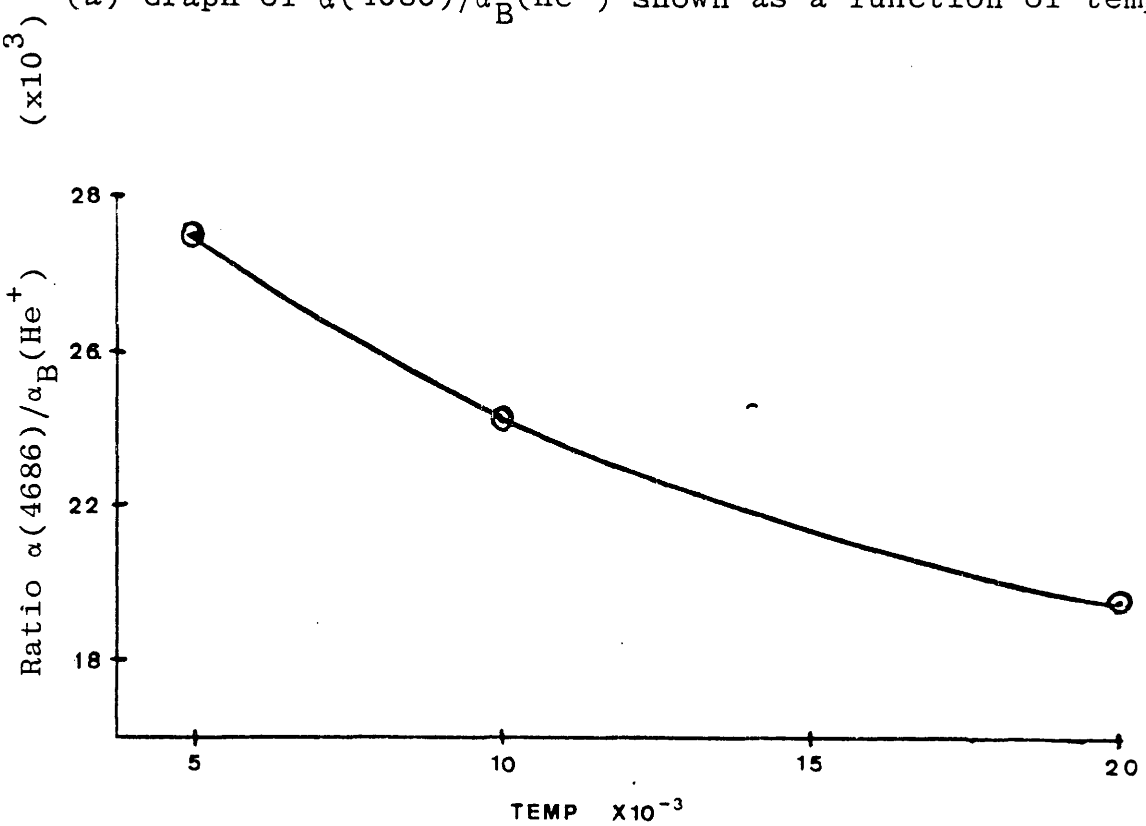

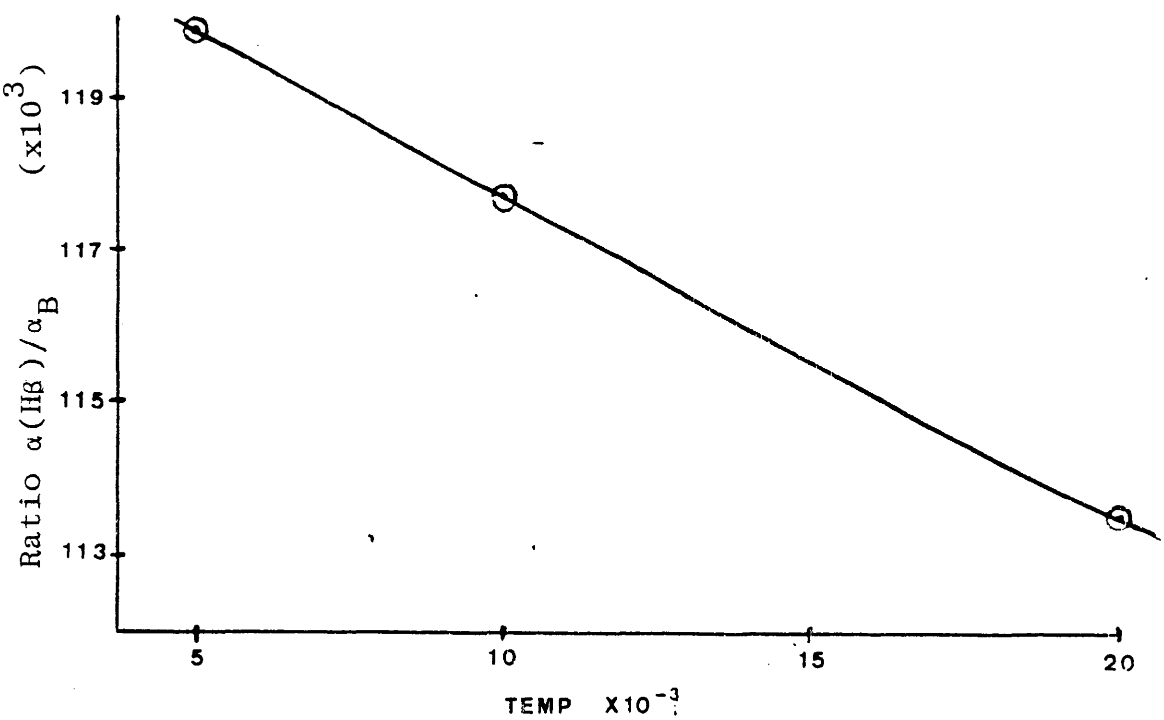

(b) Graph of $\alpha(H\beta)/\alpha_B$ shown as a function of temperature.

Table 2.1 Recombination Coefficients for H and He+.

	e- density cm^{-3}	5000 K $cm^3\ s^{-1}$	10000 K $cm^3\ s^{-1}$	20000 K $cm^3\ s^{-1}$
α(Hβ) N_e	10^2	5.391×10^{-14}	3.023×10^{-14}	1.610×10^{-14}
	10^4	5.443×10^{-14}	3.036×10^{-14}	1.612×10^{-14}
	10^5	5.504×10^{-14}	3.049×10^{-14}	1.615×10^{-14}
	10^6	5.592×10^{-14}	3.069×10^{-14}	1.618×10^{-14}
α(4686) N_e	10^4	6.915×10^{-13}	3.492×10^{-13}	1.690×10^{-13}
	10^5	6.879×10^{-13}	3.477×10^{-13}	1.686×10^{-13}
	10^6	6.691×10^{-13}	3.395×10^{-13}	1.657×10^{-13}

The above values are taken from Brocklehurst (1971).

Temperature (K)	α_B $cm^3\ s^{-1}$	$\alpha_B(4686)$ $cm^3\ s^{-1}$
4000	5.38×10^{-13}	
5000		2.56×10^{-12}
6000	3.91×10^{-13}	
8000	3.10×10^{-13}	
10000	2.58×10^{-13}	1.54×10^{-12}
12000	2.21×10^{-13}	
14000	1.94×10^{-13}	
16000	1.73×10^{-13}	
18000	1.56×10^{-13}	
20000	1.42×10^{-13}	9.08×10^{-13}

α_B values from Brown & Matthews (1970).

$\alpha_B(4686)$ values from Pottasch (1984) p170.

wavelength.

Adopting thenormal convention, the continuum flux from the central star has been measured at the visual, V band wavelength, λ=5500Å. The visual flux has been obtained from the visual magnitude determinations using the calibration of Wamsteker (1981) that:

$$F_{\lambda(vis)} = 3.68\times10^{-9}\times10^{-mv/2.5} \quad \text{ergs s}^{-1}\ \text{cm}^{-2}\ \text{Å}^{-1}$$

The fluxes in (2.2.8) are measured in units of frequency interval. More usually the continuum flux from the central star is given in units of wavelength interval, this being the case in the work presented here where the continuum flux for the stars are determined from their magnitudes in the visible. The conversion factor used is:

$$F_\nu(\text{Hz}^{-1}) = \frac{\lambda^2}{3\times10^8} F_\lambda(\text{Å}^{-1})$$

where the wavelength, λ, is in metres, m.

Rewriting (2.2.8) in terms of wavelength units then gives:

$$\frac{F(H\beta)}{F_\lambda} = \frac{15hc}{4\pi^6 k\lambda(H\beta)} \cdot \frac{L_\odot}{R_\odot^{\,2}T_\odot^{\,4}} \cdot \frac{\alpha(H\beta)}{\alpha_B} \cdot \frac{T^3 G_1(T)}{B_\lambda} \quad \text{Å} \qquad (2.2.9)$$

Here the Planck function B_λ is written in terms of wavelength. thus:

$$B_\lambda(T) = 2hc^2\lambda^{-5}\ (e^{-2.616\times10^4/T} - 1)^{-1}$$

Substituting numerical values in for the constants and taking $\alpha(H\beta)/\alpha_B$ at T_e=10⁴ K this can be written as:

$$F(H\beta)/F_\lambda = 4.126\times10^{-11}\ T^3\ G_1(T)\ (e^{2.616\times10^4/T} - 1) \quad \text{Å} \qquad (2.2.10)$$

This then enables what is known as the Hydrogen Zanstra Temperature or

Tz(H), to be determined if the ratio of the Hβ to the visual continuum for the P.N is known. The value of the integral G1(T) is shown as a function of temperature in Appendix 2.1

The HeII Zanstra Temperature, Tz(HeII) may be derived in a similar manner. Here the assumption is made that the nebula absorbs all of the photons emitted by the central star shortward of 228Å, ie the frequency limit above which Helium is doubly ionised. In this case the emission line used in an analogous fashion to the Hβ line is the transition of helium from n=3 to n=4, namely the HeII line at 4686Å. The procedure is similar to that described above. The numerical integral, $G_4(T)$ is calculated with $\nu_4=4\nu_1$, the value of this integral is tabulated in Appendix 2.3 as a function of temperature.

We have then for the case of Tz(HeII):

$$\frac{F(4686)}{F_\nu} = \frac{15h\nu(4686)}{4\pi^6 k} \cdot \frac{L_\odot}{R_\odot^2 T_\odot^4} \cdot \frac{\alpha(4686)}{\alpha(He+)} \cdot \frac{T^3 G_4(T)}{B_\nu} \quad Hz \qquad (2.2.11)$$

Again this is expressed in terms of flux in frequency interval. As in the above case it is more convenient to rewrite this in terms of wavelength interval. For the case of a nebula electron temperature of 10^4 K (2.2.11) can be written thus:

$$F(4686)/F_\lambda = 8.882\times10^{-11}\ T^3\ G_4(T)\ (e^{2.616\times10^4/T} - 1)\quad Å \qquad (2.2.12)$$

Finally it is also possible to consider what is known as the HeI Zanstra Temperature, Tz(HeI). The frequency range of the central star flux that is of interest here is the range $1.807\nu_1 < \nu < 4\nu_1$. The concern with this frequency range is that these photons may be absorbed by both H^0 and He^0. However Harman & Seaton (1966) have concluded that for those nebulae which do not have HeII emission lines, then the nebulae will be optically thick in the HeI continuum. The emission line used in determining this temperature is the HeI λ4471Å line. Using similar arguments to those in obtaining Tz(H) we can write:

$$\frac{F(4471)}{F_\nu} = \frac{15h\nu(4471)}{4\pi^6 k} \cdot \frac{L_\odot}{R_\odot^{\,2} T_\odot^{\,4}} \cdot \frac{\alpha(4471)}{\alpha(He^o)} \cdot \frac{T^3 G_{1.807}(T)}{B_\nu} \quad Hz \qquad (2.2.13)$$

Again this can be evaluated using the values of the recombination coefficients at a nebula electron temperature of 10^4 K and converting to units of wavelength to give:

$$F(4471)/F_\lambda = 3.858\times10^{-10}\ T^3\ G_{1.807}(T)\ (e^{2.616\times10^4/T} - 1)\quad Å \qquad (2.2.14)$$

The value of the integral, $G_{1.807}(T)$, is given in Appendix 2.2

These then are expressions which can be used to solve for the three temperatures; Tz(H), Tz(HeII), and Tz(HeI). In the following sections the magnitudes of the central stars studied will be determined and these will be used along with line fluxes from the literature to determine these temperatures for these nebulae.

2.3 Observational Procedure

Our observations made use of the RGO CCD at the prime focus of the 3.9m Anglo-Australian Telescope which is situated at Siding Spring, NSW, Australia. This CCD chip is based on an RCA SID 53612 thinned , back illuminated chip and has 512 × 320 pixels each of approximately 30 microns square. The chip has a quantum efficiency of some 80% at peak between 4000-7000 Å. One detected photon gives rise to one electron and the saturation level is about 1.6×10^5 electrons.

The CCD camera operated at the f/3.3 prime focus of the 3.9m telescope. The doublet corrector was used. This has an unvignetted field diameter of 25 arc minutes. The plate scale using this corrector was 16.4 arcsec/mm and hence each CCD pixel corresponds to ≈ 0.5 arc secs.

The observations were taken during three nights of March 1985. The seeing on each night was determined by examining the profiles of field stars and also of our standard stars. Generally the seeing was ≲ 1-2 arcsec.

Images were obtained through several narrow passband filters for each of the P.Ne. studied. The filters used with their wavelengths and passbands are tabulated in Table 2.2. The filters at 5500Å, 4200Å and 3600Å are the standard wide band V,B,U filters. The filter at 4788Å is a continuum filter chosen at a wavelength clear of any known emission line. The [OI] filter was chosen so that the P.Ne. could be imaged in the light of a typical 'low excitation' line, whereas the [OIII] filter was chosen to give images in a typical 'high excitation' line.

The P.Ne. that we chose to observe, the filters through which exposures were taken and the exposure times are listed in Table 2.3. In addition to these, exposures through each of the filters used were taken of spectrophotometric standard stars. These stars were taken from the lists of Landolt (1973), parameters for these standards are listed in Table

2.4. In addition to these standards we were able to use field stars in the CCD frames for a few of our sample of P.Ne. Photometry on these field stars has been done by Gathier et al (1986), Gathier (1986) and the magnitudes for these field stars have been used to calibrate the magnitudes of the P.N. to which they pertain. Details of these field stars are also listed in Table 2.4.

For the purposes of removing variations in the sensitivity across the CCD frames 'Bias' and 'Flat Field' frames were taken (Mackay, 1986). The flat field frames were obtained by illuminating the interior of the AAT dome with a standard Tungsten light source and viewing this at the CCD through each of the filters used. Bias frames were simply zero time integration frames, which gave an indication of the 'readout noise' on the CCD. It should be noted that in measuring these central stars we minimised the problems due to variations in pixel to pixel sensitivity by ensuring that the images of the central stars and the standard stars were positioned in the same area of the CCD chip.

The variation of atmospheric extinction was determined by taking observations of a standard star at different values of airmass over the three nights. We have assumed that the atmospheric extinction function remained constant over the three nights of our observations.

2.4 Preliminary Reduction

The data frames obtained at the AAT were written as standard FITS format images to magnetic tape at a density of 1600 Bpi. All preliminary analysis of this data was performed using the Groningen Image Processing System (GIPSY) at the Kapteyn Laboratorium, Groningen. I will briefly descibe in the following section the procedures which I employed in analysing this data and mention a few points concerning the GIPSY system. I have also used the STARLINK system at UCL and other sites in performing supplementary analysis.

Table 2.2

Interference Filters

Wavelength (Å)	Line observed	Filter Passband (Å)
6300	[OI]	10
5500	V	Broadband
5007	λ5007 [OIII]	15
4788	Continuum	12
4200	B	Broadband
3600	U	Broadband

Table 2.3 Observational Exposure Times.

Name of P.N.	P.K. No.	Cont. 4788Å	U	B	V	[OIII] 5007Å	[OI] 6300Å
NGC 2346	215 + 3°1	900	100	20	10		
NGC 2438	231 + 4°2	900	150	20	10		
NGC 2440	234 + 2°1	900	200	25	3		
NGC 2452	243 − 1°1	1200	180	60	60	100	1200
NGC 2818	261 + 8°1	900	300	200	200		900
NGC 2867	278 − 5°1	900	100	20	5		900
NGC 3132	272 +12°1	50	10	1	1	5	180
NGC 3211	286 − 4°1	900	500	100			
NGC 3918	294 + 4°1	900	20	5	5	60	900
NGC 5315	309 − 4°2	600	20	5			
NGC 6153	341 + 5°1	900	400	80	20		
NGC 6302	349 + 1°1	900	100	20	20		
NGC 6309	9 +14°1	900	100	20	20		
NGC 6439	11 + 5°1	900		20			
IC 2165	221 −12°1	900	100	20	5		
IC 2448	285 −14°1	900	100	20	10		
IC 4776	2 −13°1	900	30	10	5	15	
J 900	194 + 2°1	900	150	20	20	100	600
A 36	318 +41°1			20		600	
A 38	346 +12°1			200	200	900	
A 40	359 +15°1	900	150	60	60	900	
A 45	20 − 0°1			100	300		
A 58	37 − 5°1			100			
HE2-120	321 + 1°1	900	150	60	60	300	
HE2-117	321 + 2°2	900	360	180	180	360	

Table 2.3 shows the P.Ne. observed. An entry in columns 3-8 indicates that the P.N. was observed through that filter and the number gives an indication of the typical exposure time in seconds.

Table 2.4a. Details of Standard Stars.

Star I.D.	R.A.(1975) h m s	Dec(1975) ° ' "	V	B-V	U-B	Spectral Type
105-815	13 38 47	+ 0 05 25	11.44 +/-.009	+0.39 +/-.021	-0.23 +/-.019	A5 p
101-281	09 55 48	- 0 24 28	11.58 +/-.018	+0.81 +/-.021	+0.44 +/-.022	G3 V
108-475	16 35 43	- 0 31 41	11.32 +/-.021	+1.37 +/-.014	+1.49 +/-.031	K0 III

Table 2.4b Field Star Colours from the Photometry of Gathier (1984).

Star I.D.	m_v	V	(V-B)	(B-U)	(B-L)
03 039	13.11	-2.4967	0.1582		
03 042	13.37	-2.6053	0.2413		
03 043	13.71	-2.7499	0.4808		
09 199	14.49	-3.051	0.318	0.351	0.273

Table 2.4a details the spectrophotometric standard stars used, the information taken from Landolt (a). The star identification numbers in column 1 are taken from the Harvard Annals Vol 101 (Durchmusterung of Selected Areas). Columns 4, 5 and 6 give the magnitude and colour indices on the UBV photometric system along with their mean errors. The Bergedorfer Spektral Durchmusterung (BSD) spectral types are given in column 7.

Table 2.4b details the field stars taken from the photometry of Gautier (b & c). Column 1 gives his field star identification number (b). Column 2 gives the visual magnitude. Columns 3-6 give observed Walraven Log intensities.

2.4.1 Reduction Using The GIPSY Package

The data files were ported to GIPSY as FITS format files. A complete description of this system can be found in 'The Guide to GIPSY' by R.A.Allen and others which can be obtained from the Kapteyn Laboratorium. Each data frame for a P.N. was viewed and contour plots produced. A collection of these contour plots are shown in Appendix 1 of this work. Primarily we have not been concerned with the structure or morphology of the P.Ne., in viewing these images we are mainly interested in obtaining information about the central stars, and hence the images shown have only been processed in the most basic fashion. However images of this nature are scarce and hence inclusion is warranted.

2.4.2 Measurement of the Standards

Standard magnitude sequence stars were observed through each filter several times each night. The total counts in the star for each filter were obtained by integrating the CCD image under the stellar profile. The sky background was obtained from analysis of areas of dark sky in the region of the standard star, the mean value obtained in counts per pixel was then assumed to be the sky background under the stellar image. This assumption is valid due to the small area of the stellar image. Additionally, gaussian fits were made to the stellar profiles and the Full Width at Half Maximum was obtained from this in order to determine the 'seeing'.

The UBV colours of the standards and the spectral types given were used to estimate the effective surface temperature of each star. The temperature of SA 101-281 was estimated to be T = 5720 K and the temperature of SA 108-475 to be T = 4500 K. (Allen, 1973 and Selby, 1986). The uncertainties in these values are of the order of 15%. When converting the fluxes observed for the standards at the continuum wavelength of 4788Å to the visual wavelength at 5500Å the assumption was made that the stars emitted as blackbodies of temperatures as determined above. One problem that can effect this work is that the standard stars may have absorption lines within the passbands of the filters used. To determine the effect of this ideally one should have high resolution spectroscopy for each of the standard stars covering the passbands of each of the filters used. However for these stars this information is unavailable. Spectroscopic data has been obtained though of 'typical' main sequence stars having the same spectral type as our standards (Blackwell et al, 1986). From analysis of these spectra, which cover the wavelength region from approximately 3600A - 9200A, the effect of absorption lines at the wavelengths of interest to us, namely 4788A and 5500A, would appear to be minimal. Sample spectra for the cases of a G3 V and a KO III star are shown in Fig 2.2. To a first approximation the assumption of the standard stars radiating as black bodies would appear to be a reasonable one. At some future date it would be desirable to measure the energy distributions of these standard stars and use these more realistic values in the calibration of these flux standards.

2.4.3 The Treatment of the Planetary Nebulae Images.

For each P.N. we obtained, as a minimum, an image through the narrow band continuum filter, and an image through one or more of the U,B,V broadband filters. In using this imaging technique, care had to be taken to ensure that the central star of each P.N. was correctly identified. In a few cases, for example NGC 2818, the position of the central star was unclear in that nearby nebula condensations could potentially be confused with the central star. The broad band images then were used in comparison with the continuum images. Stellar like nebula condensations were enhanced in the broad band images and hence it was possible to identify the true position of the central star. For an example of this see the images of NGC 2452. (Appendix 1. Figs 4 & 5)

Generally we employed one of three methods in obtaining the flux

G3 V Main Sequence Star

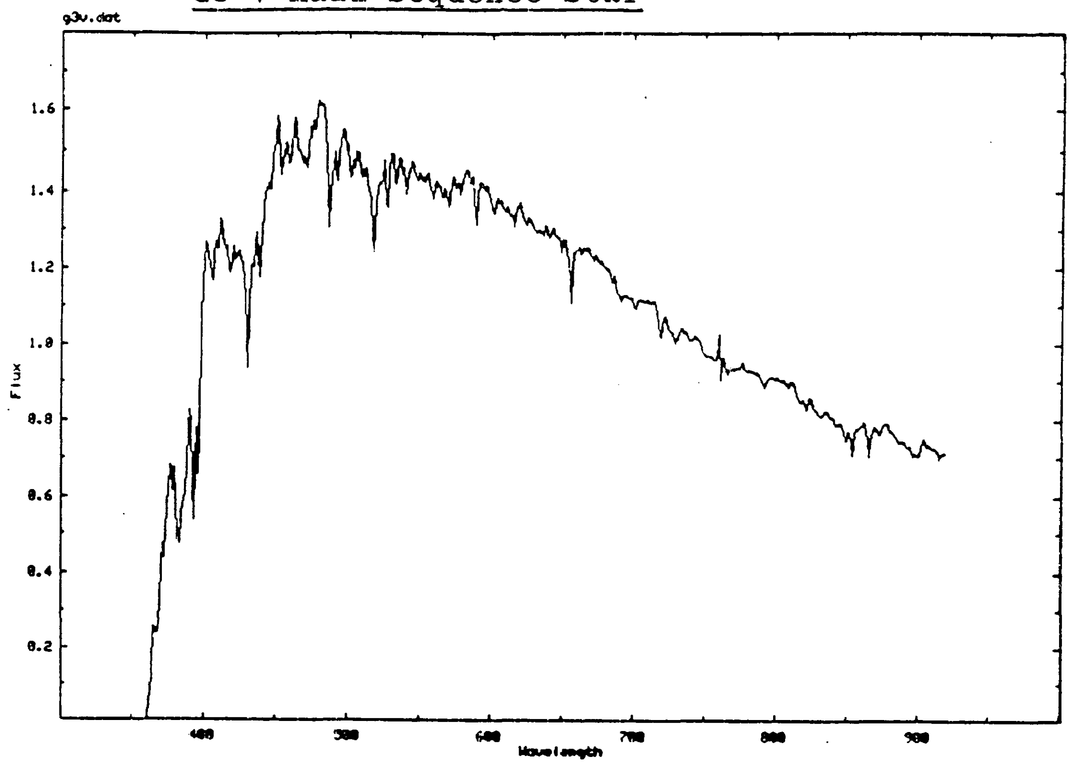

KO III Main Sequence Star

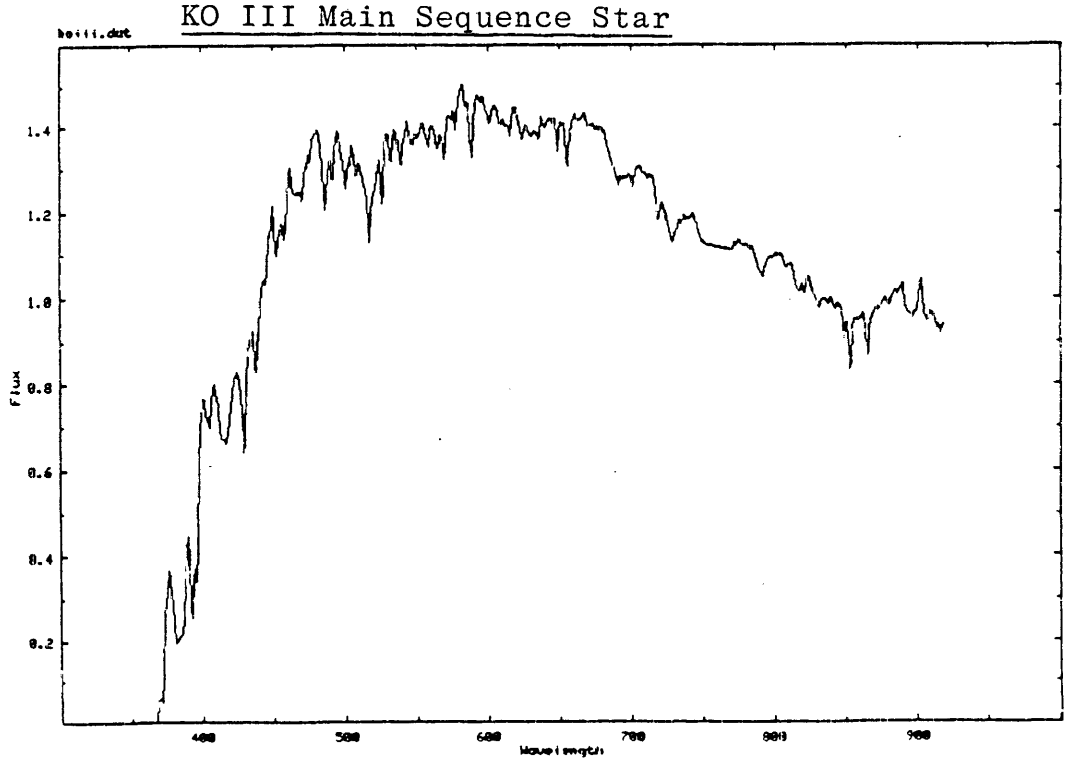

Figure 2.2 Spectra for a'Typical' G3 V, and a KO III main sequence star. Wavelength is in nanometers, Flux is in arbitary units.

contained in the central star of the P.N. for each object studied which will be discussed. In the cases of a number of the P.Ne. the central star was quite obvious above a faint nebula background, for instance NGC 3132 which has a star with $m_v = 10$ surrounded by a very faint nebula. In these cases the flux in the star was determined by integrating under the central star profile and subtracting the contribution due to the nebula, which was assumed to be constant under the stellar image. The value of this nebula background was found by taking a mean of the nebula background over a region surrounding the central star where the nebula flux was at a constant level. This method then was used for those P.Ne. for which the central star associated with that P.N. was reasonably bright ($m_v > 15$).

The second method that was employed applied to those P.Ne. with faint central stars. In these cases profiles were taken through the continuum images at the position of the central star. The corresponding profiles in position were taken from one or more of the broadband images but usually the 'B' image. In the broad band images the emission from the central star was often found to be swamped by emission from the surrounding nebula. An example of this is the case of IC 2165. In the broadband 'B' image the central star is only marginally detected. In the narrow band continuum image at 4788Å taken immediately after the 'B' image the nebula emission is surpressed relative to the central star emission and consequently the central star is clearly apparent. These images and corresponding profiles through the central star position are shown in Figs. 2.3 (a-d). From analysis of the shape of the broadband profiles the nebula contribution in the region of the central star was determined. Turning then to the narrow band continuum image, this nebula contribution was subtracted from the profiles and the integral of the remaining flux due to the central star was calculated.

For a number of the P.Ne. studied we found the central star to be located in close proximity to knots of nebulosity, for instance in the case of NGC 2440. For these P.Ne. it was sometimes difficult to

Figure 2.3a Profile thro' centre of B band image.

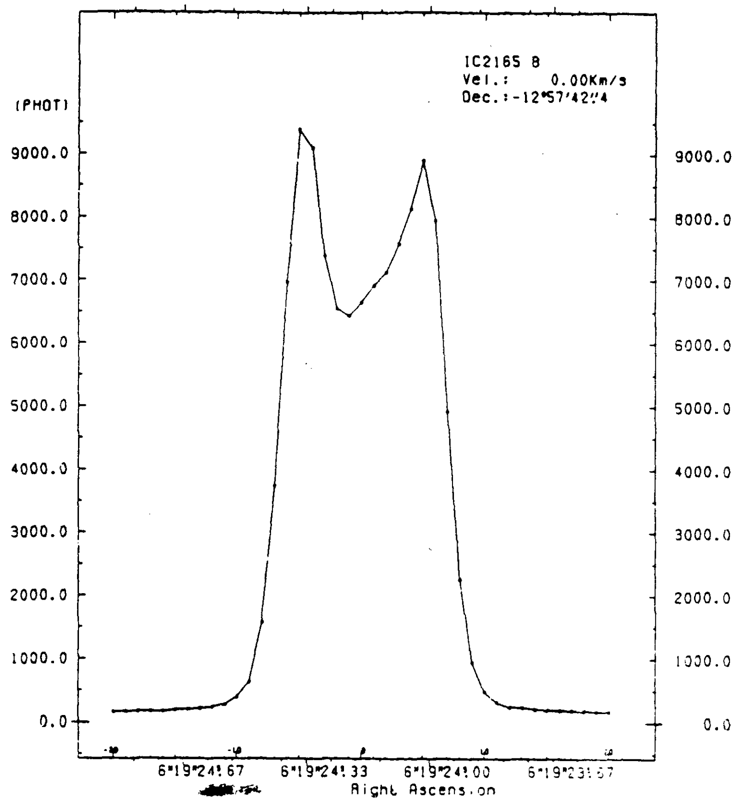

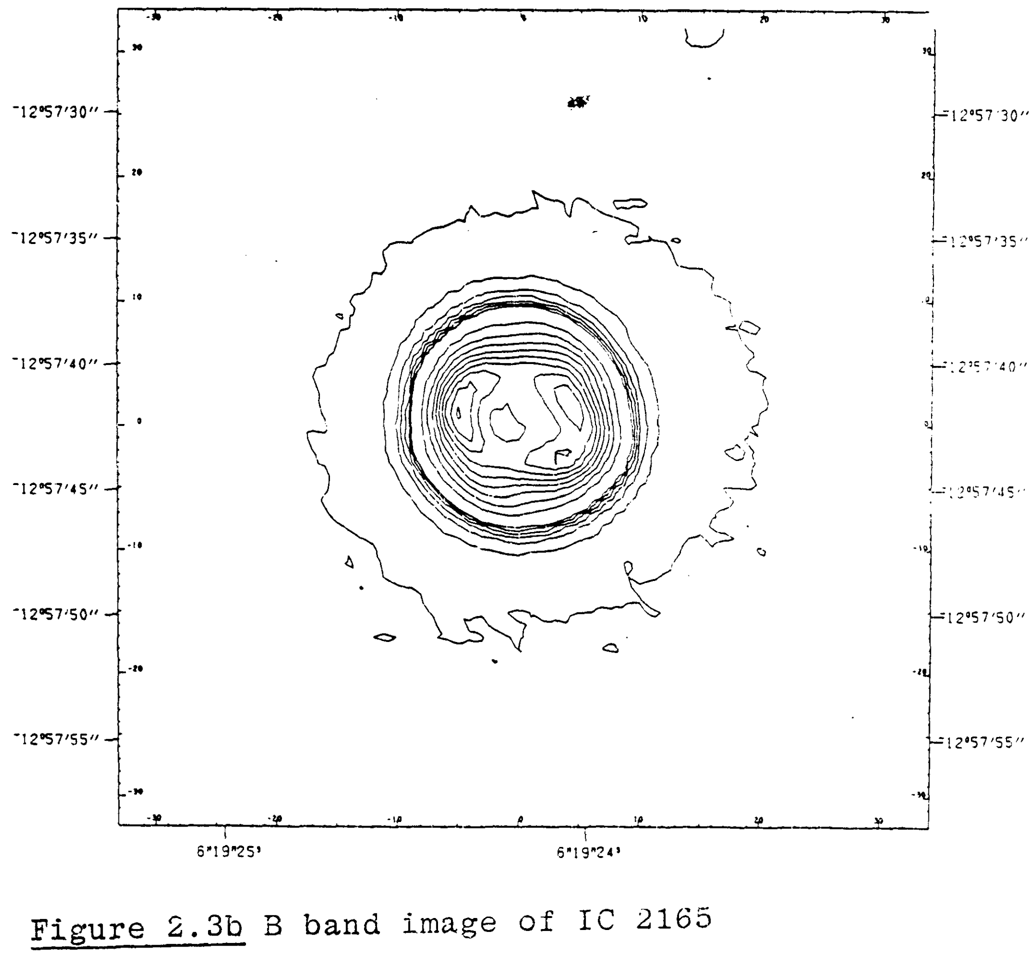

Figure 2.3b B band image of IC 2165

Figure 2.3c Profile thro' centre of 4788A image

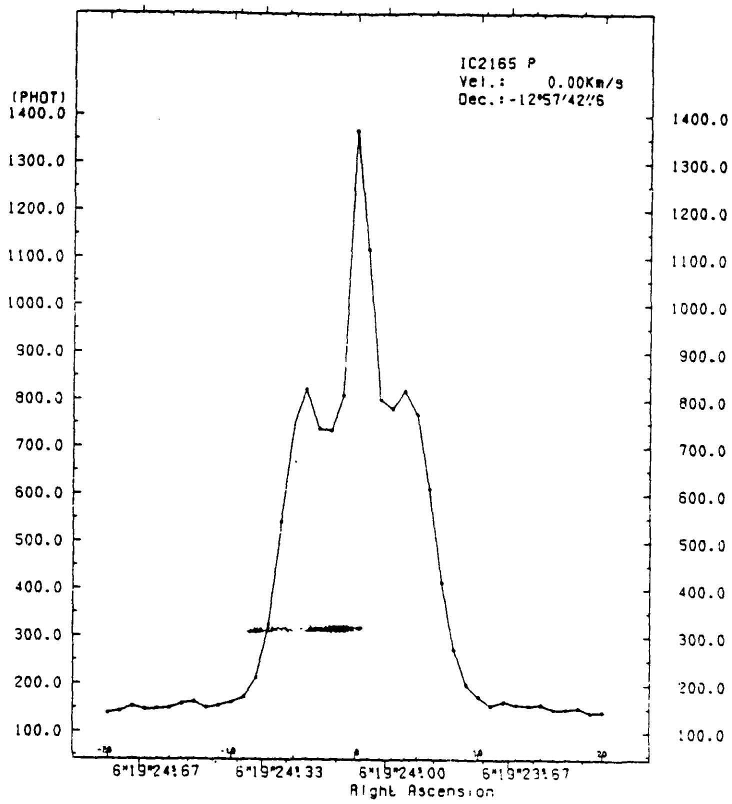

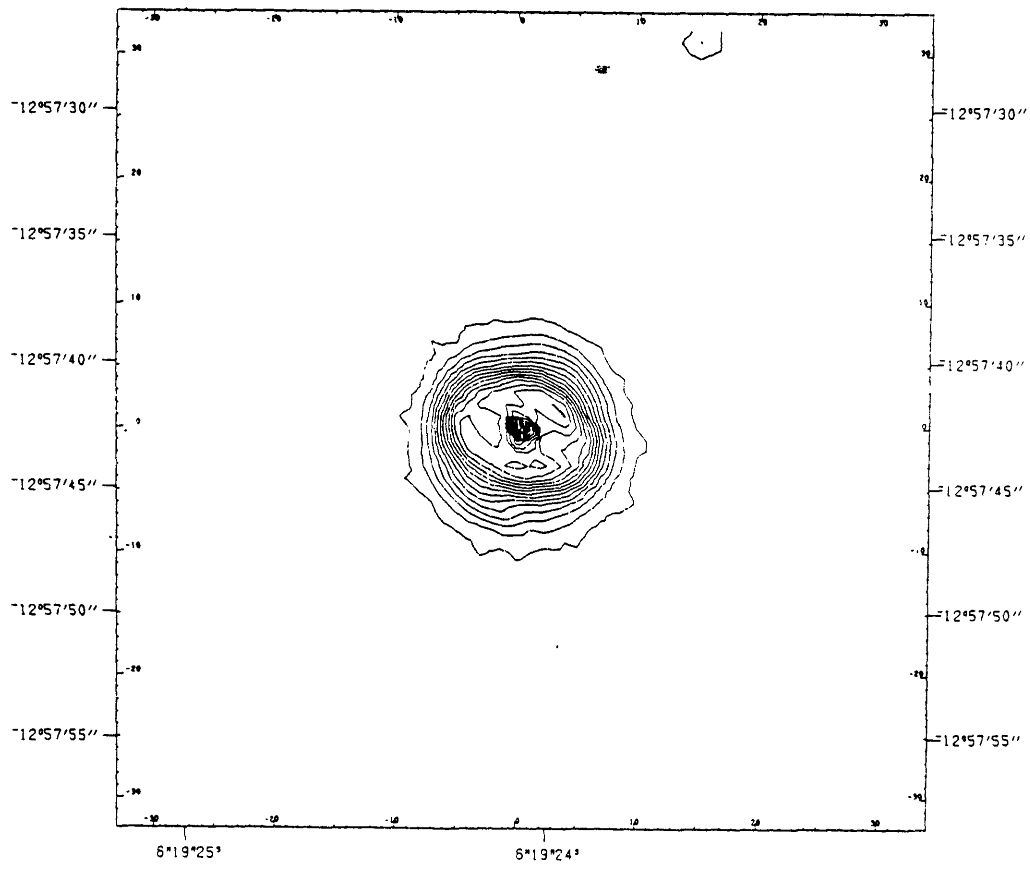

Figure 2.3d 4788A image of IC 2165

determine exactly how the continuum was behaving underneath the stellar image and hence the error in deciding the stellar flux was correspondingly higher. It was possible in some cases, especially for data obtained on the second night of these observations when the seeing was exceptionally good, for the stellar flux to be determined by making a gaussian fit to the stellar region and assuming that the baseline was flat under the stellar image. For a number of the P.Ne., e.g. NGC 3918, NGC 3211, the central star was only marginally detected above a strong nebula continuum. Here the fit of a gaussian profile proved to be unrealistic, the flux in the central star was determined by visual inspection of the profiles through the data with a best possible estimate of the continuum under the central star being made. Errors in measuring the stellar fluxes in the images for these P.Ne. were estimated by taking values of the maximuum possible changes in the contribution of the nebula contribution under the stellar image.

The final method employed was used to obtain the flux for the central star of the P.N. J900. For this nebula of rather small angula size (≈ 5 arcs) the central star was rather poorly detected in the narrow band image and completely undetected in the broadband images, where the stellar emission was swamped by nebular emission line energy. The assumption was made that in the wings of the profiles through the nebula in both the broadband and narrow band images the emission would be totally due to the nebula. Also it was assumed that the component of the flux due to the central star in the broadband image would be negligible compared to that originating from the nebula. Using the ratios of the counts contained in the wings of the images then, the broadband image was scaled to the narrow band image and then was subtracted from that. The residual resulting had a stellar like profile of FWHM equivalent to that of the 'seeing' at the time of the observation, as determined from field stars in the CCD data frame, and was centred on the position where the central star of J 900 might be expected at the centre of the nebula. The flux in this residual was determined and this was taken as being due to the central star.

Finally in the case of a few of the P.Ne. investigated no detection of the central star could be made in either the broad or narrow band images. The technique outlined above was applied to the images of NGC 6302 with no stellar like residual resulting from the fitting procedure.

2.5 Magnitude Determinations and Continuum Fluxes.

The fluxes obtained for the central stars and the standard stars from the narrow band filter at 4788Å were corrected for atmospheric extinction to a constant airmass of 1.0. All observations were taken at Zenith Distances of less than 45° so that the airmass was directly proportional to sech.

The fluxes at 4788Å had now to be converted to fluxes at 5500Å. For the purposes of this transformation both standard star and central star were assumed to radiate as blackbodies. In the case of the central stars model atmosphere calculations show that the blackbody approximation is valid overthis wavelength range. (eg Hummer & Mihalas, 1970a) For the central stars we have to also make an assumption as to what temperature to use for the blackbody. At the high temperatures of these central stars ($T > 30{,}000$ K) the ratio of the Planck functions at $\lambda = 4788$Å and $\lambda = 5500$Å varies only slightly and hence to a value of $T = 10^4$ K was used initially. However at the end of this process a value for the central star temperature is determined and this value was then used in the iteration. The relation linking the two wavelengths then is:

$$F_V = F_{(4788)} \times (B_V / B_{(4788)}) \qquad (2.5.1)$$

where F_V is the flux in counts/sec at the wavelength $\lambda = 5500$Å, $F_{(4788)}$ is the measured flux in count/sec from the 4788Å image, and B_V, $B_{(4788)}$ are the Planck Functions at those wavelengths.

Direct comparison of the fluxes of the standard stars and the central stars of the P.Ne. now enables the visual magniudes of the central stars to be determined. The relationship used is:

$$m_V \text{ (NPN)} = m_V \text{ (std)} - 2.5 \log R \qquad (2.5.2)$$

where R = flux in the NPN / flux in the std

The error in this magnitude determination was calculated taking into account the errors in calculating the fluxes in the NPN and standard stars from the 4788Å CCD images, and also the error in the quoted magnitude for the standards (although this error is rather small being of the order of 0.01 mags). The error in the visual magnitude calculated for each NPN is given by:

$$\sigma_m PN^2 = (\ \delta_m std\ )^2 + \frac{(\ 2.5\log(e)\ )^2 \delta C_{std}^2}{C_{std}^2} + \frac{(\ 2.5\log(e)\ )^2 \delta C_{NPN}^2}{C_{NPN}^2} \qquad (2.5.3)$$

where $\delta_m$std is the error in the standard star magnitude, C_{std} and δC_{std} are the flux and error (in counts/sec) found for the standard star, and C_{NPN} and δC_{NPN} are the flux and error (in counts/sec) found for the NPN.

A summary of the P.Ne. imaged and the visual magnitudes derived for their central stars from the narrow band continuum filter images is presented in Table 2.5. Column 2 gives our derived magnitudes along with the associated error whilst Column 3 gives the visual flux, uncorrected for extinction, corresponding to this magnitude as outlined below.

Knowing the visual magnitude for each of our central stars enables the visual flux from the central star to be found using the calibration of Wamsteker (1981) that 0 mag in the visual is 3.64×10^{-9} ergs cm^{-2} s^{-1} Å^{-1}, and hence:

$$F_V = 3.64 \times 10^{-9} \times 10^{-mv/2.5} \qquad (2.5.4)$$

Table 2.5 Derived Magnitudes for the P.Ne. Sample.

Name of P.N.		Magnitude m_V	F(vis) ergs cm^{-2} s^{-1} A^{-1} (× 10^{16})		Distance (kpc)	Abs. Mag. M_V
NGC 2346	a)	14.7 +/- 0.1	48.0		0.8 +/- 0.2	4.36
	b)	13.1 +/- 0.1	209			2.75
NGC 2438		18.4 +/- 0.2	1.59		1.2 +/- 0.3	6.72
NGC 2440		18.9 +/- 0.2	1.00		2.19 +/- 0.38	6.26
NGC 2452		17.9 +/- 0.2	2.52		3.57 +/- 0.47	3.76
NGC 2818		19.5 +/- 0.4	0.577	a)	2.1 +/- 0.5	7.19
				b)	3.5 +/- 0.5	6.08
NGC 2867		16.5 +/- 0.1	9.14		1.6 +/- 0.2	4.66
NGC 3132		10.2 +/- 0.1	3030		0.6 +/- 0.1	1.00
NGC 3211		17.8 +/- 0.4	2.76		1.91 +/- 0.22	5.76
NGC 3918		16.8 +/- 0.2	6.94		2.24 +/- 0.84	4.27
NGC 5315		13.3 +/- 0.2	174		2.62 +/- 0.83	0.14
NGC 6153		16.2 +/- 0.1	12.1		1.4 +/- 0.4	3.30
NGC 6302		no detection			0.53 +/- 0.12	
NGC 6309		16.5 +/- 0.1	9.14		2.1 +/- 0.5	4.58
NGC 6439		no detection			5.0 +/- 1.0	
IC 2165		17.9 +/- 0.2	2.52		2.8 +/- 0.2	4.11
IC 2448		14.5 +/- 0.1	57.7		2.8 +/- 0.2	2.11
IC 4776		13.7 +/- 0.1	121		3.4 +/- 0.2	-0.07
J 900		17.8 +/- 0.9	2.76		2.1 +/- 0.2	4.86
A 40		19.7 +/- 0.3	0.480		3.9 +/- 0.8	3.24
HE2-120		21.2 +/- 0.7	0.121		3.2 +/- 0.7	4.77
HE2-117		19.1 +/- 0.3	0.834		3.0 +/- 1.5	0.68

Notes to Table 2.5

The two values for NGC 2346 are those obtained on subsequent nights.
The two values for NGC 2818 are using different distances.

In order to calculate the unreddened visual flux of the NPN, i.e. a visual flux corrected for interstellar extinction towards each of the P.Ne., the colour excess E(B-V) must be known for each of the P.N. Following Seaton (1979) the extinction function $f(\lambda)$ is defined such that the extinction is:

$$10^{-c(\ 1+f(\lambda)\ )}$$

The value of $f(\lambda)$ is set to equal 0 at $f(H\beta)$, the wavelength of the Hβ line being 4861Å. The logarithmic extinction at Hβ then is c, hence:

$$f(\lambda) = (\ X(x)\ /\ X(H\beta)\ ) - 1$$

Where $X(x) = A_\lambda/E(B-V)$ with $x=1/\lambda(\mu m)$ and $X(H\beta)$ is the function X(x) at λ=4861Å. A_λ is the extinction in magnitudes at wavelength λ and E(B-V), the colour excess, equals $A_V - A_B$. Now $X(H\beta) = 3.68$ (Seaton, 1979) and $c = 0.4X(H\beta)E(B-V) = 1.47E(B-V)$. This follows from the definition of the interstellar extinction in magnitudes at the wavelength λ, A_λ, being defined as :

$$A_\lambda = -2.5\log(\ F_\nu\ /\ F_\nu(0)\ )$$

where $F_\nu(0)$ is the stellar flux at the surface of the earth in the absence of extinction.

Hence we can write the extinction as:

$$10^{-(\ 1.47/3.68\ )E(B-V)(\ A_\lambda/E(B-V)\ )}$$

The unreddened visual flux then is found using the above:

$$F_Vc = F_V \times 10(\ A_\lambda/E(B-V)\ )\ E(B-V)/\ 2.5 \qquad (2.5.5)$$

$A_\lambda/E(B-V)$, the extinction coefficient, is a function of wavelength.

Using a standard galactic extinction law, A_{λ} / E(B-V) = 3.10 at λ = 5500Å as tabulated in Pottasch (1984). This was taken from the average interstellar extinction curve given in Savage & Mathis (1979). $F_{V}c$ is the value of the flux corrected for extinction using the value of E(B-V).

The extinctions towards the P.Ne. have been taken from the literature, the adopted value of E(B-V) for each P.N. being listed in Table 2.6 along with the relevant references. A number of our sample of P.Ne. have recently been studied by Gathier et al (1986) who has used the 'Reddening Distance Method' to obtain distances to these P.Ne.. An important requirement of this technique is that the foreground reddening to the P.Ne must be known. Gathier has employed several methods to obtain an E(B-V) value for each of his P.N. and where possible these values have been used in this work.

The values of E(B-V) used for the P.Ne. in this work have been found largely assuming a standard interstellar extinction curve. Various authors have shown that significant deviations from this standard curve can occur in certain directions (Bless & Savage, 1972). However these deviations are most pronounced in the ultra-violet shortward of 2000Å. From measurement of E(B-V) of a number of P.Ne. using several independent techniques Pottasch (1984) concluded that the use of a standard interstellar exticton curve is valid at least for wavelengths longer than 1600Å. For the purposes of this work it should also be noted that the wavelength at which we have measured the stellar continuum flux is close to that of both the Hβ 4861Å and HeII 4686Å lines and hence extinction corrections will be unimportant to a first approximation.

These visual magnitudes and visual fluxes now enable estimates of the central star temperatures to be made if line fluxes at Hβ 4861Å and HeII 4684Å are available for the P.Ne.

2.6 Temperature Determinations

The Zanstra method for determining central star temperatures requires a knowledge of the Hβ line flux. The Hβ fluxes for each P.N. have been taken from the literature with more weight being given to recent determinations, where several are available. The fluxes are shown in column 2 of Table 2.6 along with the relevant references in column 4. These Hβ fluxes are the reddened fluxes as seen at the Earth's surface and are uncorrected for interstellar extinction. The values of extinction E(B-V) which are later used to correct these fluxes are shown in Table 2.6, column 5. The error in the Hβ fluxes are, where not shown, of the order of 0.02 in the Log, these errors being relatively negligible compared to other sources of error in computing the Zanstra temperatures. The errors inthe extinction are taken as +/- 0.05 if not indicated.

The Zanstra technique may also be applied to give as the HeII Zanstra temperature if the HeII line flux at λ=4686Å is available. Again the values of the HeII flux have been taken from the literature. It is usually the convention that these fluxes are given in a fashion such that they are expressed relative to the Hβ flux at λ=4861Å, these fluxes being shown in this fashion in Column 3 of Table 2.6 where the HeII flux is shown on the scale I(Hβ)=1.0. The small correction due to the differential reddening between Hβ and HeII λ4686Å has been applied to these values using the values of E(B-V) in column 5. The errors on these ratios are of the order of +/-0.1

Using these fluxes as the basic input data it is possible to compute the HI and HeII Zanstra temperatures for each of the P.N. of our sample. The method has been outlined in a preceeding section (2.2.5) and will not be repeated here. The derived HI and HeII Zanstra temperatures are given in columns 3 & 4 of Table 2.7 along with an estimate of the error. The analysis of the errors involved in evaluating these temperatures will be dealt with in a subsequent section (2.7.3).

Table 2.6 Hb and HeII(4686) Fluxes for the P.Ne. Sample.

Name of P.N.	-Log F(Hβ)	I(4686) ($I_{H\beta}$=1.0)	Refs	E(B-V)	Refs
NGC 2346	11.30	0.51	5,11,13	0.07+/-0.03	7
NGC 2438	11.04+/-0.07	0.41	8,16,17	0.40	8
NGC 2440	10.47	0.60	5,10,17,20,21	0.30+/-0.03	7
NGC 2452	11.44	0.57	9,17	0.43+/-0.04	7
NGC 2818	11.35	0.74	5,6,16,17	0.21	6
NGC 2867	10.56	0.28	12,17,22	0.27+/-0.03	7
NGC 3132	10.39	0.14	5,13,17,22	0.10+/-0.02	7
NGC 3211	11.02	0.70	12,17,22	0.21+/-0.03	7
NGC 3918	10.02	0.37	5,12,17,21	0.24+/-0.03	7
NGC 5315	10.41	0.11	12,17,21,22	0.35+/-0.04	7
NGC 6153	10.85	0.26	2,9	0.70+/-0.07	3
NGC 6302	10.53	0.74	9,17	1.07	15
NGC 6309	11.162	0.71	9,19	0.05+/-0.07	19
NGC 6439	11.59	0.23	9,18	0.53	18
IC 2165	10.94+/-0.03	0.56	8,12	0.51	8
IC 2448	10.84	0.29	12,17,21	0.06	15
IC 4776	10.699		19	0.34+/-0.34	19
J 900	11.225	0.50	1,9,19	0.43+/-0.09	19
A 40	13.03†		14	1.11	14
HE2-120	11.11¶		14	1.25	4
HE2-117	12.46		4	1.94	14

References to Table 2.6

1: Aller and Czyzak (1979)
2: Aller and Faulkner (1964)
3: Cahn (1976)
4: Cahn and Kaler (1971)
5: Carrasco et al (1983)
6: Dufour (1984)
7: Gathier et al (1986)
8: Kaler (1976a)
9: Kaler (1976b)
10: Kaler (1978)
11: Kaler et al (1976a)
12: Kohoutek and Martin (1981)
13: Mendez (1978)
14: Milne (1979)
15: Milne and Aller (1975)
16: O'Dell (1963b)
17: Perek (1971)
18: Pottasch (1984)
19: Shaw and Kaler (1985)
20: Shields et al (1981)
21: Torres-Peimbert and Peimbert (1977)
22: Webster (1969)

Notes to Table 2.6

†: This value of Hβ flux has been calculated from the nebula photographic magnitude (ref 13) using the method of O'Dell (1963a).

¶: This Hβ flux has been calculated from the 5Ghz radio flux given in Milne (1979) and is the flux with no extinction. (see text)

2.6.1 PNe and the Filling Factor.

In the theoretical derivation of the Zanstra temperatures in section 2.2.5 it has been assumed that the filling factor of the PNe is unity. In other words, in deriving Tz(HI) and Tz(HeII) it has been assumed that the central star is completely surrounded by the HII region and consequently no 'leakage' of hydrogen ionising photons occurs into the suurounding interstellar medium for those PNe that are optically thick to the Lyman continuum. The question must be raised as to whether this is a valid assumption to make in view of the fact that many PNe have been observed to be highly irregular in structure, with some having the appearence of a filling factor less than unity.

The filling factor accounts for for ultraviolet radiation escaping into space without ionising the nebula (Harman & Seaton, 1966). Images of PNe may be deceptive in deciding the filling factor. As reported in Kaler (1983) Young has taken slit spectra of NGC 7293 which is generally assumed to have a low filling factor. In [OII] and [NII], which are low excitation lines, the central hole is clearly evident. However when spectra in Hβ are taken this is much less evident, whilst no hole is seen in HeII. Hence it may be that the neutral hydrogen and ionised helium which actually absorb the ionising photons are distributed in a different manner than that which is suggested by broadband images of the PN. NGC 6720 provides another example. The filling factor is often assumed to be $\xi=1$ for this PN, but Atherton et al (1978) model this PN in terms of a closed shell for which $\xi=1$ on the basis of Hβ and HeII images showing a much less pronounced hole at the centre of the nebula than the [NII] image.

Pottasch (1980) has compared the electron densities, n_e, of a number of PNe as found from from the Hβ flux with n_e found from forbidden line ratios. Equality is found for a filling factor, $\xi=1$, and the conclusion is reached that most PNe are in fact fully filled.

It seems reasonable then to conclude that the PNe in our sample have a filling factor of near unity and this is assumed to be the case in the derivation of the Zanstra temperatures.

2.7 Luminosity and Radii Determinations

Before one is able to determine the luminosity or radii of the central stars it is first neccesary to know the distance to each of the P.Ne. Unfortunately in many cases the individual distances of P.Ne. are not well known, it being not unusual for different authors to quote distances differing by factors of two for even well studied nebulae.

It is fortunate however that for a number of the P.Ne. studied in this sample, we can call upon perhaps some of the most reliable distance determinations which have been made to date. Gathier (1985, Gathier et al 1986) has recently investigated the distances to a number of P.Ne, using a variety of independent methods. Where possible these distances have been used in this work. For the other P.Ne. in this sample distances have been taken from a number of sources, these distances being determined by a variety of different methods, many of which involving statistical techniques making use of assumed properties of P.N. (for instance constant Hβ luminosity) which are probably invalid for individual P.Ne. (Gathier, 1984)

The summary of the distances used is given in Table 2.5, column 4. For the relevant references please refer to section 2.7.1 where the reliability of the distances for these P.Ne. will be discussed.

Additionally in this section the question of whether the nebulae are optically thick or not will be considered. In determining many of these distances the question of whether the nebula is optically thick to hydrogen ionising radiation has been investigated. It has generally been thought that many, if not most, P.Ne. are optically thin (eg Harman &

Seaton, 1966) but recently it has been suggested by Pottasch (1980) that a considerable number of P.Ne. are optically thick. This information is important for this work as the Zanstra method to determine central star temperatures does make the assumption that the nebula surrounding the central star is optically thick to hydrogen (and/or helium) ionising radiation.

2.7.1 PNe and Optical Thickness.

Briefly it is thought (Pacynski, 1971; Schonberner, 1979; Iben, 1984) that the central stars of PNe. evolve with a slowly increasing luminosity to higher effective temperatures as they burn their residual hydrogen envelope in a shell around the C/O core. Eventually this burning ceases as the hydrogen supply is exhausted and the central star rapidly declines in luminosity as the core remnant cools down onto the white dwarf cooling track on the H-R diagram (Pacynski, 1970).

The fading time, t_f, has been defined (Iben & Renzini) to be the time taken for the central star to evolve from its 'turn on point', which is when its surface temperature gets to about 30,000 K and hence is able to emit a significant amount of hydrogen ionising photons, to a point at which its luminosity is 10 times less than at its starting value. Iben & Renzini show that t_f is extremely sensitive to the core mass of the central star going as $t_f \propto M_H^{-9.6}$, where M_H is the mass of the hydrogen exhausted core, ie the central star mass.

It was first suggested by Seaton (1966) that PNe pass through three phases in their optical depth to the Lyman ionising continuum. In the first stage the PNe. is optically thick. Schonberner (1981) and others, have shown that the hydrogen ionising photon flux from the central star increases only slowly with time during this period. The nebula surrounding the central star is expanding and hence the electron density, n_e, falls. The mass of ionised hydrogen is inversely proportional to n_e and hence increases as n_e falls. Eventually the nebula will become completely ionised and the PNe will be optically thin. Pottasch (1980) determines the ionised mass in a sample of PNe noting the $M_i \propto 1/n_e$ relationship but sees little evidence for constant M_i at low n_e. He concludes that most PNe will remain optically thick. From eqn (2.2.6) it can be seen that the number of recombinations in the nebula gas is proportional to n_e. During the optically thin phase the mass of ionised hydrogen is constant and hence as n_e continues to fall the recombination rate also falls, which leads to a decrease in the Hβ luminosity.

PNe with slowly evolving, low mass central stars ($M < 0.57\ M_\odot$) will stay optically thin as the nebula will disperse into the surrounding interstellar medium in the 30,000 years or so that the central star takes to fall to a luminosity of Log L ≈ 3 (Iben & Renzini, 1983). PNe with central stars of intermediate mass ($0.6\ M_\odot < M < 0.7\ M_\odot$) however may be expected to finally enter into another optically thick phase. During the observable lifetime of the nebula the central star undergoes a considerable evolution. As it cools the point may be reached where the ionising flux from the central star is no longer able to fully ionise the surrounding nebula. If this occurs the PNe. will once again become optically thick to the Lyman continuum.

More massive central stars though are expected to evolve much more rapidly, for instance a star with a mass of $M \approx 1.2\ M_\odot$ has a fading time of less than 100 years (Pacynski, 1971). Because of their rapid evolution it is expected that these PNe with massive central stars will be optically thick as the central stars will most probably be observed whilst cooling, being bolometrically faint, with Log L < 2.5.

Peimbert (1978) and Peimbert & Torres-Peimbert (1983) defined Type I PN to be those PNe having n(He)/n(H) > 0.123 and Log(N/O) > -0.3. These PNe are thought to be just those with high mass central stars and are hence likely to be optically thick. A number of our sample are Type I (for instance NGC 2818) and are hence classified as optically thick. A further criterion (Pottasch, 1981) is that if Tz(HI) = Tz(HeII) then the PNe is probably optically thick. This applies to a number of our sample, for instance IC 2165.

An observational criterion for optical thickness has been advanced by Harman & Seaton (1966) who found that in their sample of PNe, those which showed HeII λ4686 A emission were optically thin, this being concluded from analysis of their central stars. The exceptions to this were those PNe which have later been classified as type I. These also show HeII λ4686 A emission but are generally considered to be optically thick, being in their final stage of evolution.

In the next section the distance each PN is discussed together with whether it is optically thick or not.

2.7.2 Distances to the P.Ne.

NGC 2346: The distance to this P.N. is rather well known as it is one of that small number of P.Ne. for which the method of spectroscopic parallax can be used. This method relies on the fact that the central star is in a binary system with a companion star having a 'normal' main sequence spectral type. In the case of NGC 2346 the companion has a spectral type of A2V (Mendez & Niemela, 1981). They gave a distance of d=0.7+/-0.1 kpc. This planetary has also been carefully studied by Gathier et al (1986) (hereafter GPP86) who determined a distance of d=1.06+/-0.34 kpc. using a reddening distance method. The distance that will be adopted in this work is that given by Gathier (1984) (hereafter G84) based on a number of distance determinations.

NGC 2438: Maciel and Pottasch (1980, herafter MP80) determined a distance for this P.N. using an improved method assuming an empirical relationship between nebula ionised mass and radius, of d=1.5 kpc. No absolute error is quoted although the authors indicate that the error should be no greater than 50%. Pottasch (1984, hereafter P84) has used a method based on a standard extinction-distance diagram near to the galactic plane. From the extinction of the P.N. he devrives a distance of d=2 kpc. Acker (1978, hereafter A78) gives this nebulae as being optically thin and assuming a uniform mass for the nebula derived a distance of d=0.90+/-0.04 kpc. Daub (1982, herafter D82) also gives this nebula as being optically thin and qoutes a distance of d=1.2 kpc. The value that will be used in this work will be then d=1.2+/-0.3 kpc.

This nebula has a high nebula mass ($\approx$ 0.8 $M_\odot$) and a low n_e ($\approx 10^2$ cm^{-3}) (Pottasch, 1984) and hence may be on the verge of being optically thin. However, the hydrogen and helium Zanstra temperatures agree well for the central star, and hence this PN is most likely to be optically thick.

<u>NGC 2440</u>: This fairly bright planetary has had its distance carefully examined by G84 who gave a distance of d=2.19+/-0.38 kpc. A78 states that this P.N. is optically thin. However in Chapter 5 of this work evidence is presented showing molecular hydrogen emission originating in a thin shell at the edge of the ionised HII region. This shell is at the transition region between the HII region and the unionised HI region. Hence this P.N. must be optically thick. Additionally this PN is a Type I PN (Peimbert & Torres-Peimbert, 1983) which is a further factor to support the view that the PN is optically thick.

<u>NGC 2452</u>: This P.N. has also been studied by G84 (see also GPP86) and his value of d=3.57+/-0.47 kpc. will be used here. Whether this P.N. is optically thin or not is in dispute. A78 lists it as being optically thin whilst P84 gives it as optically thick (see also Pottasch, 1981). NGC 2452 has been classified as a Type I PN (Peimbert & Torres-Peimbert, 1983) and is hence optically thick.

<u>NGC 2818</u>: This P.N. is one of a small number of P.N. that are thought to be associated with open clusters (NGC 2438 being another). Kohoutek et al (1986) in their recent paper give two distances for this nebula,

one based on a number of statistical determinations by various authors, d=2.1 kpc, and the second based on the distance of the open cluster (also NGC 2818). This has been determined by Dufour (1984) to be d=3.5 kpc. Following Kohoutek et al use will be made of both of these distances, although they tend to the conclusion that the statisical distance is rather low and that the distance to the cluster may be more appropriate. A78 lists this P.N. as being probably optically thin. Storey (1984) however has detected the S(1) line of molecular hydrogen in this nebula indicating that it is most likely to be optically thick. This PN is also of Type I (Peimbert & Torres-Peimbert) which adds additional weight to the argument that it is optically thick.

NGC 2867: Martin (1981) has investigated this P.N. and concluded that it is optically thick to the Lyman continuum. This is confirmed in that this work shows Tz(HI) = Tz(HeII). He adopts a distance of d=3.3 kpc from the literature. Daub (1982) reaches a similar conclusion but gives a distance of d=1.2 kpc. A78 and MP80 agree on a distance of d=1.6+/-0.2 kpc, this being the distance that will be adopted here.

NGC 3132: This P.N. is another case where the central star has a normal main sequence companion of spectral type AOV. A distance obtained by the method of spectroscopic parallax has been reported by Mendez (1978) as being d=0.6+/-0.1 kpc. A78 lists this P.N. as being optically thin. However Storey (1984) has mapped this nebula in the S(1) line of molecular hydrogen showing emission in the form of a shell just outside the ionised region. This would indicate then that this nebula is ionisation bounded and hence optically thick.

NGC 3211: Using the reddening -distance method GPP86 quote a distance of d=1.91+/-0.22 kpc. for this P.N. which P84 considers to be optically thick, although A78 lists this P.N. as being possibly optically thin!

NGC 3918: GPP86 give a distance of d=2.24+/-0.84 kpc. for this small, highly luminous (in Hβ), and dense nebula (n_e ≈ 5000 cm^{-3}; Pena &

Torres-Peimbert, 1985) which is consequently most likely to be optically thick.

NGC 5315: GPP86 give a distance of d=2.62+/-0.83 kpc. This WR P.N. is probably optically thick (P84), being of Type I (Peimbert & Torres Peimbert, 1983).

NGC 6302: This P.N. is one of a small number of P.Ne. that have had neutral hydrogen detected associated with them (Rodriguez et al 1985). This confirms that this nebula is optically thick to the lyman continuum. The distance to this P.N. has been given variously as d=0.65 kpc (A78) and d=0.41 kpc (MP80). In this work a value of d=0.53+/-0.12 kpc will be adopted. This is another Type I PN.

NGC 6309: The distance determined by MP80 for this P.N. is d=2.1 kpc although following the discussion of G84 this value may be an overestimate. However A78 gives the higher value of d=2.6 kpc and lists it as being optically thin, in accordance with its rather low luminosity. However P84 gives it as being optically thick. In this work the value of d=2.3+/- 0.3 kpc will be adopted.

NGC 6153: A78 lists this P.N. as probably being optically thin and gives a distance of d=1.5+/-0.2 kpc. MP80 on the other hand determine a distance of 1.0 kpc whilst P84 gives a distance of 1.8 kpc. In this work an average distance of d=1.4+/-0.4 kpc will be used. This PN is most likely to be optically thick as Tz(HI) w Tz(HeII) as derived in this work.

NGC 6439: Values for the distance to this P.N. determined by different authors vary greatly. A78 lists this nebula as being optically thin and gives a distance of d=5.0+/-0.3 kpc. MP80 give d=3.8 kpc. whilst Pottasch (1981) gives a distance of d=1.5 kpc. and states that the nebula is optically thick, using similar data to that used by A78. Cahn (1976) and Milne & Aller (1975) give similar values of the distance at d=6.2 kpc. In this work a value of d=5 +/- 1 kpc will be used.

IC 2165: The distance to this nebula has been given by Torres-Peimbert and Peimbert (1977) to be d=2.82 kpc. This nebula is probably optically thick as this work gives Tz(HI) ≈ Tz(HeII).

IC 2448: For this nebula which A78 gives as being probably optically thin, A78 and MP80 give distances that are similar at d=2.8+/-0.2 kpc.

IC 4776: Here again A78 and MP80 are in good agreement giving the distance as d=3.4+/-0.2 kpc. Whether this P.N. is optically thick or not is not well known although its small size and relatively high electron density (n_e ≈ 8000 cm^{-3}, Pottasch, 1984) might indicate that it is optically thick.

J 900: Several authors give the distance to this small, dense, probably optically thick nebula at about 2kpc. (ie A78, d=2.25 Kpc.; MP80, d=2.0 kpc.; Pottasch (1981), d=2.1 kpc.) and hence a value of d=2.1+/-0.2 kpc will be adopted here. It being optically thick is supported as Tz(HI) ≈ Tz(HeII) which in turn agree well with its temperature as determined by the 'Stoy Method' (Preite-Martinez & Pottasch, 1983).

A 40: Daub (1982) has given the distance to this nebula (which is probably optically thin being an old evolved object; Abell, 1966) as d=3.1 kpc. whilst Maciel (1981) gives d=4.7 kpc. An average of these gives d=3.9+/-0.8 kpc.

He2-120: This rather poorly studied southern P.N. has had rather poor distance determinations. Webster (1969) gave d=3.9 kpc. whilst Daub (1982) has given d=2.5 kpc. Maciel (1981) gives d=3.2 kpc. Information as to the optical thickness of the PN is not available.

He2-117: This P.N. has had its distance measured by Maciel (1981) as d=1.7 kpc, Acker (1978) gives it as 2.5 kpc whilst Webster (1969) gives 3.24. Milne (1979) list its distance as 4.6 kpc. In this work an average distance of d=3.0 +/ 1.5 kpc will be used.

2.7.3 Theoretical Derivation of the Luminosity and Radii of the Nuclei of P.Ne. (NPN).

The luminosity of the central stars can be obtained from their m_V and T_{eff} measurements. If the spectrum of the central star is given by a blackbody function, as has been assumed in the derivation of the Zanstra temperatures, then the stellar radius can be written as:

$$R_*^2/d^2 = 1.349\times10^{-9}\ F_V\ (e^{2.616\times10^4/T} - 1) \qquad (2.7.1)$$

Here the distance, d, is in cm, whilst the visual continuum flux, F_V, is taken at λ =5500Å, as previously. This is corrected for any interstellar extinction and is obtained from the visual magnitude, m_V, using the calibration of Wamsteker (1981):

$$F_{\lambda(vis)} = 3.68\times10^{-9} \times 10^{-mv/2.5} \quad \text{ergs s}^{-1}\text{ cm}^{-2}\text{ Å}^{-1} \qquad (2.7.2)$$

The luminosity can be expressed in terms of the solar luminosity:

$$\frac{L}{L_\odot} = \frac{R_*^2\ T^4}{R_\odot^2\ T_\odot^4}$$

Hence one obtains:

$$L/L_\odot = 9.76\times10^3\ d^2\ (e^{2.616\times10^4/T} - 1)\ 10^{-mv/2.5}\ (T/5770)^4 \qquad (2.7.3)$$

which gives L in terms of the solar luminosity if m_V and the effective temperature of the central star are known. The distance hereis in kpc. The values of the stellar radius and luminosities as determined from Tz(H) are given in columns 6 & 7 respectively of Table 2.7 whilst those determined from Tz(HeII) (or for those nebula having no HeII λ4686Å

Table 2.7 Derived Zanstra Temperatures.

Name of P.N.		Tz(HI) (K) × 10^{-3}	Tz(HeII) (K) × 10^{-3}	T(EB) (K) × 10^{-3}	Ref	Radius ($R_{\odot}$) × 10^{2}	Luminosity ($L_{\odot}$)
NGC 2438		169	156			1.8	250
NGC 2440		392	280	270	1,2	1.4/1.7	4480 / 1650
NGC 2452		94.0	126	97	2	9.7/8.2	676 / 1570
NGC 2818	(a)	185	188			1.4	210
	(b)					2.3	580
NGC 2867		126	126			5.5	692
NGC 3211		132	155	129	1,2	3.2/2.9	288 / 462
NGC 3918		247	184	108	1,2	4.5/5.3	7080 / 3000
NGC 5315		49.9	75.0	47	2	76 / 59	3260 /10100
NGC 6153		92.9	109			12 / 11	994 / 1580
NGC 6309		70.6	114			7.9/6.0	143 / 564
IC 2165		162	164	101	2	6.1	2400
IC 2448		49.5	84.4	68	2	31 / 21	529 / 2330
IC 4776		45.0	-			73	2030
J 900		112	134	129	2	5.3/4.8	408 / 679
A 40		52.7	-			17	212
HE2-120		96.0	-			6.0	280
HE2-117		79.6	-			43	6830

References to Table 2.7

1 : Pottasch, 1984

2 : Preite-Martinez and Pottasch, 1983

Notes to Table 2.7

Table 2.7 gives the Tz(HI) and Tz(HeII) temperatures for the PNe listed. For comparison temperatures obtained using the "Energy Balance" method, T(EB), are listed in column 4, with references in column 5. The stellar radius of the central stars are given in column 6. Column 7 gives the Luminosity of the central stars, in units of solar luminosity, where two values are given, the first is that assuming T_{eff} = Tz(HI), whilst the second assumes T_{eff} = Tz(HeII)

(a) and (b) refer to the two distances used for NGC 2818 (see Tab 2.5) emission, their Tz(HeI)) are given in on the right hand side of the slash in columns 6 & 7 of Table 2.7.

2.7.4 Analysis of the Errors in Tz.

The errors involved in the measurements of the visual magnitudes for these. PNe have been discussed in section 2.5. This error is generally the largest error involved in determining the Zanstra temperatures for each individual PN. Other sources of error occur in a number of assumptions that have been made in the calculation of the temperatures.

The central stars have been assumed to radiate as blackbodies. It is quite possible that this is a poor assumption to make and that a model atmosphere should be used to describe the central star. It is often found in detailed photoionisation models of PNe that a model atmosphere is needed for the central star if the observed nebula abundances are to be satisfactorily modelled to compare with observational values. For example, the model atmosphere used to descibe the central star of NGC 7662 by Harrington et al (1982).

Pottasch (1984) has investigated the differences between blackbodies and a number of model atmospheres (Hummer & Mihalas, 1970; Wesemael et al, 1980; and Kudritzki et al, 1981). He concludes that in the case of Tz(HI), the values obtained using model atmospheres agree well with those from the blackbody assumption (except for low temperatures with T < 3000 K). However model atmospheres appear to differ greatly from the blackbody when Tz(HeII) is calculated, with some models giving higher temperatures than the blackbody, and others lower.

At present it is hard to say with certainty which model atmosphere should be used for any particular PN. Henry & Shipman (1986) have shown that the central stars helium abundance plays an important role in the determination of the temperature. However the composition of the central star atmospheres are difficult to determine, especially for the central stars of this sample which are intrinsically faint. The central stars can have abundances ranging from pure helium, for instance A30 and A78 (Hazard et al, 1980 and Jacoby & Ford, 1983) to more nearly solar. Clearly then the choice of model is difficult.

It is not certain that the stars radiate as blackbodies, but the error in using a blackbody is probably no greater than that in using the 'wrong' model atmosphere. Additionally Pottasch (1981) has pointed out that for high temperature stars (which is the case for the majority of the stars studied in this sample), a blackbody assumption is reasonable as electron scattering will dominate. The assumption is therefore made that the central stars radiate as blackbodies.

The flux ratios F(Hβ)/F(vis) and F(4686)/F(vis) were calculated using recombination coefficients for a PNe of $n_e=10^4$ and $T_e=10^4$. As has been shown previously in section 2.2.5 these coefficients are almost independent of n_e and only a slowly varying function of T_e. (see Table 2.1). Hence the values used here introduce a negligible error into the result.

The final possible source of error is the assumption that the nebulae are optically thick to the Lyman hydrogen ionising continuum. This has been discussed in section 2.7.1 where the conclusion was reached that most of the PNe in this sample are optically thick.

2.7.5 Analysis of the Errors in L and R.

The typical errors in the measurement of L and R have been computed using the method of error analysis outlined in Bevington (1969). the specific formulae used were as follows:

$$\frac{\delta R}{R} = \sqrt{\left[\left(\frac{\delta(d)}{d}\right)^2 + \left(\frac{\delta(F(vis))}{F(vis)}\right)^2 + \left(\frac{e^{2.665\times10^4/T}}{2(e^{2.665\times10^4/T}-1)} \cdot \frac{2.665\times10^4}{T^2} \cdot \delta T\right)^2\right]}$$

and

$$\frac{\delta L}{L} = \sqrt{\left[\left(\frac{2\delta(d)}{d}\right)^2 + \left(\frac{\ln 10\ \delta mv}{2.5}\right)^2 + \left(\frac{4\delta T}{T}\right)^2 + \left(\frac{2.665\times10^4\ e^{2.665\times10^4/T}\ \delta T}{T^2\ \left(e^{2.665\times10^4/T} - 1\right)}\right)^2\right]}$$

As can be seen, large errors occur in both L and R due to errors in the distance to the PNe. The problem of distance determination has been addressed by Gathier et al (1986) and Gathier (1984) who point out that few galactic PNe have distances measured with uncertainties < 40%. However they have considerably enlargened the sample of PNe with accurately determined distances and these distances have been used where possible.

In some cases the errors in both mv and distance are rather large, which lead to large errors in L and R. In these cases the errors shown in Chapter 6 Figure 6.1 should be taken as an indication of the size of the error and not the absolute error.

Assumptions made about the PNe and their central stars have not been included in the above estimates because of the fundamental difficulties involved in for instance, knowing whether the central star deviates substantially from a blackbody.

2.8 Discussion of the Derived Magnitudes.

It is of interest to compare the magnitudes of those central stars in this sample which have previously had their magnitudes measured by other workers.

In Figure 2.8 the magnitudes of the central stars from this work are plotted against those values as deduced by other workers. For reference the line of equivalence between the two sets of data is marked.

The measurements shown all use the method of aperture photometry except for the measurement of NGC 6153 (Reay et al, 1984b) which uses an electronographic imaging technique. The value for A40 by Abell (1966) is a photographic visual magnitude. As can be seen the values of m_V from this work are generally 1-2 magnitudes fainter than those that have been previously measured.

Recently Shaw and Kaler (1985) have presented new B and V magnitudes for 51 nuclei of planetary nebulae. They used the method of large aperture absolute photometry together with an improved method of extracting the stellar continuum fluxes from the nebula background. A number of the P.Ne. which they have measured are included in our sample. In their work they noted that most of their lower limits appeared in the neighbourhood of $m_V \approx 15$. This work would tend to confirm the fact that for central stars which they have measured at about this limit may in fact be considerably fainter. For instance in the case of NGC 2440 their appears to be a discrepancy of some 5 magnitudes between the result presented here and that which they found.

NGC 3132 is not shown in Figure 2.8. This P.N. has a star at its centre of spectral type A2 V (Mendez, 1978). This star is not hot enough to excite the nebula and hence it is thought that the exciting star for NGC 3132 must be a hot binary companion of this star (Mendez et al 1978). Kohoutek & Lausten (1977) have reported the detection of this companion

Figure 2.8 Graph comparing the visual magnitudes for the central stars measured in this work with those determined by other workers. The line shows the 1:1 correspondance.

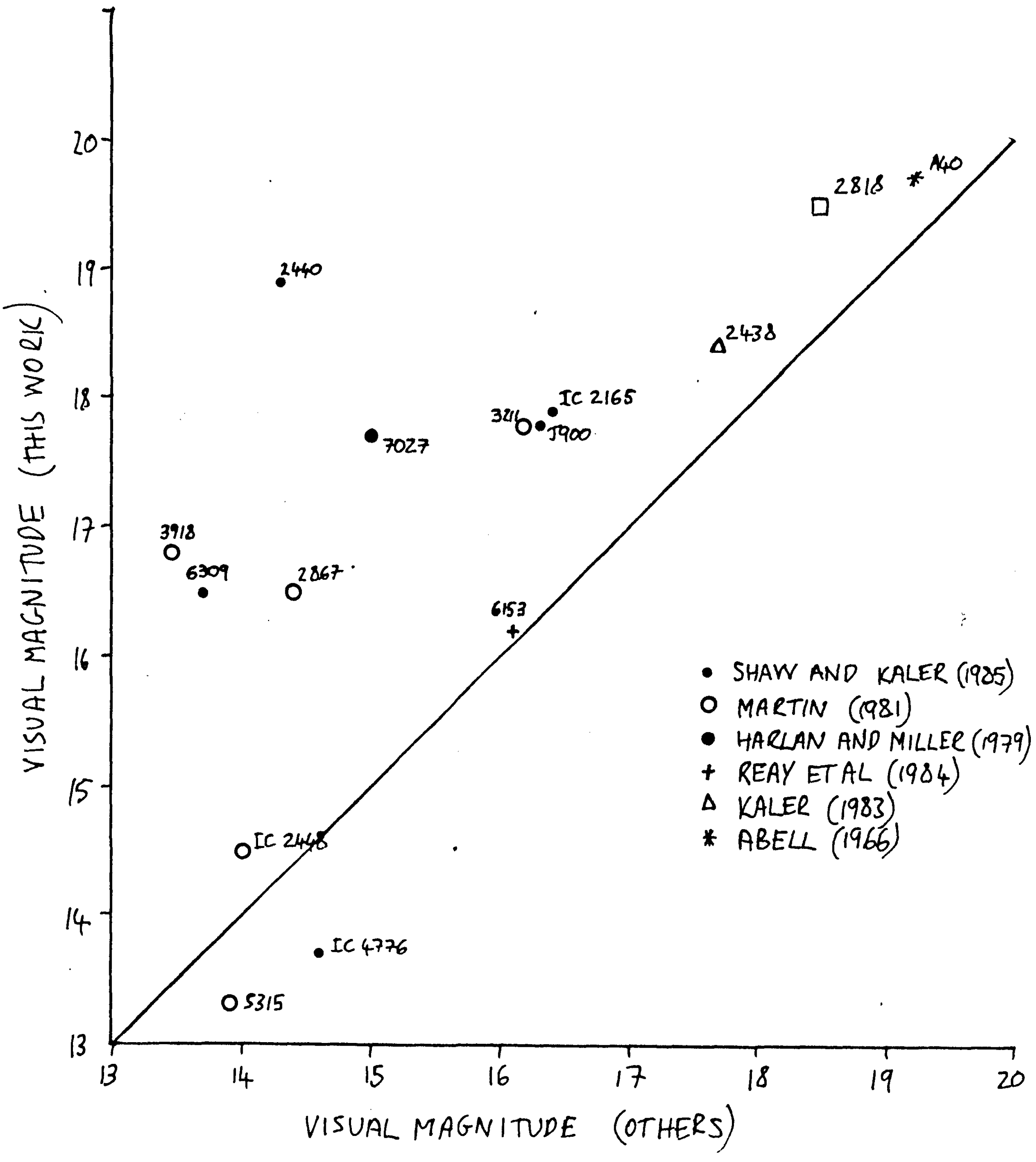

at a magnitude of ≈ m_V=14.5. In our images no detection has been made of this faint companion after extensive investigation of the various CCD images. The magnitude that is quoted for the central star of NGC 3132, then, refers to that of the A2 V star. This agrees well with previous measurements (eg Pottasch, 1984 gives m_V =10.02)

NGC 2346 is another case of a P.N. having a central star with too late a spectral type to excite the nebula. The central type for this star is A5 V (Mendez, 1978). This star is unusual in that its magnitude has been observed to vary by 2 magnitudes or more in a period of two days (Kohoutek, 1982). Two measurements of its magnitude are given in Table 2.5, these being obtained on consecutive nights. The change in magnitude of ≈ 1 mag is consistent with previous measurements.

For a limited number of the P.Ne. studied it was possible to obtain a visual magnitude directly from the V Band CCD image. This was the case for NGC 2438. Directly from the V band image m_V was determined as mv=18.3. This value is in excellent agreement with that obtained from the narrow band continuum image. This acted as a check on the method used to determine the magnitudes and indicates that the assumptions made in section 2.4 are valid.

CHAPTER 3

Chapter 3

3. Detailed Investigation of NGC 7027.

3.1 Introduction

In this Chapter I discuss in detail the planetary nebula NGC 7027. I will present new observational data which shows the unambiguous detection of the central star. I will also present velocity field maps in several lines indicating an extended faint outer halo. These data will be compared with theoretical models to give an estimate of the central star mass. The central star will be positioned in the H-R diagram and its evolution will be considered.

NGC 7027 (PK 84 -3°1) is one of the most widely studied of all P.Ne. Due to its rather amorphous appearence Perek & Kohoutek, 1967, have classified it as an irregular P.N. At radio frequencies it is in fact the brighest P.N. known even though it is of relatively small size. It is also the most luminous P.N. known in our galaxy. However, in the optical it suffers from high extinction in its direction and is hence less bright. NGC 7027 is however a rather unusual P.N. having an extremely high excitation class with as yet no positively detected central star. It has however become a standard object and has a rather well measured spectrum. Many ionic species have been found in its spectrum and more recently a number of molecules have been discovered associated with it, for instance the first detection of molecular hydrogen was detected in it by Treffers et al. (1976). In fact the first detection of any molecule in a P.N. was found in NGC 7027 when Mufson et al. (1975) found carbon monoxide emission associated with it.

Being well studied several of the input parameters needed in carrying out a determination of the central star's Zanstra temperature are rather well known, these will be discussed in a following section. However the great problem is that the central star has never been unambiguously detected, estimates of the magnitude of the central star differing widely from author to author. An early estimate was made by Berman (1937) who gave m_{pv}=11.3. Later Liller (1955) gave m_v=11.3 as a lower limit. In the same paper Liller also reported that Baade set 18 as the lower limit of the magnitude of the central star, although no observational details were reported. More recently Harlan and Miller (1979) determined m_v=15+/-1. Using a photoelectric technique Atherton et al. (1979) have given an approximate visual magnitude for the central star as mv=19.4+/-1.0. In view of this uncertainty the photoelectric imaging technique has been employed to obtain the magnitude of the central star of NGC 7027.

3.2 Observations

The observations reported here were carried out during parts of 4 nights in August 1986 at the 2.5m Isaac Newton Telescope on the island of La Palma. Kinematic observations of NGC 7027 were made with the TAURUS wide field imaging Fabry-Perot interferometer (Atherton et al. 1982) using the IPCS detector (Boksenberg, 1972) at the f/15 Cassegrain focus of the INT. An etalon of 250 μm spacing was chosen to give a velocity resolution of 3.6 kms^{-1} at 6563Å. Three narrow passband filters, having a nominal FWHM of 15Å, were used to isolate the Hα 6563Å, [OIII] 5007Å and [OI] 6300Å emission lines in the nebula. Approximately 95 frames, each of 200 pixels square, were recorded for each data cube. The observational details are listed in Table 3.1.

Each kinematic data cube was reduced following the general technique as outlined in Atherton et al. (1982). On reduction phase corrected data cubes in the light of Hα, [OIII] and [OI]of 200×200 pixels in approximately 95 frames, were produced.

Direct images were obtained with the etalon removed. In this format the TAURUS system acted as a focal reducer, with the IPCS being used in full 2 dimensional mode. Images of the nebula of 200 square pixel were taken through narrow passband filters centred on the Hβ emisiion line at 4861Å and, as descibed in section 2, the stellar continuum at 4788Å. The purpose of this filter was to record a monochromatic image of the P.N. at a wavelength clear of any nebula known nebula emission lines and hence leave just the nebula continuum to mask the central star. The Hβ image was taken to enable the nebula con estimated and to show the position of nebula features that could be confused with the central star.

For both sets of data photometric standard stars from the lists of Landolt (1983 and references therein) were observed at regular intervals throughout each night. Data from these stars enabled airmass corrections to be made although no observations were made with airmasses of greater than 1.5.

3.3 Reduction Procedures

The data were reduced using the GIPSY image processing system, with supplementary work being carried out on the STARLINK system. Contour plots of NGC 7027 taken through these two filters are shown in Fig. 3.2 a & b whilst a colour photograph of a false colour representation of a 4788Å continuum image is shown in Fig. 3.1. In this image the central star is especially obvious. It might be noted that this position corresponds well with the tentative detection of the central star reported by Atherton et al (1979) who gave a position of the central star at a point some 2 arcsecs east of the bright feature of NGC 7027.

Four images were obtained of NGC 7027 through the 4788Å continuum filter. As an initial procedure the flux contained within the central star was calculated by taking profiles through the images, estimating the continuum by eye, and taking the summation of data points to give a value of the flux. This was repeated for all frames. This value was then compared with the flux contained within the image of the standard star and this enabled a value of the magnitude of the central star of NGC

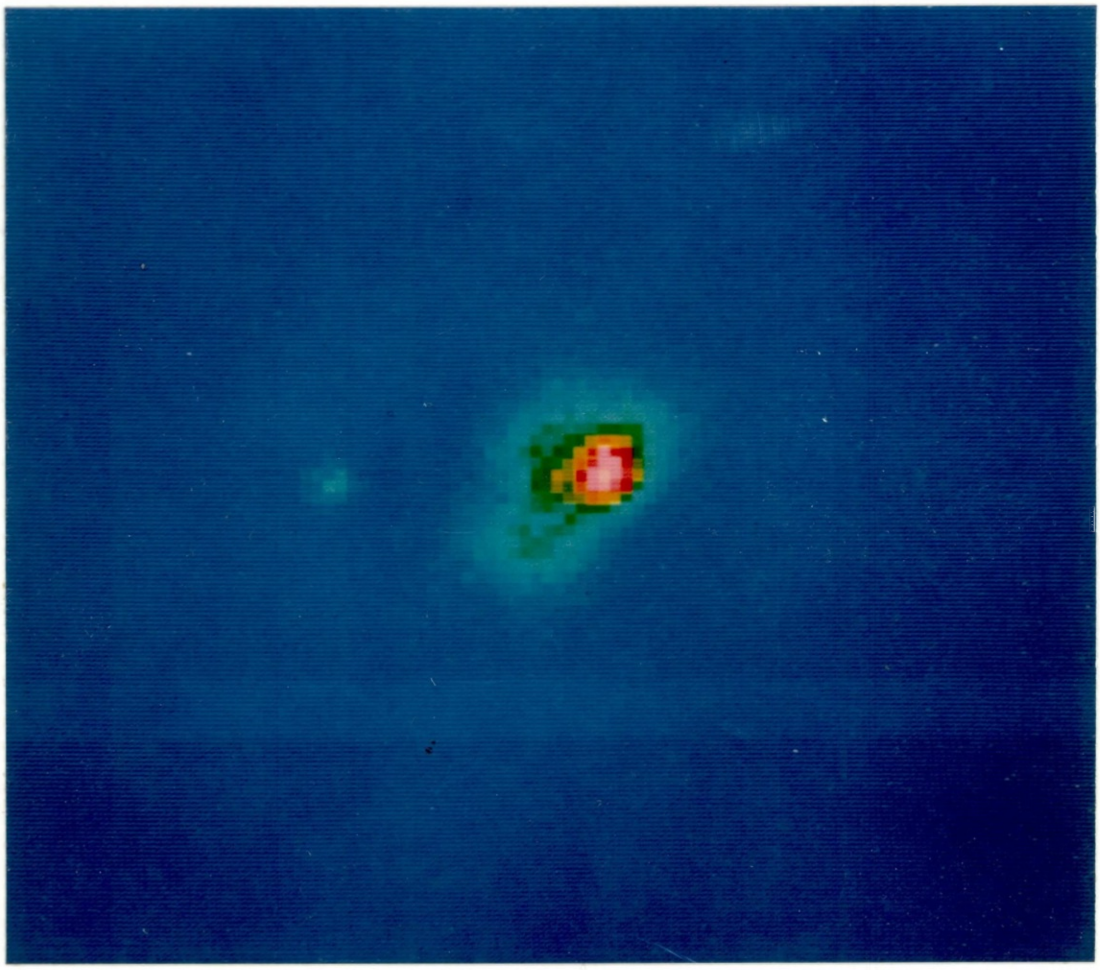

Figure 3.1

This plate shows the P.Ne. NGC 7027 as seen through the 4788 Å narrow band continuum filter. North is to the top, whilst East is to the left. One pixel is ≈ 0.5 arcsecs. The central star is clearly seen at a postion ≈ 2 arsecs to the east of the bright feature in NGC 7027.

Fig 3.2a 4788A image of NGC 7027. In this and the following plots the contours are equally spaced between the maximum and minimum values.

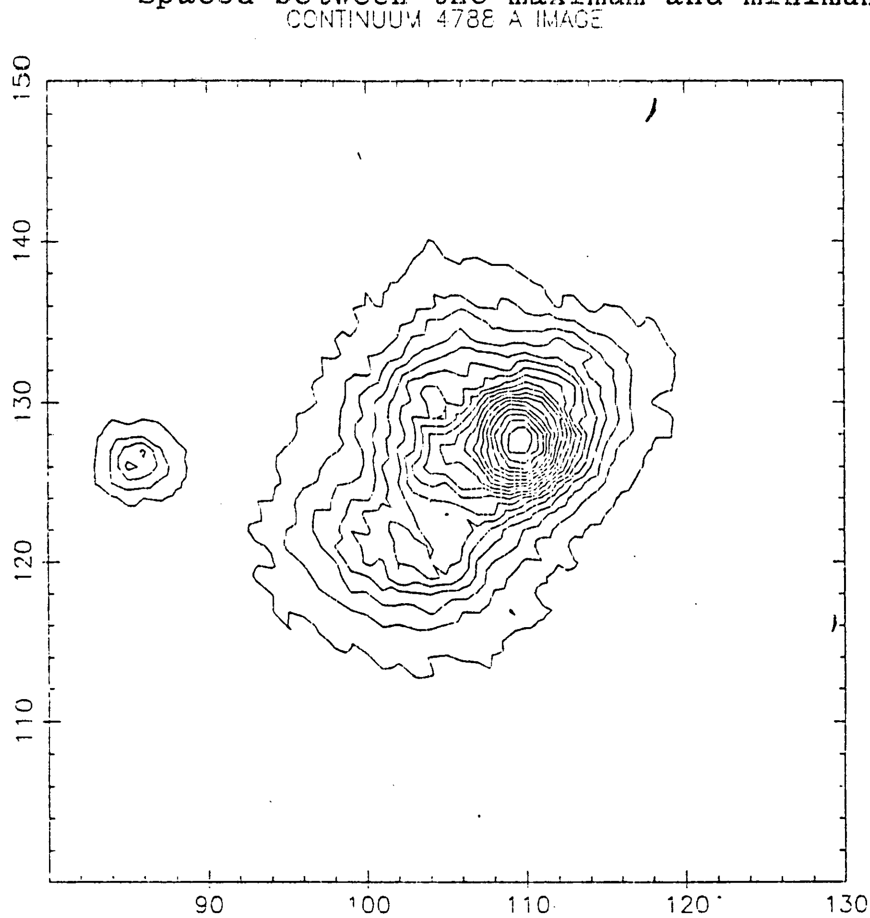

Fig 3.2b

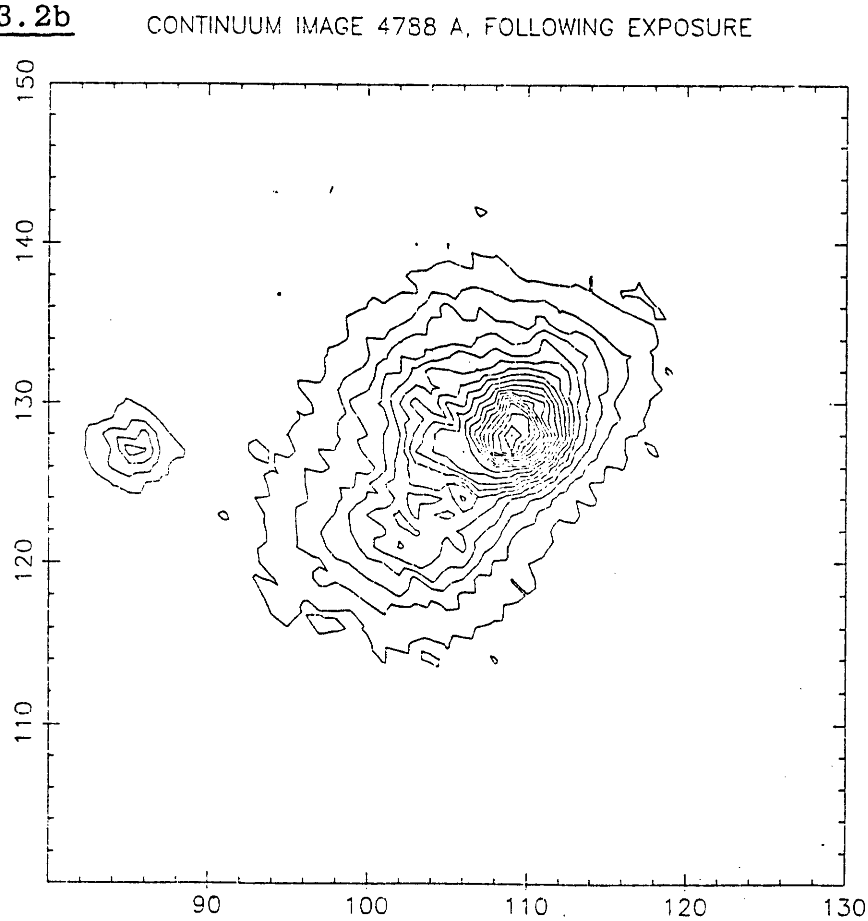

Fig 3.3a Slice through position of central star residual resulting from the subtraction of the Hb image from the 4788A image of NGC 7027

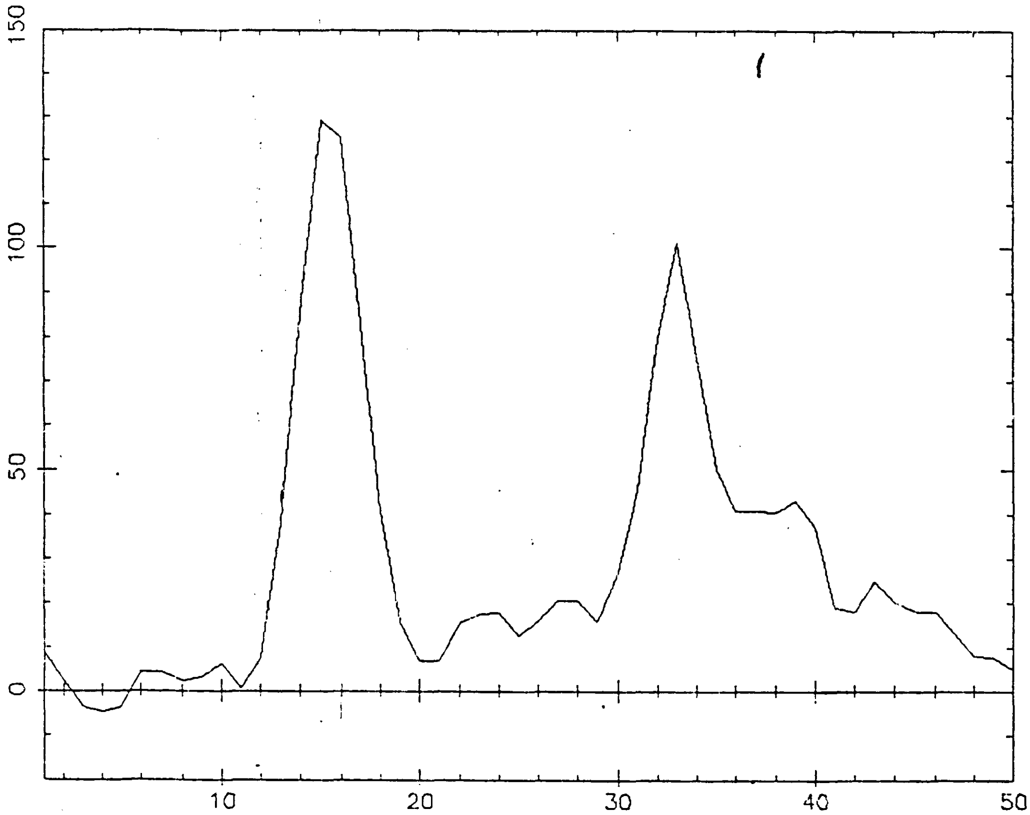

Fig 3.3b

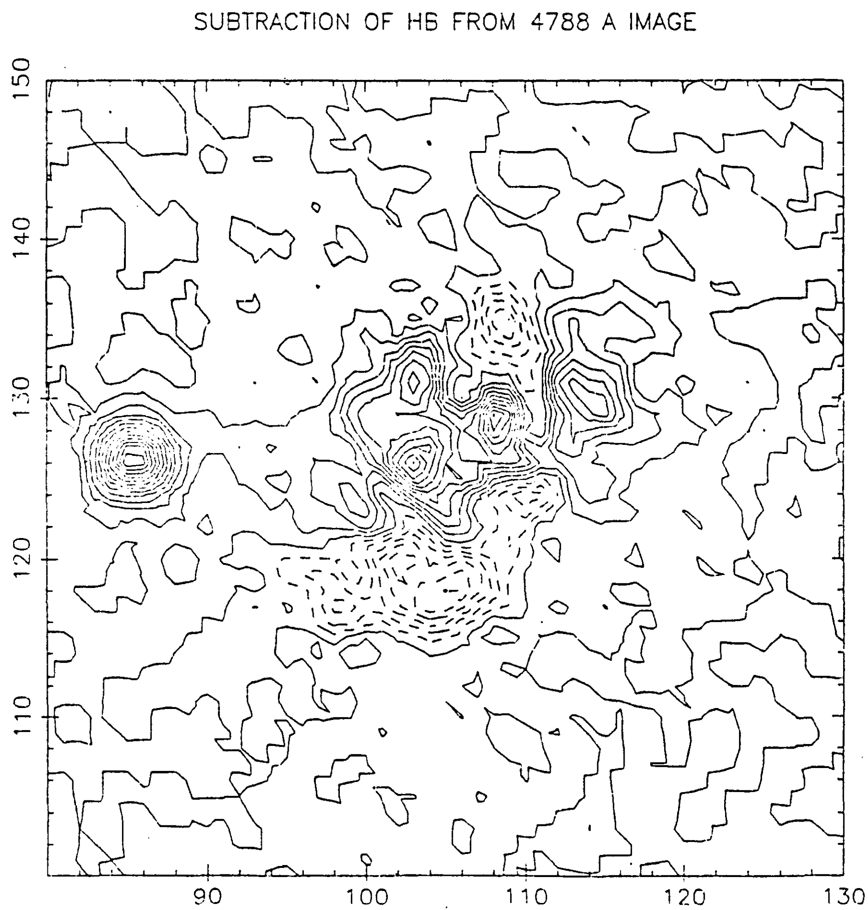

Fig 3.4b Hb image of NGC 7027

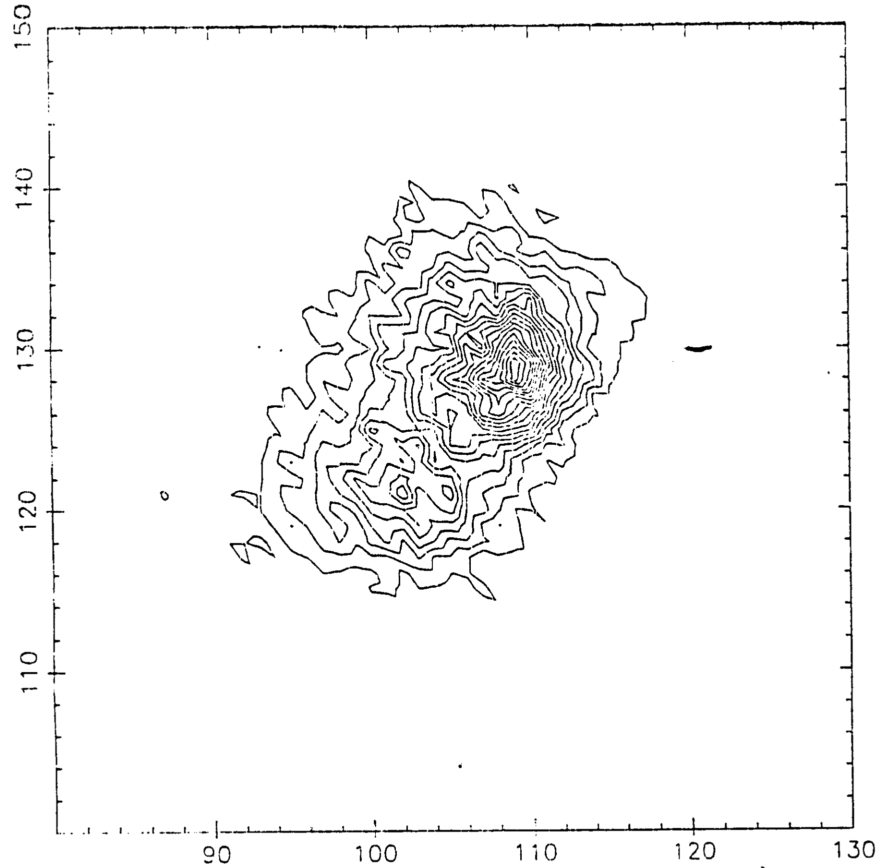

Fig 3.4b SUBTRACTION OF HB FROM DISPLACED 4788 A IMAGE

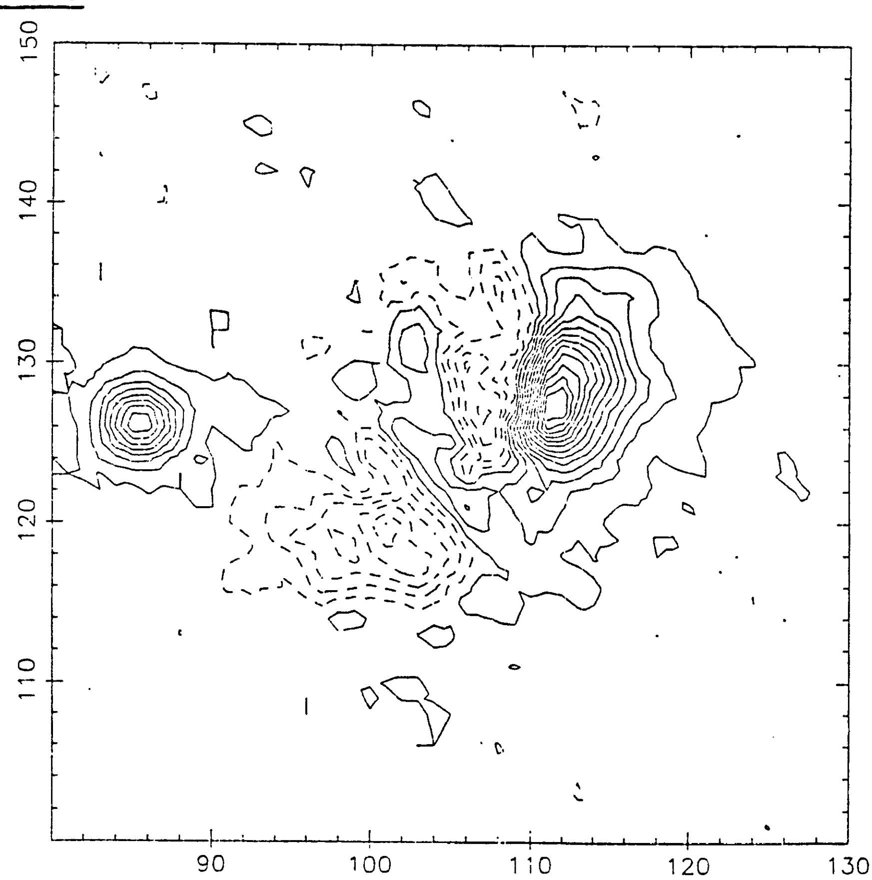

7027 at λ=4788Å to be made. Following the procedure outlined in Chapter 2, section 5, this magnitude was converted to the visual magnitude, m_v, at λ=5500Å by making the assumption that both the standard star and central star fluxes could be represented by blackbody functions.

Additionally a further technique was employed making use of the Hβ image. This image 'maps' the nebula in the Hβ emission line, this being a measure of the Balmer continuum. The 4788Å image however maps both star and nebula, this includes the sum of the continuum made up of the Hydrogen continuum, the Helium continuum and the Hydrogen two-quantum emission. At the position of the bright feature in NGC 7027, however, the emission is due just to the nebula emission. For each of the 4788Å frames the Hβ image was scaled to those frames at this point. The Hβ image was aligned with the 4788Å images using the centre of this feature and a field star (which was evident in all frames) some 40 arcsecs to the west of NGC 7027. Each appropriately scaled Hβ image was subtracted from the relevant 4788Å image.

At the expected position of the central star a residual having a gaussian like appearence with an approximate FWHM 'seeing' equivalent to that as measured from the field stars, was obtained. This was interpreted as being the central star and the volume was obtained under the gaussian. This was compared with the standard star images, as above, to derive a magnitude for the central star. Fig. 3.3b shows the the result of the subtraction of the appropriately scaled and positioned Hβ image from the continuum image. The field star is clearly seen and the central star residual is that residual located at the position of the probable central star in the continuum image (Fig. 3.2). An E-W slice through this image is shown in Fig. 3.3a, the residual due to the central star clearly having a similar FWHM as that of the field star. This lends further support to the view that this residual does represent the central star.

The validity of this technique was carefully investigated. It was found that the residuals after the subtraction process seemed to depend quite critically on the accuracy to which the Hβ and 4788Å images were overlayed. If the alignment was incorrect artificial residuals were created. An example of this is shown in Fig. 3.4b which shows a subtraction of the scaled Hβ image from the continuum image with the displacement of one image with respect to the other being different to that shown in Fig 3.3b. It was important therefore to be able to distinguish these from the central star residual and to be able to account for chance artifacts created at the position at which the central star might have been expected to have been located.

The subtractions were made for a range of possible positions of each pair of images with respect to each other. Those residuals at the expected position of the central star (Harlan & Miller, 1979; Atherton et al, 1979; and this work) in the subtractions were judged to be real. One feature was apparent in all subtractions, namely a residual at the position of the bright 'spot' of NGC 7027. Why there should be a residual at the position of the bright spot is unclear. The shape of this bright spot should be the same seen through both filters, as to why it is not may give some information as to the nature of this bright spot.

The shape of NGC 7027 in the optical has been the cause of some discussion, and in particular whether of not the bright spot is a real feature or just a region of reduced external extinction is unclear. Radio observations, eg the 5 GHz map obtained by Scott (1973), show the intrinsic shape of the nebula, as at these wavelengths the effects of interstellar extinction are much reduced. NGC 7027 is apparently a quite uniform and symetric nebula. Bentley (1982) has mapped NGC 7027 in 5 spectral bands between 8.7 and 23 μm. These maps show a remarkable similarity to the radio maps of Scott, indeed the emission from this nebula in the radio and the IR has been explained by modelling it as a simple hollow cylinder viewed at an angle from the earth.

These observations would tend to support the view that the bright feature seen in the optical is due only as an effect of external extinction. However, one possible explanation for the residual that is found in the subtraction of the scaled Hβ image from the 4788Å image could be due to this feature actually representing a density enhancement in the nebula gas. If this were so then the hydogen two-quantum emssion would be suppressed and the relative amount of continuum in the 4788Å image at the bright spot would hence be reduced. This would then lead to the residual seen as the other components of the continuum remain in the same relative proportion to each other in the two images. However the validity of this suggestion is rather uncertain. Atherton et al (1979) measured the spatial distribution of the electron density across the nebula using the ratio of the density sensitive [SII] lines at λ6717Å and λ6731Å. They found little evidence of a density gradient across the nebula although they could not rule out small size structure on scales less than 1 arcsec.

3.4 Results

Analysis of the continuum images as described in the previous section and comparison with a UBV standard star (115-273; Landolt, 1973) enabled the magnitude to be determined as m_V=17.7+/-0.5. In making this determination it has been assumed that both the central and standard stars radiate as blackbodies. This assumption is needed for the standard star when converting its flux as measured through the 4788 Å filter to that which would be expected at 5500 Å, the visual wavelength. This has been discussed in section 2.5.

The hydrogen Zanstra temperature, Tz(H), for NGC 7027 is determined using the procedure outlined in section 2.6. The calibration of Wamsteker (1981) that 0 magnitude in the visual corresponds to 3.64×10^{-9} ergs cm^{-2} s^{-1} $Å^{-1}$ means that a magnitude of m_V=17.7 corresponds to a flux in the visual, corrected for interstellar extinction using the value of E(B-V)=0.94 (Gathier, 1984), of 4.43×10^{-15} ergs cm^{-2} s^{-1} $Å^{-1}$.

The Hβ flux has been measured by several authors (Miller & Mathews, 1972; Capriotti & Daub, 1960) and most recently by Shaw & Kaler (1982) whose value of Log F(Hβ) = -10.12+/-0.01. Correction for interstellar reddening then leads to F(Hβ) = 1.08×10^{-9} ergs cm^{-2} s^{-1} A^{-1}. These values lead to a flux ratio, F(Hβ)/F(vis) = 2.436×10^{5} Å, which corresponds to a temperature, Tz(H) = 3.07×10^{5} K.

NGC 7027 has a HeII λ4686 Å flux of 42 as expressed on the usual scale where I(Hβ)=100 (Kaler, 1976b). After correcting for reddening this correponds to a flux of 4.536×10^{-10} ergs cm^{-2} s^{-1} $Å^{-1}$. Comparing with the Hβ flux gives a value, F(4686)/F(vis) = 1.024×10^{5} Å, this corresponding to a temperature of Tz(HeII) = 2.18×10^{5} K.

These temperatures are determined using the procedure of section 2.6. The errors in these measurements are due mainly to the error in the magnitude and correspond to approximately +/-20,000 K. Again the assumptions are made that central star of NGC 7027 radiates as a blackbody, that the nebula is optically thick to the Lyman hydogen ionising continuum and that it has a filling factor, ξ=1. The basic parameters descibing NGC 7027 and those parameters that have been derived are listed in Table 3.2.

3.4.1 The Central Star Temperature of NGC 7027.

The above determinations give a discrepancy between Tz(H) and Tz(HeII) with Tz(H) > Tz(HeII). Tylenda (1984) discusses the case of NGC 7027 and concludes that this PN is a candidate for a PN with a massive nucleus. Tylenda (1983) has modelled the variation of temperature with time for a 1.2 $M_\odot$ nucleus. His model A, assumes a PN with physical parameters similar to those found in NGC 7027 and predicts Tz(H) = 5.9×10^{5} and Tz(HeII) = 3.5×10^{5}. at a time of t=100 years. Tylenda (1983) indicates that Tz(HeII) gives the best estimate of the central star temperature.

Table 3.1 Observational Parameters.

Line	Filter Å	Resolution km s^{-1}	Data Cube Size
Hα	6563	4.7	200,200,93
[OI]	6300	4.7	200,200,93
[OIII]	5007	3.6	200,200,94

Table 3.2

Input and Derived Physical Parameters for NGC 7027.

Property	Value	Reference(s)
Distance......	1.2 +/- 0.4 kpc.	Pottasch et al. (1982)
E(B-V)........	0.93 mag.	Gathier (1984)
Log F(Hβ).....	-10.12 +/- 0.01 ergs cm^{-2} s^{-1}	Shaw and Kaler (1982)
F(4686)/F(Hβ).	0.42	Kaler et al. (1976b)
T_e............	15,000 +/- 2500 K	ibid
ξ (fill fac)..	1	
n(He)/n(H)....	0.116	Pottasch (1984)
n(N)/n(O).....	0.786	ibid
m_v............	17.7 +/- 0.5	
M_v............	4.42	
Tz(HI)........	307,000 K	
Tz(HeII)......	218,000 K	
T(EB).........	300,000 K	Preite-Martinez & Pottasch (1984)
Luminosity....	6470 $L_\odot$	
Radius........	0.0425 $R_\odot$	

Stasinska & Tylenda (1986) have addressed the question of whether it is possible to measure the temperatures of intermediate mass stars going through a very hot mass phase. They have investigated the Zanstra technique, concluding that at temperatures above $T=2\times10^5$ K, Tz(H) tends to give an overestimate of the true temperature, whilst Tz(HeII) gives an underestimate. Tz(H) tends to give an overestimate because recombinations resulting from He^{++} lead to more than one photon which is capable of ionising hydrogen. Tz(HeII) on the other hand gives an under estimate of the temperature because hydrogen is ionised by photons which should ionise He^+. These effects become progressively more pronounced at higher temperatures.

A further problem is that the effects of dust in the PNe may be important. In this work dust within the PN has been ignored. Helfer et al (1981) have demonstrated how the relatively small dust to gas ratio of 10^{-2} can substantially lower effective temperatures of central stars determined by the Zanstra method. This is because some Lyman continuum photons are directly absorbed by the dust and hence are not 'counted' in the Zanstra method. Their results show that the temperatures given using the Hβ flux are more prone to error than those found from the HeII λ4686 flux in that Tz(H) gives the lower (wrong) value of T_{eff}. They use Koppen's (1977) internal dust optical depths to speculate that NGC 7027 (along with NGC 6720) should show a severe discrepancy between the different Zanstra temperatures.

Support for the presence of dust in NGC 7027 is provided by Moseley (1981) who detected emission in 4 far infra-red passbands. On making certain assumptions about the grain size, density, and absorption efficiency, Moseley estimates the dust to gas ratio to be of the order of 5×10^{-3}. This may be a low limit as he assumes the mass of the nebula to be the statistical average as given by Cudworth (1974) of 0.5 $M_{\odot}$, whereas Pottasch (1984) gives the mass of the nebula to be 0.02 $M_{\odot}$. Also a distance of 0.5 kpc is used, this being considerably less than the distance found by Pottasch et al (1982). Changing these parameters would tend to increase the dust to gas ratio, although as Moseley states the value he determines is highly uncertain.

Because Tz(H) > Tz(HeII) it may be that the discrepancy between Tz(H) and Tz(HeII) is not largely due to the effects of dust although the possibility can not be ruled out. In conclusion the temperature for NGC 7027 will be estimated as 250,000+/-25,000 K.

3.4.2 L and R for NGC 7027.

With the value of T_{eff}=250,000 K for the central star of NGC 7027 its luminosity and radius may be calculated. The distance to this PN has been carefully investigated by Pottasch et al (1982) who determined a distance of d=1.2+/-0.4 kpc using various methods. Correcting for extinction the angular radius is 4.25×10^{-2} $R_{\odot}$ and the luminosity is about 6500 $L_{\odot}$. These values were computed using the procedure in Chapter 2 section 2.7.

3.5 Discussion

This chapter describes the detection of the central star of NGC 7027 with the subsequent derivation of a number of parameters describing this star. It is of interest to compare the temperature derived by the Zanstra method with that found using the 'Stoy' or 'Energy Balance' method. This has been determined for NGC 7027 by Preite-Martinez & Pottasch (1983) as T(EB) = 3×10^{5} K for their Case III, in which the nebula is assumed to be optically thick. For Case II, where the PN is assumed to be optically thick in the Ly-continuum and thin elsewhere T(EB) = 2.34×10^{5} K which is in excellent agreement with the value determined using the HeII Zanstra method. Preite-Martinez & Pottasch go on to predict a magnitude for the central star of NGC 7027 based on T(EB) = Tz(HeII) as being m_V=17.5, again in excellent agreement with the value that has been determined in this work. Is it possible then that the PN is not optically thick to the hydrogen ionising radiation?

Summarising, this Chapter presents narrow band images of NGC 7027 which unambiguously show the central star. Its visual magnitude has been determined as 17.7±0.5 implying a Zanstra temperature for the central star of 250,000±25,000 K. In Chapter 6 the mass of the central star will be investigated by comparing the parameters, T_{eff}, L_* , and R_*, derived for this central star, with theoretical models.

Preliminary results from the reduction of the TAURUS data is discussed in Chapter 6.

CHAPTER 4

Chapter 4

4. Detailed Investigation of NGC 2440.

4.1 Introduction.

In this chapter the case of the central star of NGC 2440 will be highlighted. The detection reported in Chapter 2 and Atherton et al (1986) is the first unambiguous detection of this extremely faint, hot central star. This magnitude leads to an estimate of its Zanstra temperature of 350,000 K and this makes it one of the hottest central stars observed.

For such a star all the energy in the Lyman continuum will go into ionising the surrounding nebular gas, with the energy reappearing at longer wavelengths as recombination and collisionally excited lines. It is possible to estimate the number of ionising photons emitted by the central star because each Lyman photon will result in one Balmer photon. The temperature of the star is computed from the ratio of the number of Hβ photons to the visual continuum emission, assuming either blackbody radiation or a model atmosphere. The Hβ flux from the PN is relatively easy to measure whereas the visual magnitude of a hot central star is not.

When the central star is not visible on photographs, it is possible to use large aperture photometry to measure the line and continuum strengths of the nebula and, by applying a theoretical correction to the strength of the nebula continuum, to estimate the contribution to the visual continuum from the central star (Kaler, 1976a; Kohoutek & Martin, 1981b). Such a technique is difficult to apply to stars fainter than about m_V=14 because of the noise from the background night sky and the nebula. A more sensitive search tecnique is to image the nebula using narrow-band filters to exclude all of the nebula emission lines, thus ensuring maximum contrast between the star (which is mainly a continuum source, especially for the hotter ones) and the nebula (the spectrum of which is dominated by emission lines).

NGC 2440 is a fairly bright nebula lying close to the galactic plane. Perek & Kohoutek have given this PN the designation PK 234 +2°1. Shaw & Kaler (1985) derived a lower-limit magnitude of m_V=14.3 for the central star using the technique of large area photometry. Curtis (1918) failed to find the central star on photographs in a survey which went down to m_V=19.5, and Pottasch (1981) used this lower limit to estimate the central star temperature as 5×10^5 K. Kohoutek & Martin (1981) disputed this and gave an estimate of 10^5 K. Reay et al (1984b) have given a lower limit of m_V=16.

4.2 Observations.

To resolve this controversy new observations were made at the Anglo-Australian telescope as part of a program to identify and measure the magnitudes of the central stars of a number of PNe having faint central stars. The observational procedure and details are as descibed in Chapter 2, section 2.3.

Briefly, observations were made with a CCD camera at the prime focus using a 10 Å wide filter centred at 4788 Å. This wavelength was chosen to exclude any known nebula emission lines, and thus to maximise the contrast of the star against the nebula background.

The images obtained were processed as descibed in Chapter 2, section 2.4. A contour map of the continuum image is shown in Fig. 4.1a. The central star is clearly seen between the two, bright inner condensations. The seeing for this exposure, determined from gaussian fits to the field stars in the CCD frame, was less than 1 arc sec. FWHM. Fig. 4.1b shows an observation taken using the same detector-filter combiantion one day earlier, when the seeing was 2 arc secs. The absence of the star in this image is entirely explained by the poor seeing.

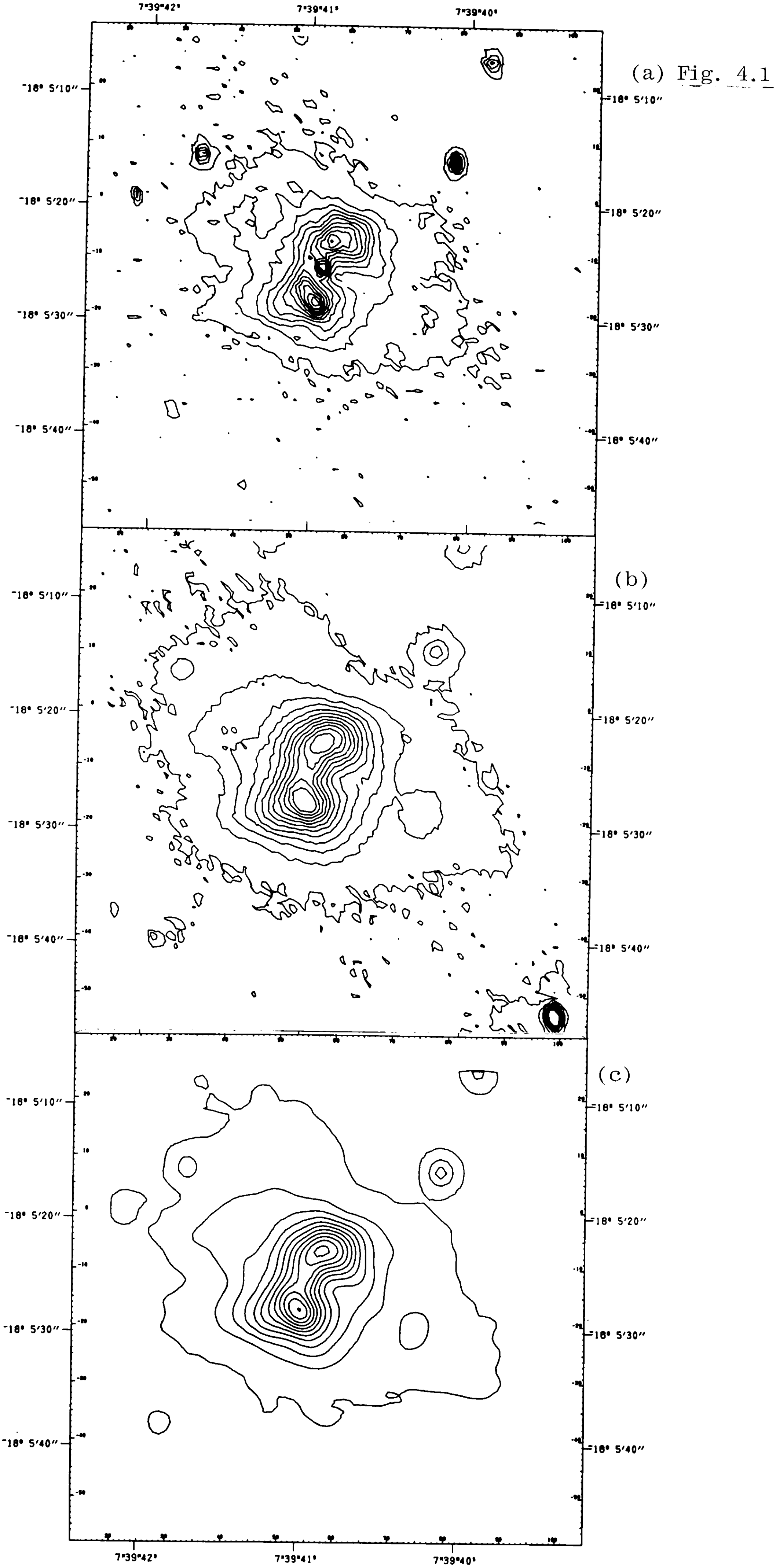
7h39m42s
7h39m41s
7h39m40s
-18° 5′10″
-18° 5′20″
-18° 5′30″
-18° 5′40″
(a) Fig. 4.1
(b)
(c)

Fig. 4.1c shows Fig. 4.1a smoothed to the same spatial resolution as Fig 4.1b and as can be seen the central star emission is 'smeared' out into the nebula continuum emission when the seeing is poor.

4.3 Results.

The magnitude of the central star was determined by interpolating and subtracting the nebula continuum from Fig. 4.1a and integrating under the stellar profile to determine the total flux. Comparison of this with similar quantities determined for two nearby field stars, the magnitudes and spectral types of which have been determined by Gathier (1984), enabled the visual magnitude of the central star to be determined. As outlined in Chapter 2, section 2.5, the assumption was made that the central star is sufficiently hot to have a Rayleigh-Jeans black-body-like spectrum in the visible and beyond, and that the comparison stars also have black body spectra.

An independent estimate of the magnitude was made by comparison with a standard (101-281) taken from the lists of Landolt (1973), of known magnitude and spectral type. Again the assumption was made that this star had a black body spectra in the mid-visible. The best value of the magnitude from these independent calibrations was m_V=19.8 +/- 0.2 for the central star of NGC 2440.

The hydrogen Zanstra temperature Tz(H) is determined as descibed in Chapter 2 section 2.6 as being Tz(H) = 390,000 K. Likewise the Helium II Zanstra temperature was determined as Tz(HeII) = 280,000 K. Errors in Tz(H) and Tz(HeII) due mainly to the error in the magnitude, amount to ±25,000 K and ±20,000 K respectively.

The difference between Tz(H) and Tz(HeII) is probably due to Tz(H) being overestimated because recombination from He^{++} yields more than one photon capable of ionising hydrogen. On the other hand, Tz(HeII) is an under estimate for the effective temperature since some of the photons capable of ionising He^+ are actually absorbed by H. Stasinska and Tylenda (1986) have shown that these effects become more noticeable at high temperatures($T > 2\times10^5$ K). A good estimate of the effective temperature, T_{eff}, is 350,000 ± 25,000 K. Pottasch (1981) notes the same effect in NGC 7027, and this is confirmed in the results presented in Chapter 3 of this work. These consistent results indicate that the nebula is most likely optically thick for photons ionising both hydrogen and helium.

A summary of the basic input parameters for NGC 2440 and the quantities derived for this PN are given in Table 4.1.

4.4 Discussion.

The Zanstra temperature may be compared with that determined from the energy balance method. Pottasch (1984) gives the temperature as 270,000 using this method if Case III assumption is made for the nebula, in other words if the nebula is optically thick. this is slightly lower than the Zanstra temperature. However Stasinska & Tylenda (1986) show that the energy balance method can lead to underestimate of the central star temperature at high temperatures. This is because some of the collisionally excited lines which need to be accounted for cannot be measured with present techniques. The most important of these are Lα, O V 1215 Å (bended with Lα), and O VI 1034 Å. The oxygen lines become particularly strong at high T_{eff} but there is no simple formulation to account for this effect. Hence if this fact is noted the energy balance method is in good agreement with the temperature determined from the Zanstra technique.

The angular radius can be computed from the visual flux (which comes from the visual magnitude using the calibration of Wamsteker (1981)). This has been outlined in Chapter 2 section 2.7.2 giving the radius as 1.5×10^{-2} $R_\odot$ if the distance of Gathier et al (1986) is used. This give a luminosity of about 3200 $L_\odot$ if the central star is assumed to radiate as

Table 4.1

Input and Derived Physical Parameters for NGC 2440.

Property	Value	Reference(s)
Distance......	2.19 +/- 0.38 kpc.	Gathier et al (1986)
E(B-V)........	0.30 +/- 0.03	ibid
Log F(Hβ).....	-10.47 +/- 0.02 ergs cm^{-2} s^{-1}	Kaler (1978); Perek (1971)
F(4686)/F(Hβ).	0.6	Shields et al (1981)
T_e(N II)......	10,000 K	ibid
ξ (fill fac)..	1	assumed
n(He)/n(H)....	0.156	Pottasch (1984)
n(N)/n(O).....	1.313	ibid
m_V............	18.9 +/- 0.2	
M_V............	6.26	
Tz(HI)........	390,000 K	
Tz(HeII)......	280,000 K	
T(EB).........	270,000 K	Pottasch (1984)
Luminosity....	3190 $L_\odot$	
Radius........	0.0152 $R_\odot$	

a blackbody.

Only one set of evolutionary calculations has been published for stars more massive than 0.7 $M_\odot$; those of Paczynski (1971) for 0.8 $M_\odot$ and 1.2 $M_\odot$. More recent calculations of the evolution of stars near 0.6 $M_\odot$ confirm the general trends of earlier models. As the shell burning proceeds in a star, its temperature increases to a maximum when the shell sources have used up essentially all the available hydrogen and helium, and then begins to decrease. The maximum temperature depends critically on the central star mass. If the models of Paczynski are correct, it can reach the value observed for NGC 2440 only when its mass is > 1.0 $M_\odot$. The high nitrogen and helium abundances (Pottasch, 1984) observed in NGC 2440 would tend to support the contention that the central star mass > 1.0 $M_\odot$. These abundances mean that NGC 2440 is a Type I PN (Peimbert & Torres Peimbert, 1983) and these are generally thought to have more massive cores (Peimbert, 1985; Kaler, 1983).

For a 1.0 $M_\odot$ model , the time taken for nuclear burning to stop is about 300 years. But the nebula must be considerably older. The age of the nebula can be determined from its diameter and expansion velocity (32 arcsecs and 23 kms^{-1}; Pottasch, 1984) as ≈ 7,000 years. But the luminosity at present indicates a cooling time of ≈ 1000 years. Hence there is some discrepancy between the observed and expected ages and probably indicates that the theory is incomplete.

Another problem which arises is the following. It is clear that the progenitor of a white dwarf of 1 $M_\odot$ must be quite massive (Peimbert, 1985). A recent discussion (Weidmann & Koester, 1983) based on a study of white dwarfs in open clusters, places this progenitor mass at 7 $M_\odot$. But the nebular mass in NGC 2440 is only 0.4 $M_\odot$ (Pottasch, 1984). Thus some 5 $M_\odot$ must have been ejected in the course of the evolution of the star, but does not appear to be present in the neighbourhood of the star. While this material could have been ejected at a very early stage in the evolution, this appears unlikely because the most active phase of mass loss appears to be at the end of Asymptotic Giant Branch stage of evolution before the transition to the Planetary Nebula stage (Renzini 1981, Renzini 1981a). Thus either the material is in some form which is as yet undetectable or present estimates of the progenitor mass are too high. One form that this 'missing mass' may be in is molecular hydrogen. In the next Chapter details of a search for molecular hydrogen in NGC 2440 are descibed and it is indeed found that there is a significant amount of molecular hydrogen associated with NGC 2440.

CHAPTER 5

Chapter 5

5. Investigations of Molecular Hydrogen Distribution in a Number of PNe

5.1 Introduction.

NGC2440 is one of a small group of Planetary Nebulae which appear to contain pairs of condensations symmetrically disposed about the position of the central star. Other members of this group include NGC7009, NGC6826 and Abell 30. Although morphologically similar there is no real evidence that these objects are representative of a particular class of nebula or indeed a particular phase of nebular evolution.

Spectroscopy of the condensations in Abell 30 (Hazard, Terlevich Morton, Sargent and Ferland 1980), for example, show that they are composed of processed hydrogen-deficient material which probably originated in the surface of a highly evolved star, implying that they were ejected at a late stage in the evolution of the central star. By contrast, spectroscopy of NGC2440 (Shields et al 1981) and NGC7009 (Aller and Epps 1975; Czyzak and Aller 1979) indicate near normal abundances in the vicinity of the condensations in these objects, although Reay and Atherton (1985) have argued that the condensations in NGC7009 must be cold (T ≈ 50 K) and dense (≈ $4\times10^{+6}$ cm^{-3}) if they are to survive in their present form for the lifetime of the nebula. If this is so, the near normal element abundances observed by Aller and Epps (1975) would be representative of the ionised skin transition regions surrounding the condensations.

In order to test the hypothesis that cold molecular condensations can exist deep within the HII regions of planetary nebulae, near to the central star, a search for the v=1-0 S(1) 2.122 μm line of molecular hydrogen in the bright condensations observed in NGC7009 and NGC2440 has been undertaken. In both of these nebulae the condensations are particularly bright in the [OI] 6300 A line which originates in HI/HII transition regions where the temperature is ≈ 5000 K. Beckwith, Persson and Gatley (1978) have shown that in NGC6720 molecular hydrogen and [OI] line emissions appear to be co-spatial.

The existence of small cool condensations has been proposed by several authors (Van Blerksom and Arny 1972; Capriotti 1973) to explain the occurence of bright [OI] 6300 A and other low excitation line emissions in planetary nebulae which have otherwise high excitation spectra. It is only in the nearby nebula NGC7293 that such condensations have been unambiguously resolved within the body of the HII region, and there are no observations reported to date which suggest that they contain molecules.

5.2 Observations.

The observations reported were made with CGSII, a 7-channel cooled grating spectrometer (Wade 1983), at the U.K. Infrared Telescope (UKIRT) on the nights of November 31 and December 1, 1984. Spectra with a resolving power ≈ 600 (velocity resolution 550 kms^{-1}) consisting of 14 sample points spaced by approximately 275 kms^{-1} were obtained centred on the 2.122 μm v=1-0 S(1) line. The entrance aperture was approximately circular with an equivalent diameter of 5.4 arcsec on the sky. An E-W chop with a beam separation of 60 arcsec was used to compensate for sky background.

Spectra of standard stars were taken against which the P.Ne. spectra were ratioed to give a flux calibration. (These were taken from the 1984 UKIRT lists of standards for JHKLL' photometry.) No correction was made for extinction because at 2 mm on Mauna Kea the extinction is less than 10% per airmass and can be zero on a good night.

Supplementary observations of NGC2440 were made with the UKIRT circular variable filter (CVF) UKT9 on December 2, 1984. The CVF had an entrance aperture of 20 arcsec and a velocity resolution of 3000 kms^{-1}. For these observations I would like to thank Drs. A Longmore & D. Whittet.

5.2.1 NGC 7009.

The observations were concentrated at the positions of the bright [OI] condensations at the ends of the major axis of the inner elliptical shells (Reay and Atherton, 1985)

In none of these observations was a significant detection of the S(1) line made. The limiting sensitivity is equivalent to an upper limit flux of $\approx 2\times10^{-17}$ W m^{-2} which corresponds to an upper limit mass $\approx 5\times10^{-6}$ $M_{\odot}$ of shock excited molecular hydrogen if we adopt the shock excitation model proposed by Kwan (1977).

5.2.2 NGC2440.

Figure 5.1 shows the positions observed in NGC2440. The crossed circles indicate points at which the S(1) line was detected. The figure shows sample spectra obtained at positions in the nebula and Table 5.1 summarises the observational parameters and line fluxes determined using BS718 and BS804 as calibration stars.

5.3 Reduction Procedure and Results.

The reduction of this data to determine the line fluxes was carried out using the DIPSO package (Howarth and Maslen, 1984) on the UCL STARLINK node. For greater accuracy the DIPSO Gaussian fitting routine ELF, written be DR. P J Storey was used. Example spectra showing the H_2 V=1-0 S(1) line are shown for NGC 2440 on Figure 5.1.

The flux measured in the line at the earth is (Hollenbach & Shull, 1977):

$$I_{ij} = f_i \, N(H_2) \, A_{ij} \, \Delta E_{ij} \, / \, 4\pi \quad \text{ergs } s^{-1} \, cm^{-2} \, sr^{-1}$$

I_{ij} is the line intensity, whilst $N(H_2)$ is the column density of H_2. ΔE_{ij} is the transition energy. f_i is the fraction of hot H_2 in that level = 1.22×10^{-2} for T_{vib} = 2000 K. A_{ij} is the Einstein transition probability. This enables the column density of H_2 to be found and hence the mass if the distance is taken as d=2.19+/-0.38 kpc (Gathier, 1984).

Results showing the masses of Θ2 at various positions in NGC 2440 are shown in Table 5.1.

5.4 Discussion of the P.Ne. NGC 7009 and NGC 2440.

In Figure 5.2 a plot of the [OI] 6300 Å intensity against the v=1-0 S(1) line intensity, for the small number of nebulae for which the intensities of both have been measured, is shown. There is clearly a correllation between the intensities of these lines which, taken with the observed spatial corellation (Beckwith et al 1978; Storey 1984) supports the view that they originate in the same region of the nebula.

From Figure 5.2 we see that for NGC7009 the [OI] intensity implies an S(1) line flux of 1.6×10^{-17} W m^{-2}. This is on the boarderline of the limiting sensitivity of the detector and may therefore explain the

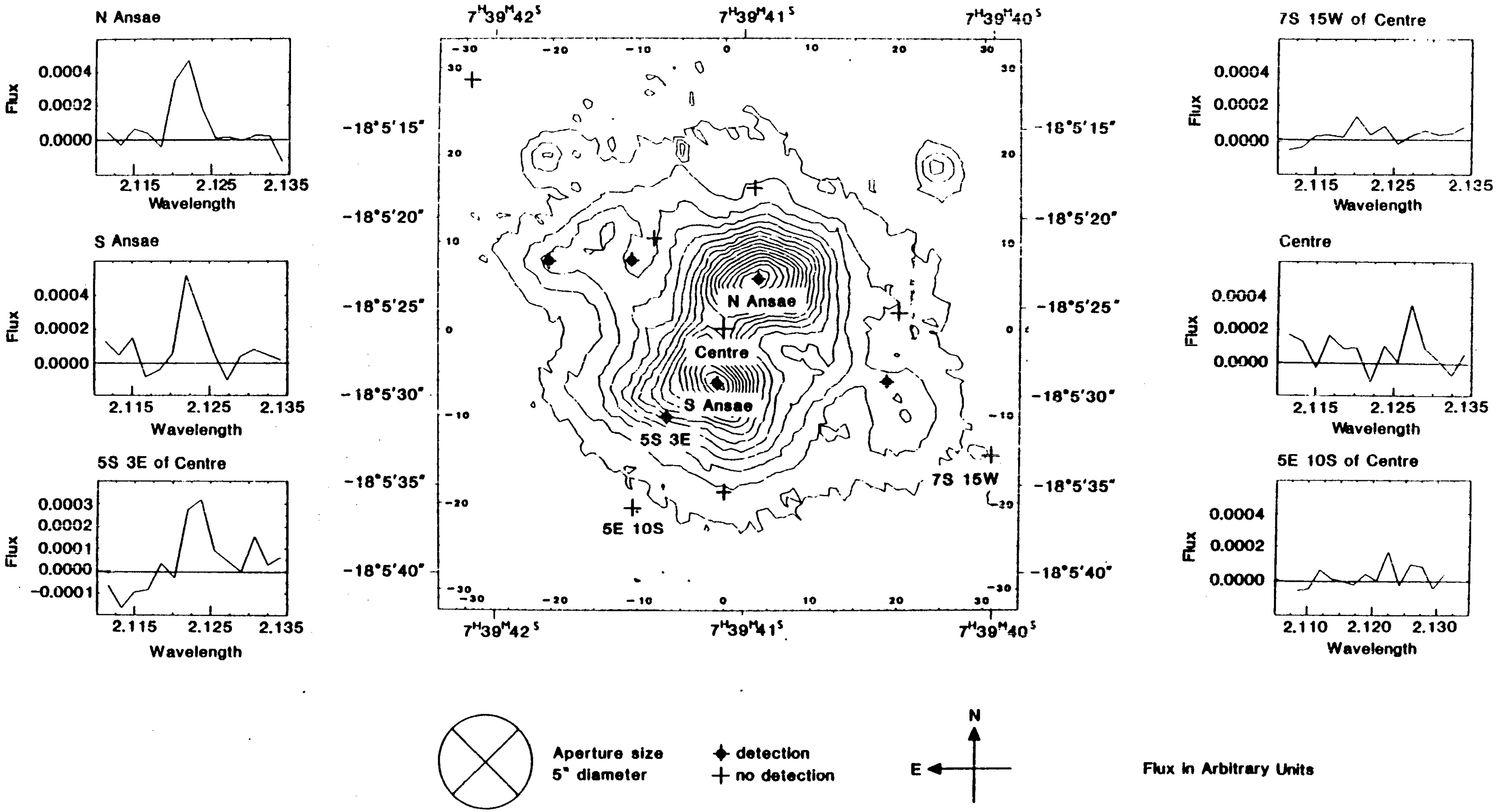

Figure 5.1 Positions of detections of molecular hydrogen superimposed on the [OI] map of NGC 2440. Also shown are sample spectra.

Figure 5.2 Graph of [OI] flux against measured H_2 v = 1→0 2.1μm for sources with measured H_2 detections

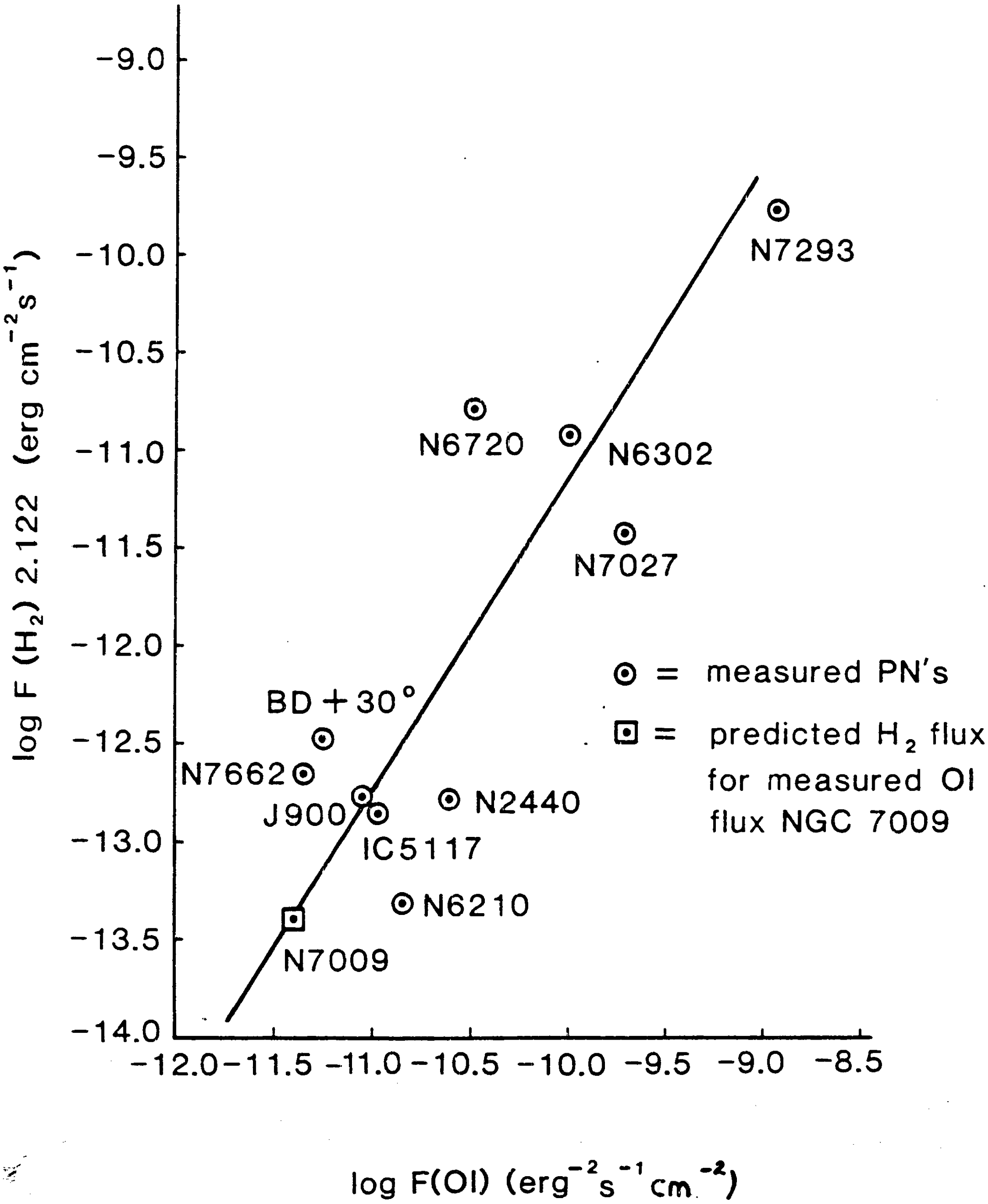

Table 5.2 Flux Measurements of the H_2 v=1-0 S(1) Line in NGC 2440.

Position*	Detector	Flux Wm^{-2}	Column Density m^{-2}	Mass H_2 $M_\odot$
N Ansa (a)	CGS2	7.96×10^{-17}	5.45×10^{21}	1.94×10^{-5}
N Ansa (b)	CGS2	9.16×10^{-17}	6.28×10^{21}	2.23×10^{-5}
S Ansa (a)	CGS2	10.36×10^{-17}	7.10×10^{21}	2.52×10^{-5}
S Ansa (b)	CGS2	10.39×10^{-17}	7.12×10^{21}	2.52×10^{-5}
3S,9W	CGS2	5.41×10^{-17}	3.71×10^{21}	1.31×10^{-5}
5S,3E	CGS2	6.71×10^{-17}	4.60×10^{21}	1.63×10^{-5}
10E,4N	CGS2	4.91×10^{-17}	3.37×10^{21}	1.19×10^{-5}
9E,4N	CGS2	6.33×10^{-17}	4.34×10^{21}	1.54×10^{-5}
Centre	CVF	3.65×10^{-16}	1.56×10^{21}	8.86×10^{-5}
20N,20E	CVF	8.49×10^{-17}	3.64×10^{20}	2.06×10^{-5}
20N,20W	CVF	1.19×10^{-16}	5.07×10^{20}	2.88×10^{-5}
20N	CVF	1.83×10^{-16}	7.83×10^{20}	4.44×10^{-5}
20S	CVF	8.48×10^{-17}	3.63×10^{20}	2.06×10^{-5}

* Note : the positions are given in arcsecs N,S,E,W of the centre.

Table 5.2

Observational parameters and fluxes for the v=1-0 S(1) line.

The aperture sizes were approximately 5 arcsecs for CGS2 and 20 arcsecs for the CVF.

non-detection of the S(1) line emission in the apparently bright [OI] condensations.

In NGC2440 the S(1) line emission clearly peaks at the positions of the inner pair of condensations (positions 1 and 2) and has a minimum in intensity between the condensations at the position of the central star (Atherton, Reay and Pottasch 1986). There is also some indication that faint S(1) line emission is present over an area of ≈ 40 arcsec centred on the central star of the nebula.

The conclusion is made that the [OI] bright condensations are molecular and therefore cool, being sufficiently dense to be self-shielding against radiation from the very hot central star. These conclusions support the view (Reay and Atherton 1985) that condensations of this nature would have to have a density ≈ $4\times10^{+6}$ cm^{-3} and temperature ≈ 50-100 K in order that they survive the lifetime of nebula.

Figure 5.3a shows contrast enhanced prime focus IIIaJ plate of NGC2440 obtained at the Anglo-Australian telescope, for which I thank Dr. David Malin of the Anglo-Australian Observatory. It can be seen that the HII region is 80 arcsec in diameter, the outer boundary is almost perfectly circular centred on the position of the central star. The complex central structure (Figure 5.1) is evident in the 'unsharp mask' print from the prime focus plate shown in figure 5.3b.

The S(1) line emission in the central regions of the nebula clearly originates in this inner structure as distinct from at the boundary of the ionisation front. This is, therfore, the first detection of molecular hydrogen emission from within the HII region of a planetary nebula. The faint, extended S(1) line emission detected with the CVF probably originates in a molecular shell located at the outer boundary of the HII region.

In Table 5.2 estimates of the mass of excited molecular hydrogen within

Figure 5.1 NGC 2440

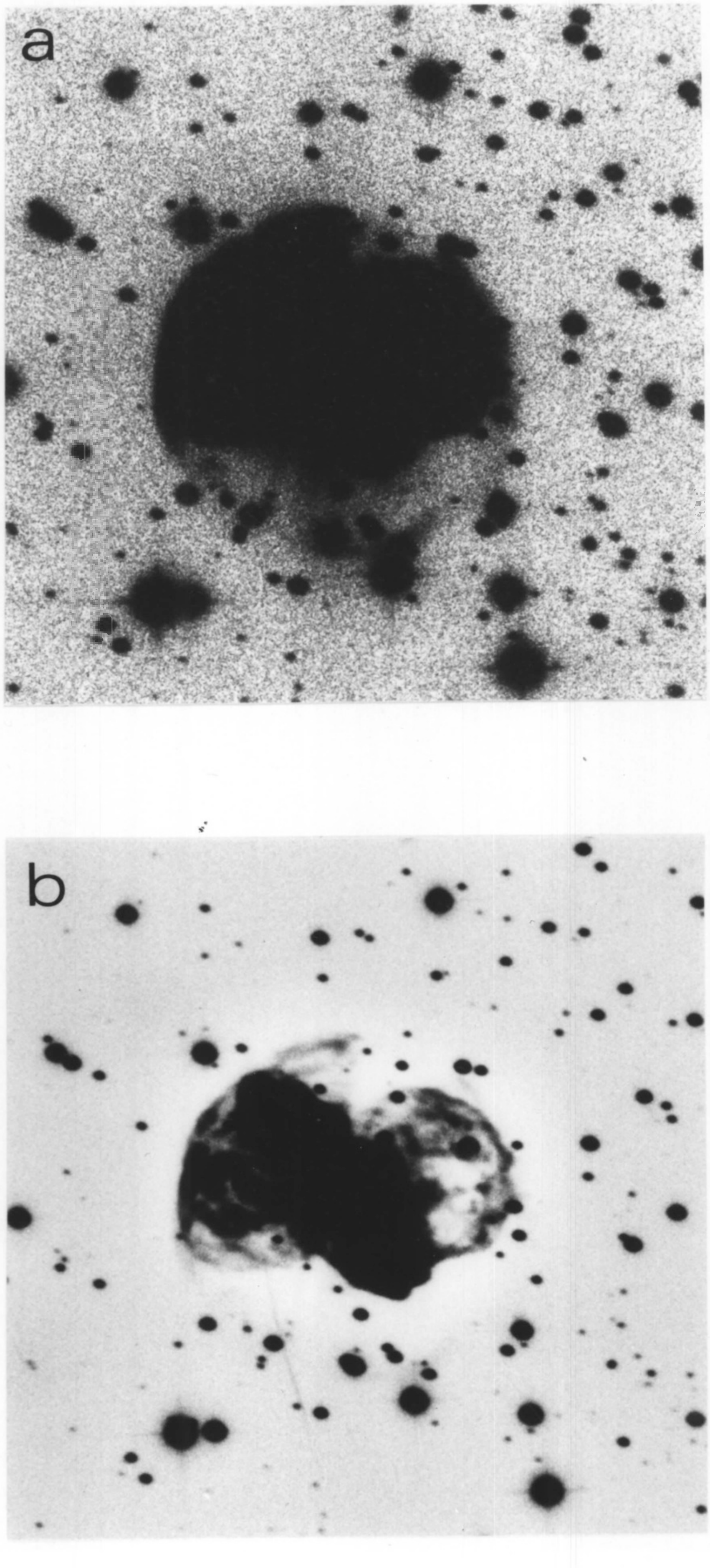

our telescope beam on the assumption of LTE at a temperature of 2000 K (Shull and Becklin 1982) are made. Using these figures the total mass of excited molecular hydrogen within, or associated with, the HII region can be made. Assuming that the pattern of molecular hydrogen emission seen is a background level originating at the boundary of the HII region superimposed upon which is the emission from the inner condensations, the background level corresponds to an excited molecular hydrogen mass of $\approx 10^{-3}$ $M_\odot$.

Taking sections in the [OI] image through the north and south condensations the sizes, and hence the masses of excited molecular hydrogen at these positions have been estimated to be 2.1×10^{-5} $M_\odot$ and 4.4×10^{-5} $M_\odot$ respectively.

5.4.1 The Excition Mechanism involved for NGC 2440.

It is of interest to look at the energetics of the molecular hydrogen excitation in the inner condensations in view of their proximity to the exceptionally hot central star.

There is reasonable evidence (Smith et al 1981; Isaacman 1984) that molecular hydrogen in planetary nebulae is shock excited, and this will assumed to be so in NGC2440.

Adopting the shock excitation model proposed by Kwan (1977) the molecular hydrogen in the inner condensations (total mass $\approx$ 6.5×10^{-5} $M_\odot$) will cool to a temperature $\approx$ 1000 K in $\approx$ 3 yrs. implying that the force driving the shock be capable of exciting w 2.2×10^{-5} $M_\odot$ yr^{-1} of molecular hydrogen. A shock velocity of 10 km s^{-1} implies a force $m\dot{v}$ of $1.5\times10^{+22}$ N.

This shock could be driven either by stellar wind outflow from the central star or by radiation pressure. For a stellar temperature of 350000 K and magnitude m_V =18.9 (Atherton, Reay and Pottasch 1985), the luminosity will be 2600 $L_\odot$ ($3.83\times10^{+27}$ W m^{-2}) for a distance of 2.2 kpc (Gathier 1984). Taking the effective diameters of the north and south condensations to be 5.7 and 7.1 arcsec respectively, the north condensation will intercept 21 percent of the stellar radiation and be subject to an acceleration L/c of $8.0\times10^{+18}$ N, and the south condensation will intercept 12 percent and be subject to an acceleration of $1.54\times10^{+18}$ N. These are clearly insufficient by a factor $\approx 10^4$ to excite the observed S(1) line emission.

An alternative source of energy to drive the shock could be stellar wind. There is no spectroscopy of the central star of NGC2440 and no direct evidence therefore for a stellar wind. If, however, the assumption that there is a stellar wind which is entirely responsible for exciting the S(1) line emission in the inner condensations, is made, the outflow rate that this implies can be estimated.

Adopting a stellar wind velocity of 2000 km s^{-1}, typical of high excitation planetary nebulae for which IUE spectra are available (Perinotto 1983), a mass outflow rate of $\approx 3\times10^{-7}$ $M_\odot$ yr^{-1} is required in order that the force mv exerted by the outflow is equal to the force required to shock 2.2×10^{-5} $M_\odot$ yr^{-1} of molecular hydrogen. This outflow rate is consistent with typical mass loss rates deduced from IUE spectra (Pottasch 1984).

5.5 Concluding Remarks.

Molecular hydrogen emission has been detected from condensations which lie deep within the HII region of the planetary nebula NGC2440. The observations imply that self-shielding molecular condensations exist very close to the exceptionally hot central star.

Radiation pressure from the star is inadequate to excite the S(1) line emission in the condensations. We estimate that a stellar mass loss rate of 3×10^{-7} $M_\odot$ yr^{-1} would be required to excite the emission.

The existence of molecular condensations within the HII region implies that they were ejected from the central star in it's pre-planetary phase of evolution, and have survived for the lifetime of the nebula. This suggestion is consistent with the model proposed by Reay and Atherton (1985) for the condensations in NGC7009.

CHAPTER 6

Chapter 6

6. Implications of the Central Star Temperatures for Stellar Evolution.

6.1 Introduction.

This Chapter will be used to briefly summarise the results presented in this thesis and indicate some possible further observational programs that might be undertaken.

6.2 The Central Stars in the H-R Diagram.

In Table 6.1 a summary of the temperatures, luminosities and radii for the central stars of the P.Ne. studied is given. Each central star is plotted on the H-R diagram in Figure 6.1. For comparison evolutionary tracks due to Paczynski (1971) are also shown. These are the only tracks available for high mass stars other authors presenting calculations for $M < 0.7\ M_{\odot}$ (Schonberner, 1979). As can be seen many of the central stars must have masses $> 0.7\ M_{\odot}$ if these evolutionary tracks are to be believed. In Table 6.2 the He/H and N/O abundances are given for each of the P.Ne. On the basis of these, those P.Ne. that are Type I (Peimbert, 1978) are indicated as such on Figure 6.1. It would appear that the Type I P.N. exist in the high mass regions of the H-R diagram which is as expected (Peimbert, 1985).

Figure 6.2 shows M_{ϕ} vs nebula radius for the P.Ne. Schonberner (1981) finds a relation of Mv with Rn and uses this to argue that most P.Ne. have cores with similar masses at about $M = 0.6\ M_{\odot}$. Based on this sample though this effect is not seen, in agreement with Gathier (1984) who argued that Schonberner's correlation was based on the distance scale to the P.Ne. which he employed.

Plates 6.1 and 6.2 are included to give an example of the effectiveness of the search technique that has been described. Plate 6.1 shows an

Table 6.1 Summary of Zanstra Temperatures and Luminosities.

Name of P.N.	T_{eff} (K) $\times 10^{-3}$	Log T_{eff} (K)	Radius ($R_\odot$) $\times 10^{2}$	Luminosity ($L_\odot$)	Log L
NGC 2438	160	5.204	1.8	250	2.398
NGC 2440	350	5.544	1.5	3190	3.504
NGC 2452	110	5.041	8.8	1040	3.017
NGC 2818	186	5.270	2.3	580	2.763
NGC 2867	126	5.100	5.5	692	2.840
NGC 3211	145	5.161	3.1	390	2.591
NGC 3918	220	5.342	4.8	4940	3.694
NGC 5315	50	4.699	75	3200	3.505
NGC 6153	100	5.000	11	1260	3.100
NGC 6309	85	4.929	7.0	210	2.322
NGC 7027	250	5.398	4.3	6500	3.813
IC 2165	162	5.210	6.1	2400	3.380
IC 2448	68	4.833	26	1300	3.115
IC 4776	45	4.653	73	2030	3.307
J 900	125	5.097	5.0	570	2.757
A 40	52	4.716	17	212	2.326
HE2-120	96	4.982	6.0	280	2.447
HE2-117	80	4.903	43	6830	3.834

Figure 6.1 Luminosity as a Fuction of T_{eff} for the P.Ne. Central Stars.

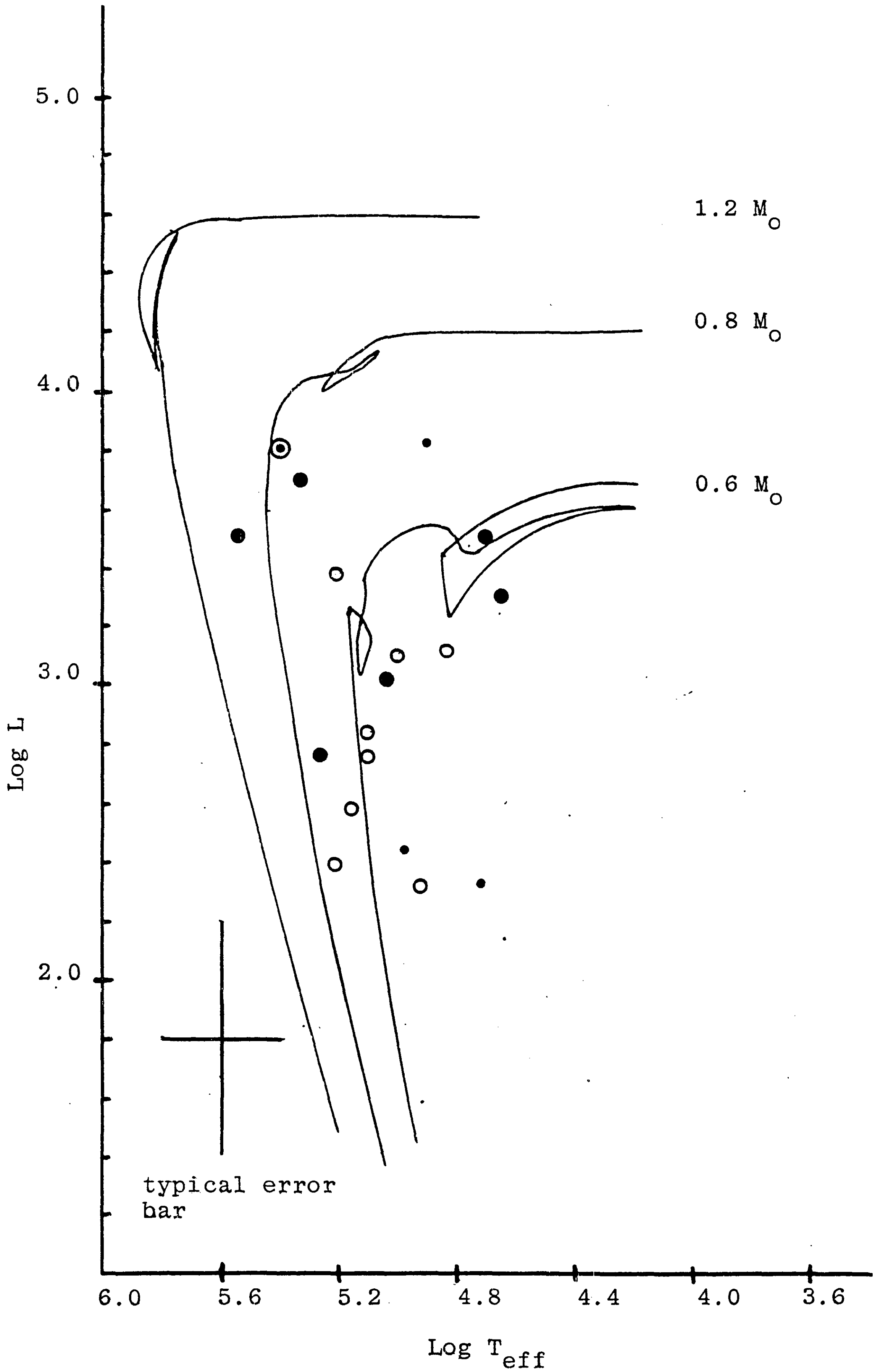

image of IC 2165 as seen through the standard 'B' broadband filter. No central star is apparent in this image, even though the seeing was ≈ 1 arcsec. Hua & Grundseth (1985) recently investigated this P.N. using an imaging technique through emission line filters. Even though they claimed seeing of < 1 arcsec they were unable to detect the central star. Plate 6.2 shows the image taken after the B image, through the narrow band continuum filter. Here the central star is quite obvious against the much reduced nebula background, and a good estimate of $m_V = 17.9$ could be made.

In summary it is shown how many central stars of P.Ne. may have previously had their brightnesses overestimated. Hence hot central stars have been discriminated against. It is probable that these hot central stars are the more massive of the nuclei of P.Ne. These stars had massive progenitors. A search for mass from the progenitor of NGC 2440 has lead to the detection of a substantial amount of H_2.

6.3 Prospects for Further Work.

Massive central stars evolve very quickly along the horizontal part of the H-R diagram, for instance a $1.2M_\odot$ star exhausts its nuclear burning material in about 10 years (Pacynski, 1971). Hence it is unlikely that it will be posiible to study a central star in this phase. However as the star cools to become a white dwarf it may be possible to gain an insight into the stars earlier history by investigating its associated nebula.

A recent suggestion has been made that the existence of a faint recombining halo around the brighter ionised inner region of a planetary nebula may indicate the existence of a hot, luminous central star which is cooling rapidly towards the White Dwarf stage of its evolution (Tylenda, 1986). It is postulated that for a radiation bounded P.N. the maximum size of the ionised region will be reached when the central star reaches its hottest and most luminous position during its horizontal

Table 6.2 Helium and Nitrogen abundances for the sample PNe.

Name of P.N.	n(He)/n(H)	ref	n(N)/n(O)	ref
NGC 2346	0.133	1	0.464	1
NGC 2438	0.104	1	0.280	3
NGC 2440	0.156	1	1.313	1
NGC 2452	0.107	1	1.150	1
NGC 2818	>0.069	2	≈1	2
NGC 2867	0.108	1	0.311	1
NGC 3132	0.126	1	0.333	1
NGC 3211	0.119	1	0.174	2
NGC 3918	0.115	1	0.417	1
NGC 5315	0.122	2	0.955	2
NGC 6153				
NGC 6302	0.180	1	1.417	1
NGC 6309	0.124	1	0.169	1
NGC 6439				
NGC 7027	0.116	1	0.786	1
IC 2165	0.133	2	0.174	2
IC 2448	0.095	2	0.517	1
IC 4776	0.86	1	0.933	3
J 900	0.102	1	0.161	1
A 40				
HE2-120				
HE2-117				

References to Table 6.2.

1 : compilation by Pottasch (1984)

2 : Torres-Peimbert & Peimbert (1977)

3 : compilation by Kaler (1979)

evolution across the H-R diagram. When the central star has depleted its hydrogen shell through burning it rapidly cools and its luminosity consequently falls. Because of this the ionising flux from the central star will also be reduced and the ionisation front of the P.N. will recede. High excitation lines (e.g. [OIII]) will rapidly fade as their recombination times are short. However for lower excitation lines (e.g. [SII], [OI]) the timescales for recombination can be much longer. Hence a useful test as to whether a faint halo is in fact recombining, rather than being a result of a varying density distribution, is to be able to compare the images in high excitation lines with those in low excitation lines. For recombining halo's the low excitation lines should be dominant with little high excitation line emission for the reasons explained above.

Two other factors have also to be satisfied, that the central star is hot ($T > 10^5$K) and luminous ($L/L_\odot > 10^2$) and also that the bright central part of the P.N. is radiation bounded. If this second criteria is not satisfied then the halo is just ionised by flux from the central star. However the sample to be investigated should be chosen on the basis that they show strong low excitation line emission from the central areas indicating that their central parts are optically thick to H-ionising radiation.

For these suspected hot objects the central star magnitudes are poorly determined as the stars are rather faint in the visible. This is because the bulk of their energy is output in the UV whilst they emit a great number of ionising photons which cause their surrounding nebulae to emit strongly in emision, especially in the optical. Accurate visual magnitude determinations are essential if the temperatures and luminosities of these objects are to be more accurately assessed.

As described in Chapter 3 TAURUS was use at the INT to investigate the kinematics of a number of P.N. and in particular how stellar winds shape the P.N. This data is now under preliminary reduction. One of the

Figure 6.1 Absolute magnitude for the P.Ne. as a function of nebula radius.

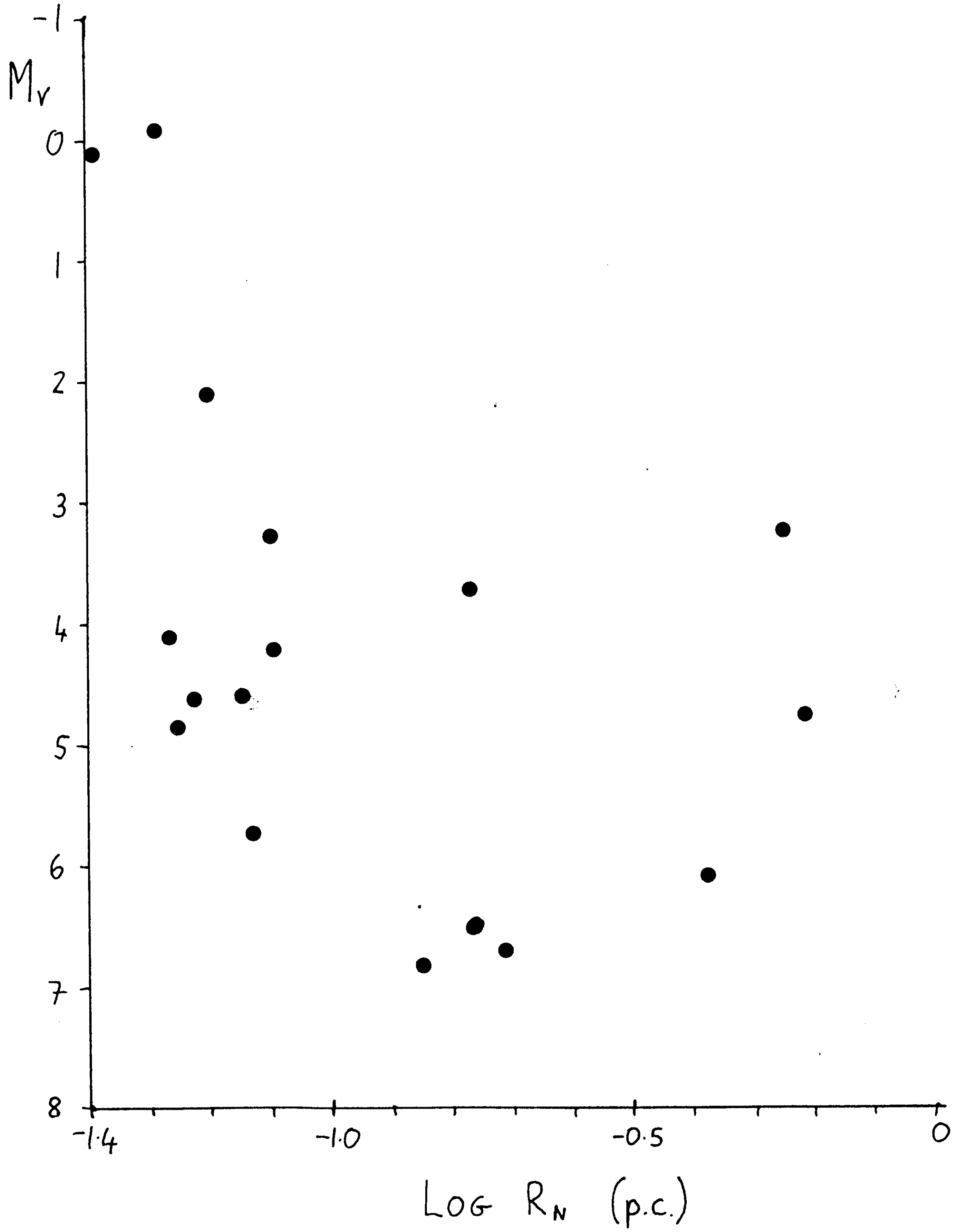

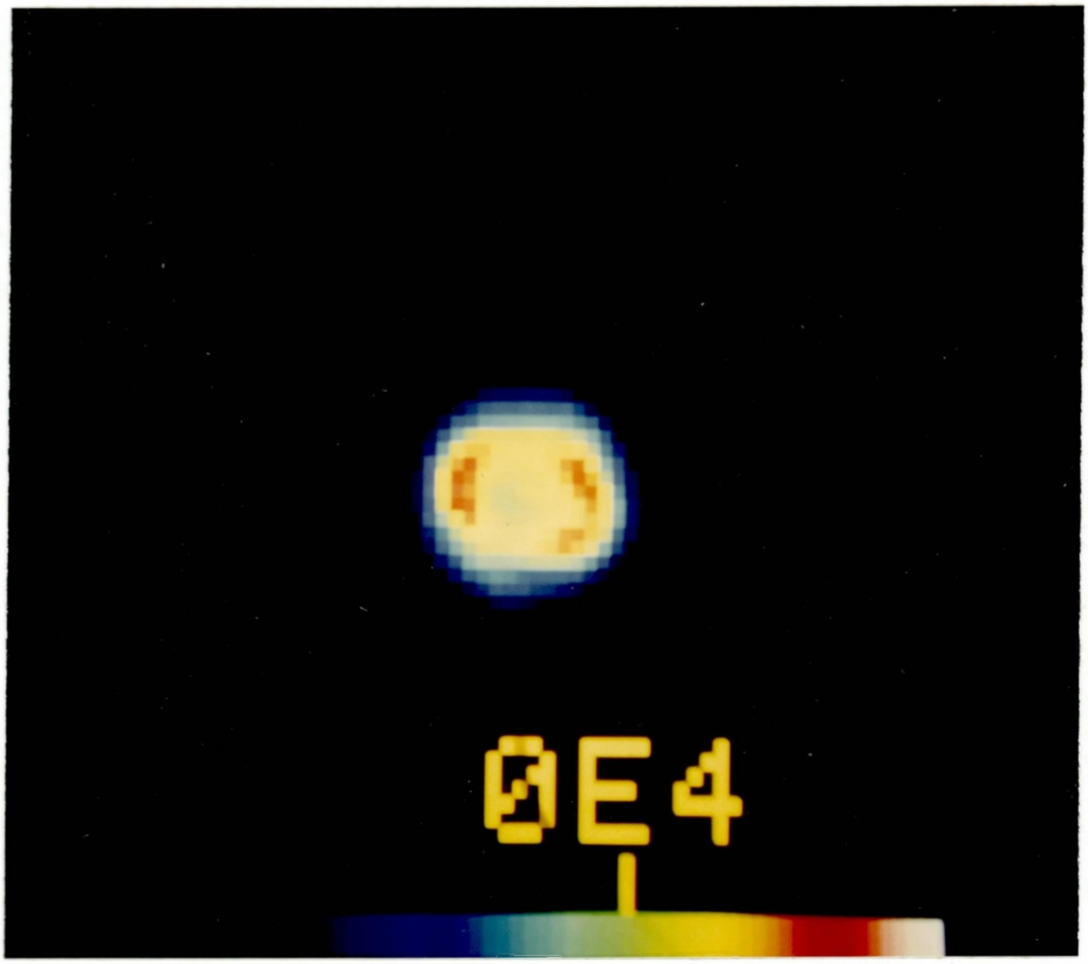

Plate 6.1

This plate shows the P.N. IC 2165 as seen through the 'B' broadband filter. As can be seen the central star is completely swamped by the nebula emission.

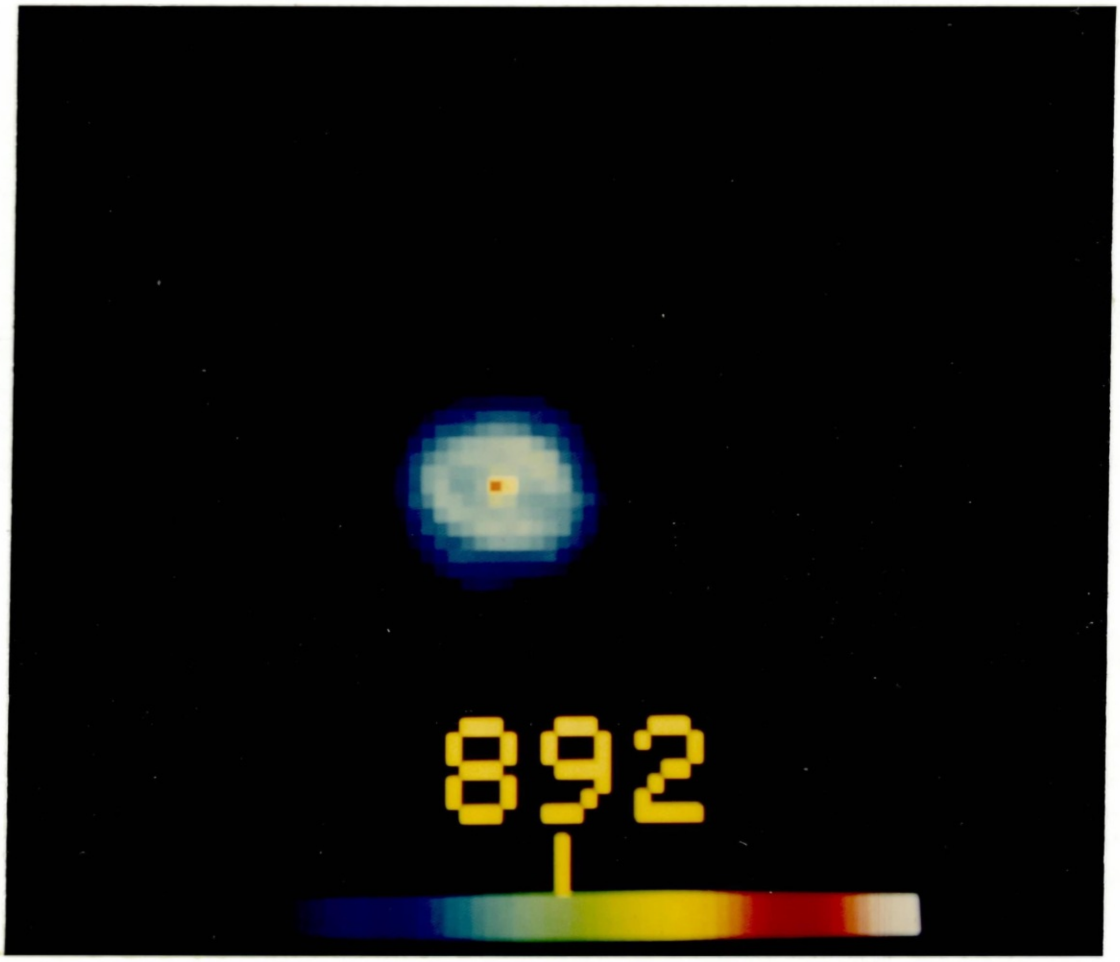

Plate 6.2

This plate shows the IC 2165 as imaged through the 4788 Å narrow band continuum filter. Comparing this with the previous plate (6.1) the central star is now quite obvious as the contrast between star and nebula is maximised using the technique descibed in Chapter 2.

objects studied was NGC 7027. We obtained data cubes in Hα and [OIII]λ5007A for this object. Contour maps for this object which seem to show a faint outer halo extending nearly twice as far as has previously been seen (Atherton et al 1979). However due to the nature of that observing program and the dynamic range limitations of the IPCS only tentative conclusions can be made about this finding as our signal to noise in the faint outer regions is rather poor . Hence I will seek to make deeper exposures on this interesting object using the CCD in order to be able to make a more qualatative assessment of the nature of this outer halo. The central star of NCG 7027 is thought to be extremely hot implying a high progenitor mass but the observed mass of the nebula and central star falls some $4M_\odot$ short of the required mass. Hence if this halo is in fact real it would account for some of this 'missing' mass that must have been shred by the progenitor of the central star.

In summary it is proposed to confirm or otherwise the recombining nature of the faint outer halo's of the P.N. For the recombining halo's, the relative importance of the various emission lines will be compared with theoretical estimates (Tylenda, 1984). This, together with improved estimates for the central star magnitude will enable further constraints to be placed on the evolution of the central stars studied. Estimates of the central stars masses will also be possible.

APPENDICES

Appendix 1.

The following appendix contains contour plots of the PNe studied in this work. For most of the PNe a 'broad band' image (either U, B or V) is shown along with the narrow band, 4788 A, 'continuum' image. The name of the P.N., following the normal convention is given followed by a code letter to identify through which filter the image was obtained. These codes correspond to the following filters as follows:

U - U filter at 3600 Å
B - B filter at 4200 Å
V - V filter at 5500 Å
P - Narrow band 'continuum' filter at 4788 Å
Q - Narrow band [OIII] filter at 5007 Å
R - Narrow band [OI] filter at 6300 Å

The contour levels plotted are indicated on each figure along with the minimum amd maximum values in the image. Generally the levels are set spaced evenly between the maximum and minimum values in the data, although in some of the plots extra contours are used at low levels to detail faint structure. Additionally in some of the plots the contours are set to emphasise the central star of the P.N.

The images of NGC 3132 show the central star to be saturated with flux spilling into adjacent pixels. These over-exposures were taken to show the faint structure of the P.N. For estimates of the central star brightness shorter exposures, which did not saturate at the central star were taken.

In some of the plots a saturated band of pixels running across the frame may be seen. This is the result of saturation in a faulty set of pixels in the CCD detector. It should be noted that due to the reduction of the original hardcopy output for inclusion in this appendix, that the scales/mm given under SCALES are in fact incorrect.

Appendix 2.

This appendix contains values of the numerical integrals $G_1(T)$, $G_{1.807}(T)$ and $G_4(T)$ used in the calculation of the Zanstra Temperatures. These were computed using a numerical integration. The routine to compute $G_1(T)$ is shown in Program 3, in Appendix 3, with this being run with suitably adjusted limits, over which the integral was integrated, to find $G_{1.807}(T)$ and $G_4(T)$

Appendix 3.

This appendix contains the programs used in the computation of the magnitudes, Zanstra temperatures, radii and luminosities of the central stars studied in this work. The programs were written using the VIEW word processor on the BBC microcomputer. These text files could be 'executed' using the system command *EXEC to give the BASIC program, which could then be run in the usual manner. Listed here are the VIEW text files. A brief description of the purpose of each of the programs is given at the beginning of each program.

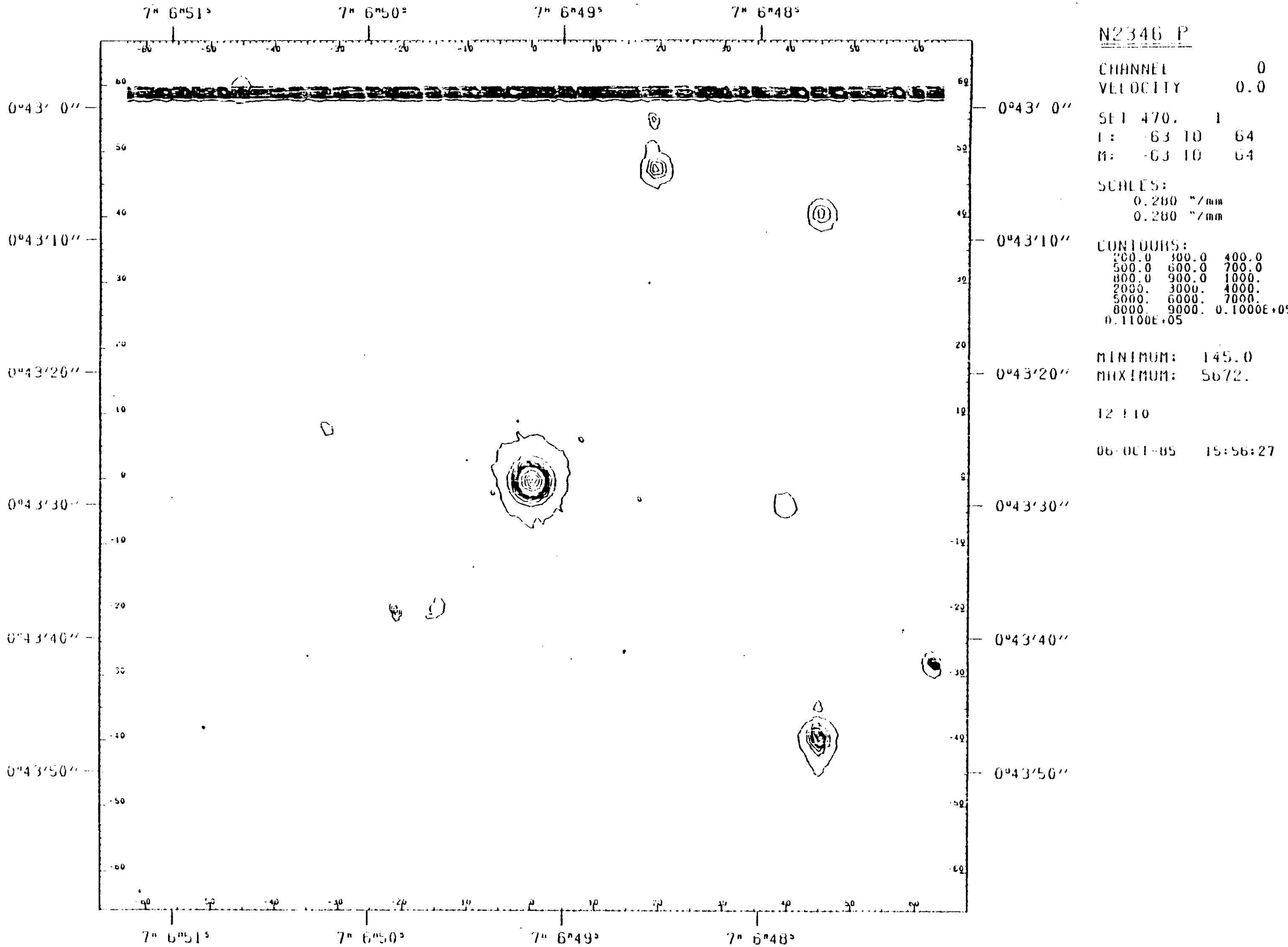
7h 6m51s
7h 6m50s
7h 6m49s
7h 6m48s
0°43′ 0″
0°43′10″
0°43′20″
0°43′30″
0°43′40″
0°43′50″
N2346 P
CHANNEL 0
VELOCITY 0.0
SET 470. 1
L: -63 10 64
M: -63 10 64
SCALES:
0.280 "/mm
0.280 "/mm
CONTOURS:
200.0 300.0 400.0
500.0 600.0 700.0
800.0 900.0 1000.
2000. 3000. 4000.
5000. 6000. 7000.
8000. 9000. 0.1000E+05
0.1100E+05
MINIMUM: 145.0
MAXIMUM: 5672.
12 110
06-OCT-85 15:56:27

Fig A1.1

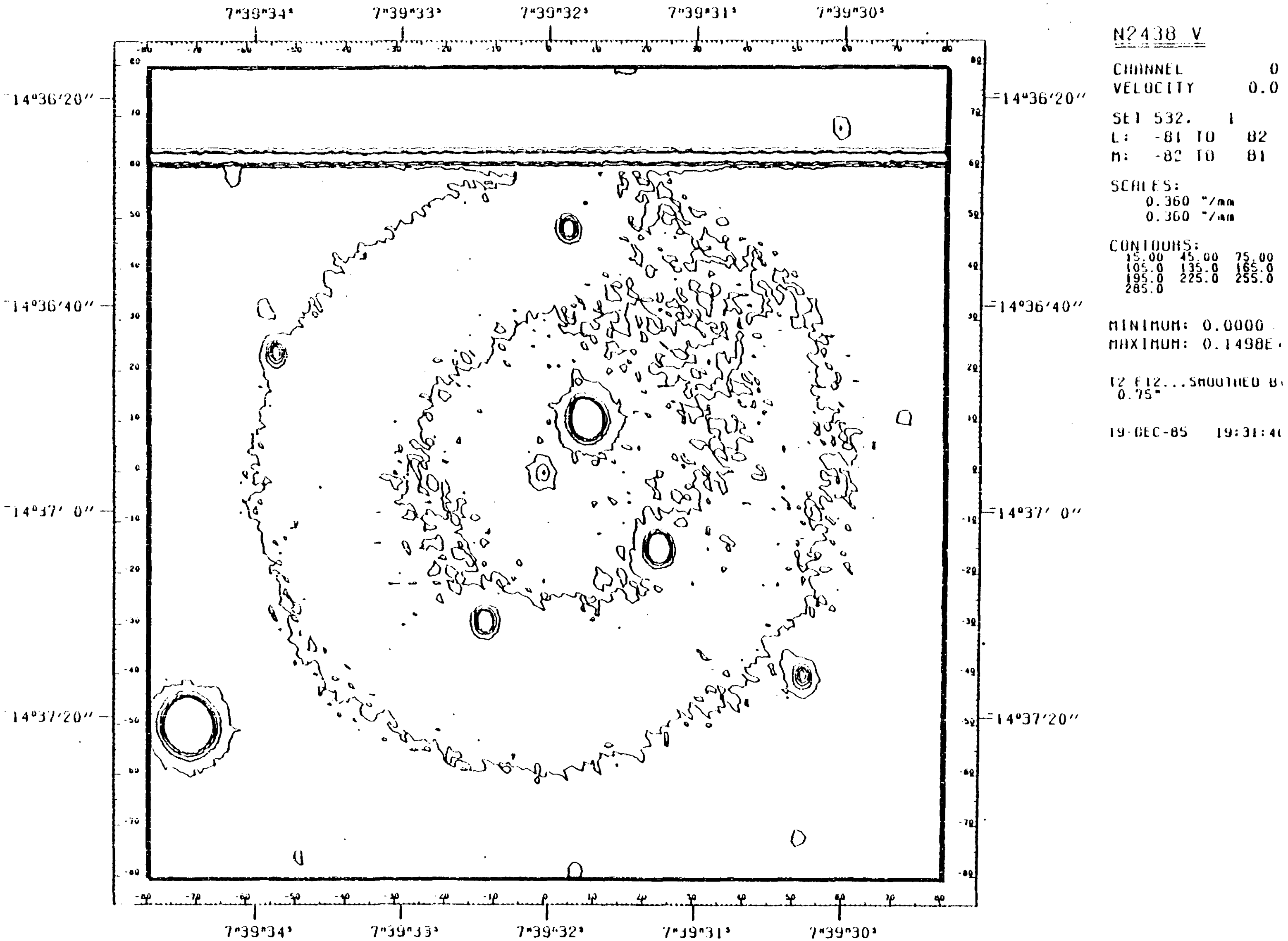
7h39m34s
7h39m33s
7h39m32s
7h39m31s
7h39m30s
-14°36′20″
-14°36′40″
-14°37′ 0″
-14°37′20″
N2438 V
CHANNEL 0
VELOCITY 0.0
SEl 532. 1
L: -81 TO 82
M: -82 TO 81
SCALES:
0.360 "/mm
0.360 "/mm
CONTOURS:
15.00 45.00 75.00
105.0 135.0 165.0
195.0 225.0 255.0
285.0
MINIMUM: 0.0000
MAXIMUM: 0.1498E
I2 FI2...SHOOTHED B
0.75"
19-DEC-85 19:31:4

Fig A1.2

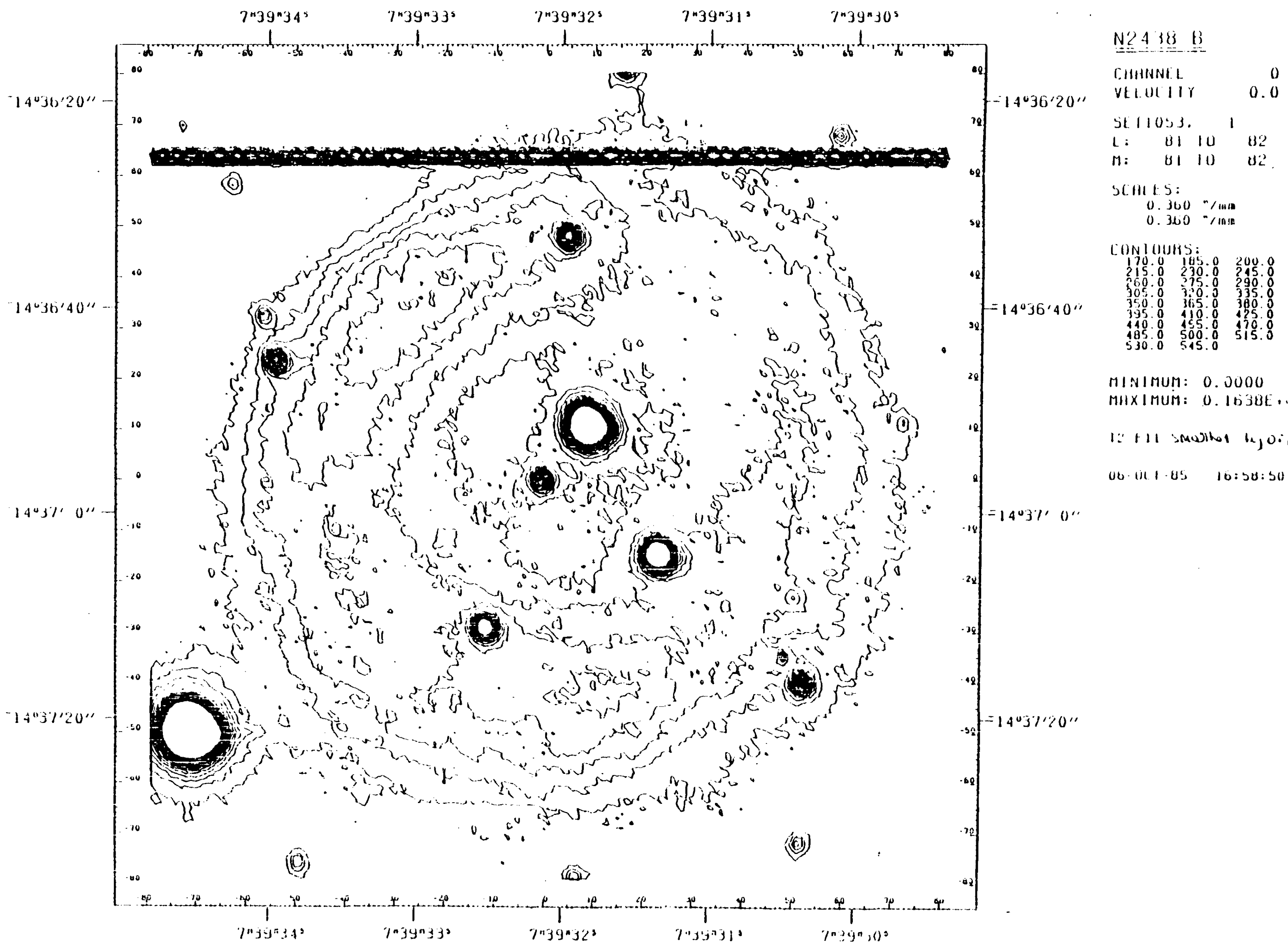
7h39m34s
7h39m33s
7h39m32s
7h39m31s
7h39m30s
-14°36′20″
-14°36′40″
-14°37′ 0″
-14°37′20″
N2438 B
CHANNEL 0
VELOCITY 0.0
SETT053. 1
L: 81 10 82
M: 81 10 82
SCALES:
0.360 "/mm
0.360 "/mm
CONTOURS:
170.0 185.0 200.0
215.0 230.0 245.0
260.0 275.0 290.0
305.0 320.0 335.0
350.0 365.0 380.0
395.0 410.0 425.0
440.0 455.0 470.0
485.0 500.0 515.0
530.0 545.0
MINIMUM: 0.0000
06-OCT-85 16:58:50

Fig A1.3

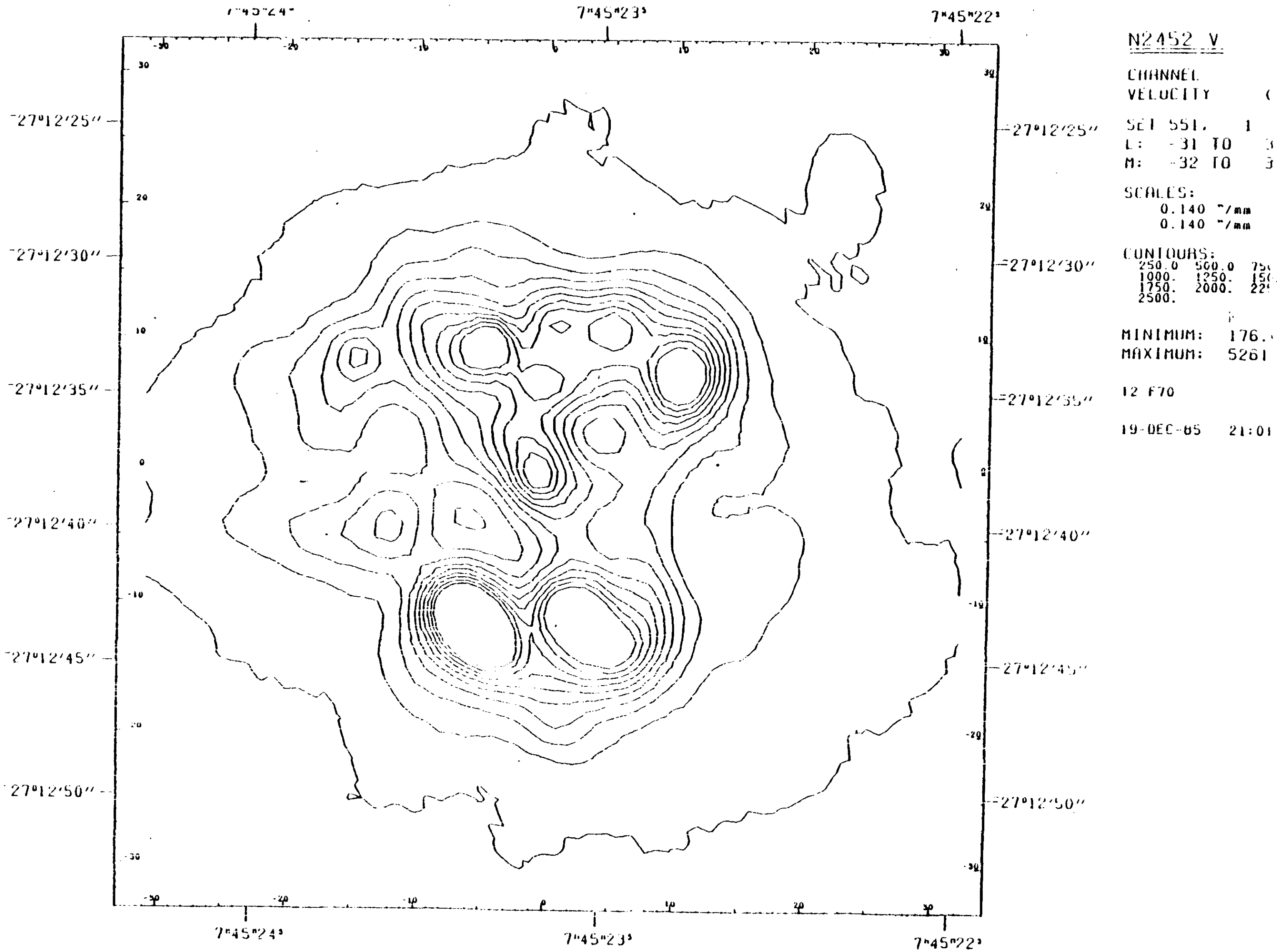
7h45m24s
7h45m23s
7h45m22s
-27°12'25"
-27°12'30"
-27°12'35"
-27°12'40"
-27°12'45"
-27°12'50"
N2452 V
CHANNEL
VELOCITY
SET 551.
L: -31 TO
M: -32 TO
SCALES:
0.140 "/mm
0.140 "/mm
CONTOURS:
250.0 500.0
1000. 1250.
1750. 2000.
2500.
MINIMUM: 176.
MAXIMUM: 5261
12 F70
19-DEC-85 21:01

Fig A1.4

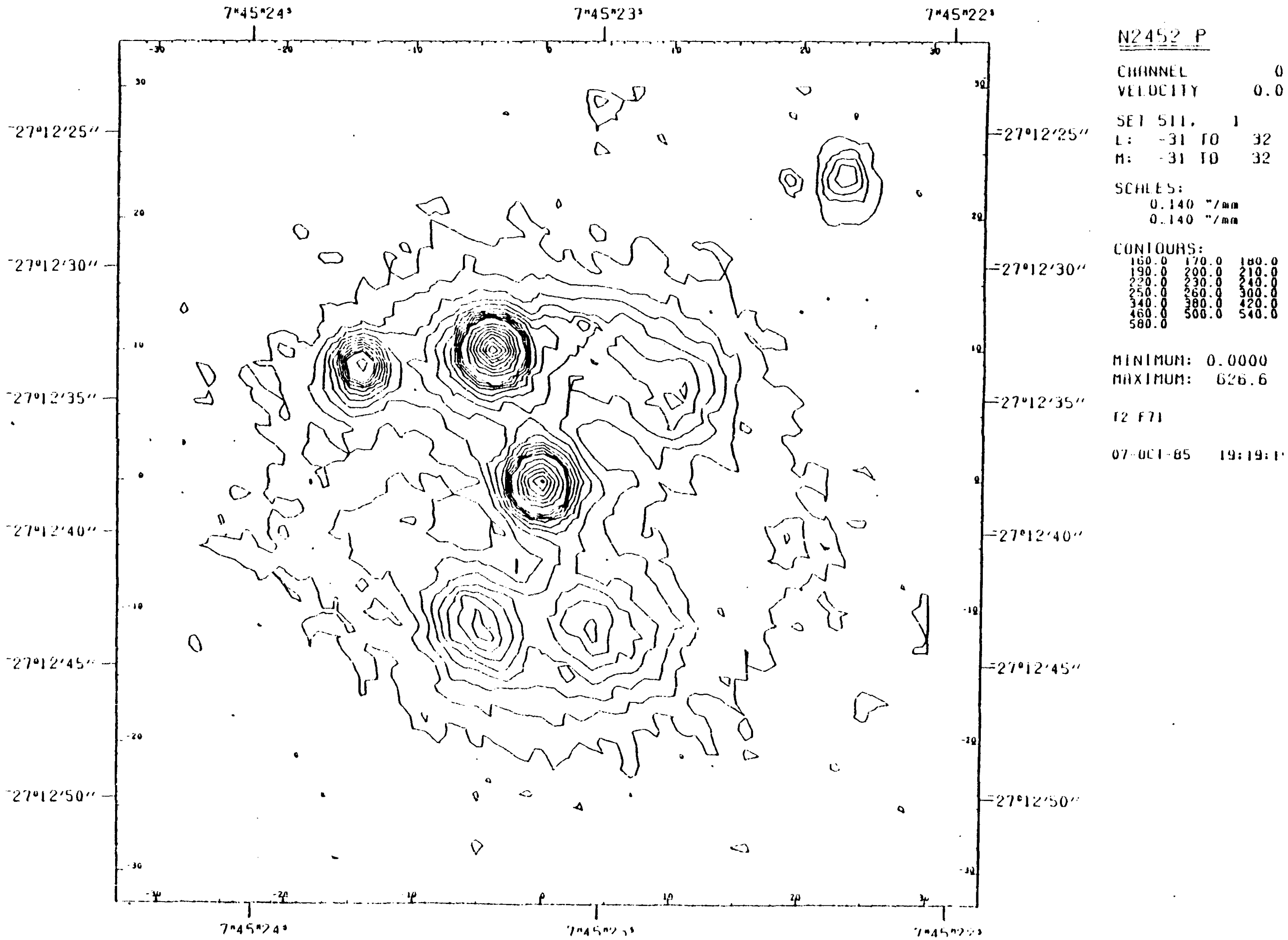
7h45m24s
7h45m23s
7h45m22s
-27°12'25"
-27°12'30"
-27°12'35"
-27°12'40"
-27°12'45"
-27°12'50"
N2452 P
CHANNEL 0
VELOCITY 0.0
SET 511, 1
L: -31 TO 32
M: -31 TO 32
SCALES:
0.140 "/mm
0.140 "/mm
CONTOURS:
160.0 170.0 180.0
190.0 200.0 210.0
220.0 230.0 240.0
250.0 260.0 300.0
340.0 380.0 420.0
460.0 500.0 540.0
580.0
MINIMUM: 0.0000
MAXIMUM: 626.6
T2 F71
07-OCT-85 19:19:1

Fig A1.5

Fig A1.6

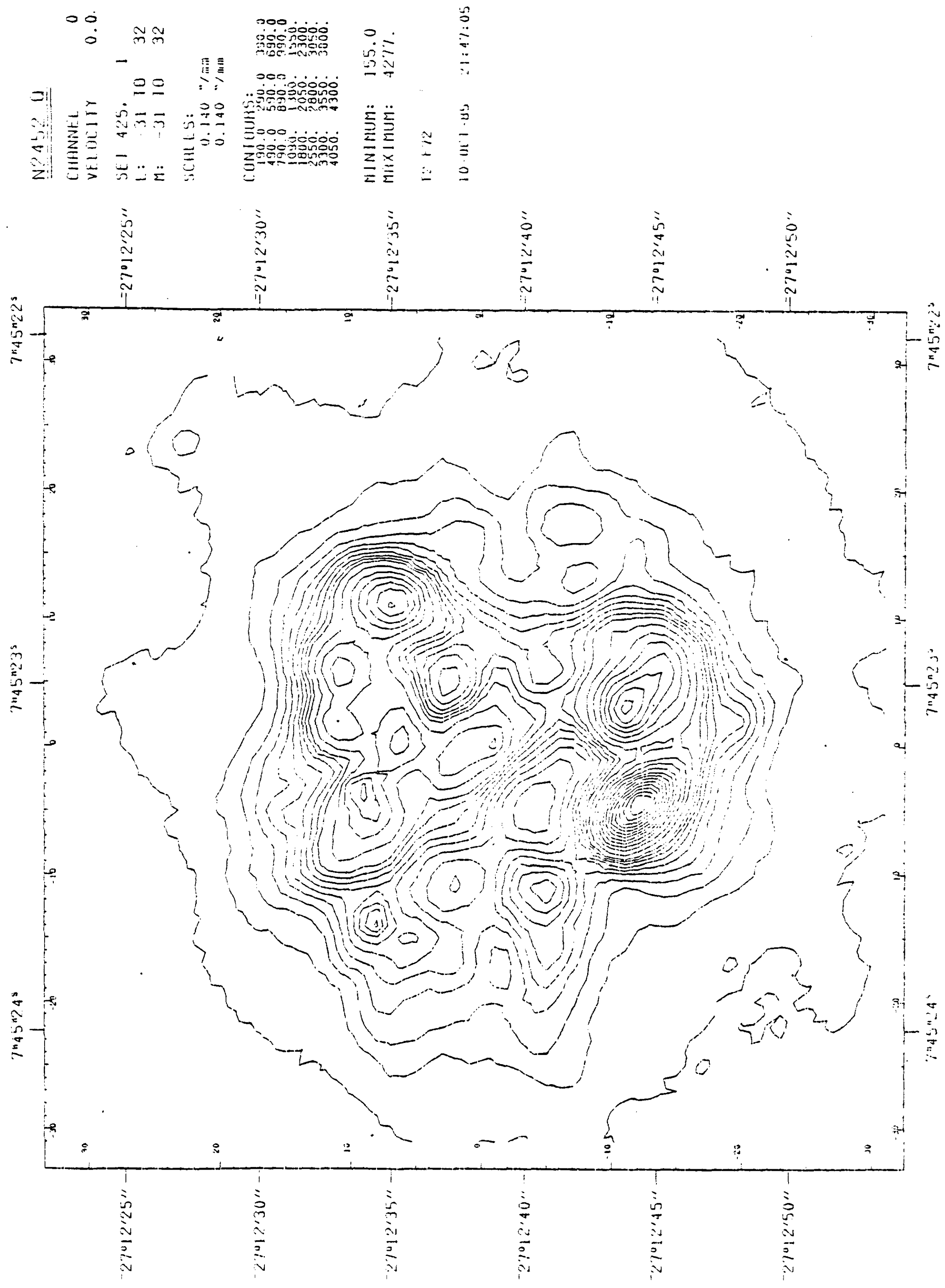
N2452 0
CHANNEL 0
VELOCITY 0.0
MINIMUM: 155.0
-27°12'25"
-27°12'30"
-27°12'35"
-27°12'40"
-27°12'45"
-27°12'50"
7h45m22s
7h45m23s
7h45m24s

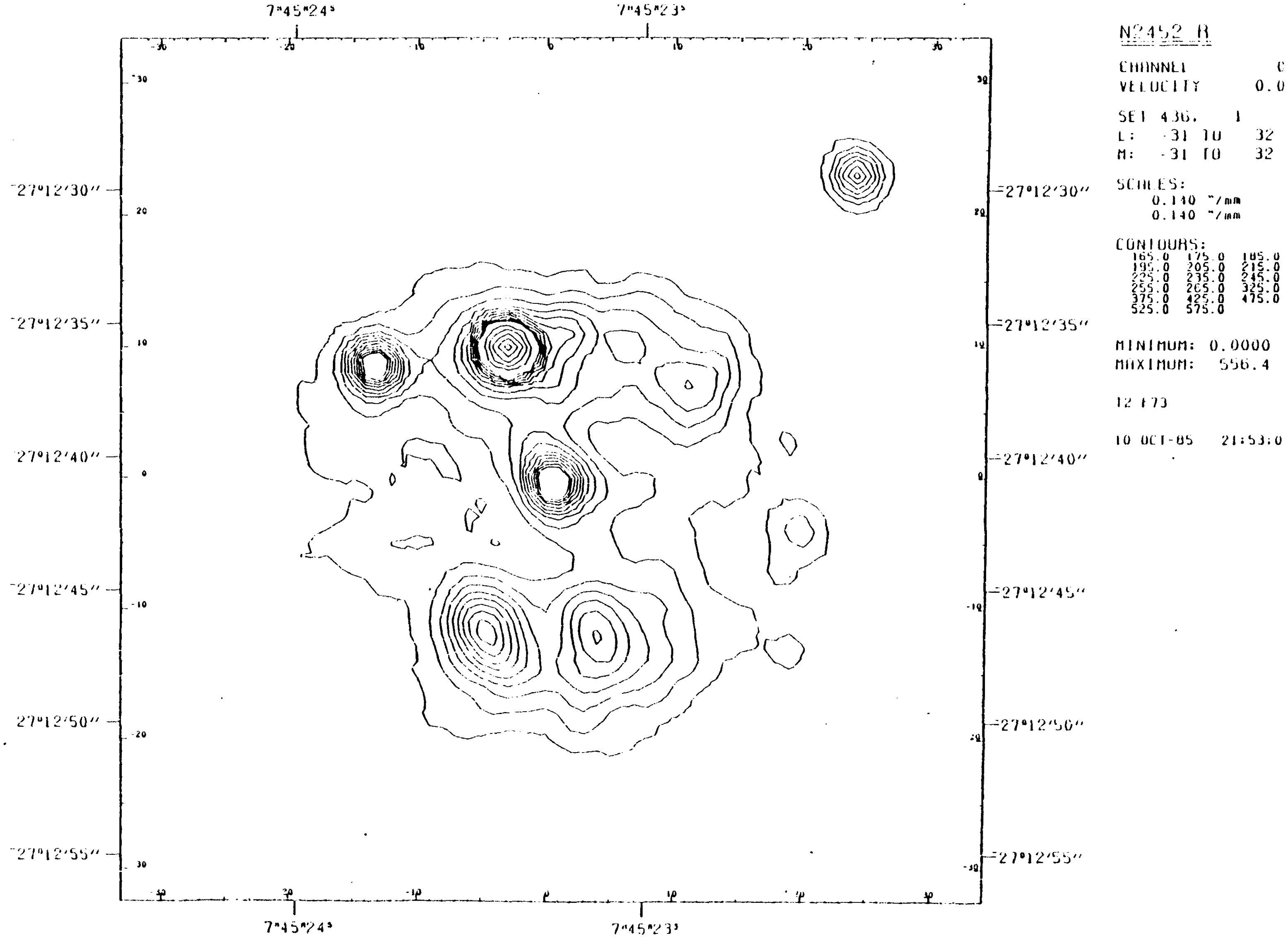

7h45m24s
7h45m23s
-27°12'30"
-27°12'35"
-27°12'40"
-27°12'45"
-27°12'50"
-27°12'55"
N2452 B
CHANNEL C
VELOCITY 0.0
SET 436. 1
L: -31 TO 32
M: -31 TO 32
SCALES:
0.140 "/mm
0.140 "/mm
CONTOURS:
165.0 175.0 185.0
195.0 205.0 215.0
225.0 235.0 245.0
255.0 265.0 325.0
375.0 425.0 475.0
525.0 575.0
MINIMUM: 0.0000
MAXIMUM: 556.4
12 F73
10 OCT-85 21:53:0

Fig A1.7

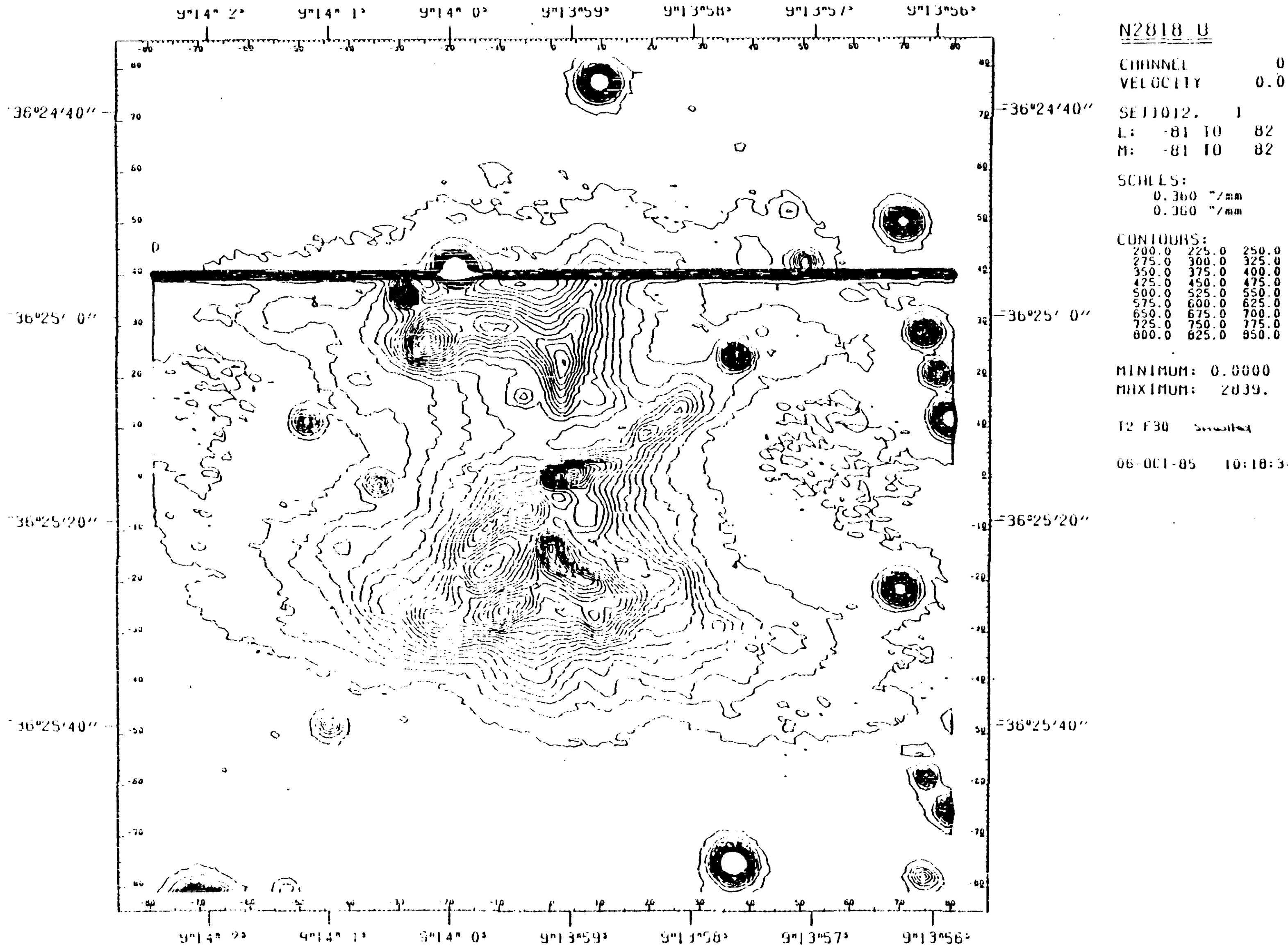
N2818 U
CHANNEL 0
VELOCITY 0.0
SETJ012. 1
L: -81 TO 82
M: -81 TO 82
SCALES:
0.360 "/mm
0.360 "/mm
CONTOURS:
200.0 225.0 250.0
275.0 300.0 325.0
350.0 375.0 400.0
425.0 450.0 475.0
500.0 525.0 550.0
575.0 600.0 625.0
650.0 675.0 700.0
725.0 750.0 775.0
800.0 825.0 850.0
MINIMUM: 0.0000
MAXIMUM: 2839.
06-OCT-85 10:18:3
9h14m 2s
9h14m 1s
9h14m 0s
9h13m59s
9h13m58s
9h13m57s
9h13m56s
-36°24'40"
-36°25' 0"
-36°25'20"
-36°25'40"

Fig A1.3

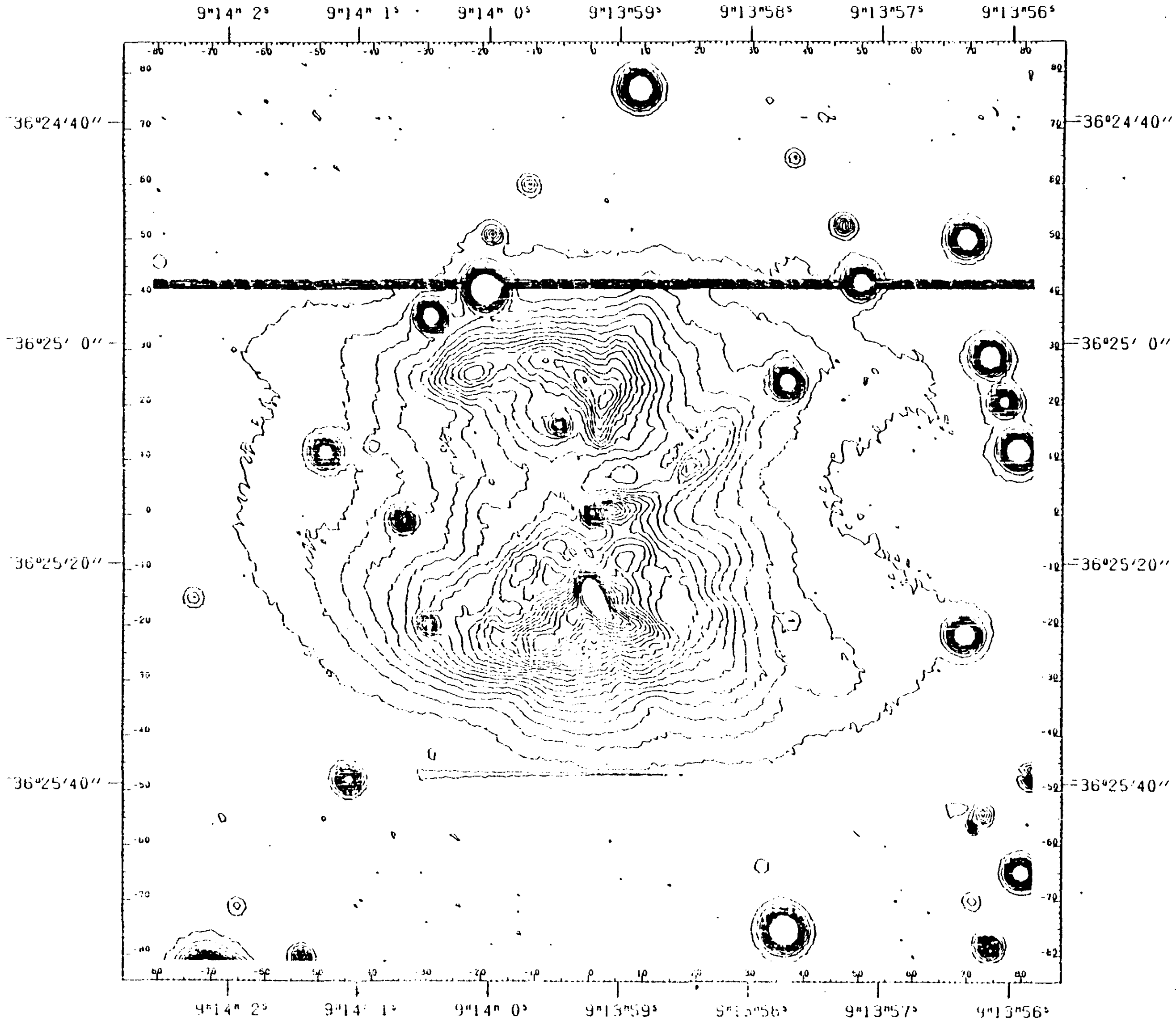

N2818 B

CHANNEL 0
VELOCITY 0.0

SET 811. 1
L: -81 TO 82
M: -81 TO 82

SCALES:
0.360 "/mm
0.360 "/mm

CONTOURS:
300.0 400.0 500.0
600.0 700.0 800.0
900.0 1000. 1100.
1200. 1300. 1400.
1500. 1600. 1700.
1800. 1900. 2000.
2100. 2200. 2300.
2400. 2500.

MINIMUM: 186.0
MAXIMUM: 0.1638E+05

T2 F32

05-OCT-85 20:41:46

Fig A1.9

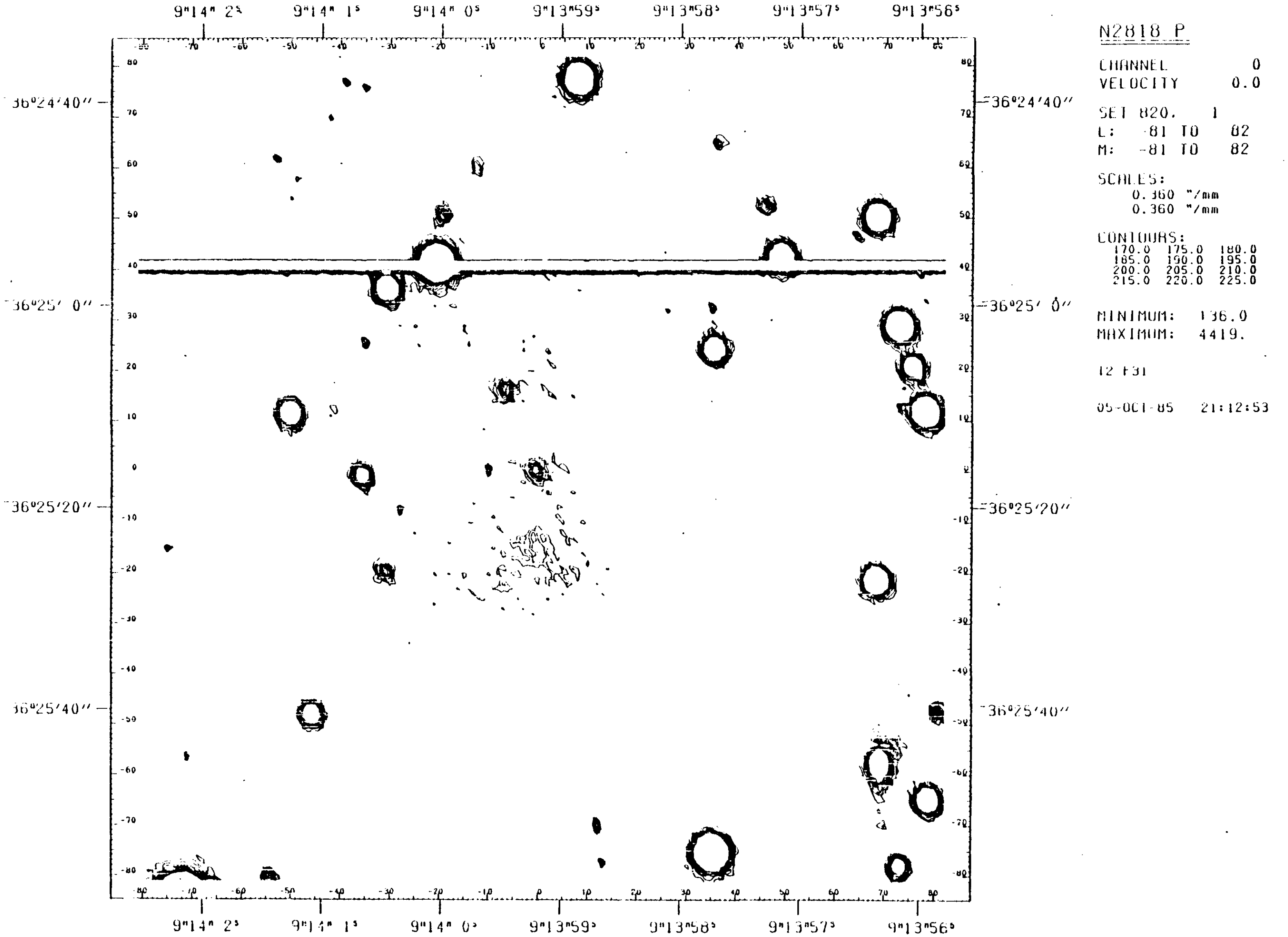
9h14m 2s
9h14m 1s
9h14m 0s
9h13m59s
9h13m58s
9h13m57s
9h13m56s
36°24′40″
36°25′ 0″
36°25′20″
36°25′40″
N2818 P
CHANNEL 0
VELOCITY 0.0
SET 820. 1
L: -81 TO 82
M: -81 TO 82
SCALES:
0.360 "/mm
0.360 "/mm
CONTOURS:
170.0 175.0 180.0
185.0 190.0 195.0
200.0 205.0 210.0
215.0 220.0 225.0
MINIMUM: 136.0
MAXIMUM: 4419.
12 F31
05-OCT-85 21:12:53

Fig A1.10

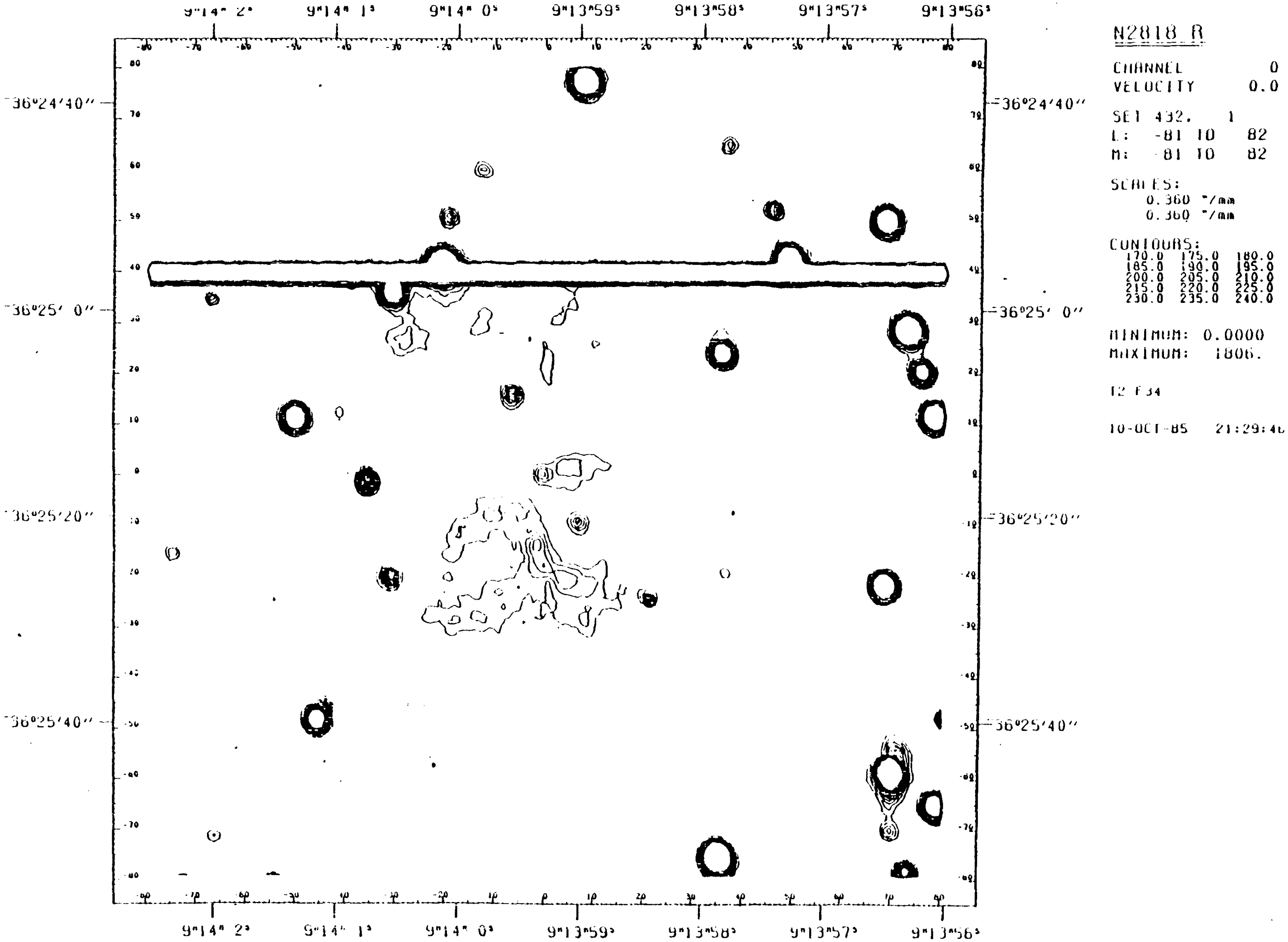
N2818 R
CHANNEL 0
VELOCITY 0.0
SET 432. 1
L: -81 10 82
M: -81 10 82
SCALES:
0.360 "/mm
0.360 "/mm
CONTOURS:
170.0 175.0 180.0
185.0 190.0 195.0
200.0 205.0 210.0
215.0 220.0 225.0
230.0 235.0 240.0
MINIMUM: 0.0000
MAXIMUM: 1806.
10-OCT-85 21:29:46

Fig A1.11

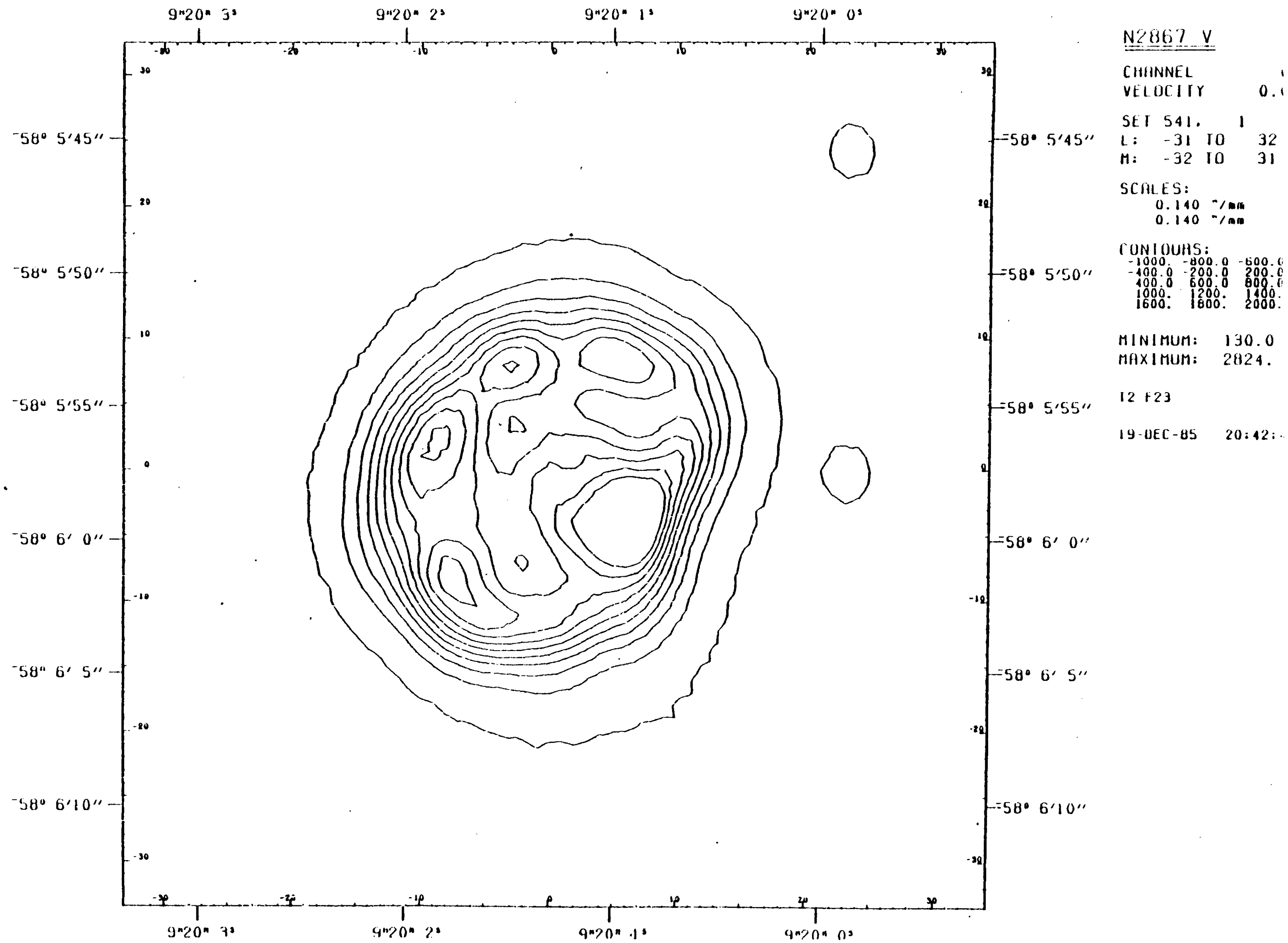
9h20m 3s
9h20m 2s
9h20m 1s
9h20m 0s
-58° 5'45"
-58° 5'50"
-58° 5'55"
-58° 6' 0"
-58° 6' 5"
-58° 6'10"
N2867 V
CHANNEL
VELOCITY 0.
SET 541. 1
L: -31 TO 32
M: -32 TO 31
SCALES:
0.140 "/mm
0.140 "/mm
CONTOURS:
-1000. -800.0 -600.0
-400.0 -200.0 200.0
400.0 600.0 800.0
1000. 1200. 1400.
1600. 1800. 2000.
MINIMUM: 130.0
MAXIMUM: 2824.
I2 F23
19-DEC-85 20:42:

Fig A.12

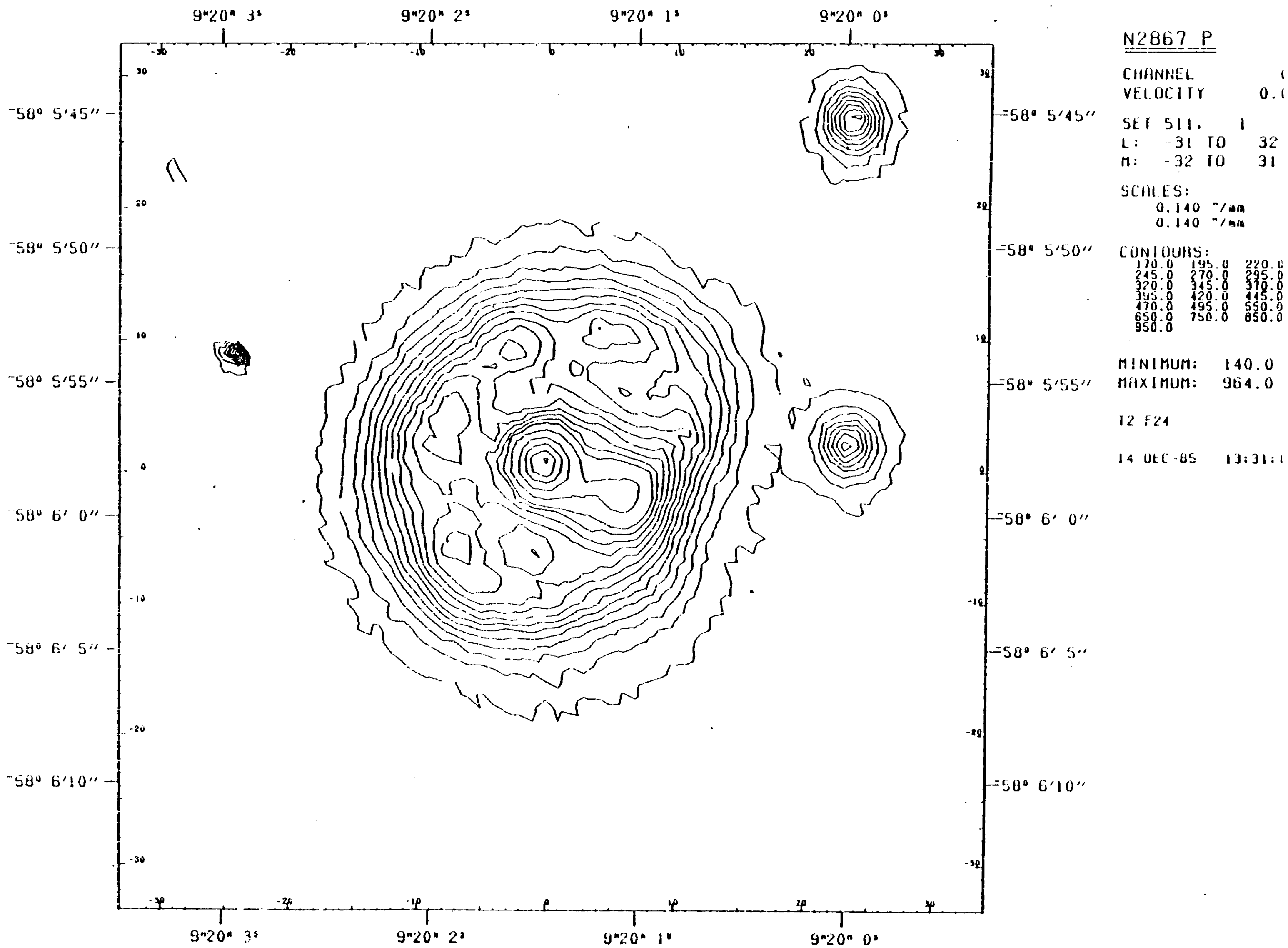

N2867 P
CHANNEL
VELOCITY 0.
SET SII. 1
L: -31 TO 32
M: -32 TO 31
SCALES:
0.140 "/mm
0.140 "/mm
CONTOURS:
170.0 195.0 220.0
245.0 270.0 295.0
320.0 345.0 370.0
395.0 420.0 445.0
470.0 495.0 550.0
650.0 750.0 850.0
950.0
MINIMUM: 140.0
MAXIMUM: 964.0
I2 F24
14 DEC-85 13:31:
9h20m 3s
9h20m 2s
9h20m 1s
9h20m 0s
-58° 5′45″
-58° 5′50″
-58° 5′55″
-58° 6′ 0″
-58° 6′ 5″
-58° 6′10″

Fig A1.13

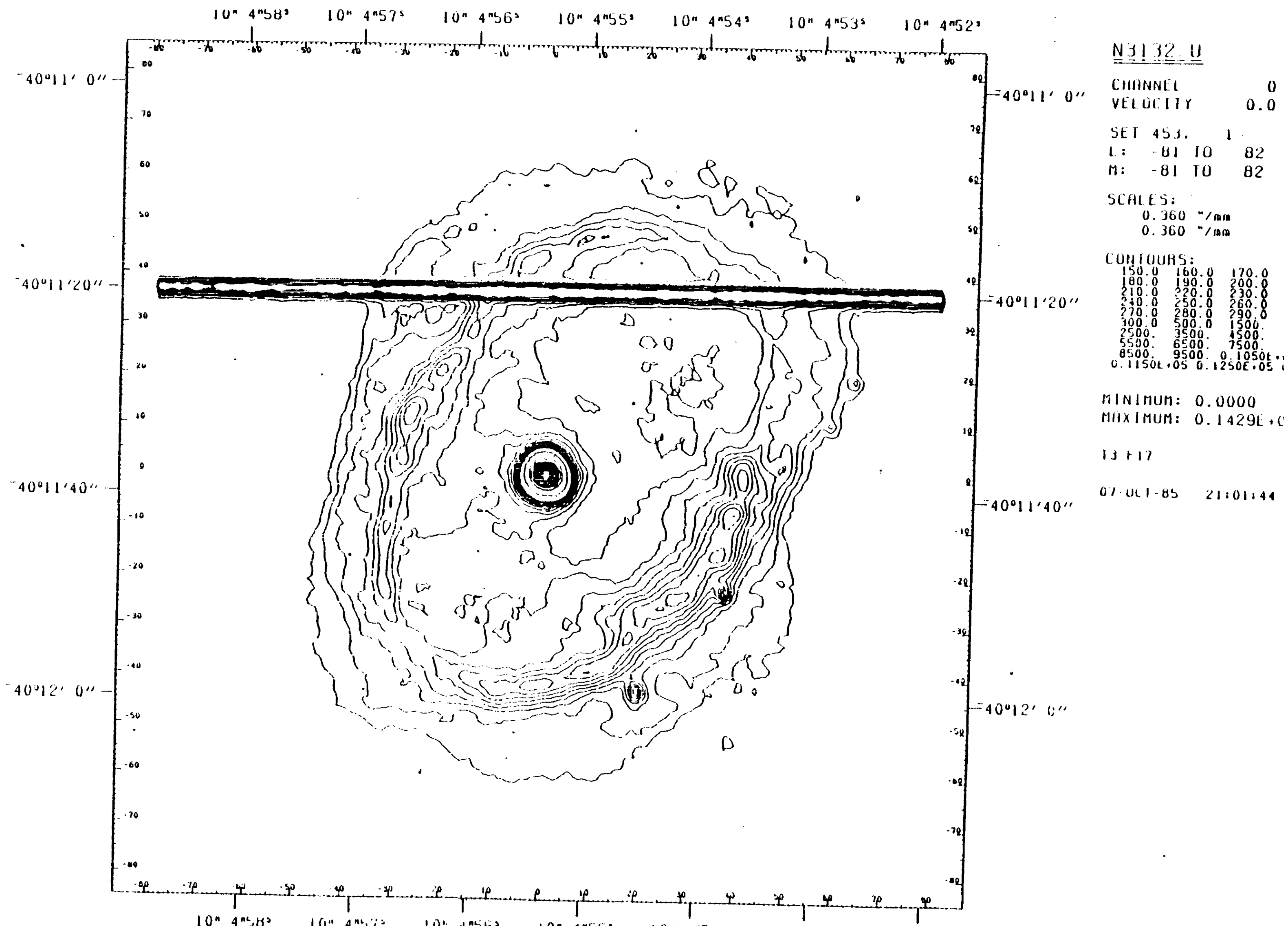
N3132 U
CHANNEL 0
VELOCITY 0.0
SET 453. 1
L: -81 TO 82
M: -81 TO 82
SCALES:
0.360 "/mm
0.360 "/mm
CONTOURS:
150.0 160.0 170.0
180.0 190.0 200.0
210.0 220.0 230.0
240.0 250.0 260.0
270.0 280.0 290.0
300.0 500.0 1500.
2500. 3500. 4500.
5500. 6500. 7500.
8500. 9500. 0.1050E+
0.1150E+05 0.1250E+05
MINIMUM: 0.0000
MAXIMUM: 0.1429E+0
07-OCT-85 21:01:44
-40°11′ 0″
-40°11′20″
-40°11′40″
-40°12′ 0″
10h 4m58s
10h 4m57s
10h 4m56s
10h 4m55s
10h 4m54s
10h 4m53s
10h 4m52s

Fig A1.14

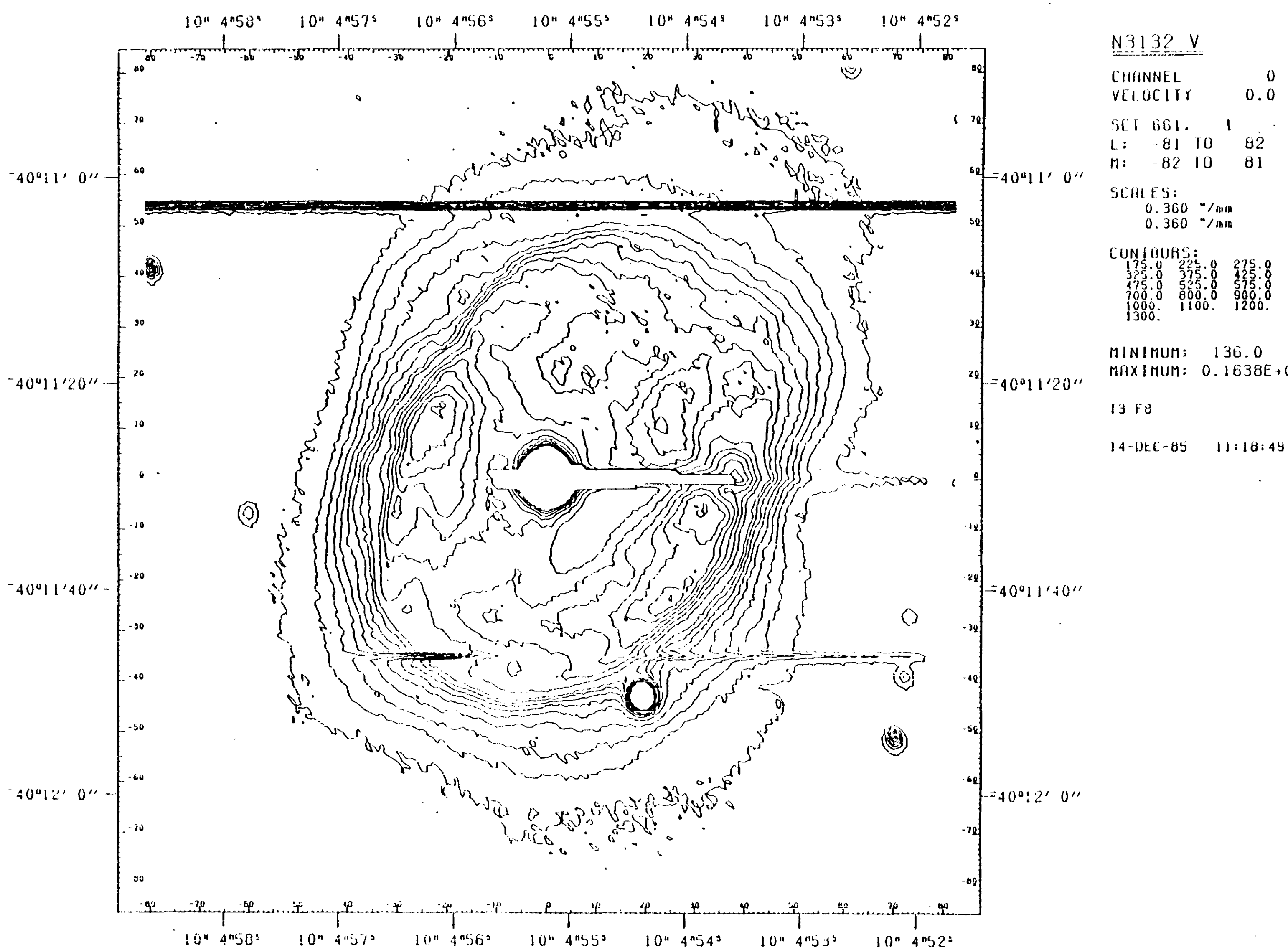
10ʰ 4ᵐ58ˢ 10ʰ 4ᵐ57ˢ 10ʰ 4ᵐ56ˢ 10ʰ 4ᵐ55ˢ 10ʰ 4ᵐ54ˢ 10ʰ 4ᵐ53ˢ 10ʰ 4ᵐ52ˢ
-40°11′ 0″
-40°11′20″
-40°11′40″
-40°12′ 0″
N3132 V
CHANNEL 0
VELOCITY 0.0
SET 661. 1
L: -81 TO 82
M: -82 TO 81
SCALES:
0.360 "/mm
0.360 "/mm
CONTOURS:
175.0 225.0 275.0
325.0 375.0 425.0
475.0 525.0 575.0
700.0 800.0 900.0
1000. 1100. 1200.
1300.
MINIMUM: 136.0
MAXIMUM: 0.1638E+(
T3 F8
14-DEC-85 11:18:49

Fig A1.15

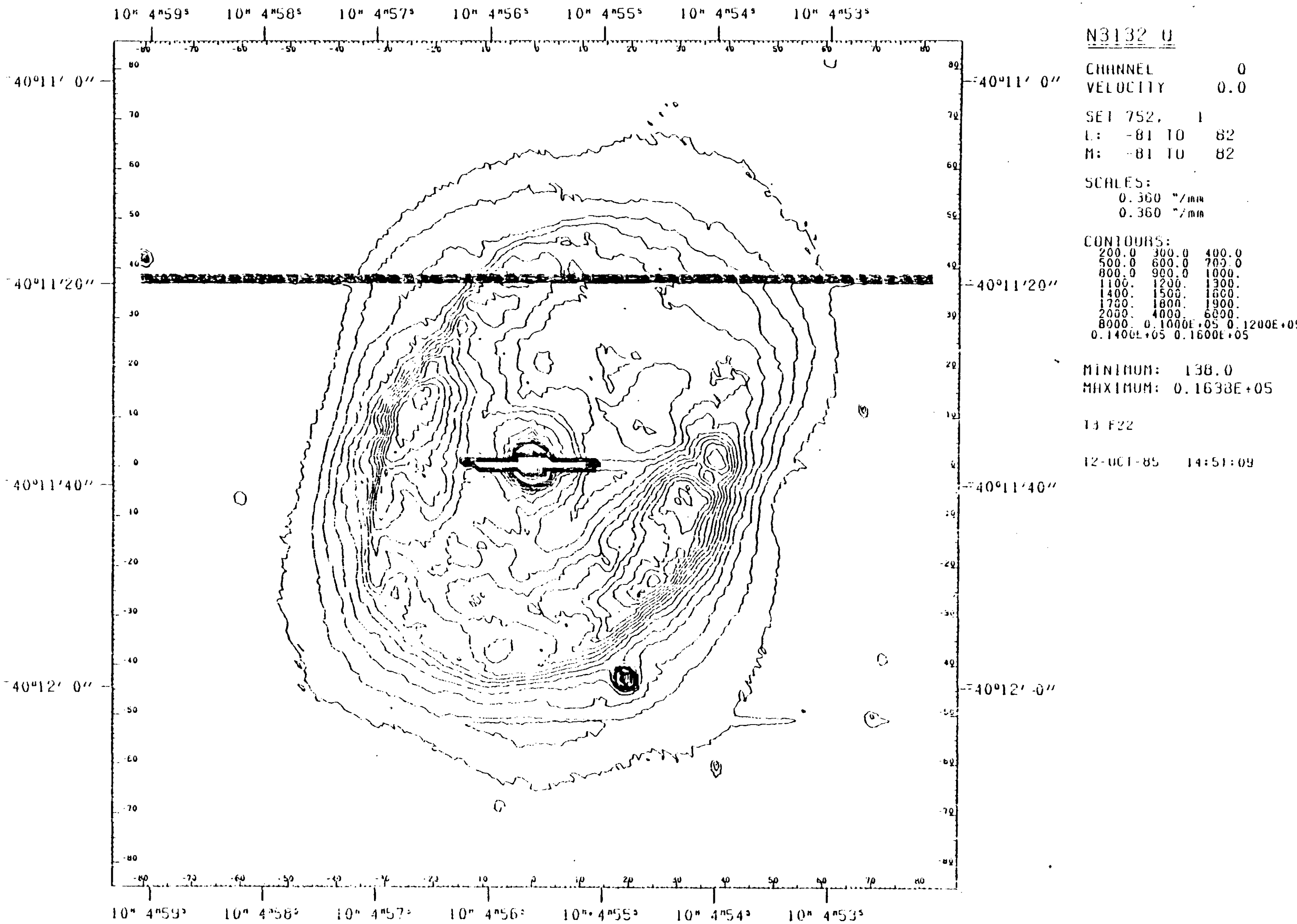
10h 4m59s
10h 4m58s
10h 4m57s
10h 4m56s
10h 4m55s
10h 4m54s
10h 4m53s
40°11′ 0″
40°11′20″
40°11′40″
40°12′ 0″
N3132 U
CHANNEL 0
VELOCITY 0.0
SET 752, 1
L: -81 TO 82
M: -81 TO 82
SCALES:
0.360 "/mm
0.360 "/mm
CONTOURS:
200.0 300.0 400.0
500.0 600.0 700.0
800.0 900.0 1000.
1100. 1200. 1300.
1400. 1500. 1600.
1700. 1800. 1900.
2000. 4000. 6000.
8000. 0.1000E+05 0.1200E+05
0.1400E+05 0.1600E+05
MINIMUM: 138.0
MAXIMUM: 0.1638E+05
T3 F22
12-OCT-85 14:51:09

Fig A1.16

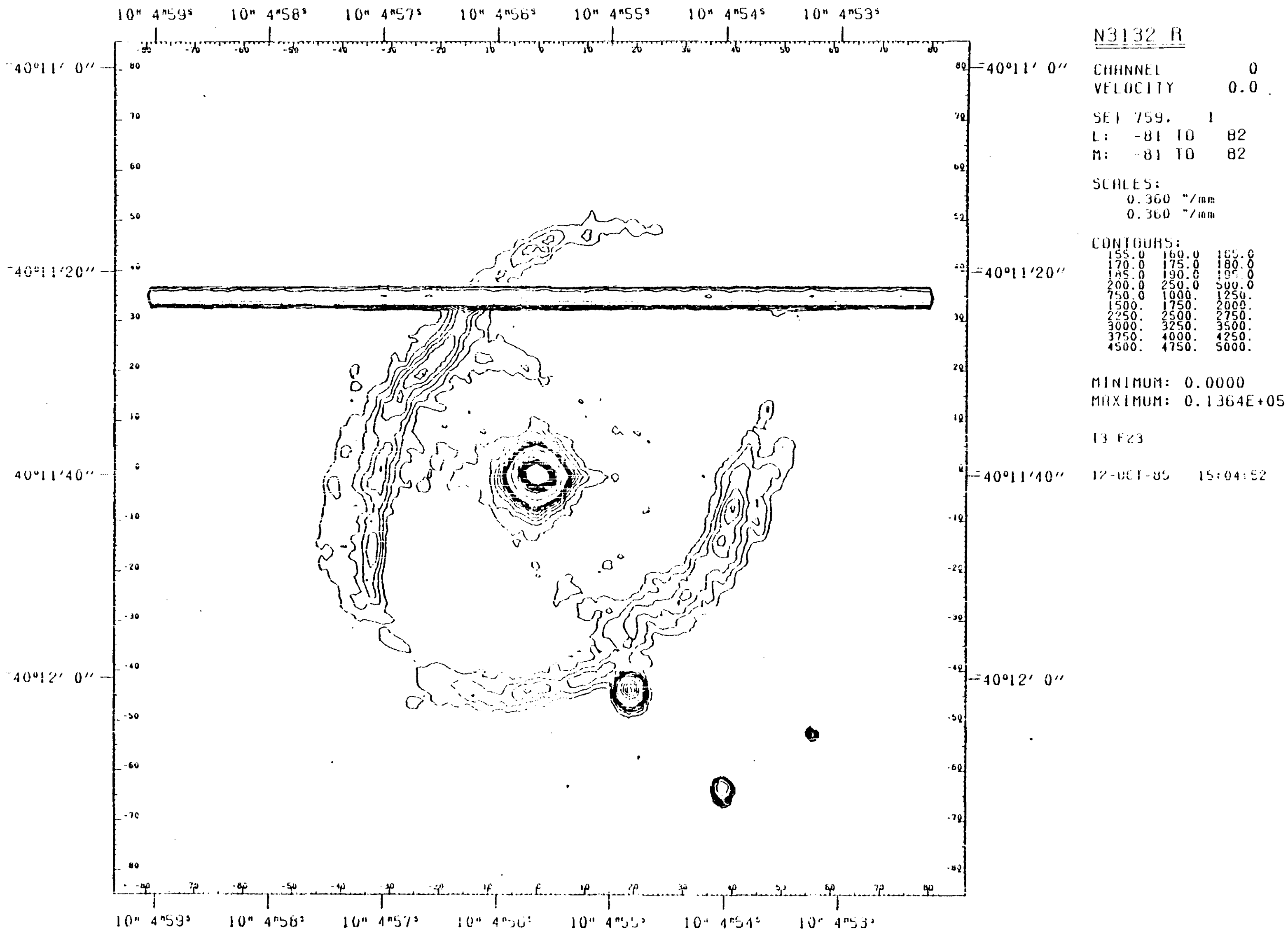
N3132 R
CHANNEL 0
VELOCITY 0.0
SET 759. 1
L: -81 TO 82
M: -81 TO 82
SCALES:
0.360 "/mm
0.360 "/mm
CONTOURS:
155.0 160.0 165.0
170.0 175.0 180.0
185.0 190.0 195.0
200.0 250.0 500.0
750.0 1000. 1250.
1500. 1750. 2000.
2250. 2500. 2750.
3000. 3250. 3500.
3750. 4000. 4250.
4500. 4750. 5000.
MINIMUM: 0.0000
MAXIMUM: 0.1364E+05
12-OCT-85 15:04:52
-40°11′ 0″
-40°11′20″
-40°11′40″
-40°12′ 0″
10h 4m59s
10h 4m58s
10h 4m57s
10h 4m56s
10h 4m55s
10h 4m54s
10h 4m53s

Fig A1.17

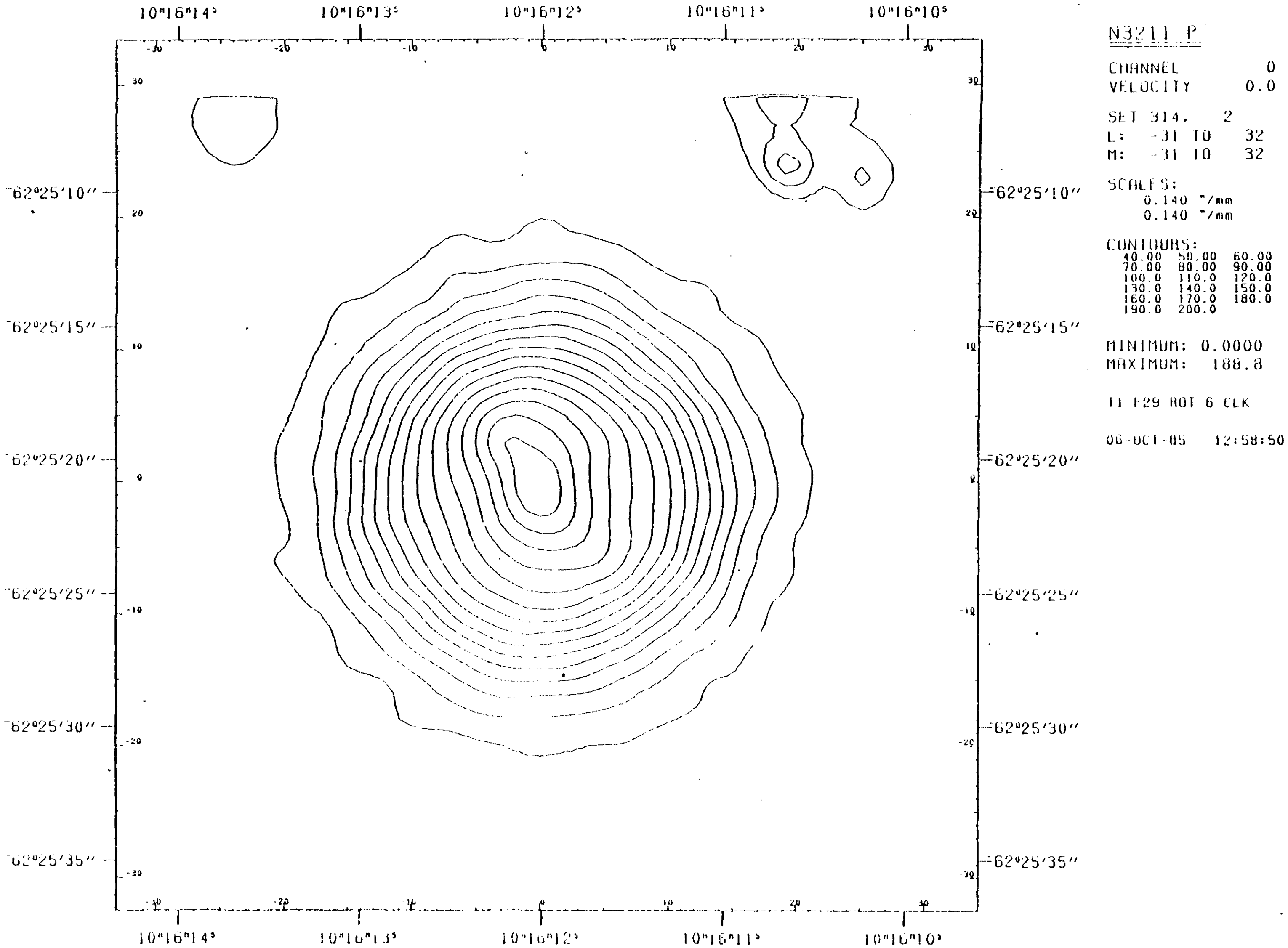
10ʰ16ᵐ14ˢ
10ʰ16ᵐ13ˢ
10ʰ16ᵐ12ˢ
10ʰ16ᵐ11ˢ
10ʰ16ᵐ10ˢ
-62°25′10″
-62°25′15″
-62°25′20″
-62°25′25″
-62°25′30″
-62°25′35″
N3211 P
CHANNEL 0
VELOCITY 0.0
SET 314, 2
L: -31 TO 32
M: -31 TO 32
SCALES:
0.140 "/mm
0.140 "/mm
CONTOURS:
40.00 50.00 60.00
70.00 80.00 90.00
100.0 110.0 120.0
130.0 140.0 150.0
160.0 170.0 180.0
190.0 200.0
MINIMUM: 0.0000
MAXIMUM: 188.8
I1 F29 ROT 6 CLK
06-OCT-85 12:58:50

Fig A1.18

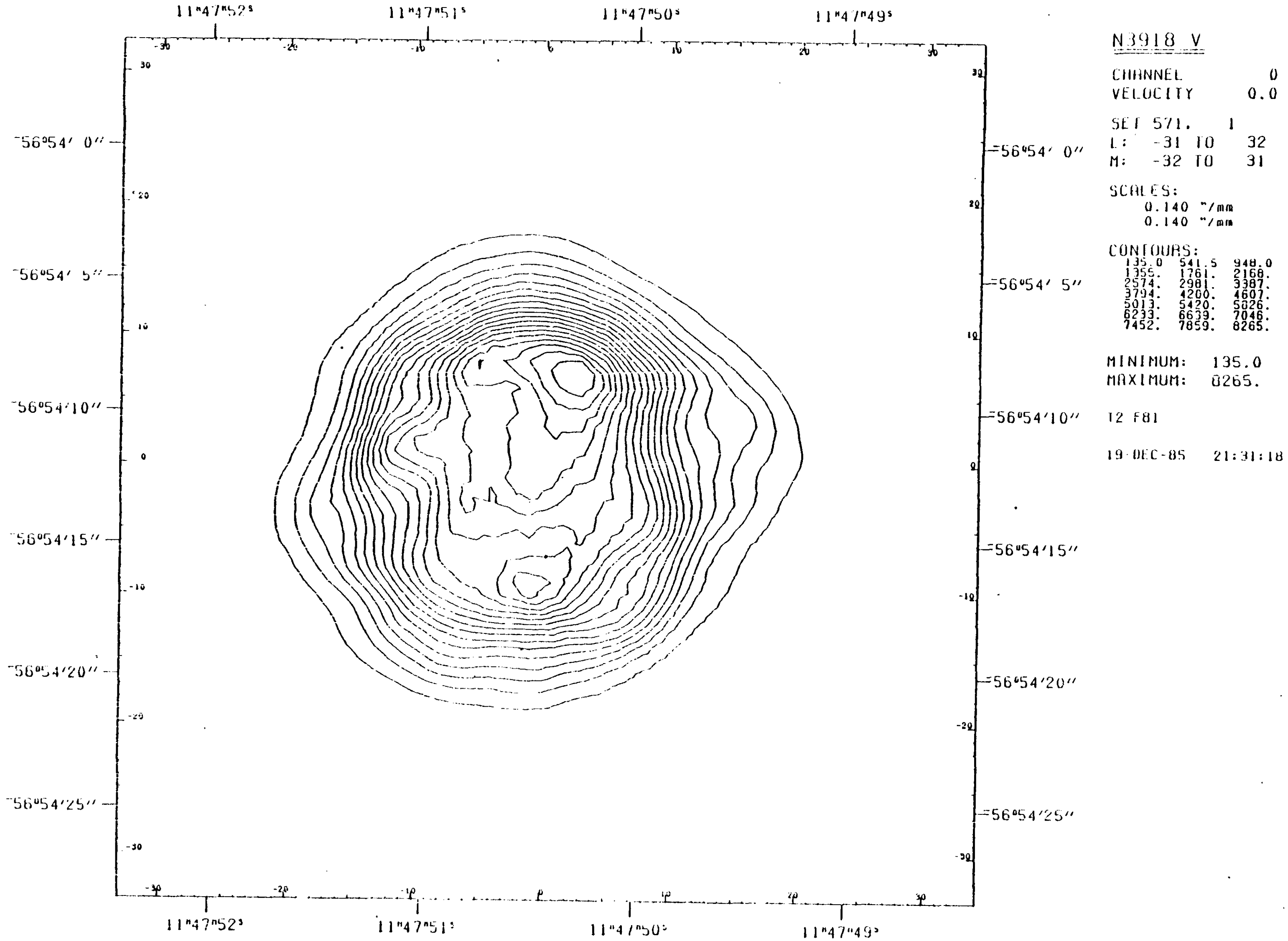
11h47m52s
11h47m51s
11h47m50s
11h47m49s
-56°54′ 0″
-56°54′ 5″
-56°54′10″
-56°54′15″
-56°54′20″
-56°54′25″
N3918 V
CHANNEL 0
VELOCITY 0.0
SET 571. 1
L: -31 TO 32
M: -32 TO 31
SCALES:
0.140 ″/mm
0.140 ″/mm
CONTOURS:
135.0 541.5 948.0
1355. 1761. 2168.
2574. 2981. 3387.
3794. 4200. 4607.
5013. 5420. 5826.
6233. 6639. 7046.
7452. 7859. 8265.
MINIMUM: 135.0
MAXIMUM: 8265.
12 F81
19-DEC-85 21:31:18

Fig A1.19

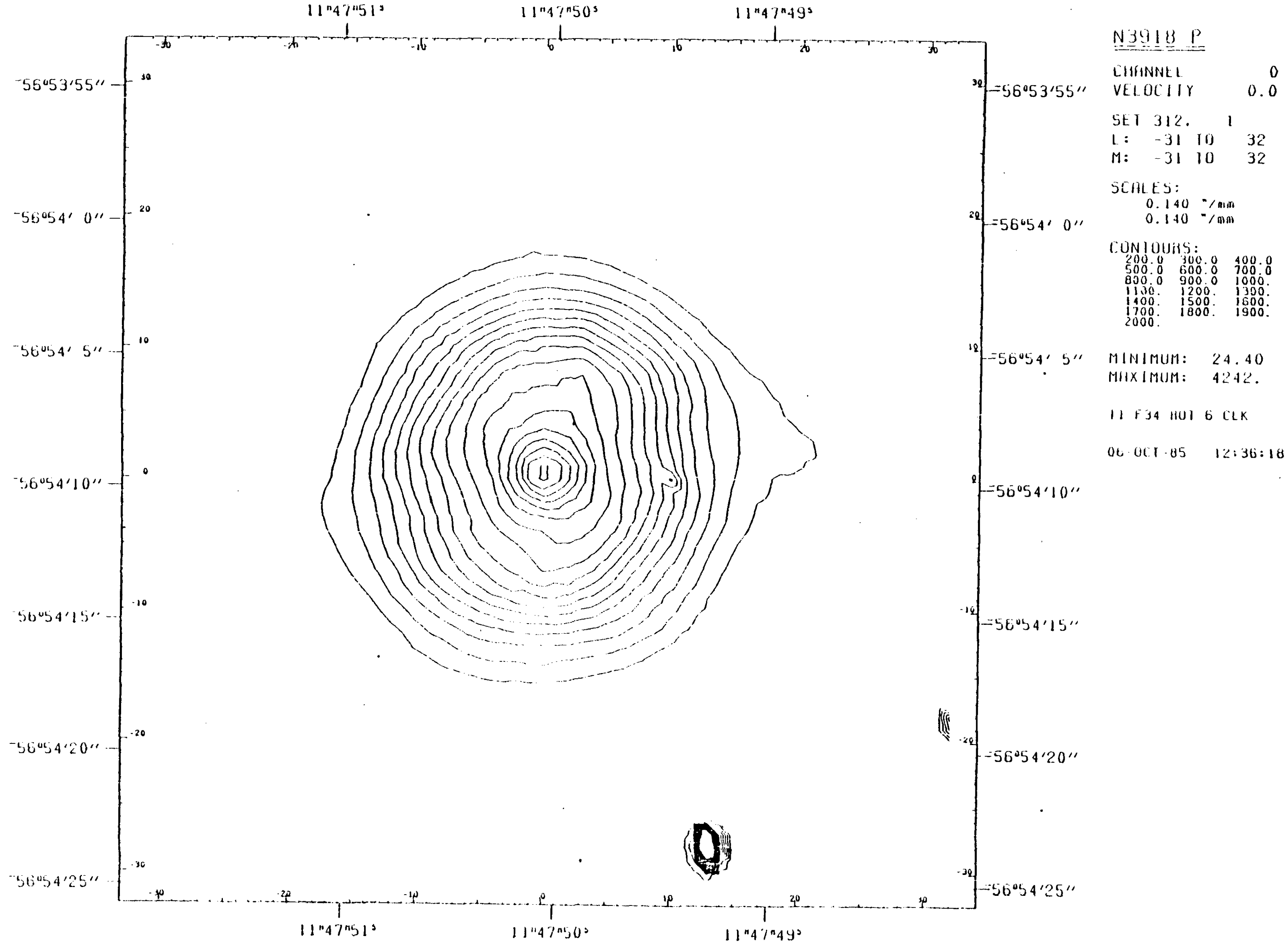
11ʰ47ᵐ51ˢ
11ʰ47ᵐ50ˢ
11ʰ47ᵐ49ˢ
-56°53′55″
-56°54′ 0″
-56°54′ 5″
-56°54′10″
-56°54′15″
-56°54′20″
-56°54′25″
N3918 P
CHANNEL 0
VELOCITY 0.0
SET 312. 1
L: -31 TO 32
M: -31 TO 32
SCALES:
0.140 ″/mm
0.140 ″/mm
CONTOURS:
200.0 300.0 400.0
500.0 600.0 700.0
800.0 900.0 1000.
1100. 1200. 1300.
1400. 1500. 1600.
1700. 1800. 1900.
2000.
MINIMUM: 24.40
MAXIMUM: 4242.
II F34 HOT 6 CLK
06-OCT-85 12:36:18

Fig A1.20

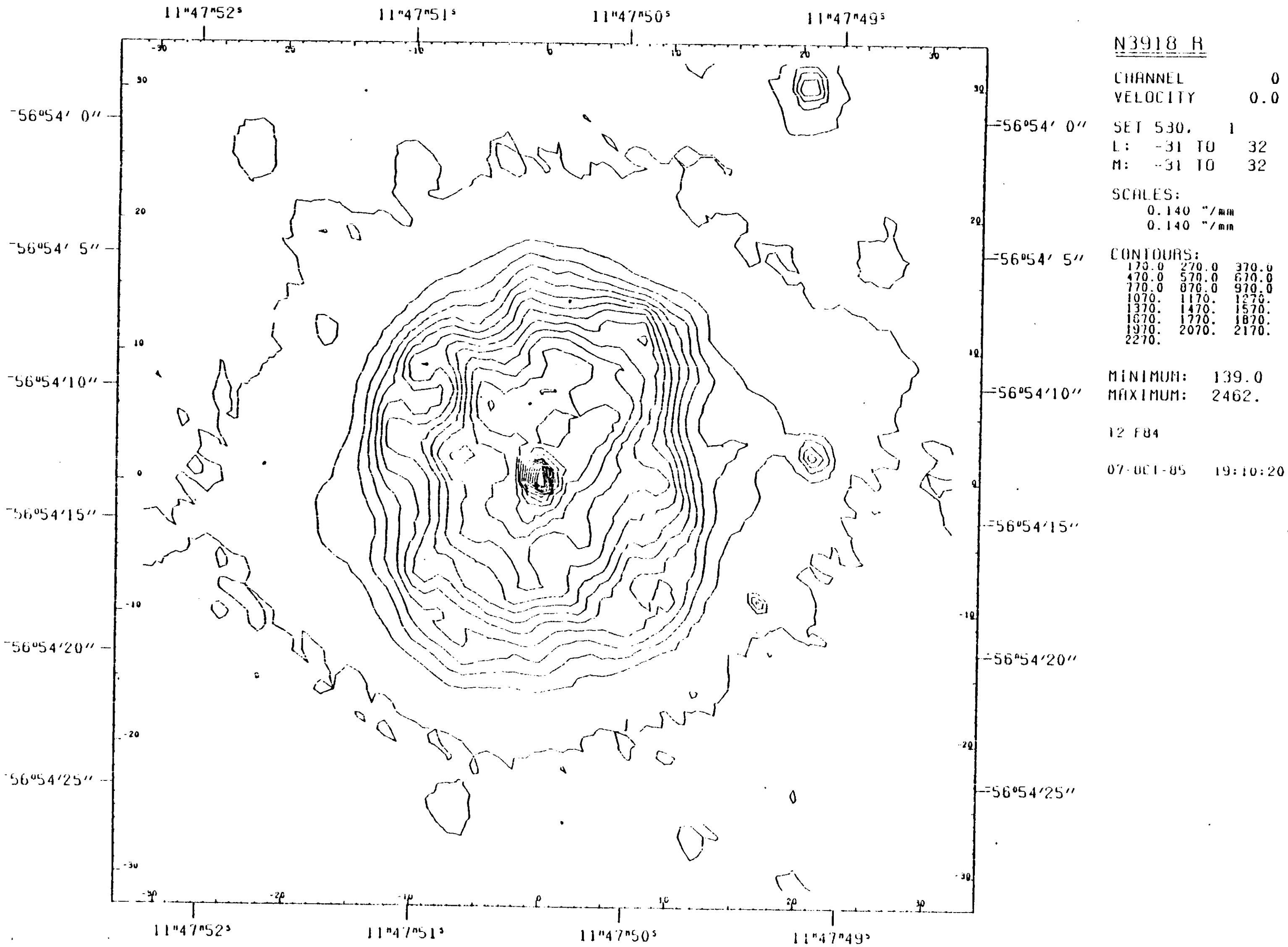

11h47m52s
11h47m51s
11h47m50s
11h47m49s
-56°54′ 0″
-56°54′ 5″
-56°54′10″
-56°54′15″
-56°54′20″
-56°54′25″
N3918 R
CHANNEL 0
VELOCITY 0.0
SET 530, 1
L: -31 TO 32
M: -31 TO 32
SCALES:
0.140 "/mm
0.140 "/mm
CONTOURS:
170.0 270.0 370.0
470.0 570.0 670.0
770.0 870.0 970.0
1070. 1170. 1270.
1370. 1470. 1570.
1670. 1770. 1870.
1970. 2070. 2170.
2270.
MINIMUM: 139.0
MAXIMUM: 2462.
12 F84
07-OCT-85 19:10:20

Fig A1.21

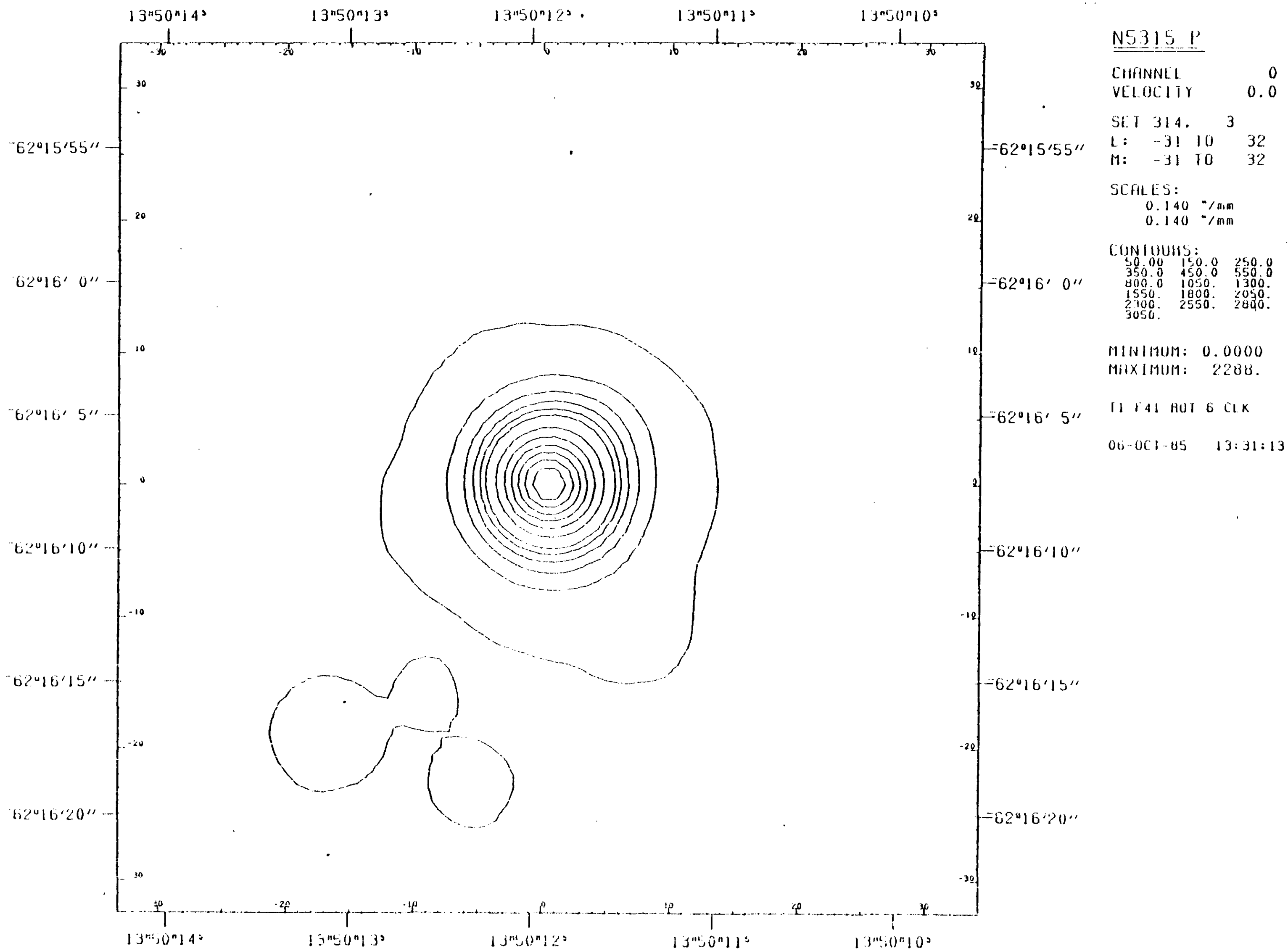
13ʰ50ᵐ14ˢ
13ʰ50ᵐ13ˢ
13ʰ50ᵐ12ˢ
13ʰ50ᵐ11ˢ
13ʰ50ᵐ10ˢ
-62°15′55″
-62°16′ 0″
-62°16′ 5″
-62°16′10″
-62°16′15″
-62°16′20″
N5315 P
CHANNEL 0
VELOCITY 0.0
SET 314. 3
L: -31 TO 32
M: -31 TO 32
SCALES:
0.140 "/mm
0.140 "/mm
CONTOURS:
50.00 150.0 250.0
350.0 450.0 550.0
800.0 1050. 1300.
1550. 1800. 2050.
2300. 2550. 2800.
3050.
MINIMUM: 0.0000
MAXIMUM: 2288.
TI F41 ROT 6 CLK
06-OCT-85 13:31:13

Fig A1.22

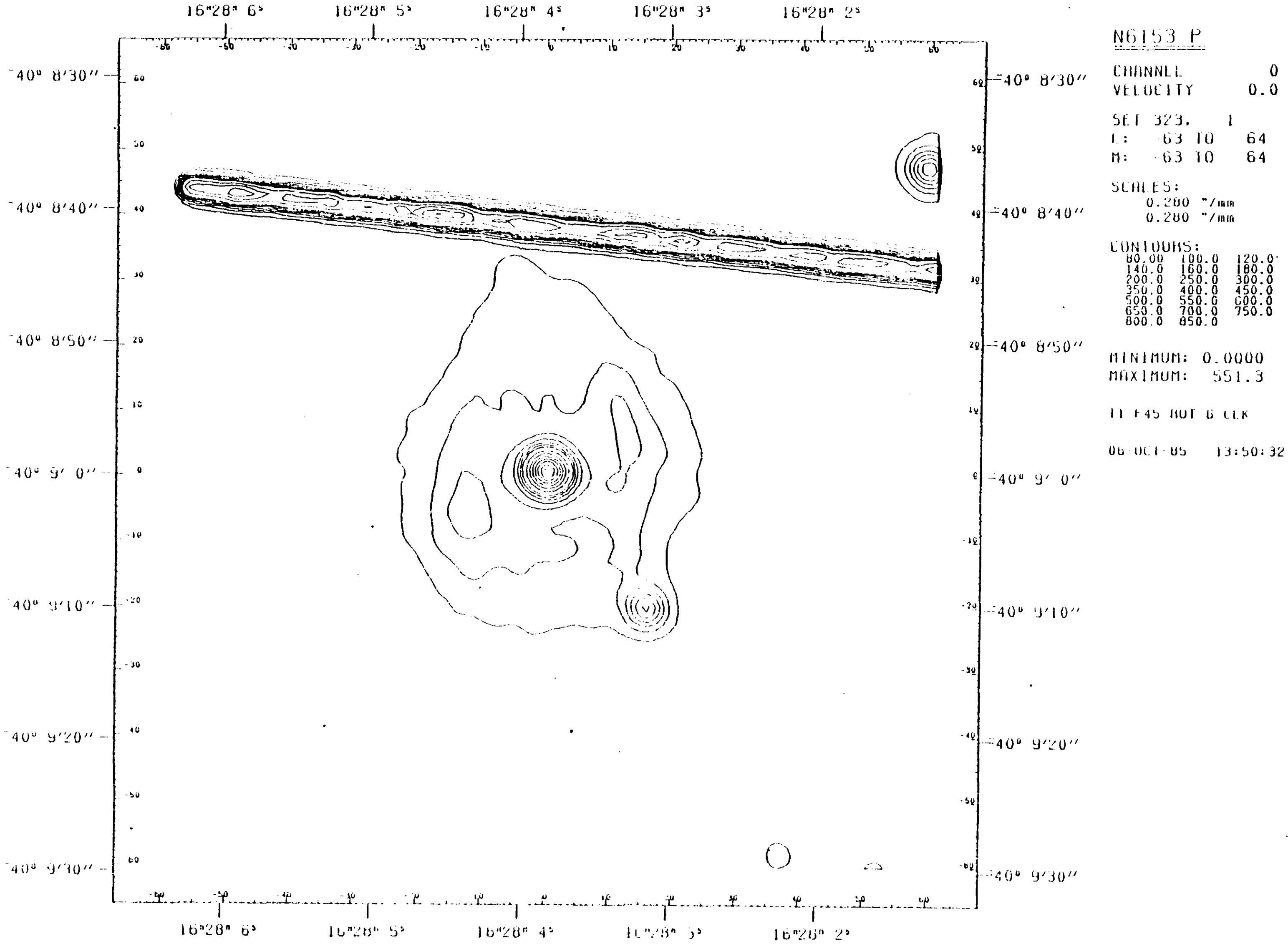
16h28m 6s
16h28m 5s
16h28m 4s
16h28m 3s
16h28m 2s
-40° 8′30″
-40° 8′40″
-40° 8′50″
-40° 9′ 0″
-40° 9′10″
-40° 9′20″
-40° 9′30″
N6153 P
CHANNEL 0
VELOCITY 0.0
SET 323. 1
L: -63 TO 64
M: -63 TO 64
SCALES:
0.280 "/mm
0.280 "/mm
CONTOURS:
80.00 100.0 120.0
140.0 160.0 180.0
200.0 250.0 300.0
350.0 400.0 450.0
500.0 550.0 600.0
650.0 700.0 750.0
800.0 850.0
MINIMUM: 0.0000
MAXIMUM: 551.3
06-OCT-85 13:50:32

Fig A1.23

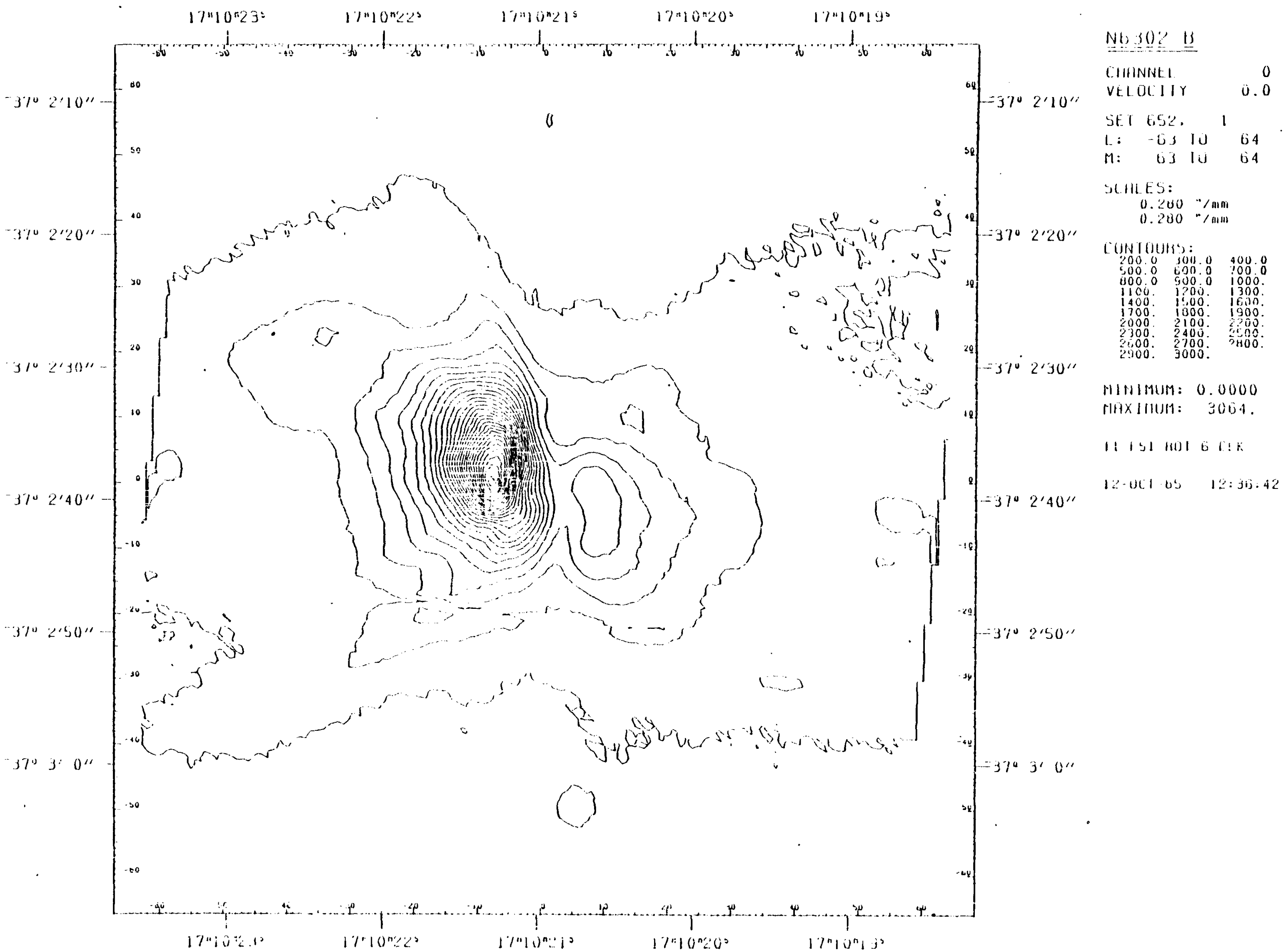
17h10m23s
17h10m22s
17h10m21s
17h10m20s
17h10m19s
-37° 2′10″
-37° 2′20″
-37° 2′30″
-37° 2′40″
-37° 2′50″
-37° 3′ 0″
N6302 B
CHANNEL 0
VELOCITY 0.0
SET 652. 1
L: -63 TO 64
M: 63 TO 64
SCALES:
0.280 "/mm
0.280 "/mm
CONTOURS:
200.0 300.0 400.0
500.0 600.0 700.0
800.0 900.0 1000.
1100. 1200. 1300.
1400. 1500. 1600.
1700. 1800. 1900.
2000. 2100. 2200.
2300. 2400. 2500.
2600. 2700. 2800.
2900. 3000.
MINIMUM: 0.0000
MAXIMUM: 3064.
12-OCT-85 12:36:42

Fig A1.24

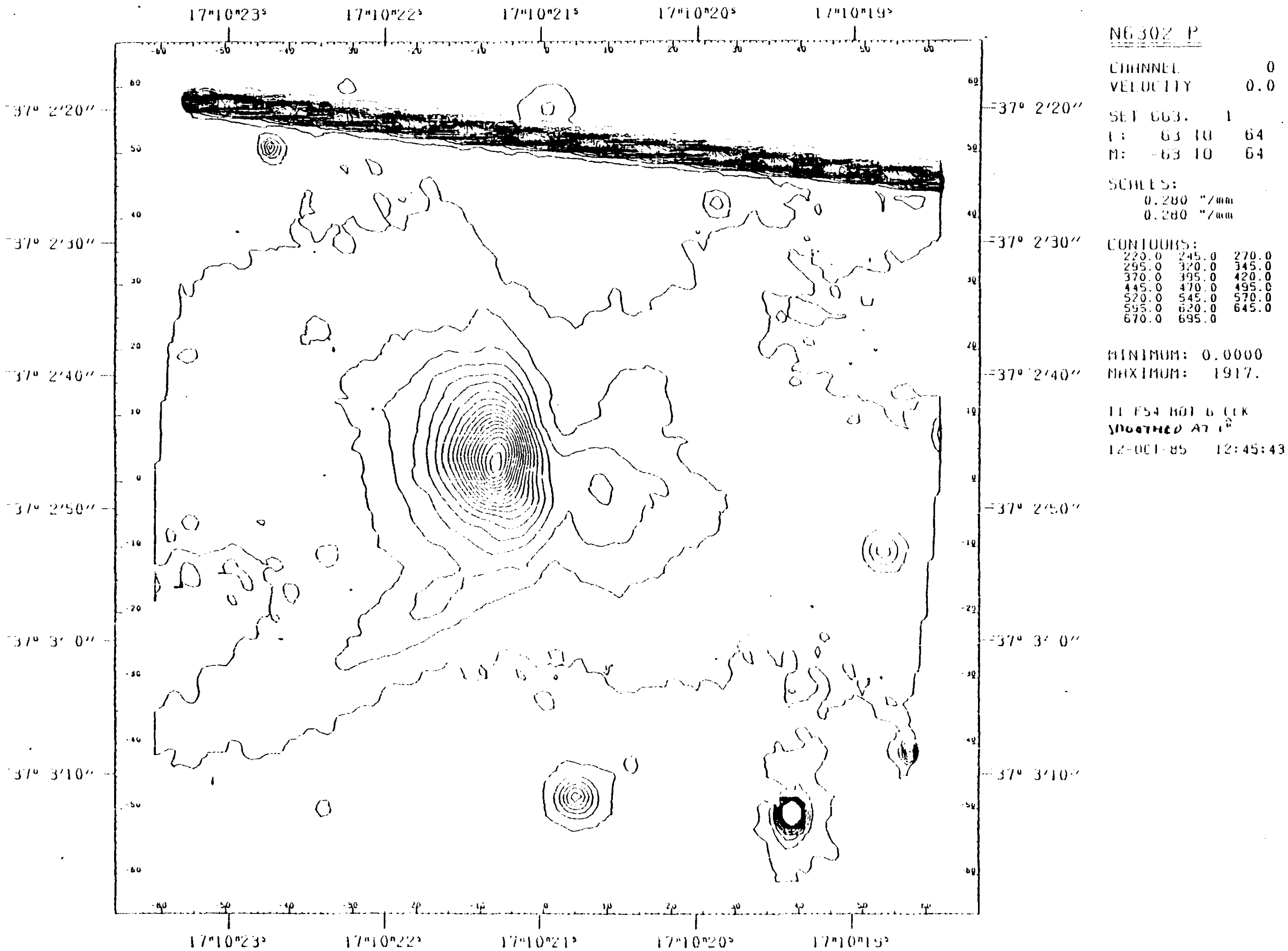
17ʰ10ᵐ23ˢ
17ʰ10ᵐ22ˢ
17ʰ10ᵐ21ˢ
17ʰ10ᵐ20ˢ
17ʰ10ᵐ19ˢ
-37° 2′20″
-37° 2′30″
-37° 2′40″
-37° 2′50″
-37° 3′ 0″
-37° 3′10″
NG302 P
CHANNEL 0
VELOCITY 0.0
SET 663. 1
L: 63 10 64
M: -63 10 64
SCALES:
0.280 "/mm
0.280 "/mm
CONTOURS:
220.0 245.0 270.0
295.0 320.0 345.0
370.0 395.0 420.0
445.0 470.0 495.0
520.0 545.0 570.0
595.0 620.0 645.0
670.0 695.0
MINIMUM: 0.0000
MAXIMUM: 1917.
12-OCT-85 12:45:43

Fig A1.25

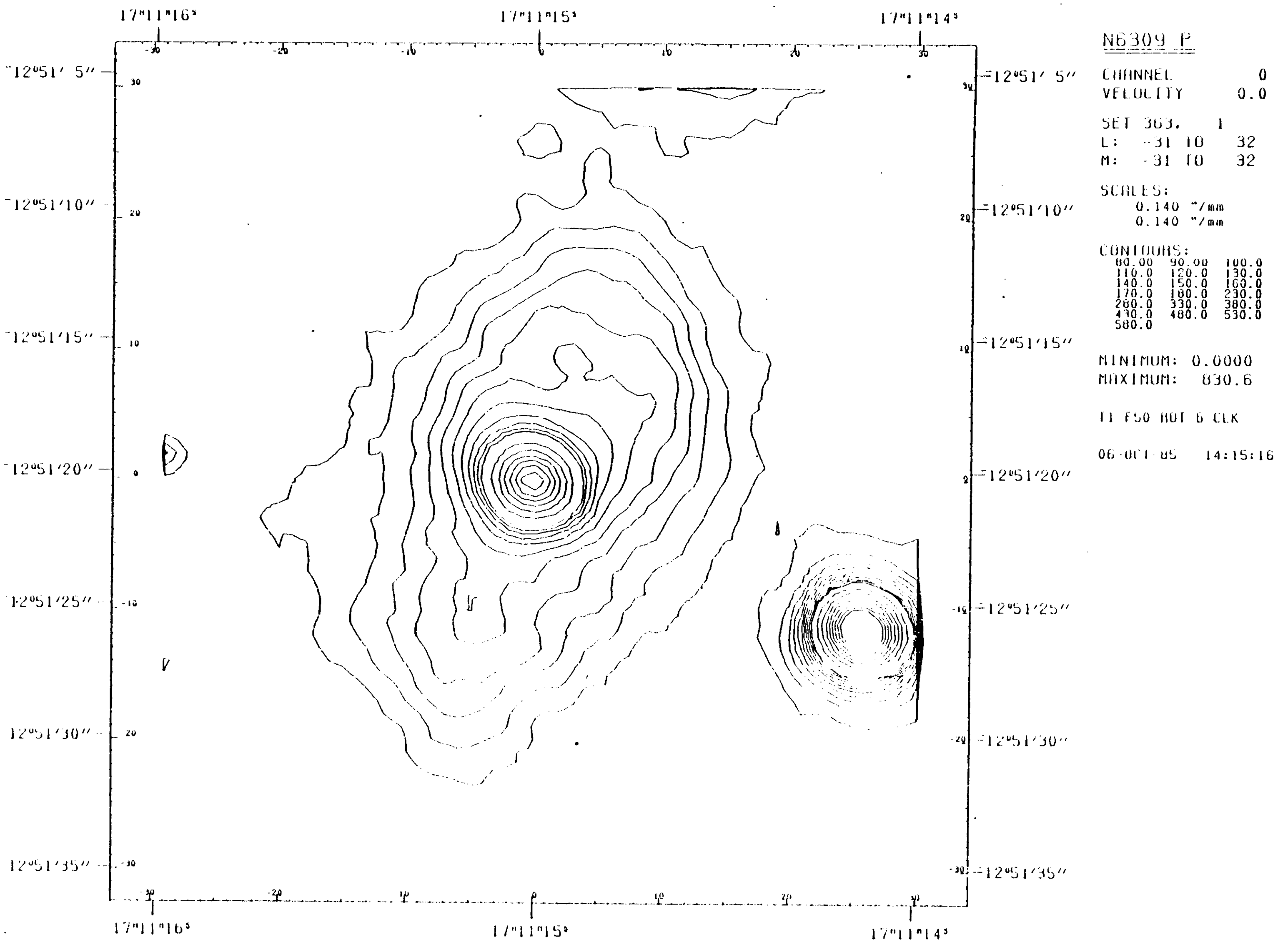
17h11m16s
17h11m15s
17h11m14s
-12°51′5″
-12°51′10″
-12°51′15″
-12°51′20″
-12°51′25″
-12°51′30″
-12°51′35″
N6309 P
CHANNEL 0
VELOCITY 0.0
SET 363, 1
L: -31 TO 32
M: -31 TO 32
SCALES:
0.140 "/mm
0.140 "/mm
CONTOURS:
80.00 90.00 100.0
110.0 120.0 130.0
140.0 150.0 160.0
170.0 180.0 230.0
280.0 330.0 380.0
430.0 480.0 530.0
580.0
MINIMUM: 0.0000
MAXIMUM: 830.6
II F50 HOT 6 CLK
06-OCT-85 14:15:16

Fig A1.26

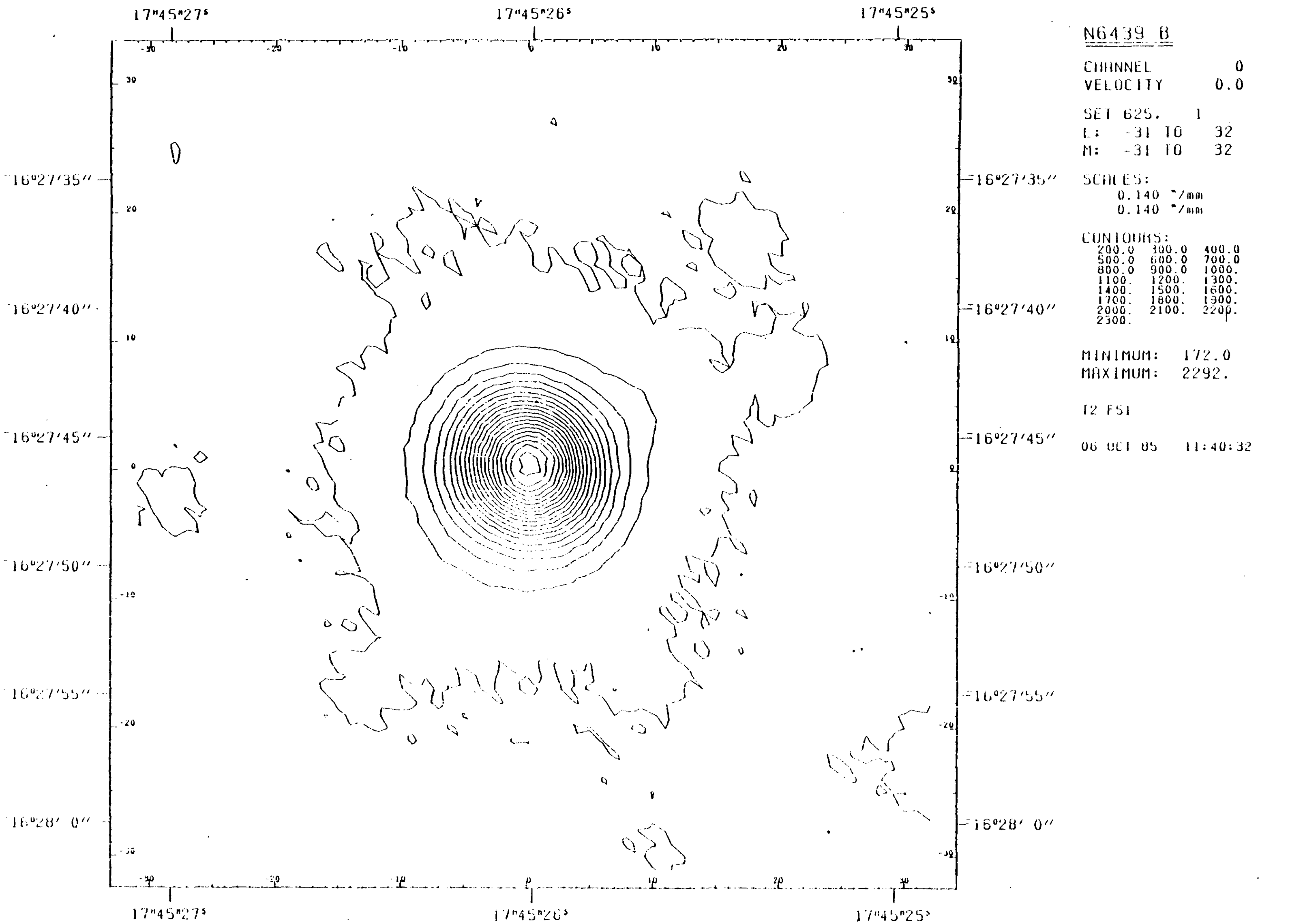
17ʰ45ᵐ27ˢ
17ʰ45ᵐ26ˢ
17ʰ45ᵐ25ˢ
-16°27′35″
-16°27′40″
-16°27′45″
-16°27′50″
-16°27′55″
-16°28′ 0″
N6439 B
CHANNEL 0
VELOCITY 0.0
SET 625. 1
L: -31 TO 32
M: -31 TO 32
SCALES:
0.140 "/mm
0.140 "/mm
CONTOURS:
200.0 300.0 400.0
500.0 600.0 700.0
800.0 900.0 1000.
1100. 1200. 1300.
1400. 1500. 1600.
1700. 1800. 1900.
2000. 2100. 2200.
2300.
MINIMUM: 172.0
MAXIMUM: 2292.
T2 FS1
06 OCT 85 11:40:32

Fig A1.27

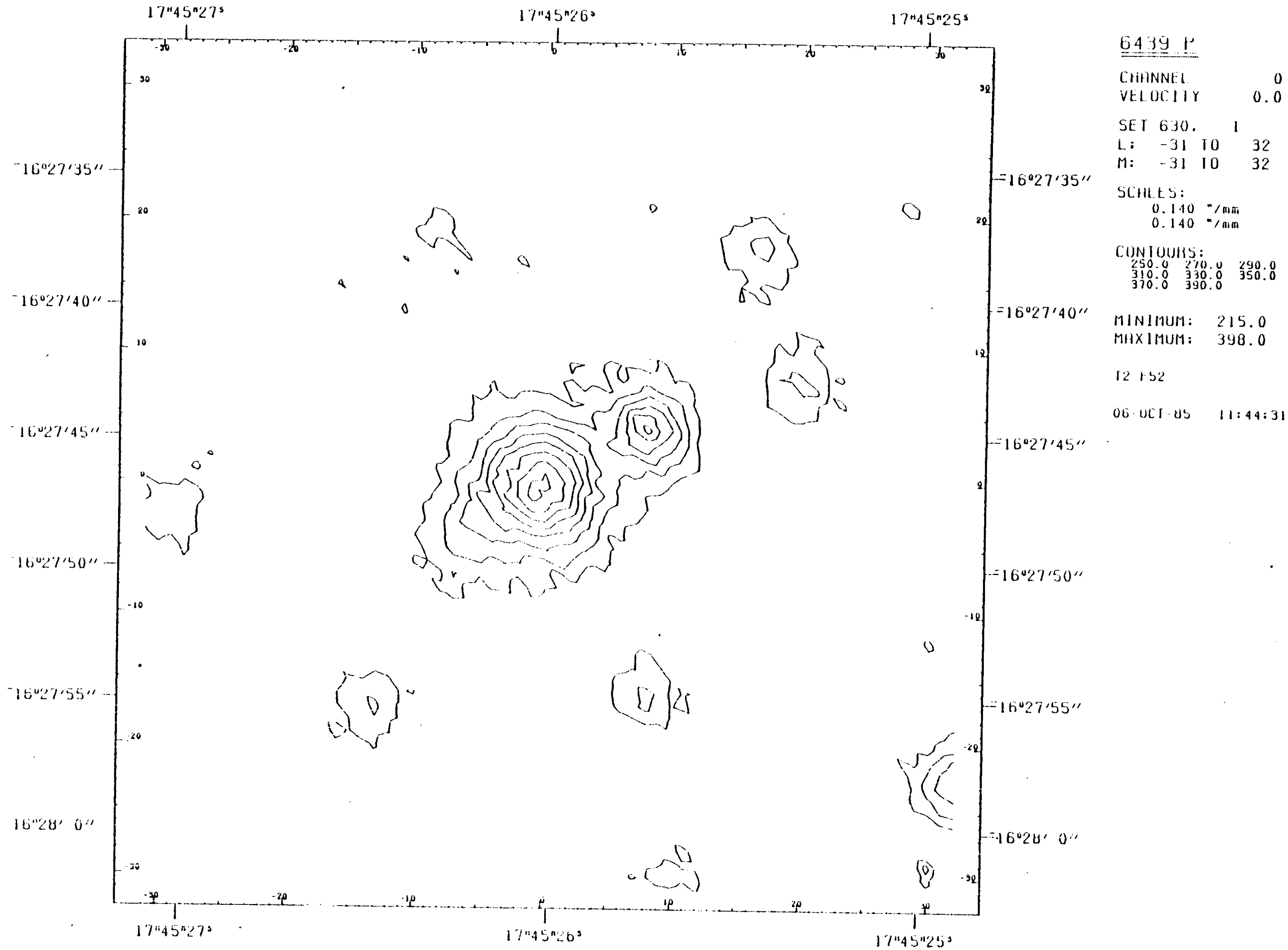

17ʰ45ᵐ27ˢ
17ʰ45ᵐ26ˢ
17ʰ45ᵐ25ˢ
-16°27′35″
-16°27′40″
-16°27′45″
-16°27′50″
-16°27′55″
-16°28′ 0″
6439 P
CHANNEL 0
VELOCITY 0.0
SET 630. 1
L: -31 TO 32
M: -31 TO 32
SCALES:
0.140 ″/mm
0.140 ″/mm
CONTOURS:
250.0 270.0 290.0
310.0 330.0 350.0
370.0 390.0
MINIMUM: 215.0
MAXIMUM: 398.0
I2 F52
06-OCT-85 11:44:31

Fig A1.28

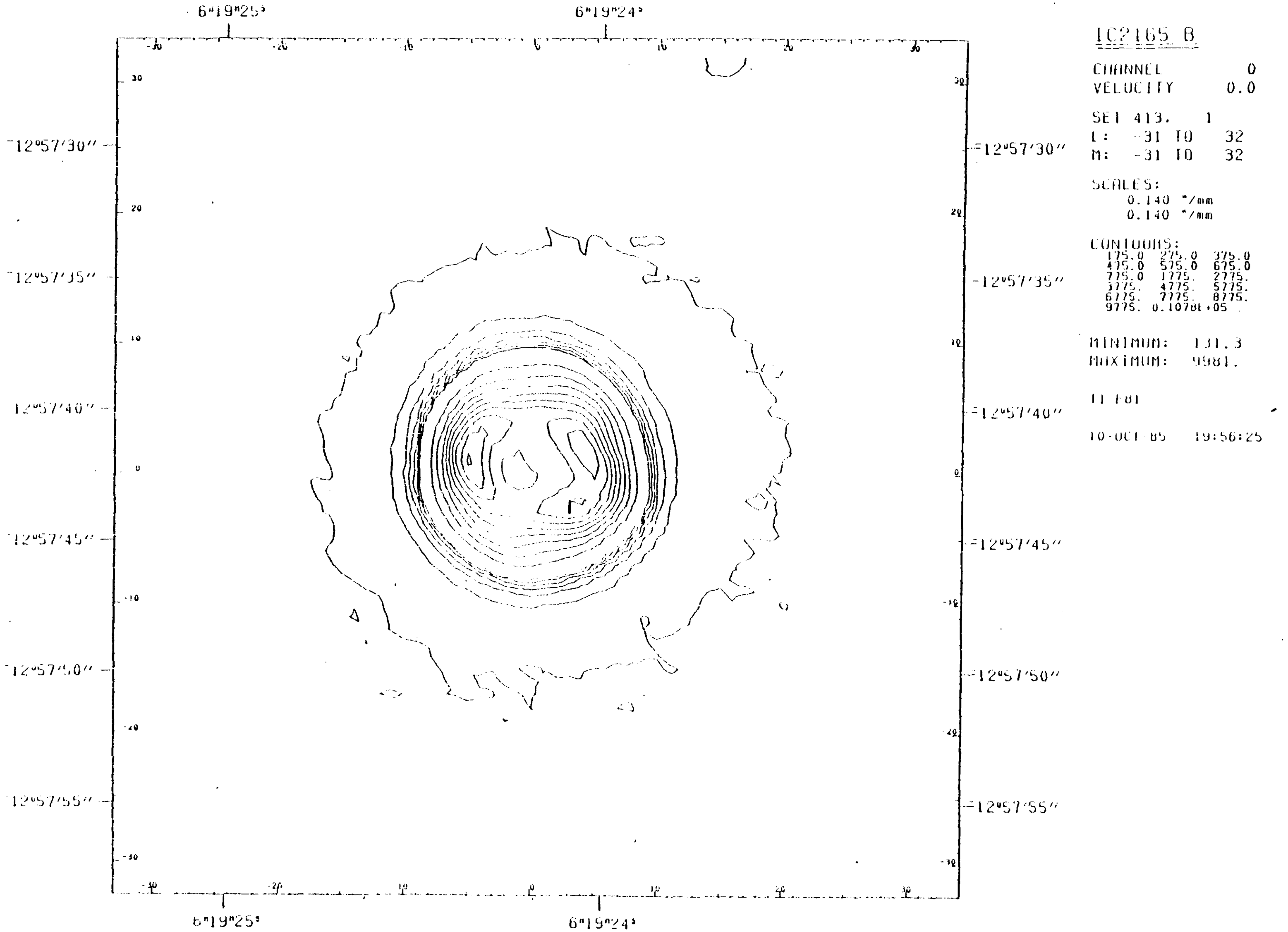

6h19m25s
6h19m24s
-12°57′30″
-12°57′35″
-12°57′40″
-12°57′45″
-12°57′50″
-12°57′55″
IC2165 B
CHANNEL 0
VELOCITY 0.0
SET 413. 1
L: -31 TO 32
M: -31 TO 32
SCALES:
0.140 "/mm
0.140 "/mm
CONTOURS:
175.0 275.0 375.0
475.0 575.0 675.0
775.0 1775. 2775.
3775. 4775. 5775.
6775. 7775. 8775.
9775. 0.1078E+05
MINIMUM: 131.3
MAXIMUM: 9981.
10-OCT-85 19:56:25

Fig A1.31

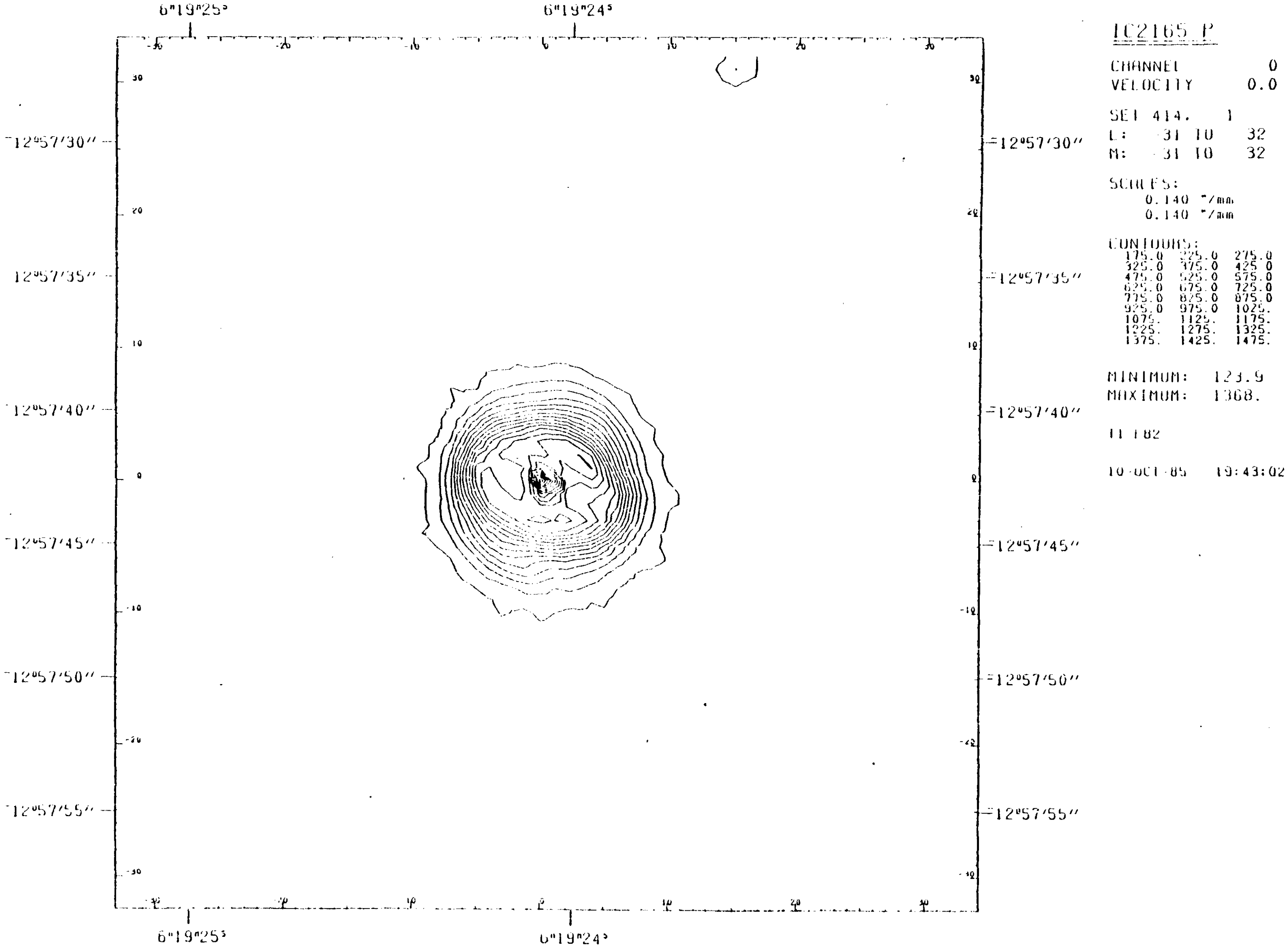
6h19m25s
6h19m24s
-12°57'30"
-12°57'35"
-12°57'40"
-12°57'45"
-12°57'50"
-12°57'55"
IC2165 P
CHANNEL 0
VELOCITY 0.0
SET 414. 1
L: -31 10 32
M: -31 10 32
SCALES:
0.140 "/mm
0.140 "/mm
CONTOURS:
175.0 225.0 275.0
325.0 375.0 425.0
475.0 525.0 575.0
625.0 675.0 725.0
775.0 825.0 875.0
925.0 975.0 1025.
1075. 1125. 1175.
1225. 1275. 1325.
1375. 1425. 1475.
MINIMUM: 123.9
MAXIMUM: 1368.
10-OCT-85 19:43:02

Fig A1.32

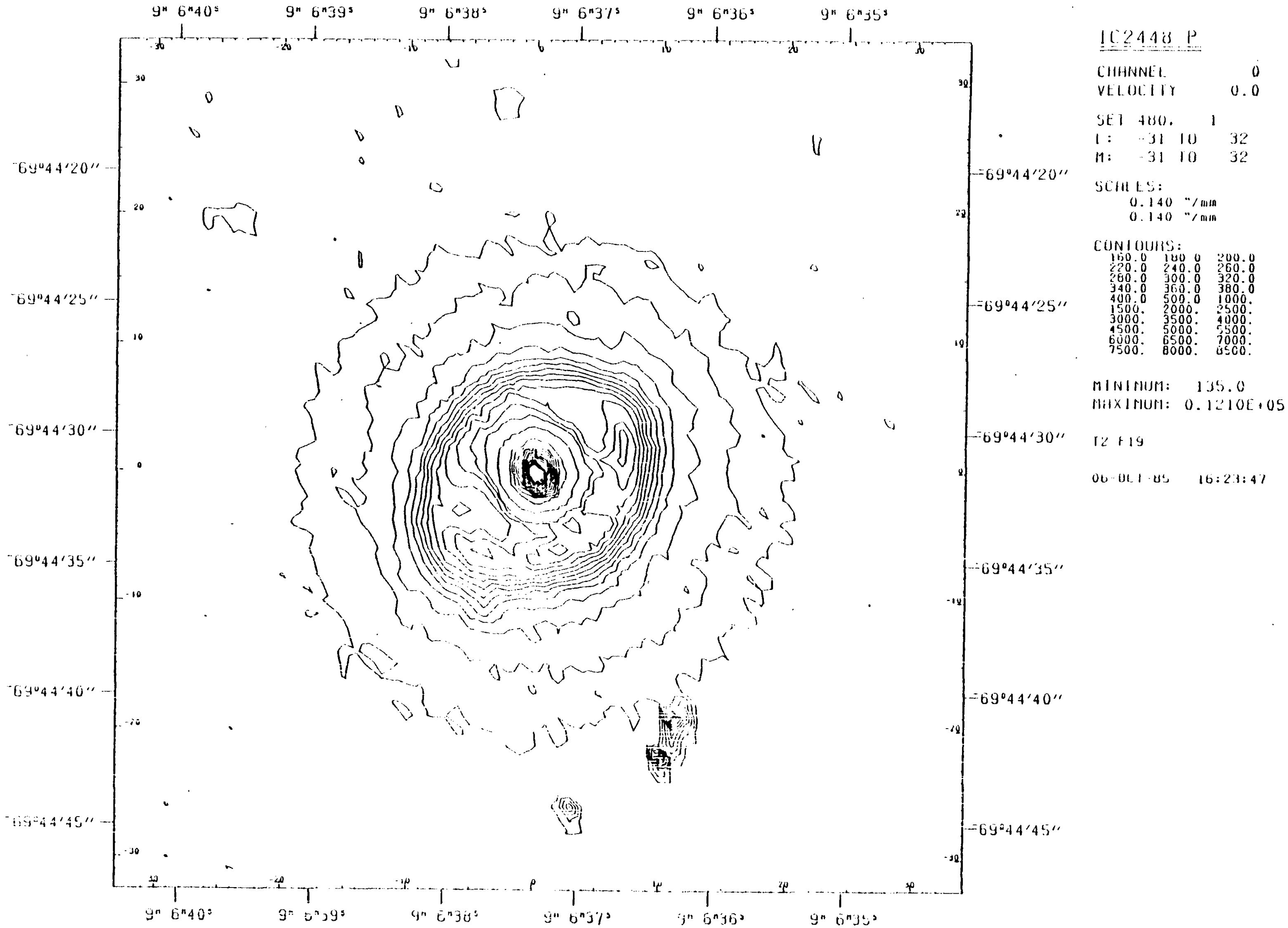

IC2448 P
CHANNEL 0
VELOCITY 0.0
SET 480. 1
L: -31 10 32
M: -31 10 32
SCALES:
0.140 "/mm
0.140 "/mm
CONTOURS:
160.0 180.0 200.0
220.0 240.0 260.0
280.0 300.0 320.0
340.0 360.0 380.0
400.0 500.0 1000.
1500. 2000. 2500.
3000. 3500. 4000.
4500. 5000. 5500.
6000. 6500. 7000.
7500. 8000. 8500.
MINIMUM: 135.0
MAXIMUM: 0.1210E+05
T2 F19
06-OCT-85 16:23:47
9h 6m40s
9h 6m39s
9h 6m38s
9h 6m37s
9h 6m36s
9h 6m35s
-69°44′20″
-69°44′25″
-69°44′30″
-69°44′35″
-69°44′40″
-69°44′45″

Fig A1.33

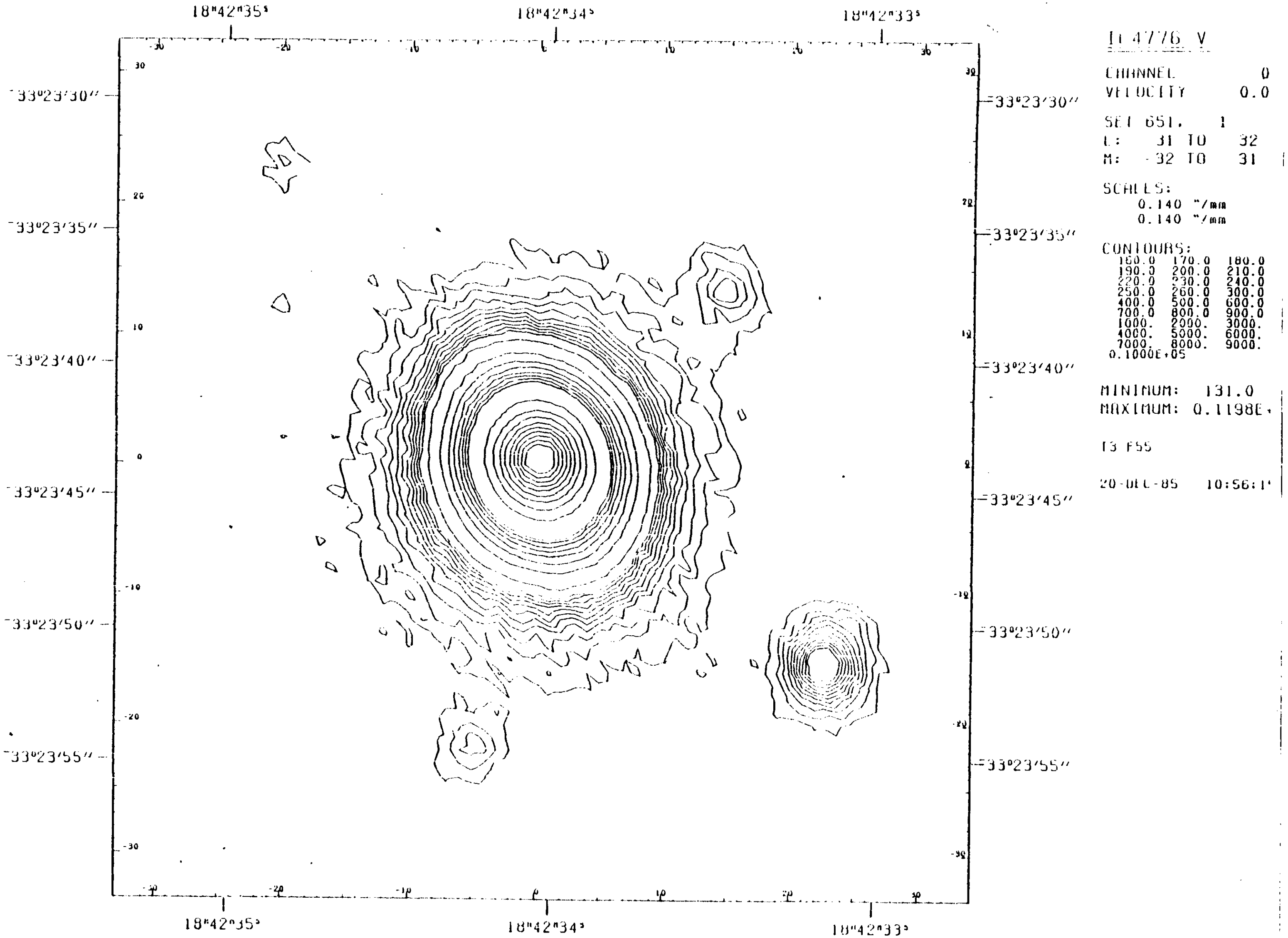
18h42m35s
18h42m34s
18h42m33s
-33°23′30″
-33°23′35″
-33°23′40″
-33°23′45″
-33°23′50″
-33°23′55″
IC 4776 V
CHANNEL 0
VELOCITY 0.0
SET 651. 1
L: 31 TO 32
M: -32 TO 31
SCALES:
0.140 "/mm
0.140 "/mm
CONTOURS:
160.0 170.0 180.0
190.0 200.0 210.0
220.0 230.0 240.0
250.0 260.0 300.0
400.0 500.0 600.0
700.0 800.0 900.0
1000. 2000. 3000.
4000. 5000. 6000.
7000. 8000. 9000.
0.1000E+05
MINIMUM: 131.0
MAXIMUM: 0.1198E
13 FSS
20-DEC-85 10:56:1

Fig A1.34

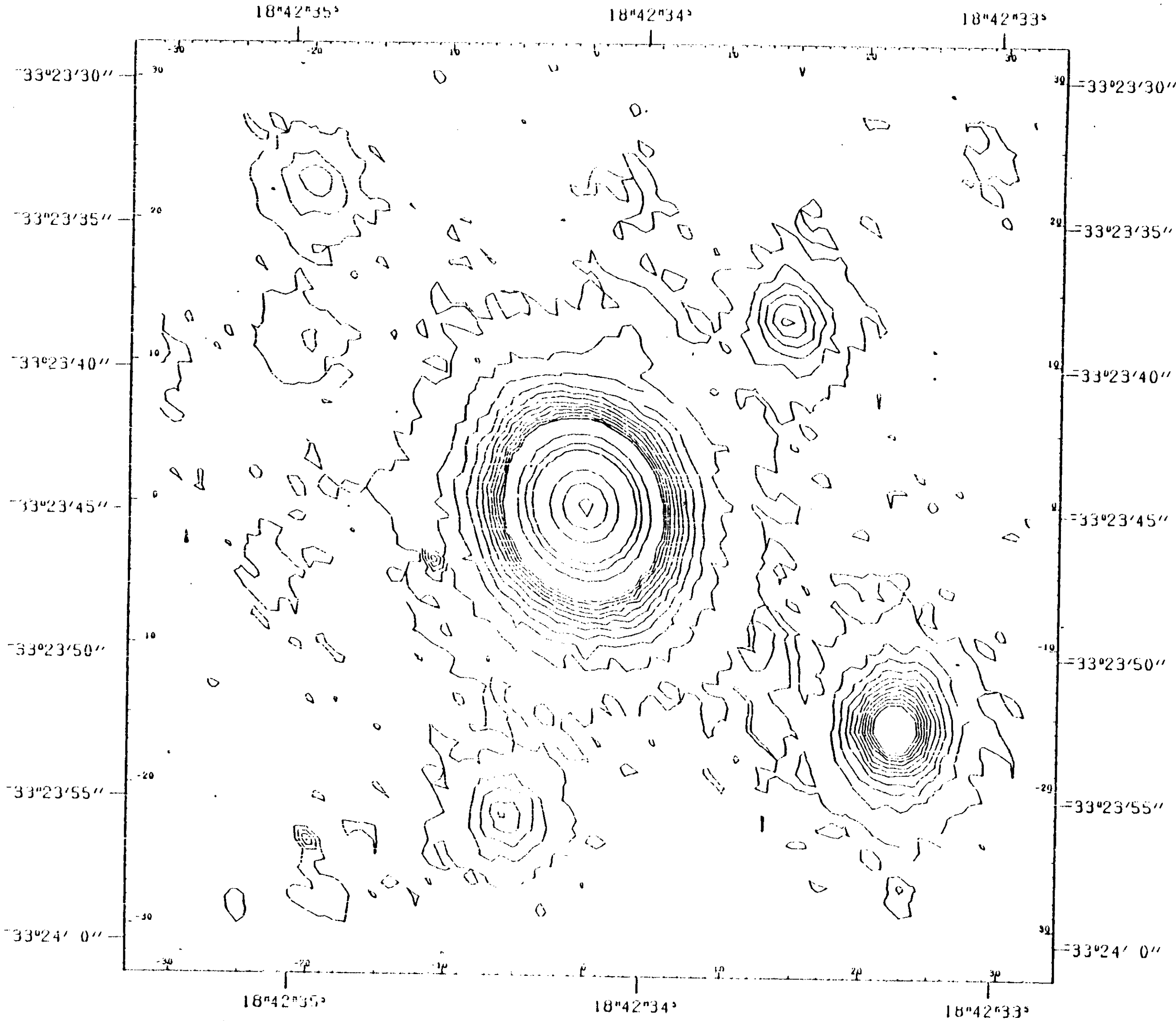

IC4776 P

CHANNEL 0
VELOCITY 0.0

SET 656. 1
L: -31 TO 32
M: -32 TO 31

SCALES:
0.140 "/mm
0.140 "/mm

CONTOURS:
180.0 200.0 220.0
240.0 260.0 280.0
300.0 320.0 340.0
360.0 380.0 400.0
600.0 800.0 1000.
1000. 2000. 3000.
4000.

MINIMUM: 157.0
MAXIMUM: 4307.

T3 F56

20-DEC-85 10:42:00

Fig A1.35

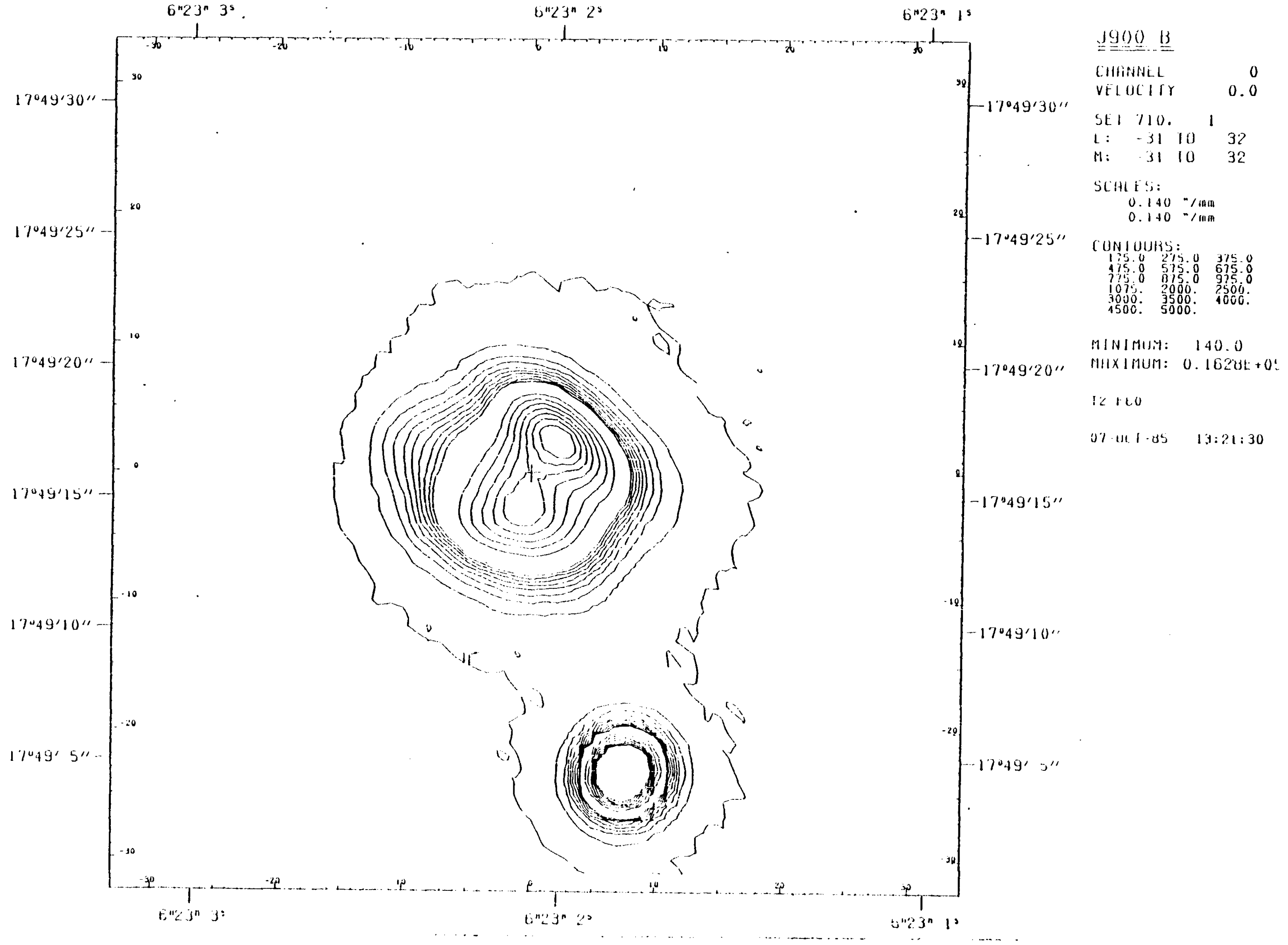
6h23m 3s
6h23m 2s
6h23m 1s
17°49'30"
17°49'25"
17°49'20"
17°49'15"
17°49'10"
17°49' 5"
J900 B
CHANNEL 0
VELOCITY 0.0
SET 710. 1
L: -31 TO 32
M: -31 TO 32
SCALES:
0.140 "/mm
0.140 "/mm
CONTOURS:
175.0 275.0 375.0
475.0 575.0 675.0
775.0 875.0 975.0
1075. 2000. 2500.
3000. 3500. 4000.
4500. 5000.
MINIMUM: 140.0
MAXIMUM: 0.1628E+05
I2 FLO
07-OCT-85 13:21:30

Fig A1.36

Fig A1.37

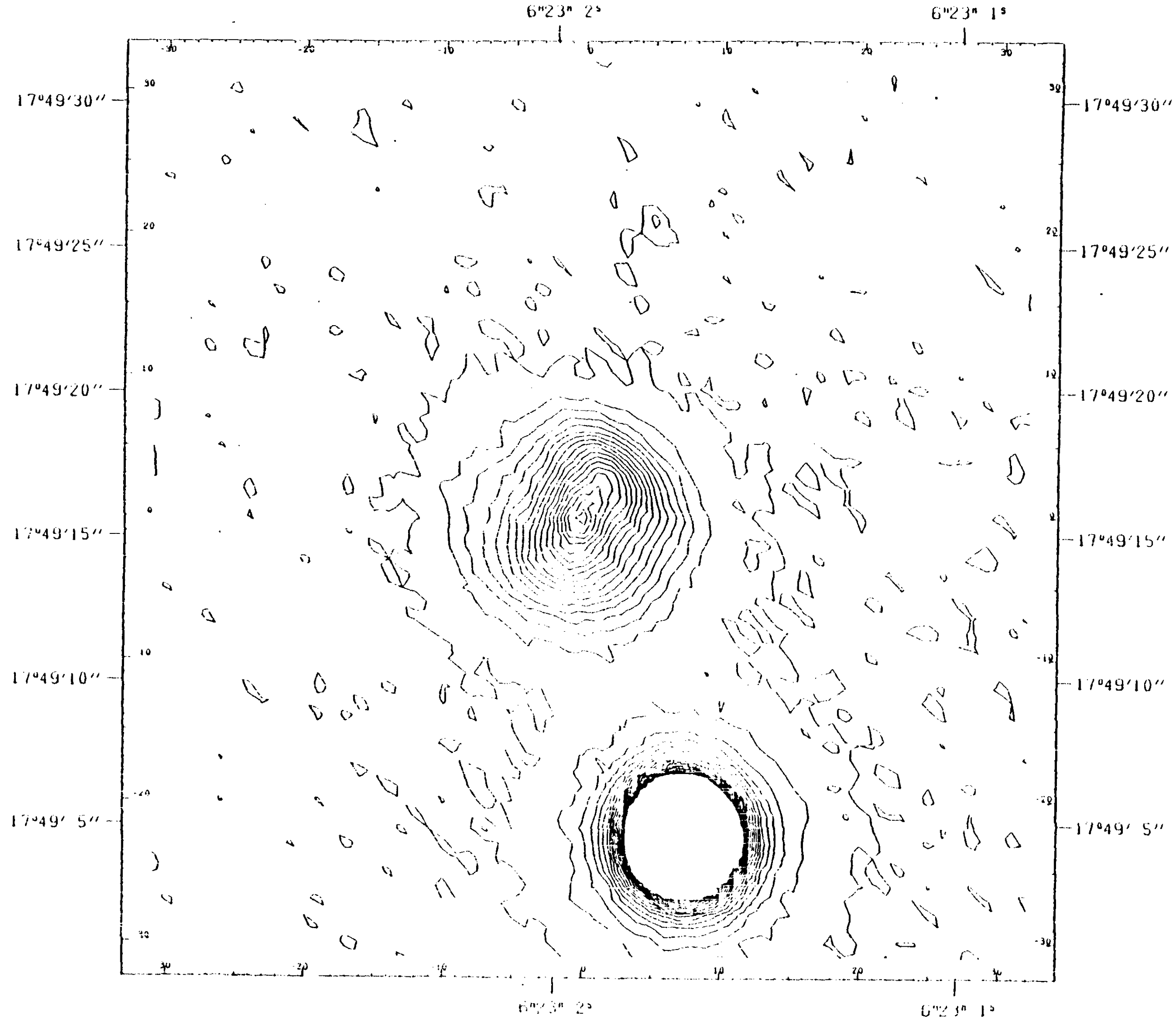

J900 P

CHANNEL 0
VELOCITY 0.0

SET 720. 1
L: -31 TO 32
M: -31 TO 32

SCALES:
0.140 "/mm
0.140 "/mm

CONTOURS:

160.0	185.0	210.0
235.0	260.0	285.0
310.0	335.0	360.0
385.0	410.0	435.0
460.0	485.0	510.0
535.0	560.0	585.0
610.0		

MINIMUM: 141.0
MAXIMUM: 0.1137E+05

12 F63

07-OCT 85 13:37:43

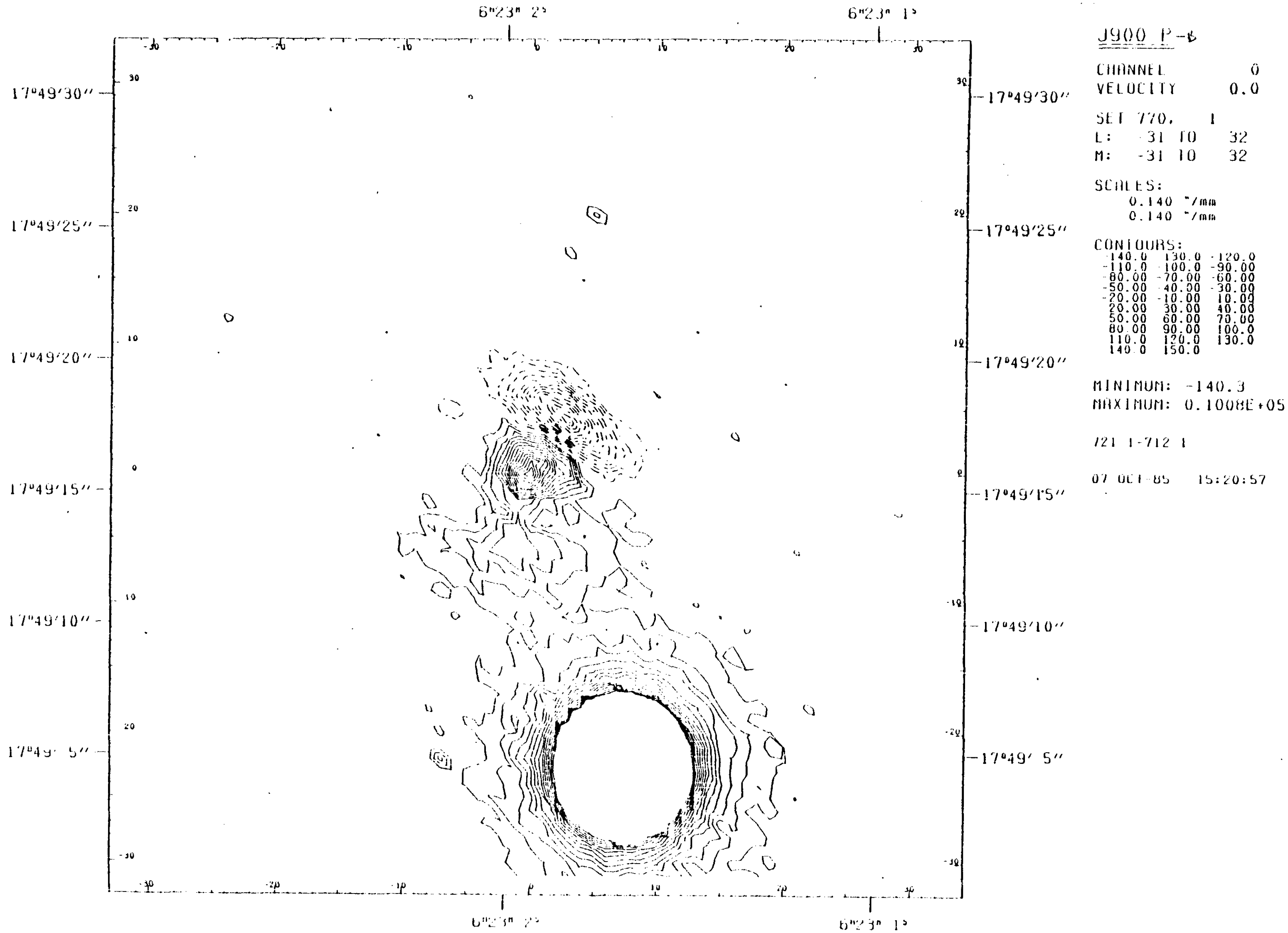
6h23m 2s
6h23m 1s
17°49'30"
17°49'25"
17°49'20"
17°49'15"
17°49'10"
17°49' 5"
J900 P-B
CHANNEL 0
VELOCITY 0.0
SET 770, 1
L: -31 TO 32
M: -31 TO 32
SCALES:
0.140 "/mm
0.140 "/mm
CONTOURS:
-140.0 -130.0 -120.0
-110.0 -100.0 -90.00
-80.00 -70.00 -60.00
-50.00 -40.00 -30.00
-20.00 -10.00 10.00
20.00 30.00 40.00
50.00 60.00 70.00
80.00 90.00 100.0
110.0 120.0 130.0
140.0 150.0
MINIMUM: -140.3
MAXIMUM: 0.1008E+05
721 1-712 1
07 OCT 85 15:20:57

Fig A1.38

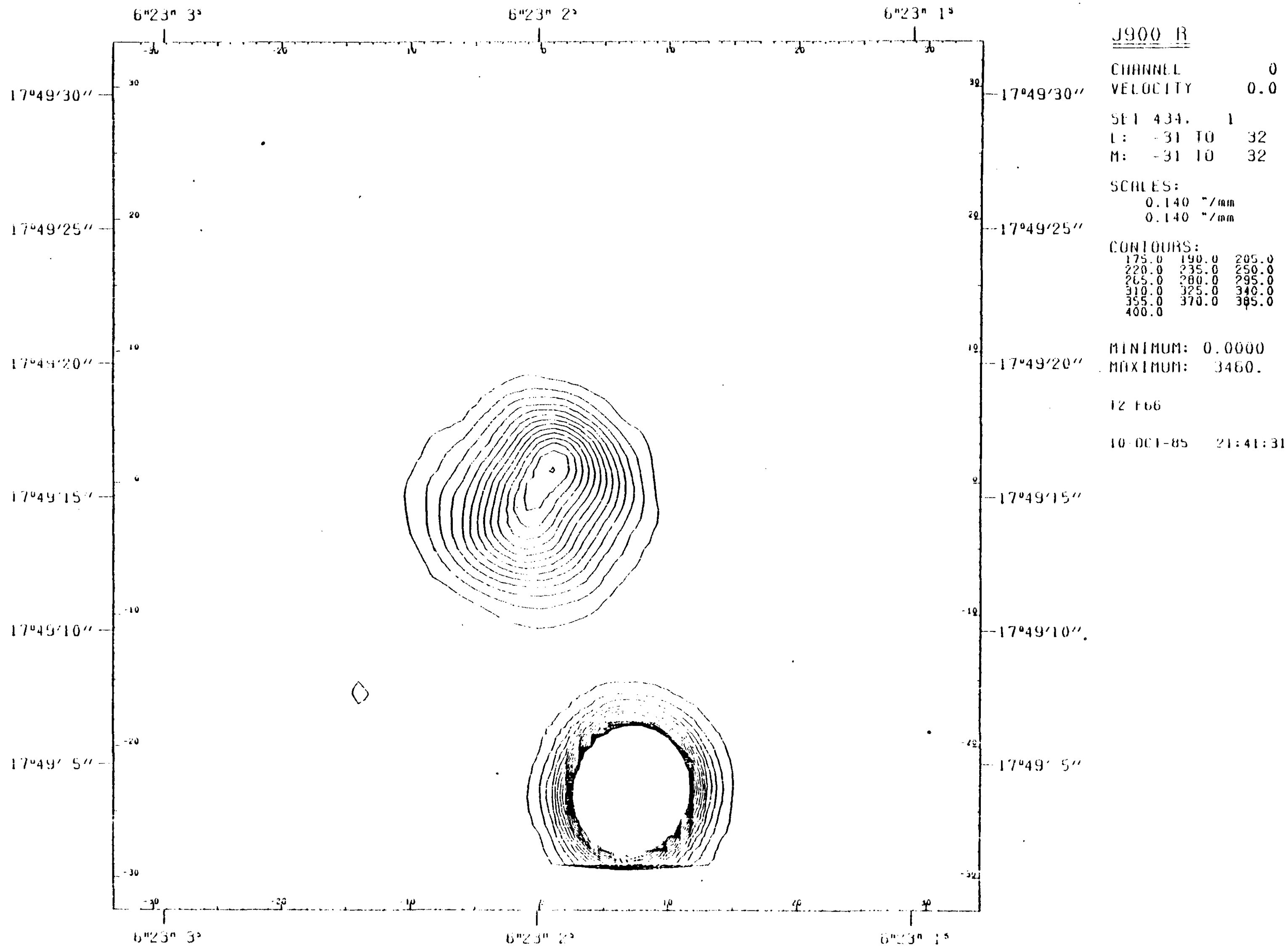

J900 R
CHANNEL 0
VELOCITY 0.0
SET 434. 1
L: -31 TO 32
M: -31 TO 32
SCALES:
0.140 "/mm
0.140 "/mm
CONTOURS:
175.0 190.0 205.0
220.0 235.0 250.0
265.0 280.0 295.0
310.0 325.0 340.0
355.0 370.0 385.0
400.0
MINIMUM: 0.0000
MAXIMUM: 3460.
12 F66
10-OCT-85 21:41:31
6h23m 3s
6h23m 2s
6h23m 1s
17°49'30"
17°49'25"
17°49'20"
17°49'15"
17°49'10"
17°49' 5"

Fig A1.39

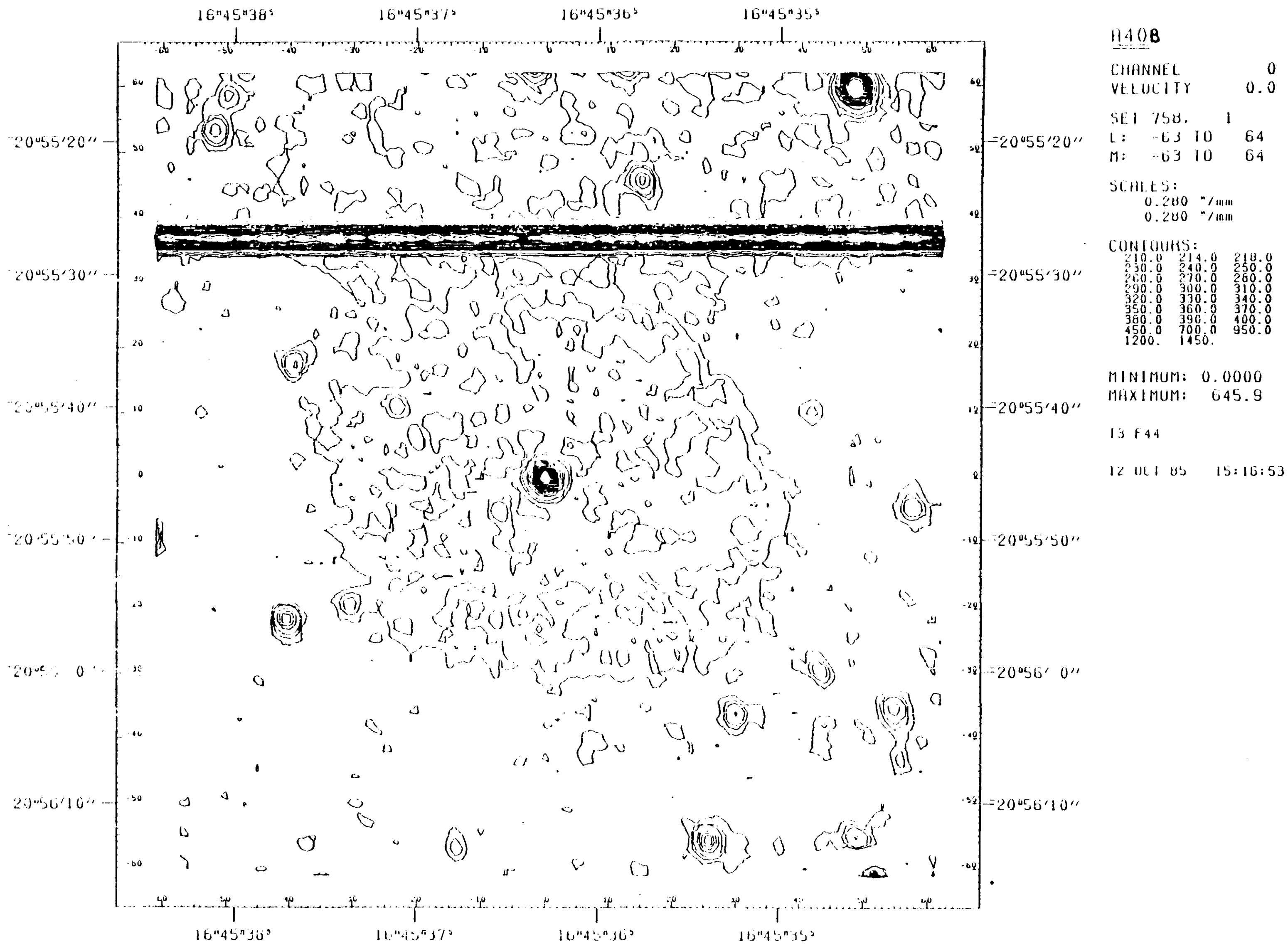
16ʰ45ᵐ38ˢ
16ʰ45ᵐ37ˢ
16ʰ45ᵐ36ˢ
16ʰ45ᵐ35ˢ
20°55'20"
20°55'30"
20°55'40"
20°55'50"
20°56'0"
20°56'10"
A40B
CHANNEL 0
VELOCITY 0.0
SET 758. 1
L: -63 TO 64
M: -63 TO 64
SCALES:
0.280 "/mm
0.280 "/mm
CONTOURS:
210.0 214.0 218.0
230.0 240.0 250.0
260.0 270.0 280.0
290.0 300.0 310.0
320.0 330.0 340.0
350.0 360.0 370.0
380.0 390.0 400.0
450.0 700.0 950.0
1200. 1450.
MINIMUM: 0.0000
MAXIMUM: 645.9
13 F44
12 OCT 85 15:16:53

Fig A1.40

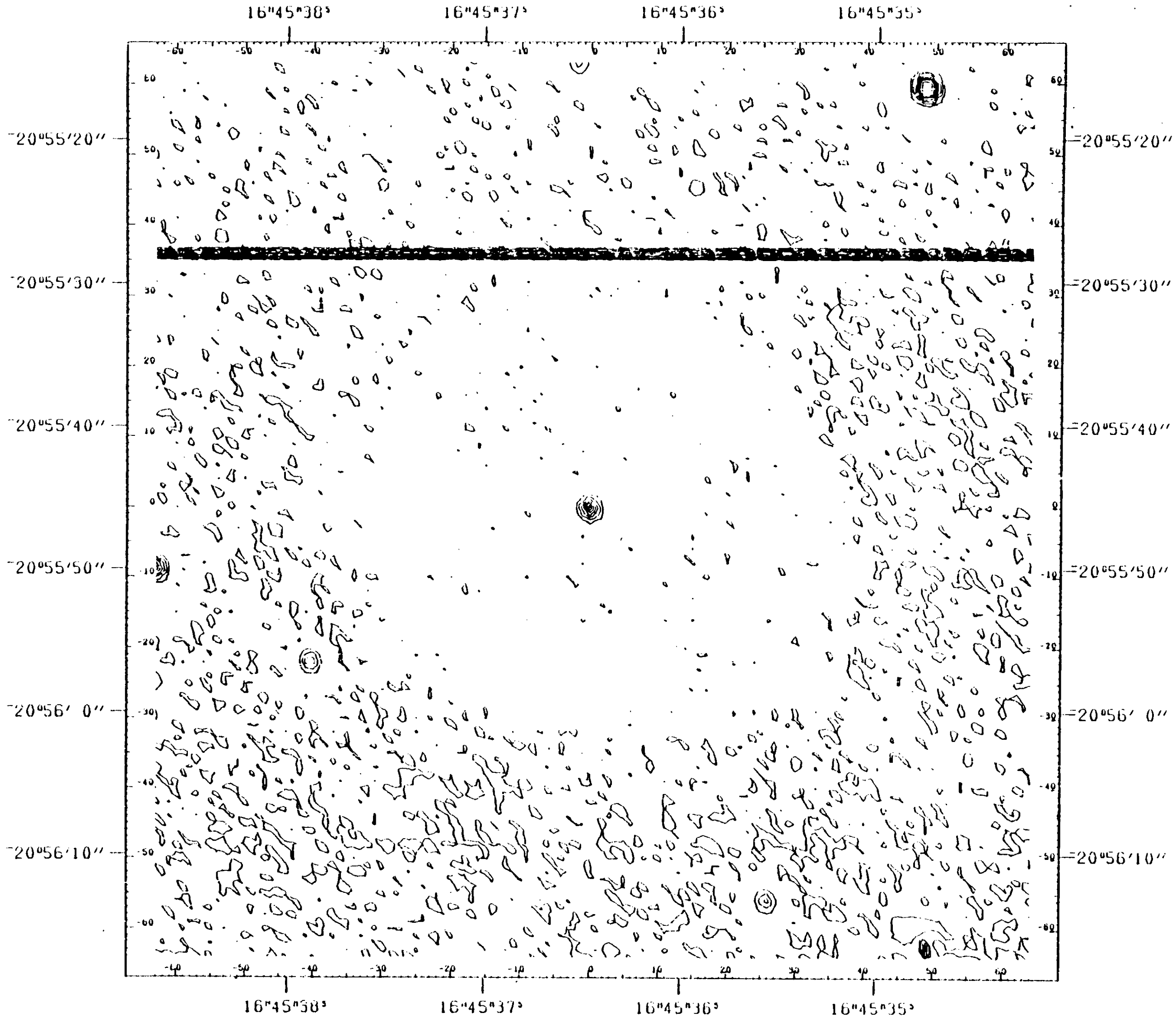

A40 V

CHANNEL 0
VELOCITY 0.0

SET 631. 1
L: -63 TO 64
M: -64 TO 63

SCALES:
0.280 "/mm
0.280 "/mm

CONTOURS:
163.0 226.3 293.6
358.9 424.2 489.5
554.8 620.1 685.4
750.7 816.0 946.6
1208. 1469.

MINIMUM: 163.0
MAXIMUM: 1469.

13 F47

14-DEC-85 09:37:14

Fig A1.41

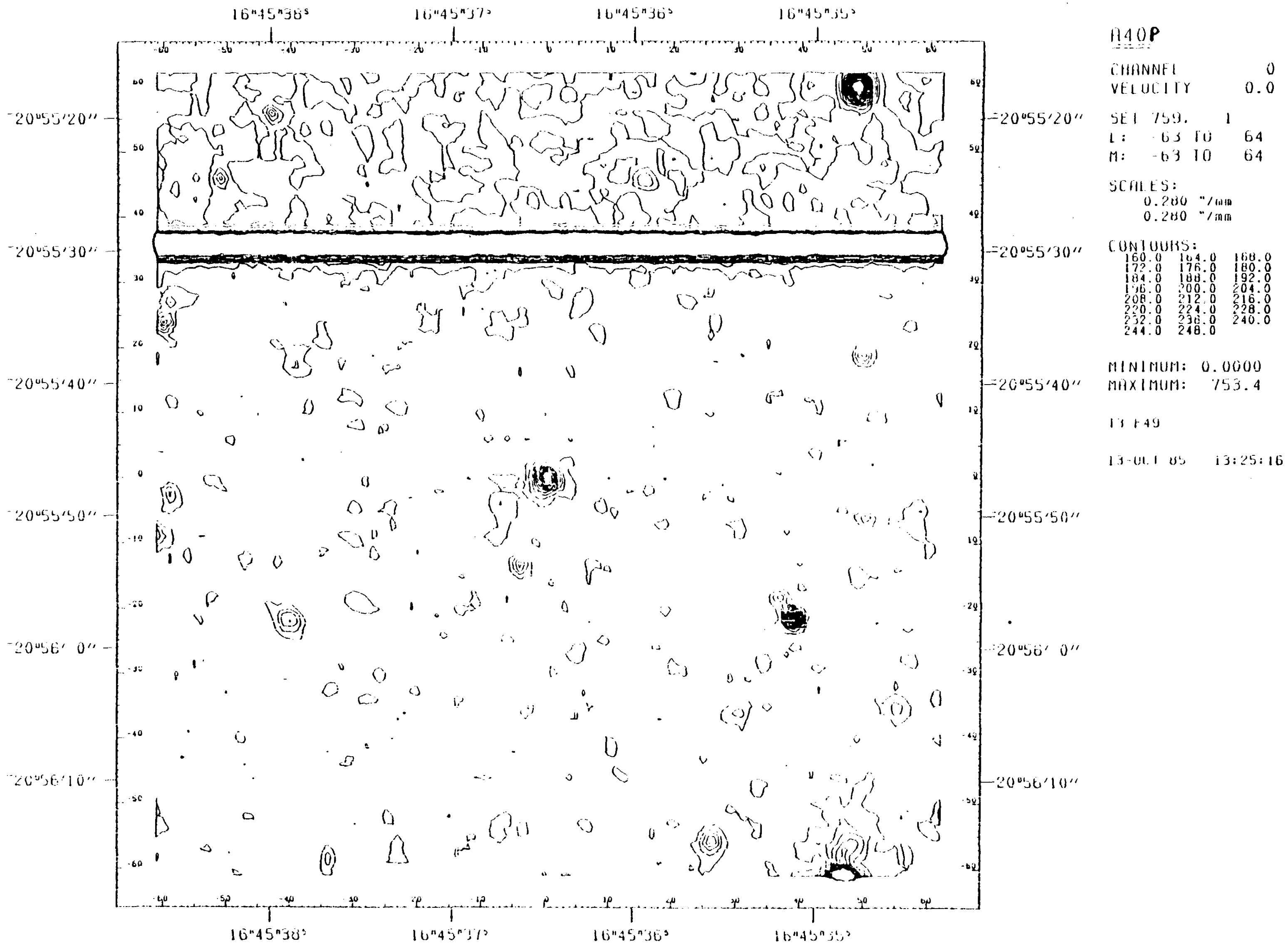
16h45m38s
16h45m37s
16h45m36s
16h45m35s
-20°55'20"
-20°55'30"
-20°55'40"
-20°55'50"
-20°56' 0"
-20°56'10"
A40P
CHANNEL 0
VELUCITY 0.0
SET 759. 1
L: -63 TO 64
M: -63 TO 64
SCALES:
0.280 "/mm
0.280 "/mm
CUNTUURS:
160.0 164.0 168.0
172.0 176.0 180.0
184.0 188.0 192.0
196.0 200.0 204.0
208.0 212.0 216.0
220.0 224.0 228.0
232.0 236.0 240.0
244.0 248.0
MINIMUM: 0.0000
MAXIMUM: 753.4
13 F49
13-OCT 85 13:25:16

Fig A1.42

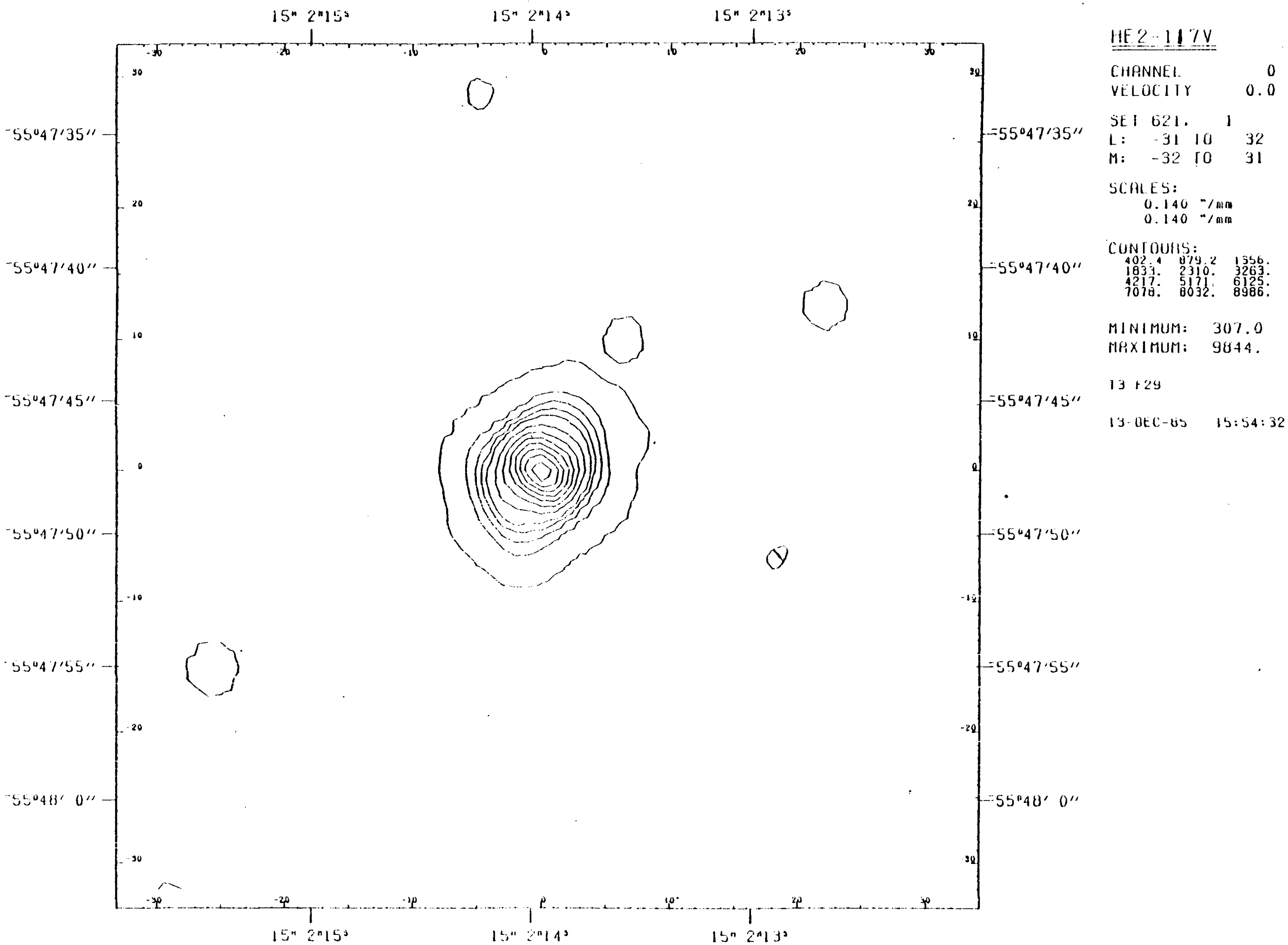

15ʰ 2ᵐ15ˢ
15ʰ 2ᵐ14ˢ
15ʰ 2ᵐ13ˢ
-55°47′35″
-55°47′40″
-55°47′45″
-55°47′50″
-55°47′55″
-55°48′ 0″
HE2-117V
CHANNEL 0
VELOCITY 0.0
SET 621. 1
L: -31 TO 32
M: -32 TO 31
SCALES:
0.140 ″/mm
0.140 ″/mm
CONTOURS:
402.4 879.2 1356.
1833. 2310. 3263.
4217. 5171. 6125.
7078. 8032. 8986.
MINIMUM: 307.0
MAXIMUM: 9844.
13 F29
13-DEC-85 15:54:32

Fig A1.43

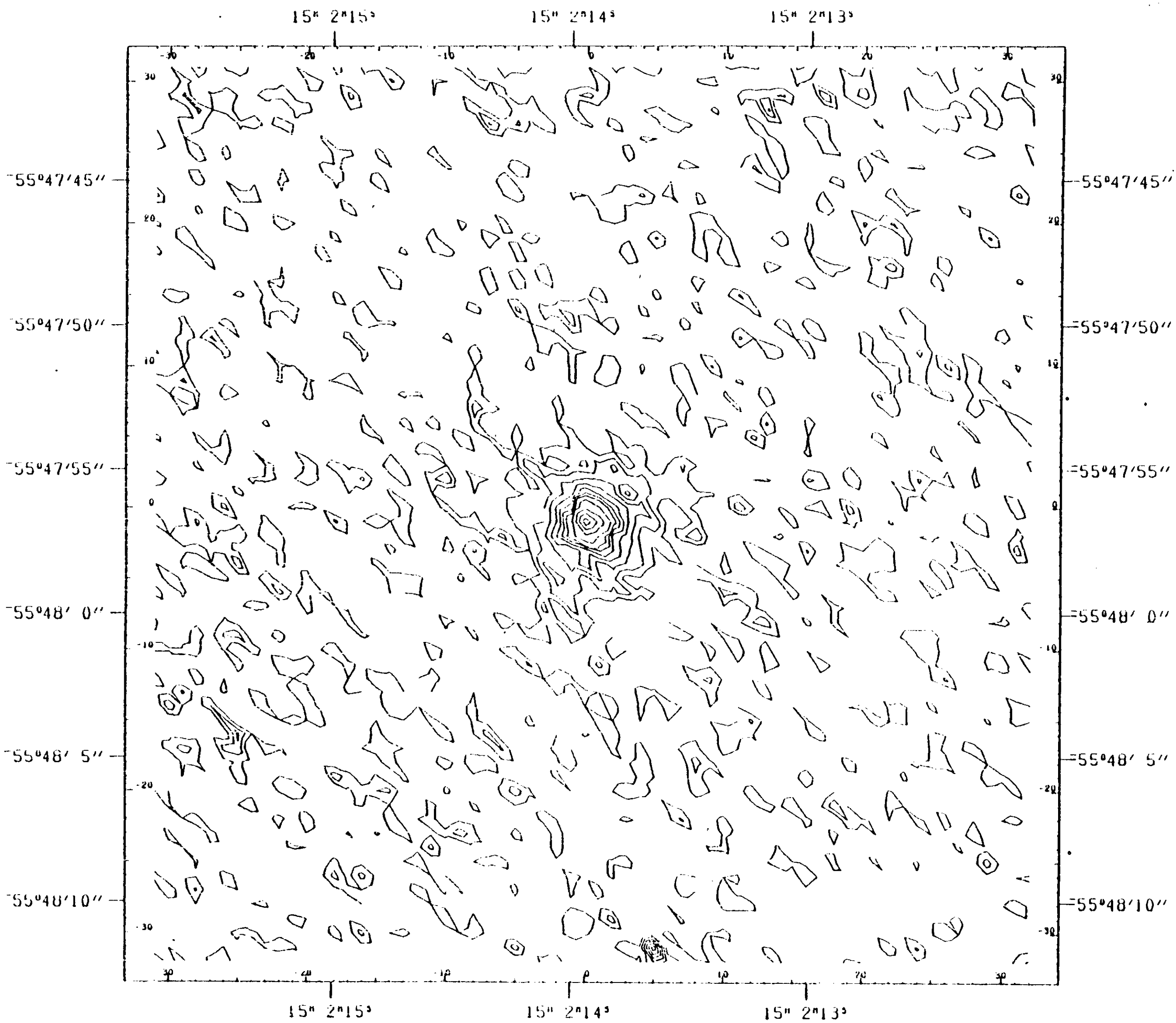

HE2-117P

CHANNEL 0
VELOCITY 0.0

SET 581. 1
L: -31 TO 32
M: -32 TO 31

SCALES:
0.140 "/mm
0.140 "/mm

CONTOURS:
150.0 155.0 160.0
165.0 170.0 175.0
180.0 190.0 210.0
230.0 250.0 270.0

MINIMUM: 135.0
MAXIMUM: 264.0

T3 F30

20-DEC-85 09:46:44

Fig A1.44

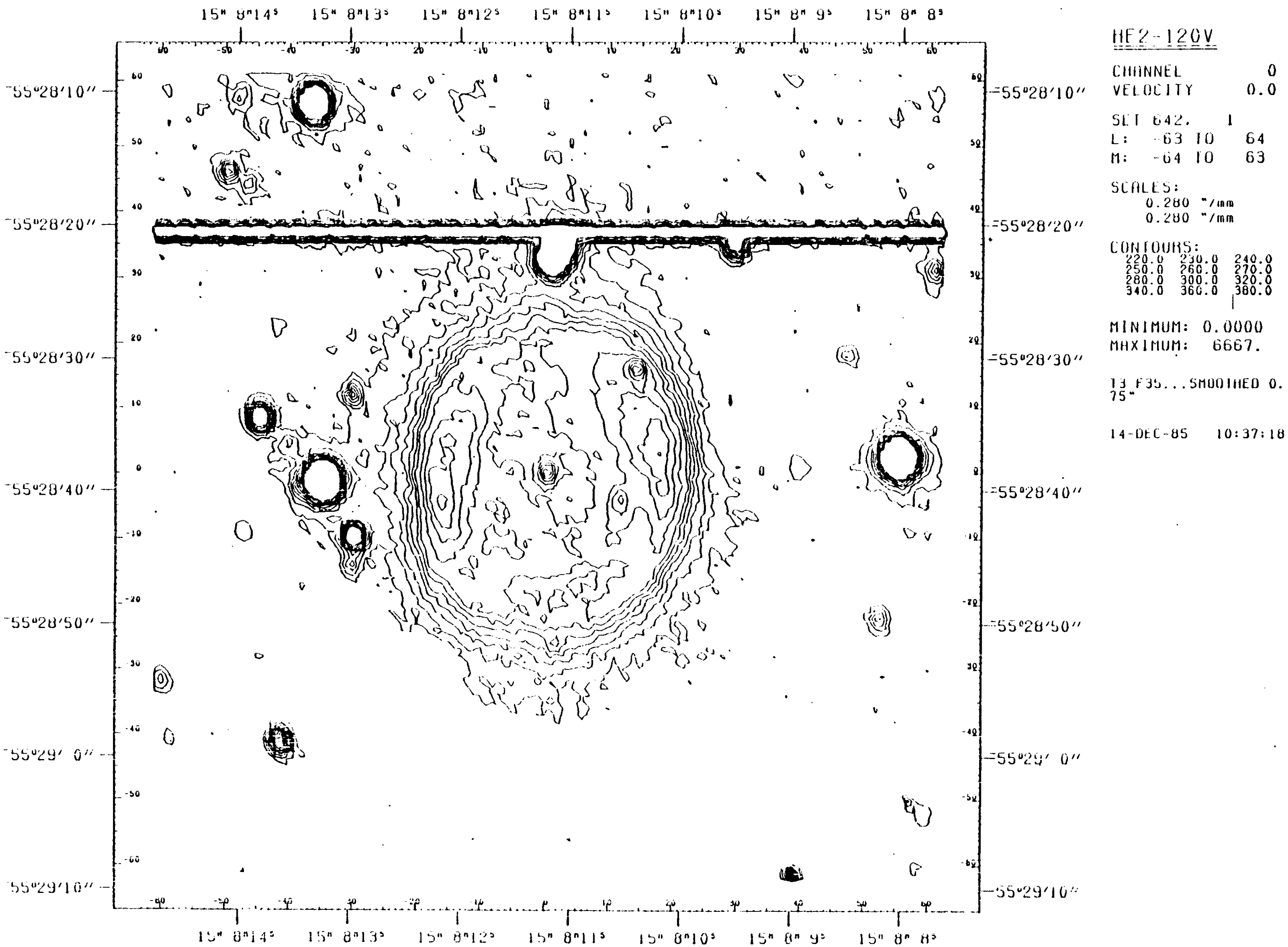

HF2-120V
CHANNEL 0
VELOCITY 0.0
SET 642. 1
L: -63 TO 64
M: -64 TO 63
SCALES:
0.280 "/mm
0.280 "/mm
CONTOURS:
220.0 230.0 240.0
250.0 260.0 270.0
280.0 300.0 320.0
340.0 360.0 380.0
MINIMUM: 0.0000
MAXIMUM: 6667.
T3 F35...SMOOTHED 0.75"
14-DEC-85 10:37:18
15h 8m14s
15h 8m13s
15h 8m12s
15h 8m11s
15h 8m10s
15h 8m 9s
15h 8m 8s
-55°28′10″
-55°28′20″
-55°28′30″
-55°28′40″
-55°28′50″
-55°29′ 0″
-55°29′10″

Fig A1.45

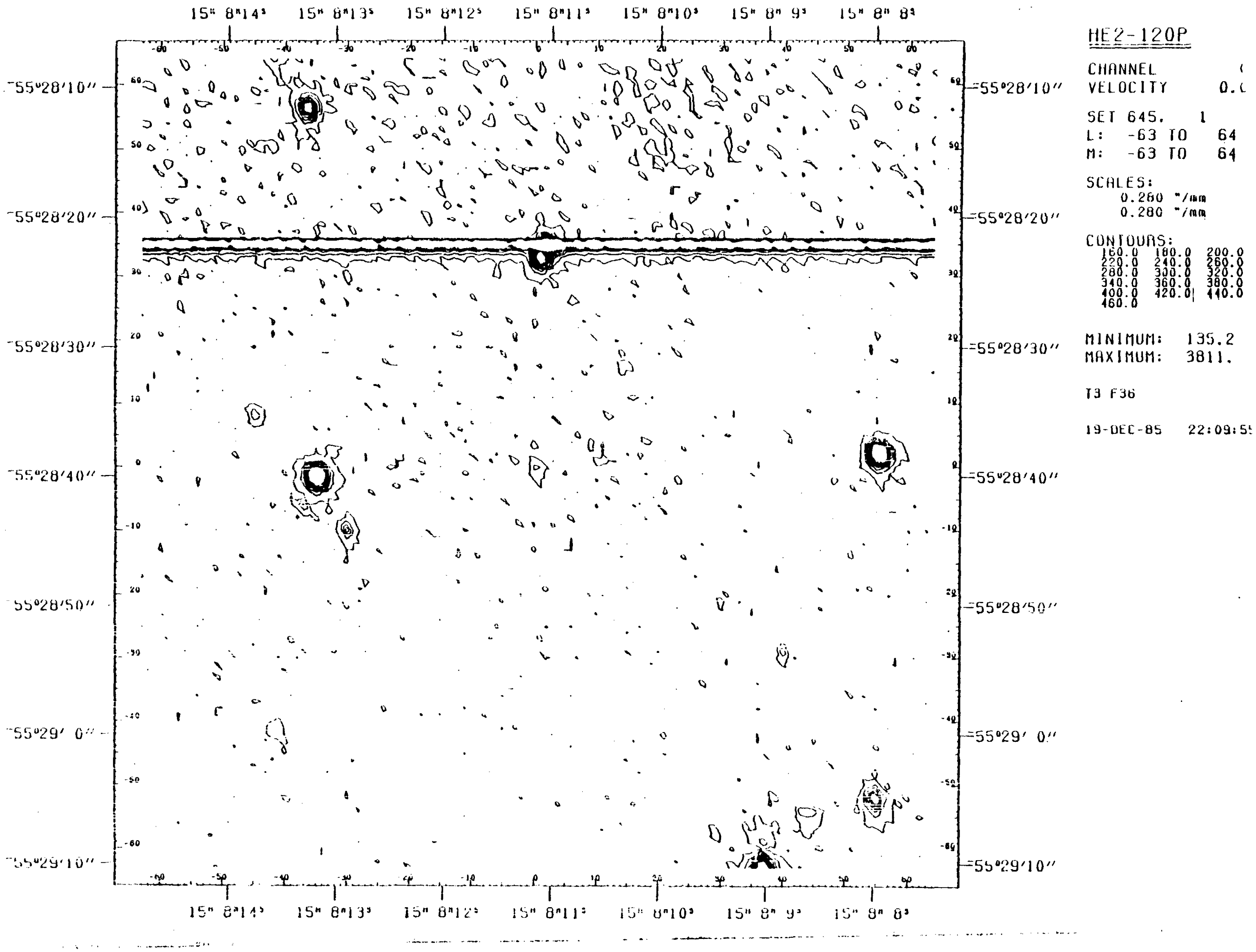
HE2-120P
CHANNEL
VELOCITY 0.
SET 645. 1
L: -63 TO 64
M: -63 TO 64
SCALES:
0.280 "/mm
0.280 "/mm
CONTOURS:
160.0 180.0 200.0
220.0 240.0 260.0
280.0 300.0 320.0
340.0 360.0 380.0
400.0 420.0 440.0
460.0
MINIMUM: 135.2
MAXIMUM: 3811.
T3 F36
19-DEC-85 22:09:5
15h 8m14s 15h 8m13s 15h 8m12s 15h 8m11s 15h 8m10s 15h 8m 9s 15h 8m 8s
-55°28'10" -55°28'20" -55°28'30" -55°28'40" -55°28'50" -55°29' 0" -55°29'10"

Fig A1.46

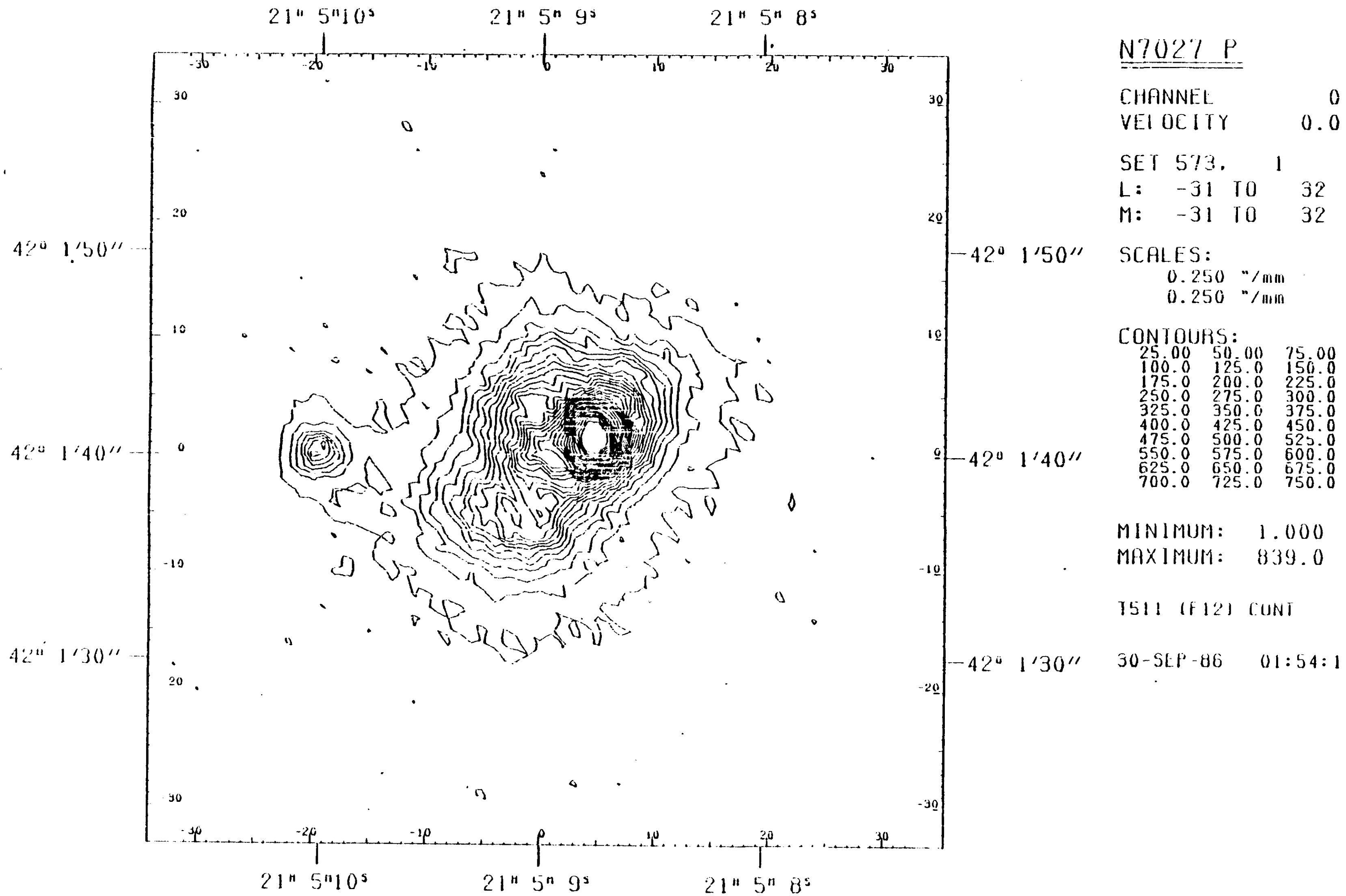
21h 5m10s
21h 5m 9s
21h 5m 8s
42° 1′50″
42° 1′40″
42° 1′30″
N7027 P
CHANNEL 0
VELOCITY 0.0
SET 573. 1
L: -31 TO 32
M: -31 TO 32
SCALES:
0.250 "/mm
0.250 "/mm
CONTOURS:
25.00 50.00 75.00
100.0 125.0 150.0
175.0 200.0 225.0
250.0 275.0 300.0
325.0 350.0 375.0
400.0 425.0 450.0
475.0 500.0 525.0
550.0 575.0 600.0
625.0 650.0 675.0
700.0 725.0 750.0
MINIMUM: 1.000
MAXIMUM: 839.0
TSII (F12) CONT
30-SEP-86 01:54:11

Fig A1.47

Appendix 2.1

Temp (K)	$G_1(T)$
2.2000E4	5.1978E-2
2.4000E4	8.1405E-2
2.6000E4	1.1792E-1
2.8000E4	1.6081E-1
3.0000E4	2.0910E-1
3.2000E4	2.6174E-1
3.4000E4	3.1769E-1
3.6000E4	3.7596E-1
3.8000E4	4.3568E-1
4.0000E4	4.9611E-1
4.2000E4	5.5662E-1
4.4000E4	6.1671E-1
4.6000E4	6.7595E-1
4.8000E4	7.3404E-1
5.0000E4	7.9074E-1
5.2000E4	8.4587E-1
5.4000E4	8.9931E-1
5.6000E4	9.5098E-1
5.8000E4	1.0008E0
6.0000E4	1.0489E0
6.2000E4	1.0950E0
6.4000E4	1.1394E0
6.6000E4	1.1820E0
6.8000E4	1.2229E0
7.0000E4	1.2621E0
7.2000E4	1.2997E0
7.4000E4	1.3357E0
7.6000E4	1.3702E0
7.8000E4	1.4033E0
8.0000E4	1.4350E0
8.2000E4	1.4653E0
8.4000E4	1.4944E0
8.6000E4	1.5223E0
8.8000E4	1.5490E0
9.0000E4	1.5746E0
9.2000E4	1.5992E0
9.4000E4	1.6228E0
9.6000E4	1.6454E0
9.8000E4	1.6672E0
1.0000E5	1.6880E0
1.0200E5	1.7081E0
1.0400E5	1.7273E0
1.0600E5	1.7458E0
1.0800E5	1.7636E0
1.1000E5	1.7807E0
1.1200E5	1.7972E0
1.1400E5	1.8131E0
1.1600E5	1.8283E0
1.1800E5	1.8430E0
1.2000E5	1.8572E0

Temp (K)	$G_1(T)$
1.2200E5	1.8709E0
1.2400E5	1.8840E0
1.2600E5	1.8967E0
1.2800E5	1.9090E0
1.3000E5	1.9208E0
1.3200E5	1.9323E0
1.3400E5	1.9433E0
1.3600E5	1.9540E0
1.3800E5	1.9643E0
1.4000E5	1.9743E0
1.4200E5	1.9839E0
1.4400E5	1.9932E0
1.4600E5	2.0023E0
1.4800E5	2.0110E0
1.5000E5	2.0195E0
1.5200E5	2.0277E0
1.5400E5	2.0356E0
1.5600E5	2.0433E0
1.5800E5	2.0508E0
1.6000E5	2.0580E0
1.6200E5	2.0651E0
1.6400E5	2.0719E0
1.6600E5	2.0785E0
1.6800E5	2.0849E0
1.7000E5	2.0912E0
1.7200E5	2.0972E0
1.7400E5	2.1031E0
1.7600E5	2.1089E0
1.7800E5	2.1144E0
1.8000E5	2.1198E0
1.8200E5	2.1251E0
1.8400E5	2.1302E0
1.8600E5	2.1352E0
1.8800E5	2.1401E0
1.9000E5	2.1448E0
1.9200E5	2.1494E0
1.9400E5	2.1539E0
1.9600E5	2.1582E0
1.9800E5	2.1625E0
2.0000E5	2.1666E0
2.0200E5	2.1707E0
2.0400E5	2.1746E0
2.0600E5	2.1784E0
2.0800E5	2.1822E0
2.1000E5	2.1858E0
2.1200E5	2.1894E0
2.1400E5	2.1929E0
2.1600E5	2.1963E0
2.1800E5	2.1996E0
2.2000E5	2.2028E0
2.2200E5	2.2060E0

Temp (K)	$G_1(T)$
2.2400E5	2.2091E0
2.2600E5	2.2121E0
2.2800E5	2.2150E0
2.3000E5	2.2179E0
2.3200E5	2.2207E0
2.3400E5	2.2235E0
2.3600E5	2.2262E0
2.3800E5	2.2288E0
2.4000E5	2.2314E0
2.4200E5	2.2339E0
2.4400E5	2.2364E0
2.4600E5	2.2388E0
2.4800E5	2.2412E0
2.5000E5	2.2435E0
2.5200E5	2.2457E0
2.5400E5	2.2480E0
2.5600E5	2.2501E0
2.5800E5	2.2522E0
2.6000E5	2.2543E0
2.6200E5	2.2564E0
2.6400E5	2.2584E0
2.6600E5	2.2603E0
2.6800E5	2.2622E0
2.7000E5	2.2641E0
2.7200E5	2.2660E0
2.7400E5	2.2678E0
2.7600E5	2.2696E0
2.7800E5	2.2713E0
2.8000E5	2.2730E0
2.8200E5	2.2747E0
2.8400E5	2.2763E0
2.8600E5	2.2779E0
2.8800E5	2.2795E0
2.9000E5	2.2811E0
2.9200E5	2.2826E0
2.9400E5	2.2841E0
2.9600E5	2.2855E0
2.9800E5	2.2870E0
3.0000E5	2.2884E0
3.0200E5	2.2898E0
3.0400E5	2.2912E0
3.0600E5	2.2925E0
3.0800E5	2.2938E0
3.1000E5	2.2951E0
3.1200E5	2.2964E0
3.1400E5	2.2976E0
3.1600E5	2.2989E0
3.1800E5	2.3001E0
3.2000E5	2.3012E0
3.2200E5	2.3024E0
3.2400E5	2.3036E0

Temp (K)	$G_1(T)$
3.2600E5	2.3047E0
3.2800E5	2.3058E0
3.3000E5	2.3069E0
3.3200E5	2.3080E0
3.3400E5	2.3090E0
3.3600E5	2.3101E0
3.3800E5	2.3111E0
3.4000E5	2.3121E0
3.4200E5	2.3131E0
3.4400E5	2.3140E0
3.4600E5	2.3150E0
3.4800E5	2.3159E0
3.5000E5	2.3169E0
3.5200E5	2.3178E0
3.5400E5	2.3187E0
3.5600E5	2.3196E0
3.5800E5	2.3204E0
3.6000E5	2.3213E0
3.6200E5	2.3221E0
3.6400E5	2.3230E0
3.6600E5	2.3238E0
3.6800E5	2.3246E0
3.7000E5	2.3254E0
3.7200E5	2.3262E0
3.7400E5	2.3269E0
3.7600E5	2.3277E0
3.7800E5	2.3284E0
3.8000E5	2.3292E0
3.8200E5	2.3299E0
3.8400E5	2.3306E0
3.8600E5	2.3313E0
3.8800E5	2.3320E0
3.9000E5	2.3327E0
3.9200E5	2.3334E0
3.9400E5	2.3341E0
3.9600E5	2.3347E0
3.9800E5	2.3354E0
4.0000E5	2.3360E0
4.0200E5	2.3366E0
4.0400E5	2.3373E0
4.0600E5	2.3379E0
4.0800E5	2.3385E0
4.1000E5	2.3391E0
4.1200E5	2.3397E0
4.1400E5	2.3402E0
4.1600E5	2.3408E0
4.1800E5	2.3414E0

Temp (K)	$G_{1.807}(T)$
2.8000E5	2.0393E0
2.8500E5	2.0498E0
2.9000E5	2.0598E0
2.9500E5	2.0694E0
3.0000E5	2.0786E0
3.0500E5	2.0874E0
3.1000E5	2.0959E0
3.1500E5	2.1041E0
3.2000E5	2.1119E0
3.2500E5	2.1195E0
3.3000E5	2.1267E0
3.3500E5	2.1337E0
3.4000E5	2.1404E0
3.4500E5	2.1469E0
3.5000E5	2.1532E0
3.5500E5	2.1592E0
3.6000E5	2.1650E0
3.6500E5	2.1707E0
3.7000E5	2.1761E0
3.7500E5	2.1813E0
3.8000E5	2.1864E0
3.8500E5	2.1913E0
3.9000E5	2.1960E0
3.9500E5	2.2006E0
4.0000E5	2.2050E0
4.0500E5	2.2093E0
4.1000E5	2.2134E0
4.1500E5	2.2175E0
4.2000E5	2.2213E0
4.2500E5	2.2251E0
4.3000E5	2.2288E0
4.3500E5	2.2323E0
4.4000E5	2.2358E0
4.4500E5	2.2391E0
4.5000E5	2.2424E0
4.5500E5	2.2455E0
4.6000E5	2.2486E0
4.6500E5	2.2516E0
4.7000E5	2.2544E0
4.7500E5	2.2572E0
4.8000E5	2.2600E0
4.8500E5	2.2626E0
4.9000E5	2.2652E0
4.9500E5	2.2677E0
5.0000E5	2.2702E0
5.0500E5	2.2726E0
5.1000E5	2.2749E0
5.1500E5	2.2771E0
5.2000E5	2.2793E0
5.2500E5	2.2815E0
5.3000E5	2.2836E0

Temp (K)	$G_4(T)$
2.8000E5	1.2621E0
2.8500E5	1.2858E0
2.9000E5	1.3089E0
2.9500E5	1.3313E0
3.0000E5	1.3532E0
3.0500E5	1.3744E0
3.1000E5	1.3952E0
3.1500E5	1.4153E0
3.2000E5	1.4350E0
3.2500E5	1.4541E0
3.3000E5	1.4727E0
3.3500E5	1.4908E0
3.4000E5	1.5085E0
3.4500E5	1.5257E0
3.5000E5	1.5424E0
3.5500E5	1.5588E0
3.6000E5	1.5746E0
3.6500E5	1.5901E0
3.7000E5	1.6052E0
3.7500E5	1.6199E0
3.8000E5	1.6342E0
3.8500E5	1.6482E0
3.9000E5	1.6618E0
3.9500E5	1.6751E0
4.0000E5	1.6880E0
4.0500E5	1.7006E0
4.1000E5	1.7129E0
4.1500E5	1.7249E0
4.2000E5	1.7367E0
4.2500E5	1.7481E0
4.3000E5	1.7592E0
4.3500E5	1.7701E0
4.4000E5	1.7807E0
4.4500E5	1.7911E0
4.5000E5	1.8012E0
4.5500E5	1.8111E0
4.6000E5	1.8208E0
4.6500E5	1.8302E0
4.7000E5	1.8394E0
4.7500E5	1.8484E0
4.8000E5	1.8572E0
4.8500E5	1.8658E0
4.9000E5	1.8742E0
4.9500E5	1.8824E0
5.0000E5	1.8904E0
5.0500E5	1.8983E0
5.1000E5	1.9060E0
5.1500E5	1.9135E0
5.2000E5	1.9208E0
5.2500E5	1.9280E0
5.3000E5	1.9351E0

Appendix 2.2

Temp.(K)	$G_{1.807}(T)$
2.5000E4	1.7215E-3
3.0000E4	8.2845E-3
3.5000E4	2.4498E-2
4.0000E4	5.3753E-2
4.5000E4	9.7062E-2
5.0000E4	1.5335E-1
5.5000E4	2.2029E-1
6.0000E4	2.9512E-1
6.5000E4	3.7513E-1
7.0000E4	4.5797E-1
7.5000E4	5.4170E-1
8.0000E4	6.2486E-1
8.5000E4	7.0633E-1
9.0000E4	7.8535E-1
9.5000E4	8.6140E-1
1.0000E5	9.3417E-1
1.0500E5	1.0035E0
1.1000E5	1.0693E0
1.1500E5	1.1316E0
1.2000E5	1.1906E0
1.2500E5	1.2462E0
1.3000E5	1.2987E0
1.3500E5	1.3482E0
1.4000E5	1.3948E0
1.4500E5	1.4388E0
1.5000E5	1.4802E0
1.5500E5	1.5193E0
1.6000E5	1.5561E0
1.6500E5	1.5909E0
1.7000E5	1.6237E0
1.7500E5	1.6548E0
1.8000E5	1.6841E0
1.8500E5	1.7118E0
1.9000E5	1.7380E0
1.9500E5	1.7629E0
2.0000E5	1.7864E0
2.0500E5	1.8088E0
2.1000E5	1.8299E0
2.1500E5	1.8501E0
2.2000E5	1.8692E0
2.2500E5	1.8874E0
2.3000E5	1.9047E0
2.3500E5	1.9211E0
2.4000E5	1.9368E0
2.4500E5	1.9518E0
2.5000E5	1.9661E0
2.5500E5	1.9797E0
2.6000E5	1.9927E0
2.6500E5	2.0052E0
2.7000E5	2.0171E0
2.7500E5	2.0284E0

Appendix 2.3

Temp(K)	$G_4(T)$
3.0000E4	3.8953E-7
3.5000E4	5.2433E-6
4.0000E4	3.9414E-5
4.5000E4	1.8322E-4
5.0000E4	6.1311E-4
5.5000E4	1.6220E-3
6.0000E4	3.6032E-3
6.5000E4	7.0057E-3
7.0000E4	1.2278E-2
7.5000E4	1.9819E-2
8.0000E4	2.9940E-2
8.5000E4	4.2849E-2
9.0000E4	5.8645E-2
9.5000E4	7.7328E-2
1.0000E5	9.8814E-2
1.0500E5	1.2295E-1
1.1000E5	1.4954E-1
1.1500E5	1.7834E-1
1.2000E5	2.0910E-1
1.2500E5	2.4156E-1
1.3000E5	2.7546E-1
1.3500E5	3.1055E-1
1.4000E5	3.4659E-1
1.4500E5	3.8336E-1
1.5000E5	4.2066E-1
1.5500E5	4.5830E-1
1.6000E5	4.9611E-1
1.6500E5	5.3396E-1
1.7000E5	5.7170E-1
1.7500E5	6.0923E-1
1.8000E5	6.4646E-1
1.8500E5	6.8328E-1
1.9000E5	7.1964E-1
1.9500E5	7.5548E-1
2.0000E5	7.9074E-1
2.0500E5	8.2539E-1
2.1000E5	8.5940E-1
2.1500E5	8.9273E-1
2.2000E5	9.2537E-1
2.2500E5	9.5731E-1
2.3000E5	9.8854E-1
2.3500E5	1.0191E0
2.4000E5	1.0489E0
2.4500E5	1.0779E0
2.5000E5	1.1063E0
2.5500E5	1.1340E0
2.6000E5	1.1610E0
2.6500E5	1.1872E0
2.7000E5	1.2129E0
2.7500E5	1.2378E0

Temp (K)	$G_{1.807}(T)$
5.3500E5	2.2856E0
5.4000E5	2.2876E0
5.4500E5	2.2895E0
5.5000E5	2.2914E0
5.5500E5	2.2933E0
5.6000E5	2.2951E0
5.6500E5	2.2968E0
5.7000E5	2.2985E0
5.7500E5	2.3002E0
5.8000E5	2.3018E0
5.8500E5	2.3034E0
5.9000E5	2.3050E0
5.9500E5	2.3065E0
6.0000E5	2.3080E0
6.0500E5	2.3094E0
6.1000E5	2.3109E0
6.1500E5	2.3123E0
6.2000E5	2.3136E0
6.2500E5	2.3149E0
6.3000E5	2.3162E0
6.3500E5	2.3175E0
6.4000E5	2.3188E0
6.4500E5	2.3200E0
6.5000E5	2.3212E0
6.5500E5	2.3223E0
6.6000E5	2.3235E0
6.6500E5	2.3246E0
6.7000E5	2.3257E0
6.7500E5	2.3268E0
6.8000E5	2.3278E0
6.8500E5	2.3288E0
6.9000E5	2.3299E0
6.9500E5	2.3308E0
7.0000E5	2.3318E0
7.0500E5	2.3328E0
7.1000E5	2.3337E0
7.1500E5	2.3346E0
7.2000E5	2.3355E0
7.2500E5	2.3364E0
7.3000E5	2.3373E0
7.3500E5	2.3381E0
7.4000E5	2.3389E0
7.4500E5	2.3397E0
7.5000E5	2.3405E0

Temp (K)	$G_4(T)$
5.3500E5	1.9420E0
5.4000E5	1.9487E0
5.4500E5	1.9553E0
5.5000E5	1.9617E0
5.5500E5	1.9681E0
5.6000E5	1.9743E0
5.6500E5	1.9803E0
5.7000E5	1.9863E0
5.7500E5	1.9921E0
5.8000E5	1.9978E0
5.8500E5	2.0034E0
5.9000E5	2.0089E0
5.9500E5	2.0142E0
6.0000E5	2.0195E0
6.0500E5	2.0246E0
6.1000E5	2.0297E0
6.1500E5	2.0346E0
6.2000E5	2.0395E0
6.2500E5	2.0443E0
6.3000E5	2.0490E0
6.3500E5	2.0535E0
6.4000E5	2.0580E0
6.4500E5	2.0625E0
6.5000E5	2.0668E0
6.5500E5	2.0711E0
6.6000E5	2.0752E0
6.6500E5	2.0793E0
6.7000E5	2.0834E0
6.7500E5	2.0873E0
6.8000E5	2.0912E0
6.8500E5	2.0950E0
6.9000E5	2.0987E0
6.9500E5	2.1024E0
7.0000E5	2.1060E0
7.0500E5	2.1096E0
7.1000E5	2.1131E0
7.1500E5	2.1165E0
7.2000E5	2.1198E0
7.2500E5	2.1232E0
7.3000E5	2.1264E0
7.3500E5	2.1296E0
7.4000E5	2.1327E0
7.4500E5	2.1358E0
7.5000E5	2.1389E0

PROGRAM 1 - v.planck.

```
*B.
AUTO
MODE 3

REM written - 12-05-86
REM updated - 07-03-87
REM program - v.planck
REM purpose - to convert the measured counts of the object from those at
REM         - 4788A to the visual at 5500A using a Blackbody relationship

@% = &30A
max = 0
A = 0
DIM X( 100 )
DIM Rat( 100 )
DIM Vcts( 100 )
DIM Verr( 100 )
DIM Name$( 100 )
DIM T( 100 )
CLS

PROCintro
REPEAT
   PROCenter
   PROCcounts
   UNTIL FNstop
PROCsave
PROCend
END


DEF PROCintro

   P. "This program will evaluate the ratio of the Planck function at  "
   P. "two specified wavelengths.  Ratio = P1 / P2                       "
   P. "You are required to enter......."
   P. "WAVELENGTH's in ANGSTROM's"
   P. "TEMPERATURE's in KELVIN's"
   PRINT "Push any key to continue......                  "
   A$ = GET$                                   : REM waits for key to be hit
   CLS

ENDPROC


DEF PROCsave

   INPUT "Name for output file.....        " file$
```

```
   X = OPENOUT( file$ )
   C = max

   REPEAT
       C = C - 1
       PRINT Name$( C ),Rat( C ),Vcts( C ),Verr( C ),T( C )
       PRINT#X,Name$( C ),Rat( C ),Vcts( C ),Verr( C ),T( C )
       UNTIL C = 0
   CLOSE#0
   PRINT ' "Data saved in file " file$

ENDPROC


DEF PROCenter

   INPUT "Please enter the first wavelength in angstrom's.    " A1
   A1 = A1 * 1E-08
   INPUT "Please enter the second wavelength in angstrom's.   " A2
   A2 = A2 * 1E-08
   INPUT "Please enter the temperature in Kelvin.             " T
   PRINT
   M1 = FNplanck( A1 , T )
   M2 = FNplanck( A2 , T )
   X( A ) = M1
   X( A + 1 ) = M2
   Rat = M1 / M2
   PRINT "The ratio of the Planck function's is....." Rat
   PRINT
   A = A + 2

ENDPROC


DEF PROCcounts

   REM this procedure converts the P counts to equivalent V counts
   INPUT "Enter the P counts for the P.N. (per sec.)      " Pcts
   INPUT "Enter the error on the count.                   " Err
   INPUT "Enter the name of the P.N.                      " Name$
   Vcts = Rat * Pcts
   PctsT = Pcts + Err
   PctsB = Pcts - Err
   VctsT = PctsT * Rat
   VctsB = PctsB * Rat
   Verr = ( VctsT - VctsB ) / 2
   P. ' "The V counts/sec for the P.N. " Name$ " is " Vcts " +/- " Verr
   T( max ) = T
   Rat( max ) = Rat
   Vcts( max ) = Vcts
   Verr( max ) = Verr
```

```
   Name$( max ) = Name$
   max = max + 1

ENDPROC


DEF PROCend

   PRINT ' "Bye for now.......        "
   @% = 10

ENDPROC


DEF FNplanck(A,B)
LOCAL X
X=1.43882/(A*B)
=(1.19104E-05/A^5)*(1/(EXP(X)-1))

DEF FNstop
PRINT "Repeat? (n=STOP)      "
REPLY$=GET$
= (REPLY$="N") OR (REPLY$="n")
```

PROGRAM 2 - v.pnmag.

```
*BASIC
AUTO
MODE 3
@% = &0002040A
CLS

REM  written - 15-05-86
REM  updated - 07-03-87
REM  program - v.pnmag
REM  purpose - Calculates magnitude of NPN by ratioing NPN counts with
REM          - those of the standard star. Includes errors.

PROCintro
REPEAT
   PROCdo
   UNTIL FNstop
PROCend

END


DEF PROCintro

   INPUT "Enter the mag of the std star.                     " stdmag
   INPUT "Enter the error of the std star mag.               " stdmagerr
   INPUT "Enter the V counts for the std star.               " stdcts
   INPUT "Enter the error of the V counts of the std.        " stdctserr
   PRINT
   INPUT "Enter the name for the output file.                " out$

   X = OPENOUT(out$)

   PRINT "Hit any key to continue........."
   A$ = GET$
   CLS


DEF PROCdo

   INPUT "Enter the counts of the P.N.                       " pncts
   INPUT "Enter the error on this.                           " pnctserr
   INPUT "Enter the P.N. name.                               " name$

   pnmag = FNpnmag(stdmag,pncts,stdcts)

   REM calculate error in log term
   REM this comes from differential of log term
   pnflxerr  = ( ( 2.5 * LOG( 10 ) * pnctserr ) / pncts ) ^ 2
```

```
   stdflxerr = ( ( 2.5 * LOG( 10 ) * stdctserr ) / stdcts ) ^ 2
   errlog    = pnflxerr + stdflxerr

   REM calc total error
   errtot = SQR( ( stdmagerr ^ 2 ) + errlog )

   PRINT "P.N. " name$ " mag is " pnmag " +/- " errtot
   PRINT#X,name$,pncts,pnmag,errtot

ENDPROC


DEF PROCend

   CLOSE#X
   PRINT "Bye for now........"
   @% = 10

ENDPROC


DEF FNpnmag(m2,f1,f2)

= m2 - ( 2.5 * LOG( f1 / f2) )


DEF FNstop

PRINT "Do you want to compute for another P.N.? (n=STOP).    "
REPLY$ = GET$
= (REPLY$="N") OR (REPLY$="n")
```

PROGRAM 3 - v.workout

```
*BASIC
AUTO
MODE 3

REM written - 09-05-86
REM amended - 25-02-87
REM purpose - To evaluate the theoretical ratio of F(Hb)/F(vis),
REM         - corrected for interstellar reddening using the expression
REM         - as derived in Chapter 2, equation 2.2.10. Additionally
REM         - the function G1(T) is evaluated for a grid of T.

  Y=OPENOUT("HI")
  Z=OPENOUT("G1")

  DIM temper( 200 )
  DIM ratio_5( 200 )            :REM ratio for Te = 5000 K
  DIM ratio_10( 200 )           :REM                10000 K
  DIM ratio_20( 200 )           :REM                20000 K

  Lim = 18          : REM this is the max loop lim in FNGi
  DIM Int(  Lim )   : REM these are the arrays for FNGi
  DIM Rom(  Lim )
  DIM Temp( Lim )

  T1 = 20000        : REM starting temperature
  Step = 2000       : REM step size for T
  max = 199
  C = 0

  REPEAT

     C = C + 1
     T1 = T1 + Step
     G1 = FNGi
     val_5  = FNzan_5
     val_10 = FNzan_10
     val_20 = FNzan_20
     temper( C ) = T1
     ratio_5( C ) = val_5
     ratio_10( C ) = val_10
     ratio_20( C ) = val_20
     PRINT "temp is " T1 " ratios are " val_5,val_10,val_20
     PRINT#Y,T1,val_5,val_10,val_20
     PRINT "file loaded with T1,values"
     PRINT#Z,T1,G1
     PRINT "file loaded with T1, G1 val"
  UNTIL C = max
```

```
  CLOSE#0

END


DEF FNGi

  REM this function evaluates Gi(T)

  LOCAL  T, B, H, I, N, Sum, A%, B%, M%, K, J, L, Dev, P

  T = 88.0
  B = 6.626E-27 * 3.2895E15 / ( 1.381E-16 * T1 )

  PRINT "The function to be integrated is f(X)= X^2/(exp(X)-1)      "
  PRINT
  PRINT "The upper limit is infinity and will be approximated by x=88"
  PRINT
  PRINT "                Upper limit is " T
  PRINT
  PRINT "The lower limit is hv/kT (where v=freq. of the Lyman Limit)"
  PRINT "                Lower limit is " B
  PRINT

  H = T - B
  Int( 1 ) =  ( FNf( B ) + FNf( T ) ) * H / 2.0

  I = 2
  REPEAT

     N = ( 2 ^ I ) + 1
     H = ( T - B ) / ( N - 1 )

     Sum = 0

     REM    FOR M = 2 TO N-1
     REM    X = B + (M-1)*H
     REM    Sum = Sum + FNf(X)
     REM    NEXT M

     A% = 1
     B% = N - 2
     FOR M% = A% TO B%
        Sum = Sum + FNf( B + ( M% * H ) )
     NEXT

     Int( I ) = ( ( 2 * Sum ) + FNf(B) + FNf(T) ) * H / 2

     FOR K = 1 TO I
        Rom( K ) = Int( K )
     NEXT
```

```
    FOR K = 2 TO I

       FOR J = K - 1 TO I
          Temp( J ) = Rom( J )
       NEXT

       FOR L = K TO I
          P = 2 ^ K
          Rom( L ) = ( ( P * Temp( L ) ) - Temp( L - 1 ) ) / ( P - 1 )
       NEXT

    NEXT

    Dev = Rom( I ) - Rom( I - 1 )

    P. "After" N-1 " intervals the integral is  " Rom(I) " Change " Dev

    Dev = ABS( Dev )

    I = I + 1
  UNTIL ( I > Lim ) OR ( Dev < 1.0E-6 )

  IF I > Lim THEN P. '"ROUNDING ERRORS NOW DOMINATING; stopping" : STOP

  PRINT
  PRINT "INTEGRATION COMPLETE"
  PRINT "Gi(T) is " Rom( I - 1 )

= Rom( I - 1 )

DEF FNf(X)=X^2/(EXP(X)-1)        : REM this is the integral in FnGi


REM these functions evaluate ratio F(HB)/F(vis) , see red book 2 page 35

REM evaluated at Te of 5,000 K
DEF FNzan_5
=  4.1914E-11 * T1 ^ 3 * G1 * ( EXP( 2.616E4 / T1 ) - 1 )

REM evaluated at Te of 10,000 K
DEF FNzan_10
=  4.1296E-11 * T1 ^ 3 * G1 * ( EXP( 2.616E4 / T1 ) - 1 )

REM evaluated at Te of 20,000 K
DEF FNzan_20
=  3.9884E-11 * T1 ^ 3 * G1 * ( EXP( 2.616E4 / T1 ) - 1 )
```

PROGRAM 4 - v.hetrue2

```
*BASIC
AUTO
MODE 3
@% = &00030A

REM Written - 18-05-86
REM Updated - 06-03-87
REM Program - v.hetrue2
REM Purpose - The visual magnitudes, Hb & HeII fluxes for a P.N. are
REM         - entered, the HeII flux being expressed as a fraction of
REM         - the Hb flux, along with the reddening, E(B-V).
REM         - The flux ratios F(HeII) to F(vis) & F(Hb) to F(vis)
REM         - corrected for reddening are computed.

REM VDU2
PROCintro
PROCstart
PROCinput
PROCratio
PROCherat
PROCraterr
PROCsave
PROCend
REM VDU3
END

DEF PROCstart

   X = OPENOUT(out$)
   Y = OPENOUT(rat$)
   Z = OPENOUT(herat$)
   A4861 = 3.63                 : REM A coeffs for wavelength in angstrom
   A5500 = 3.10                 : REM see Pottasch P 96.

   max = 25

   DIM mv( max )
   DIM emv( max )
   DIM LHB( max )
   DIM HB( max )
   DIM EBV( max )
   DIM eEBV( max )              : REM error in E(B-V)
   DIM name$( max )
   DIM FRAT( max )
   DIM FRATmax( max )
   DIM FRATmin( max )
   DIM eFRATmax( max )
   DIM eFRATmin( max )
```

```
   DIM eRAT( max )
   DIM eFRAT( max )              : REM error in FRAT
   DIM HEHBRAT( max )
   DIM HEII( max )
   DIM HERAT( max )
   DIM EHERAT( max )
   DIM HERATmax( max )
   DIM HERATmin( max )
ENDPROC


DEF PROCintro

   PRINT "Prog computes the F(Hb)/F(vis) and F(HeII)/F(vis) ratios    "
   PRINT "for a given star. "
   PRINT "Input F(HB) flux in LOG erg s-1 cm-2 units.                  "
   PRINT "Visual magnitude is converted to F(vis).                     "
   PRINT "These values should be those uncorrected for extinction.     "
   PRINT "You will also be asked for a value of the extinction E(B-V)."
   PRINT "and the value of the HEII 4686 flux in terms of the hb flux "
   PRINT "ie as a fraction. This value should be corrected for extn.   "
   PRINT
   INPUT "Input the name of the o/p file for mv & extn........ " out$
   INPUT "Input name of o/p file to contain Hb flux ratio..... " rat$
   INPUT "Input name of o/p file for HeII/f(vis) ratio........ " herat$
   PRINT
ENDPROC


DEF PROCinput

   A = 0
   number = 0

   REPEAT
       A = A + 1
       INPUT "Enter the P.N. name.....                           " name$
       name$( A ) = name$
       INPUT "Enter the mag mv of this P.N.....                  " pnmag
       mv( A ) = pnmag
       INPUT "Enter the error in this.....                       " errtot
       emv( A ) = errtot
       INPUT "Enter the HB flux for the P.N. in LOG units.. " LHB( A )
       INPUT "Enter E(B-V) for the nebula.....                   " EBV( A )
       INPUT "Enter the error in E(B-V)......                    " eEBV(A)
       INPUT "Enter HEII/HB for the nebula.....                  " HEHBRAT(A)
       number = A
       UNTIL FNstop
ENDPROC
```

```
DEF PROCratio

   A = 0

   REPEAT
       A = A + 1
       HB( A ) = 10 ^ LHB( A )
       FRAT( A ) = FNratio( HB( A ),EBV( A ),mv( A ) )
       UNTIL A = number
ENDPROC


DEF PROCraterr       REM see R2 page 76

   A = 0

   REPEAT
       A = A + 1
       eRAT( A ) = SQR( ( emv( A ) ^ 2 ) + ( 0.5 * eEBV( A ) ) ^ 2 )
       eFRAT( A ) = eRAT( A ) * FRAT( A )
       FRATmax( A ) = FRAT( A ) + eFRAT( A )
       FRATmin( A ) = FRAT( A ) - eFRAT( A )
       UNTIL A = number
ENDPROC


DEF PROCherat

   A = 0

   REPEAT
       A = A + 1
       HEII( A ) = HB( A ) * HEHBRAT( A )
       HERAT( A ) = FNratio( HEII( A ),EBV( A ),mv( A ) )
       eRAT( A ) = SQR( ( emv( A ) ^ 2 ) + ( 0.5 * eEBV( A ) ) ^ 2 )
       EHERAT( A ) = eRAT( A ) * HERAT( A )
       HERATmax( A ) = HERAT( A ) + EHERAT( A )
       HERATmin( A ) = HERAT( A ) - EHERAT( A )
       UNTIL A = number
ENDPROC


DEF PROCsave

   A = 0

   REPEAT
       A = A + 1
       P.
       P. "Values of reddened corrected P.N. " name$(A) " are: "
       P. "F(Hb)/F(vis) ratio is...... " FRAT( A ) " +/- " eFRAT( A )
```

```
        P. "F(HeII)/F(vis) ratio is.... " HERAT( A ) " +/- " EHERAT( A )
        P.#X,name$( A ),mv( A ),emv( A ),EBV( A ),eEBV( A )
        P.#Y,name$( A ),FRAT( A ),eFRAT( A ),FRATmax( A ),FRATmin( A )
        P. name$( A ),FRAT( A ),eFRAT( A ),FRATmax( A ),FRATmin( A )
        P.#Z,name$(A),HERAT( A ),EHERAT( A ),HERATmax( A ),HERATmin( A )
        P. name$( A ),HERAT( A ),EHERAT( A ),HERATmax( A ),HERATmin( A )
        P.
        UNTIL A = number

ENDPROC

DEF PROCend

   CLOSE#0
   PRINT "Magnitudes and extinctions saved in ...... " out$
   PRINT "F(Hb)/F(vis) ratios saved in ............. " rat$
   PRINT "F(HeII)/F(vis) ratios saved in ........... " herat$
   PRINT
   PRINT "Bye for now.......                 "

ENDPROC


DEF FNratio( hb,extn,mag )

REM ratio is Hb(corr)/Fvis(corr)
REM Hb(corr) = Hb * 10^(3.63/2.5 * E(B-V)
REM Fvis(corr) = 3.64*10-9 * 10^(-mv/2.5) * 10^(3.10/2.5 * E(B-V))
REM so these reduce to:

= ( 1 / ( 3.64E-9 ) ) * hb * ( 10 ^ ( 0.4 * ( mag + ( 0.53 * extn ) )))


DEF FNstop

PRINT " Repeat ? ( n = STOP ) "
REPLY$ = GET$
= (REPLY$ = "N") OR (REPLY$ = "n")
```

PROGRAM 5 - v.zan2

```
*BASIC
AUTO
MODE 3

REM written - 18-05-87
REM updated - 07-02-87
REM purpose - Program ZAN2 takes the flux ratio F(Hb)/F(vis) for the P.N
REM         - and computes the Temp., Luminosity and Radius for the NPN.
REM         - this version also computes errors.
REM         - Can also be used for F(HeII)/F(vis) ratio!

PROCask
PROCstart
PROCintro

REM VDU 2
C = 0
   REPEAT
       C = C + 1
       YOUT( C ) = FNfind( FRAT( C ) )      : REM find nearest T for FRAT
       P. name$( C ), YOUT( C ), C
       P. "FRATmax= " FRATmax( C ) " for " name$( C )
       YOUTmax( C ) = FNfind( FRATmax( C ) )
       P. name$( C )" max", YOUTmax( C ), C
       P. "FRATmin= " FRATmin( C ) " for " name$( C )
       YOUTmin( C ) = FNfind( FRATmin( C ) )
       P. name$( C )" min ", YOUTmin( C ), C
       eYOUT( C ) = ( YOUTmax( C ) - YOUTmin( C ) ) * 0.5
       UNTIL C = number
REM VDU 3

PROCradius
PROClumin
PROCend
END


DEF PROCask

   REM VDU 2
   INPUT "Enter name of theoretical data................ " thec$
   INPUT "Enter name of file with P.N. flux ratios...... " rat$
   INPUT "Enter name of P.N. data file.................. " lum$
   INPUT "Enter name for output file.................... " out$
   REM VDU 3
   CLS

ENDPROC
```

```
DEF PROCstart

   Lim = 200                                : REM No. of values in TvsRAT
   Max = 25                                 : REM No. of P.N.'s

   DIM X( Lim )                             : REM Temp calculated
   DIM Y( Lim )                             : REM Ratio calculated
   DIM FRAT( Max )                          : REM Ratio for P.N.
   DIM eFRAT( Max )
   DIM FRATmax( Max )
   DIM FRATmin( Max )
   DIM name$( Max )                         : REM Names of P.N.
   DIM mv( Max )                            : REM mags of P.N.
   DIM emv( Max )
   DIM mvc( Max )                           : REM mags corrected for extinc
   DIM emvc( Max )
   DIM FvisC( Max )                         : REM corrected vis. fluxes
   DIM FvisCmax( Max )
   DIM FvisCmin( Max )
   DIM eFvisC( Max )
   DIM EBV( Max )                           : REM extinction of P.N.
   DIM eEBV( Max )
   DIM Dis( Max )                           : REM distance to the P.N.
   DIM eDis( Max )                          : REM error in the distance
   DIM YOUT( Max )                          : REM calc. temps of P.N.
   DIM YOUTmax( Max )
   DIM YOUTmin( Max )
   DIM eYOUT( Max )
   DIM Rad( Max )                           : REM calc. radii of P.N.
   DIM eRad( Max )
   DIM lumin( Max )                         : REM calc. lumin. of P.N.
   DIM elumin( Max )

   W = OPENIN(rat$)
   X = OPENIN(theo$)
   Y = OPENIN(lum$)
   Z = OPENOUT(out$)

   A = 0
   B = 0

ENDPROC


DEF PROCintro

   PRINT "This program evaluates a Zanastra temp for the named P.N."
   REM load in all the data into the arrays.
```

```
   REPEAT
       INPUT#X,T,RAT
       PRINT TAB(0,5) "Temp is            Ratio is                 "
       PRINT TAB(0,5) "Temp is " T " Ratio is " RAT
       A = A + 1
       X( A ) = T
       Y( A ) = RAT
       PRINT TAB(0,7) "X(            )  is            "
       PRINT TAB(29,7) " and Y(            ) is            "
       PRINT TAB(0,7) "X( "A" ) is " X( A ) " and Y( "A" ) is " Y( A )
       UNTIL EOF#X
   N = A

   B = 0

   REPEAT
       B = B + 1
       INPUT#W,name$,FRAT,eFRAT,FRATmax,FRATmin
       name$( B ) = name$
       FRAT( B ) = FRAT
       eFRAT( B ) = eFRAT
       FRATmax( B ) = FRATmax
       FRATmin( B ) = FRATmin
REM         VDU 2
       PRINT "loading " name$( B ) " ratio " FRAT( B ) " file " B
REM         VDU 3
       UNTIL EOF#W
   number = B

   B = 0

   REPEAT

       B = B + 1
       INPUT#Y,name$(B),mv(B),emv(B),EBV( B ),eEBV( B )
   REM VDU 2
       P. name$( B ),mv( B ),emv( B ),EBV(B),eEBV(B)
       P. "Enter the distance (kpc) to the P.N. " name$( B )
       INPUT Dis( B )
       INPUT "Enter the error in the distance (kpc) " eDis( B )
   REM VDU 3
       UNTIL EOF#Y
   number = B

ENDPROC


DEF PROCradius

   B = 0
```

```
   REPEAT
       B = B + 1
       FvisC( B ) = 3.64E-9 * 10^(-mv( B ) / 2.5) * 10^( 1.24*EBV( B ) )
       eFvisC( B )=SQR(( 0.848 * emv( B ) ) ^ 2 + ( 8.2 * eEBV( B ) )^2)
       eFvisC( B )= FvisC( B ) * eFvisC( B )
       Rad( B ) = FNradius(Dis( B ),FvisC( B ),YOUT( B ))
       eRad(B) = FNraderr(eDis(B),Dis(B),eFvisC(B),FvisC(B),eYOUT(B),YOUT(B))
       UNTIL B = number

ENDPROC


DEF PROClumin

   B = 0

   REPEAT
       B = B + 1
       mvc( B ) = mv( B ) - ( 3.10 * EBV( B ) )
       emvc( B ) = SQR( ( emv( B ) ^ 2 ) + ( 3.1 * eEBV( B ) ) ^ 2 )
       lumin( B ) = FNlumin( Dis( B ),YOUT( B ),mvc( B ) )
       elumin(B)=FNlumerr(eDis(B),Dis(B),emvc(B),mvc(B),eYOUT(B),YOUT(B))
       UNTIL B = number

ENDPROC


DEF PROCend

   REM VDU 2
   B = 0
   @% = &30A

   REPEAT
       B = B + 1
       PRINT name$(B),FRAT(B),YOUT(B),eYOUT(B),Rad(B),eRad(B),lumin(B),elumin(B)
       PRINT#Z,name$(B),FRAT(B),YOUT(B),eYOUT(B),Rad(B),eRad(B),lumin(B),elumin(
       UNTIL B = number

   PRINT "Ending now........."
   CLOSE#0
   REM VDU 3
   @% = 10

ENDPROC


DEF FNradius(D,Fvis,T)     : REM see R2 page 56
REM units of this are solar radii
REM Ro = 6.96e10 cm, 1 kpc = 3.08e21 cm
```

```
= SQR( ( D ^ 2 ) * ( 2.6268E12 ) * Fvis * ( EXP( 2.6161E4 / T ) - 1 ) )


DEF FNraderr(ED,D,EF,F,ET,T)

LOCAL X,Y,Z,W

X = ( ED / D ) ^ 2
Y = ( ( EF / F ) * 0.5 ) ^ 2
W = EXP( 2.6161E4 / T ) / ( EXP( 2.6161E4 / T ) - 1 )
Z = ( ( 0.5 * W * 2.6161E4 * ET ) / ( T ^ 2 ) ) ^ 2

= SQR( X + Y + Z )


DEF FNlumin(D,T,MV)        : REM see R2 page 70

= 9.760E3*(D^2)*(EXP(2.6161E4/T)-1)*(10^(-MV/2.5 ) ) * (( T / 5770 )^4)


DEF FNlumerr(ed,d,em,m,eT,T)

LOCAL X,Y,Z,W,U

X = ( ( ED / D ) * 0.5 ) ^ 2
Y = ( ( LN( 10 ) * em ) / 2.5 ) ^ 2
W = EXP( 2.6161E4 / T ) / ( EXP( 2.6161E4 / T ) - 1 )
Z = ( ( 2.6161E4 * W * eT ) / ( T ^ 2 ) ) ^ 2
U = ( ( 4 * eT ) / T ) ^ 2

= SQR( X + Y + Z + U )


DEF FNfind( help )

REM this routine fits a 4th degree polynomial to the grid of theoretical
REM flux ratios to find T. for the observed flux ratio. See Bevington,
REM Data reduction and error analysis for the physical sciences, page 261.

       A = 0
       Val = 0


       REPEAT
           A = A + 1
           Val = help - Y( A )
           UNTIL ( Val < 0.0 ) OR ( A = N )


       IF A - N = 0 THEN PRINT " !!! warning this result is incorrect !!! "
       IF A - N = 0 THEN A = 10
```

```
        Ntemp = X( A )
        PRINT "Diff is " Val " Nearest Temp is " Ntemp
        X1 = Y( A - 2 ) : Y1 = X( A - 2 )  : REM X is the flux ratio
        X2 = Y( A - 1 ) : Y2 = X( A - 1 )  : REM Y is the temperature
        X3 = Y( A )     : Y3 = X( A )
        X4 = Y( A + 1 ) : Y4 = X( A + 1 )
        X5 = Y( A + 2 ) : Y5 = X( A + 2 )
        PRINT "Ratios... " X1,X2,X3,X4,X5
        PRINT "Temps.... " Y1,Y2,Y3,Y4,Y5
        D = ( help - X1 ) / ( X2 - X1 )
        D2 = 1.0
        D3 = ( X3 - X1 ) / ( X2 - X1 )
        D4 = ( X4 - X1 ) / ( X2 - X1 )
        D5 = ( X5 - X1 ) / ( X2 - X1 )
        A1 = Y1
        A2 = ( Y2 - A1 ) / D2
        A3 = ( Y3 - ( A2 * D3 ) - A1 ) / ( D3 * ( D3 - D2 ) )
        A4 = ( Y4 - ((A3*D4)*(D4-D2))-(A2*D4)-A1) / (D4*(D4-D2)*(D4-D3))
        Top = ( Y5-A1-(D5*A2)-(A3*(D5-D2))-(A4*(D5-D3)*(D5-D2)) )
        Bottom = ( D5 * ( D5 - D4 ) * ( D5 - D3 ) * ( D5 - D2 ) )
        A5 = Top / Bottom
        P1 = A1 + ( A2 * D ) + ( A3 * D * ( D - D2 ) )
        P2 = ( A4 + D * ( D - D2 ) * ( D - D3 ) )
        P3 = ( A5 + D * ( D - D2 ) * ( D - D3 ) * ( D - D4 ) )
= P1 + P2 + P3
```

PUBLICATIONS

Mon. Not. R. astr. Soc., (1986) **218**, *Short Communication*, 13P–17P

Extra-nuclear molecular hydrogen in NGC 1068

N. K. Reay *Astrophysics Group, Blackett Laboratory, Imperial College, London SW72BZ*

P. D. Atherton *Kapteyn Astronomical Institute, 9700-A V Groningen, Netherlands*

N. A. Walton *Astrophysics Group, Blackett Laboratory, Imperial College, London SW72BZ*

Accepted 1985 October 28. Received 1985 October 14

Summary. We report observations of the $v=1-0$ S(1) line of molecular hydrogen in the nucleus and inner spiral arms of the Seyfert galaxy NGC 1068. Spectra of the nucleus, for which the $v=2-1$ S(1) line was also observed, confirm that the lines are collisionally excited. Significant detections were made at two of the seven positions at which spectra were recorded in the inner spiral arms. The inner region of NGC 1068 is known to be turbulent, with Hα linewidths of up to $\sim 100\,\mathrm{km\,s^{-1}}$ and little correlation between linewidth and the positions of the bright H II regions. We have suggested in a previous publication that this turbulence may be the result of nuclear outflow interacting with the galactic disc. We suggest here that the molecular hydrogen is excited by a shock driven by this outflow.

1 Introduction

Thompson, Lebovsky & Rieke (1978) detected molecular hydrogen in the nucleus of NGC 1068 using a Fourier Transform Spectrometer (FTS). Subsequently Hall *et al.* (1981) have obtained spectra of the nucleus, through a 3.8-arcsec aperture, in the 2.0–2.4-μm region at a resolution of $5\,\mathrm{cm^{-1}}$ (velocity resolution $350\,\mathrm{km\,s^{-1}}$). They suggested that the emission arises in molecular clouds which are confined to the central 200 pc of the galaxy, the kinematics of which are determined by the gravitational potential of the nucleus. The ratio of the $v=1-0$ S(1) to $v=2-1$ S(1) lines is reported by both groups of authors to be consistent with shock excitation of the molecules rather than UV fluorescence.

In this note we report the first detection of extra-nuclear molecular hydrogen in NGC 1068. The $v=1-0$ S(1) line was detected at two positions in the inner spiral arm of the galaxy, both of which lie within the region containing turbulent H II complexes (Atherton, Reay & Taylor 1985) which is co-spatial with the 3-kpc infrared disc reported by Telesco, Becklin & Wynn-Williams (1984).

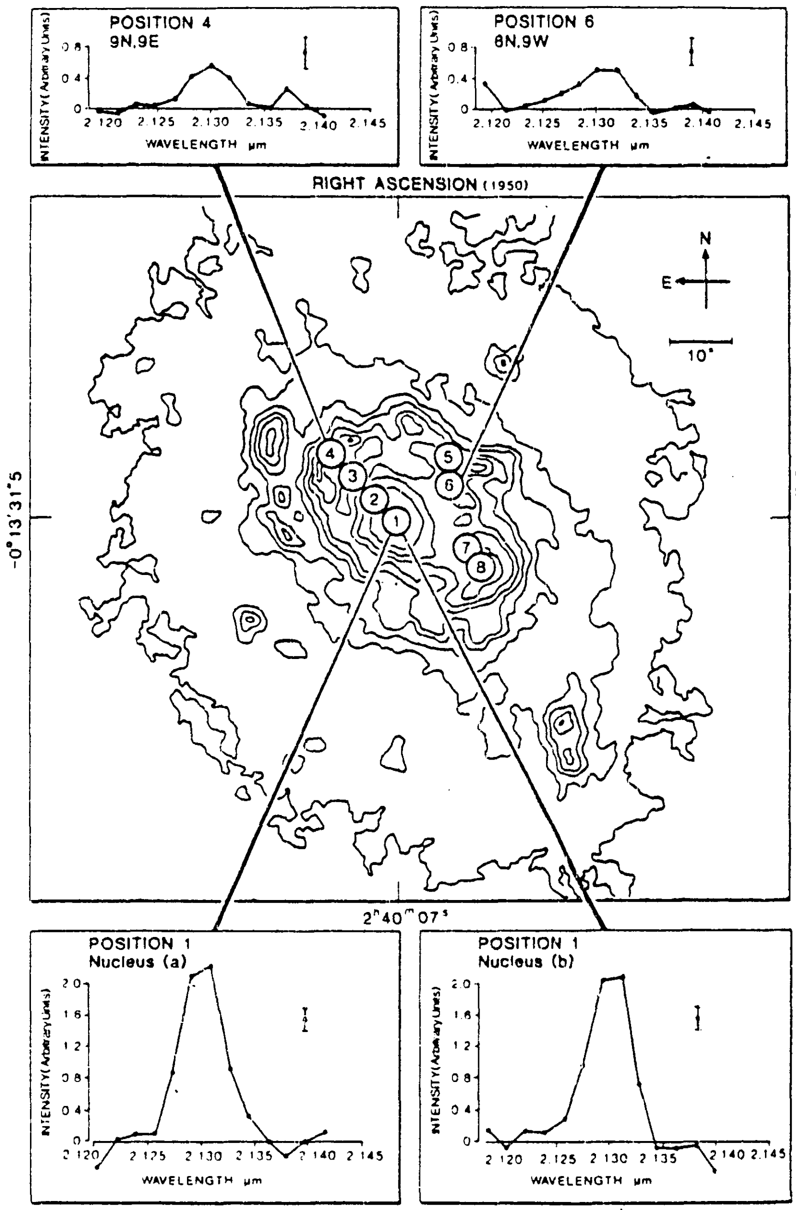

Figure 1. Positions at which observations of the S(1) $v=1-0$ line were made shown superimposed on an Hα-line contour map. Significant detections were made at position 1 (the nucleus) and positions 4 and 6. The spectra obtained at these positions are illustrated. They have been ratioed with a standard star, smoothed with a top-hat function of width 275 km s^{-1} and the base-lines have been subtracted.

2 Observations

The observations were made with a 7-channel cooled grating spectrometer (Wade 1983) at the UK Infrared Telescope (UKIRT) on the night of 1984 November 31 and December 1. Spectra with a resolving power ~600 (velocity resolution 550 km s^{-1}), Consisting of 14 sample points spaced by approximately 275 km s^{-1}, were obtained centred on the anticipated position of the redshifted 2.122-μm $v=1-0$ S(1) line.

Table 1. Observational parameters and fluxes for the $v=1-0$ S(1) line.

Position	Co-ordinates*	Integration Time (s)	Flux ($W m^{-2}$)	Luminosity ($L_⊙$)
1	nucleus (a)	320	1.53×10^{-16}	1.35×10^{6} (mean value)
	nucleus (b)	320	1.48×10^{-16}	
2	3N, 3E	320	... null detection ...	
3	6N, 6E	640	... null detection ...	
4	9N, 9E	640	3.75×10^{-17}	3.4×10^{5}
5	9N, 9W	320	... null detection ...	
6	6N, 3W	1280	3.9×10^{-17}	3.5×10^{5}
7	6S, 12W	980	... null detection ...	
8	7.5S, 13W	640	... null detection ...	

* Measured in arcseconds north (N), south (S), east (E), or west (W) from the nucleus.

The entrance aperture was approximately circular with an equivalent diameter of 5.4 arcsec on the sky. An E–W chop with a beam separation of a 60 arcsec was used to compensate for sky background.

Spectra obtained at the nucleus, and two other positions where significant detections were obtained, are shown superimposed on an Hα contour map (Fig. 1) produced from data obtained with TAURUS (Atherton *et al.* 1982) at the Anglo-Australian Telescope.

Table 1 summarizes the observational parameters and the line fluxes and luminosities determined using calibration spectra obtained for the standard stars BS718 and BS804.

The two spectra obtained at the nucleus give fluxes of 1.48×10^{-16} and $1.53\times10^{-16}\,W\,m^{-2}$, with a mean value of $1.5\times10^{-16}\,W\,m^{-2}$ corresponding to a luminosity of $1.35\times10^{6}\,L_⊙$ if we adopt a distance of 18.1 Mpc (Sandage & Tammann 1975). At positions 4 and 6 the fluxes are 3.75×10^{-16} and $3.9\times10^{-16}\,W\,m^{-2}$ respectively, corresponding to luminosities of 3.4×10^{5} and $3.5\times10^{5}\,L_⊙$.

Positions 4 and 6 both lie on the ridge of H II regions which delinate the inner spiral arm to the north of the nucleus of NGC 1068. In this region Atherton *et al.* (1985) have measured Hα linewidths of up to 85 km s^{-1}. H II regions in normal galaxies have Hα linewidths of typically 20 km s^{-1} (Gallagher & Hunter 1983) while some exceptional H II regions have been reported with linewidths of up to 75 km s^{-1} (Jaffe, Perola & Tarenghi 1978). The inner spiral arms of NGC 1068 are, by comparison, exceptionally turbulent and it is attractive to suggest that the molecular hydrogen emission in these regions is shock-excited.

In the very bright H II region 15 arcsec to the south-west of the nucleus, Atherton *et al.* (1985) reported Hα linewidths of greater than 130 km s^{-1}. At this position we failed to detect the S(1) line.

Joseph, Wright & Wade (1984) have recently pointed out that in Orion the ratio of the luminosity in the $v=1-0$ S(1) line of molecular hydrogen to the total infrared luminosity $L[S(1)]/L[IR]$ has a value of $\sim1.2\times10^{-5}$, which they suggest may be expected to be a characteristic value of this ratio in regions of star formation. They argue that a value of this ratio in excess of that observed in Orion may be indicative of shock-excitation of molecular hydrogen.

Adopting an IR luminosity of $1.4\times10^{11}\,L_⊙$ for the nucleus of NGC 1068 (Telesco *et al.* 1984), we find a value of the ratio $L[S(1)]/L[IR]\sim1.0\times10^{-5}$, consistent with the value observed in Orion.

At positions 4 and 6 the 10-μm flux densities (Telesco *et al.* 1984) are 125 mJy (3.8×10^{-14} W m^{-2} on the assumption of a full bandwidth of 3×10^{13} Hz) and 75 mJy (2.2×10^{-14} W m^{-2}) respectively. There are no measurements of the total IR flux in these regions, but adopting an estimate for both regions of 15 times the 10-μm flux leads to values of the ratio L[S(1)]/L[IR] of 7×10^{-5} for position 4 and 12×10^{-5} for position 6. These are significantly in excess of the value observed in Orion.

The optically bright H II region to the south-west of the nucleus (position 8) is a factor 2 or more brighter at 10 μm (Telesco *et al.* 1984) than positions 4 and 6 and the inner spiral arm in general. Our failure to detect the S(1) line at this position suggests that the L[S(1)]/L[IR] ratio may have a considerable variation from one H II region to another.

Finally it is of interest to look at the energetics of the molecular hydrogen excitation process. There is remarkably little correlation between structure in the linewidth map and in the intensity map (Atherton *et al.* 1985). The H II regions which show so distinctively in the latter are, in general, hardly distinguishable against the background in the former. Furthermore, the linewidth map shows a general tendency for decreasing linewidths with increasing distance from the nucleus. We suggest that this essentially galacto-centric turbulence pattern may indicate a nuclear origin of the molecular hydrogen excitation process.

Assuming LTE at a temperature of 2000 K (Shull & Beckwith 1982), the mean S(1) line flux of 3.82×10^{-17} W m^{-2} at positions 4 and 6 implies an upper limit to the mass of excited molecular hydrogen of $\sim$700 $M_\odot$. This gas will cool to a temperature of 1000 K in approximately 10^8 s (Kwan 1977), implying that the energy source must be capable of exciting $\sim$230 $M_\odot$ yr^{-1}. The force required to excite this mass of molecular hydrogen in a 10 km s^{-1} shock will be $\sim1.5\times10^{29}$ N.

In comparison, a molecular hydrogen emitting region of 5 arcsec diameter (the telescope beamwidth) at a distance $\sim$11 arcsec from the nucleus will intercept $\sim$1.5 per cent of the nuclear luminosity. Adopting a value of 1.4×10^{11} $L_\odot$ (Telesco *et al.* 1984) for the nuclear luminosity L, the maximum radiative force L/c driving the shock will be $\sim3\times10^{27}$ N, insufficient by a factor $\sim$50 to excite the observed molecular hydrogen.

An alternative source of energy to drive the shock may be nuclear outflow. Atherton *et al.* (1985) suggested outflow in the form of 'cloudlets' at a velocity of $\sim$1500 km s^{-1} or more to explain their kinematic data. Although no attempt was made by these authors to quantify the level of outflow, we can make a crude estimate by asking how much would be required to explain the observed molecular hydrogen emission as arising in an outflow-driven shock. For the force mv exerted by the outflow to equal the force required to shock 230 $M_\odot$ yr^{-1} of molecular hydrogen, the mass outflow rate m must be $\sim$100 $M_\odot$ yr^{-1} if the outflow velocity is 1500 km s^{-1}.

3 Conclusions

In conclusion we can say that we have detected molecular hydrogen in emission external to the nucleus of NGC 1068. The signal-to-noise ratio is poor, but there is some evidence that the emission may be localized in the ridge of H II regions which delineate the inner spiral arm of the galaxy.

Radiation pressure from the nucleus appears to be inadequate to drive the exciting shock. On the other hand, outflow from the nucleus may be responsible for the turbulence observed in the inner spiral arms, and also for the observed molecular hydrogen emission providing the mass outflow rate is $\gtrsim$100 $M_\odot$ yr^{-1}.

Acknowledgments

We gratefully acknowledge the professional assistance and hospitality provided by the UKIRT staff. In particular we thank Dr Andy Longmore for his assistance in making the observations.

References

Atherton, P. D., Reay, N. K. & Taylor, K., 1985. *Mon. Not. R. astr. Soc.*, **216**, 17P.

Atherton, P. D., Taylor, K., Pike, C. D., Harmer, C. F. W., Parker, N. M. & Hook, R., 1982. *Mon. Not. R. astr. Soc.*, **201**, 661.

Gallagher, J. S. & Hunter, D. A., 1983. *Astrophys. J.*, **274**, 141.

Hall, D. N. B., Kleinmann, S. G., Scoville, N. Z. & Ridgeway, S. T., 1981. *Astrophys. J.*, **248**, 898.

Jaffe, W. J., Perola, G. C. & Tarenghi, M., 1978. *Astrophys. J.*, **244**, 808.

Joseph, R. D., Wright, G. S. & Wade, R., 1984. *Nature*, **311**, 132.

Kwan, J., 1977. *Astrophys. J.*, **216**, 713.

Sandage, A. & Tammann, G. A., 1975. *Astrophys. J.*, **196**, 313.

Shull, J. M. & Beckwith, S., 1982. *Ann. Rev. Astr. Astrophys.*. **20**, 163

Telesco, C. M., Becklin, E. E. & Wynn-Williams, C. G., 1984. *Astrophys. J.*, **282**, 427.

Thomspon, R. I., Lebovsky, M. J. & Rieke, G. H., 1978. *Astrophys. J.*, **222**, L49.

Wade, R., 1983. *Proceedings of S.P.I.E.*, **445**, 47.

MAGNITUDES OF SELECTED CENTRAL STARS OF PLANETARY NEBULAE

N.A.Walton N.K.Reay S.R.Pottasch P.D.Atherton

Astrophysics Group,
Blackett Laboratory,
Imperial College,
London SW7 2BZ,
U.K.

Kapteyn Astronomical Institute
University of Groningen
Post Box 800
9700 AV Groningen
The Netherlands

ABSTRACT

We have taken narrow band continuum images of 21 Planetary Nebulae using a CCD camera at the prime focus of the Anglo-Australian Telescope. These nebulae were selected on the basis that their central stars had been previously poorly detected or undetected. Using these images we have determined visual magnitudes for the nuclei of the Planetary Nebulae and calculated their corresponding Zanstra temperatures. The distribution of the Planetary Nebulae on the Log L-Log T plane is presented and briefly discussed in terms of present theories of the evolution of the nuclei of Planetary Nebulae. A number of the central stars studied have high temperatures which can be explained with present theories if their masses are about 1 $M_{\odot}$.

Keywords: planetary nebulae-temperatures of stars

1. INTRODUCTION

There is some argument concerning the evolutionary tracks of the central stars of Planetary Nebulae (PNe) on the H-R diagram. In order to accurately position the central stars in the H-R diagram one needs to know their distances and temperatures. In this paper we concentrate on determining the temperatures of a number of central stars that have previously been poorly determined.

Theories of the evolution of intermediate mass stars predict that some will pass through a high temperature phase with temperatures greater than 2×10^5 K (Ref. 1).These very hot stars will emit the bulk of their energy in the ultraviolet (Ref. 2) and hence will appear as the fainter central stars in the visible. Most of the PNe that we chose to observe were just those with faint nuclei.

In measuring the temperatures of these central stars we have made use of the Zanstra method which requires a knowledge of the number of ionising photons from the star and its visual continuum flux and relies on the fact that the nebula is optically thick in the Lyman continuum. All the energy from the exciting star in the Lyman continuum will go into ionising the surrounding nebula gas. This energy will emerge at longer wavelengths in the form of recombination and collisionally excited lines. If the Hβ flux from the PN is known then the total number of ionising Lyman photons can be determined because each Lyman photon eventually leads to the production of a Balmer photon. The visual flux from the star can be calculated directly from its visual magnitude. The ratio of these two quantities leads to the hydrogen Zanstra temperature assuming either a black body or model atmosphere for the central star.

The ratio of the number of ionising photons to the stellar continuum flux in the visible increases with temperature. The nebula flux is determined by the ionising photon flux. As a consequence of this the hotter the exciting star the brighter the nebula will be relative to the stars visual continuum meaning that hot stars will be less easily seen in the visible above the background nebula flux. It is easy to measure the Hβ flux from a PN but for hot stars it is harder to measure the central star magnitude.

One method that has recently been used by Shaw and Kaler (Ref. 3) to determine the magnitudes of central stars uses aperture photometry to measure the total line and continuum flux coming from the PN (which includes the contribution from the central star). Theoretical models are used to predict the nebula contribution to this flux and hence the remaining flux is that from the exciting star. However for fainter central stars ($m_V < 14$) noise from the nebula and the background night sky can make this method difficult to apply.
Another method makes use of the IUE telescope. Here the UV continuum for PNe can be obtained from IUE SWP and LWR images. The theoretical nebulà continuum is calculated and deconvolved from the observed continuum to leave the stellar component which is usually assumed to be a blackbody. From this stellar flux an estimate of the visual magnitude of the star can be made. The magnitude of NGC 3918 has been determined in this way by Clegg et al (Ref. 4).

As an alternative to these methods we decided to make use of a technique using an imaging detector. A narrow band filter was used to image the nebulae, thus excluding all known nebula emission lines so as to ensure the maximum possible contrast between the star and the nebula. (The star is largely a continuum source whilst the nebula spectrum is dominated by emission lines.) As has been noted by Pottasch (Ref. 5) and others the greatest contrast between star and nebula occurs at wavelengths below 2000Å. However we have observed in the visible where large ground based telescopes coupled with sensitive detectors offsets the reduced discrimination.

In this work we present new visual magnitudes for 21 central stars. Hydrogen Zanstra temperatures are calculated for these stars and they are shown positioned on the H-R diagram.

2. OBSERVATIONS

The method used was a refinement of the technique previously employed by Reay et al (Ref. 6). To ensure maximum discrimination between the central star and the nebula monochromatic images of the nebulae were recorded at a wavelength well clear of any known emission lines. Images were also taken through U,B and V broadband filters. For some of the nebulae studied we also obtained [OI] and [OIII] images. These supplementary images together with the narrow band continuum exposures enabled us to identify the central star in those cases where it might have been confused with knots and condensations within the nebula envelope.

The observations were made with a CCD camera at the prime focus of the Anglo-Australian telescope during three nights of March 1985. The continuum filter had a bandwidth of 10Å and was centred at 4788Å. The spatial resolution of the CCD detector was ≈ 0.5 arcsecs. The seeing at the time of observation was determined from the FWHM of field stars in the image frame or by taking the FWHM of the nearest (time) standard star frame.

Between observations of the PNe, images of spectrophotometric standard stars were recorded through each of the six filters used. The standard stars were taken from the lists of Landolt (Ref. 7). Flat fields using each of the filters were taken on each of the three nights. Also read out noise on the CCD was determined by reading out the CCD after a zero time integration.

For two of the PNe in our sample (NGC 2440 and NGC 3918) Gathier (Ref. 8) has photometric data on nearby field stars which appear in our images. These enabled an independent estimate of the central star magnitude to be made, giving us a check on our calibration technique.

The data obtained was reduced at two sites. The bulk of the reduction was carried out using the GIPSY image processing system at The University of Groningen. Supplementary reduction was performed using the STARLINK image processing system running at University College, London.

A sample of the images that we obtained are shown as contour maps in Figs. 1-2. We found that the seeing pertaining at the time of each exposure was critically important in determining the observability of some of the central stars. For instance, NGC 2440 is shown in Fig. 1. In Fig. 1a the central star is clearly seen when the seeing was ≈ 1 arcsec. However in an earlier exposure Fig. 1b, when the seeing was ≈ 2 arcsec the central star is no longer apparent. Fig. 1c shows the effect of smoothing Fig. 1a to 2 arcsec resolution showing how the central star is merged into the nebula emission when the seeing is poor.

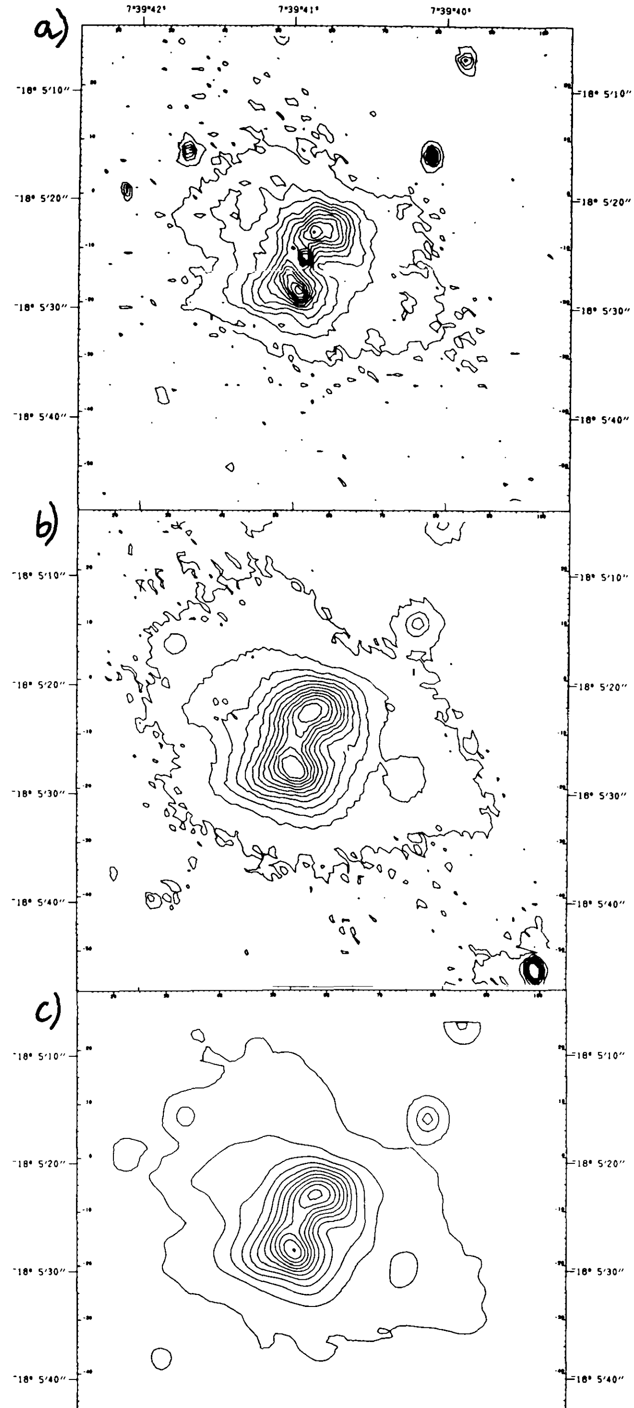

Fig 1 (a) A narrow band CCD image of NGC 2440 obtained through a continuum filter centred at λ = 4788Å. Here the star is clearly seen, the seeing being about 1 arcsec. (b) With seeing of 2 arcsec on a previous observation the star is no longer apparent. (c) The result of smoothing (a) to 2 arcsec resolution showing that with bad seeing the central star is swamped by the nebula background.

The standard star intensities for each exposure were obtained from the images. By observing the same standard at varying angles from the zenith it was possible to find the solution for atmospheric extinction. It was found that this did not change over the three nights and so a standard airmass correction was applied to each of the PN.

To enable the magnitudes of the central stars to be determined the intensity of the central stars in the continuum images were found by interpolating and subtracting the nebula continuum and integrating under the stellar profile. These were corrected for atmospheric extinction and compared with similar quantities determined for the standard stars. Field stars were used as an additional calibration in the cases of NGC 2440 and NGC 3918.

3. MAGNITUDES

The visual magnitudes of the central stars were found by comparing the flux in the central star to the flux in the standard. All observations were corrected for atmospheric extinction. In order to make the correction from our observed continuum wavelength at $\lambda = 4788Å$ to the V band (at $\approx 5500Å$) we made the assumption that the central stars are sufficiently hot to have Rayleigh-Jeans black body spectra in the visible. We also assumed that the standard stars emit as black bodies in the wavelength range that we were concerned with.

On making these assumptions we obtained unreddened visual magnitudes for the central stars which are shown in the second column of Table 1. Shown in column 3 are visual magnitudes which have been recently determined by other workers as referenced in column 4.

In order to obtain the corresponding visual continuum fluxes for each of these central stars it was neccessary to first correct the visual magnitudes for interstellar extinction. Gathier (Ref. 8) has obtained the colour excess E(B-V) for a number of the PNe in our sample. Additional E(B-V) values were taken from the compilation of Pottasch (Ref. 5). For the objects A40, HE2-120 and HE2-177 estimates of the reddening correction were obtained from Abell (Ref. 9) and Webster (Ref.10). The central star fluxes were then obtained from the de-reddened magnitudes using the calibration of Wamsteker (Ref.11) that 0 mag in the visual is 3.64×10^{-9} ergs cm^{-2} s^{-1} A^{-1}. The reddened fluxes are shown in column 2 of Table 2.

4. TEMPERATURE DETERMINATION

If the Hβ flux for the PNe is known then this together with the visual flux can be used to determine the Hydrogen Zanstra temperatures of the central stars. Column 3 of Table 2 shows the Hβ fluxes for our PNe with the corresponding references in column 4. The fluxes shown are not corrected for interstellar extinction. (It should be noted that only an approximate value of the extinction is needed so long as the extinction does not occur within the nebula. This is because to determine the Zanstra temperature the ratio of the Hβ and visual fluxes are used, with our continuum wavelength being approximately equal to the Hβ wavelength.) The derived hydrogen Zanstra temperatures Tz (HI), using the method Harman et al (Ref. 12) as described in Pottasch (Ref. 5), are shown in column 5 of Table 2.
It has been argued by Stasinska and Tylenda

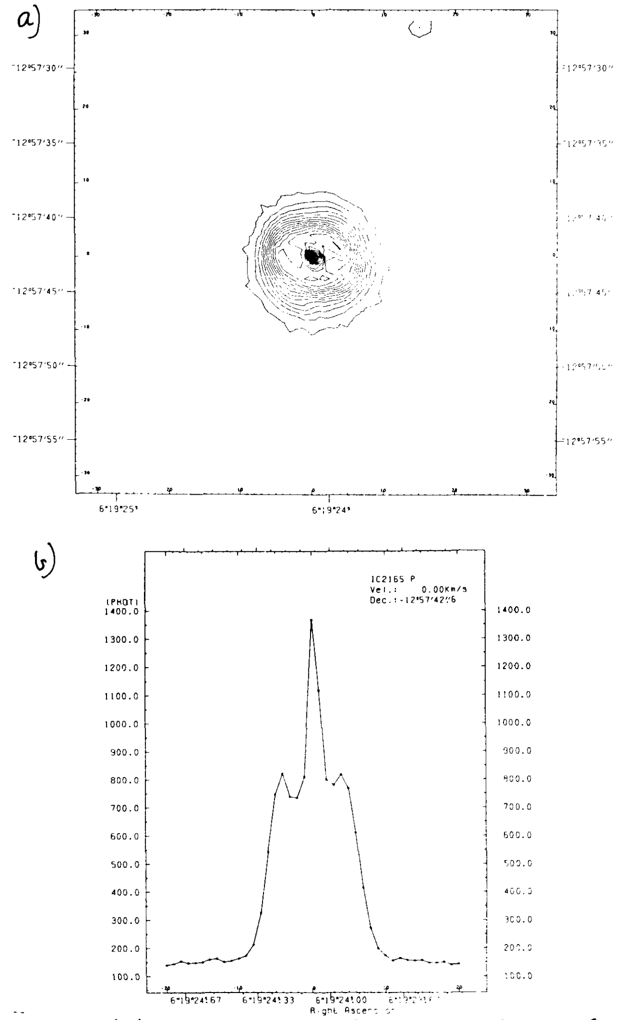

Fig 2 (a) A narrow band CCD image of IC 2165 obtained through a continuum filter centred on $\lambda = 4788Å$. (b) A profile taken through the centre of the nebula. The star is clearly seen demonstrating the effectivness of this technique in enhancing the central star against the nebula background.

(Ref. 1) that the Zanstra temperature derived from the Hβ line may give an overestimate of the effective temperature of the central star. This is because more than one hydrogen ionising photon is produced from each He^{2+} recombination. This effect is only important for derived HI Zanstra temperatures greater than 2×10^5 K. Column 6 of Table 2 shows the adjusted temperatures taking this point into account. The errors shown here are largely due to the error in the stellar magnitude.

Knowing the visual magnitude of the central star and its effective temperature it is possible to determine the luminosity of the central star. The distances to the PNe were taken from recent measurements by Gathier (Ref. 8), Maciel and Pottasch (Ref. 13), Maciel (Ref. 14) and the compilation in Pottasch (Ref. 5). The luminosity of each of our sample of PNe is shown plotted as a function of temperature on the Log L- Log T H-R Diagram in Fig. 3. Typical error bars are indicated. Superimposed on this Fig. 3 are the evolutionary calculations made by Pacynski (Ref. 15) for hydrogen and helium shell burning stars of masses $0.6M_\odot$, $0.8M_\odot$ and $1.2M_\odot$.

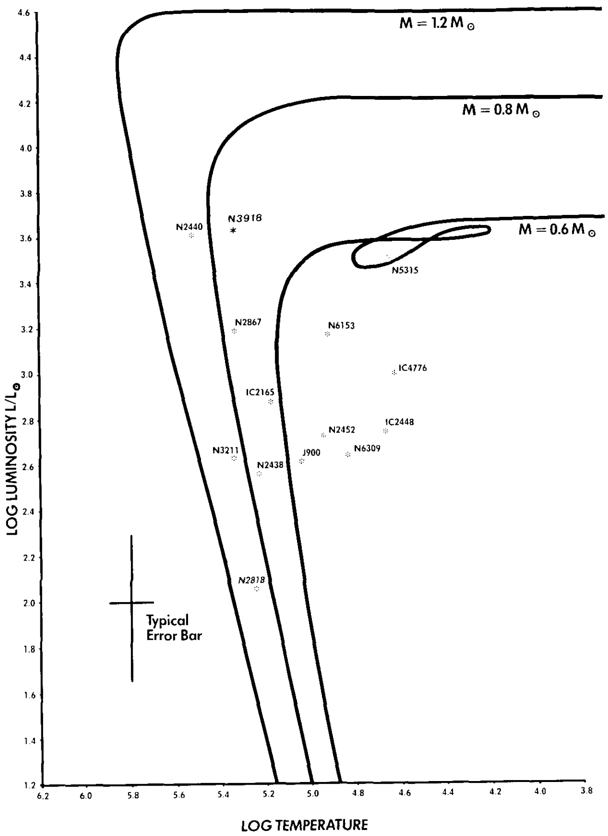

Fig 3 The Hertzsprung-Russell diagram for *planetary nebulae*. The luminosity L of the central star (log units of solar luminosity $L_\odot$) is plotted against its hydrogen Zanstra temperature (log units). The objects are identified by their nebulae identifications. The lines are the theoretical calculations made by Paczynski (Acta Astron. **21**, 419, 1971) for $0.6M_\odot$, $0.8M_\odot$ and $1.2M_\odot$ central stars.
A Typical error bar is shown in the bottom left corner.

5. DISCUSSION

In this work then we detect a number of central stars with temperature greater than 10^5 K. It is also interesting to note that we have detected three stars having temperatures above 2×10^5 K, namely NGC 2440, NGC 3211 and NGC 3918. The case of NGC 2440 has been described in more detail in a previous paper by Atherton et al. (ref. 2). The positions of these central stars on the H-R diagram can be explained if they have masses greater than $0.8M_\odot$. These PN have relatively high Nitogen and Helium abundances (Ref. 5) which is thought to be an indicator of more massive central stars.

An advantage of this technique is that the observations can be made without prior knowledge of the position of the central star. This is particularly useful for those nebulae whose central stars are faint or below the visual threshold. Once obtained, the data can be searched for candidate central stars (making use of supplementary images at other wavelenghts to identify nebula features) and image processing techniques can be applied to separate stellar flux from the nebula background. This is a distinct advantage over methods using data obtained from IUE where a significant nebula flux must be modelled and removed from the observed spectrum in order to obtain the stellar contribution.

Our technique is an effective method of detecting and positioning central stars, this information aiding subsequent observations with instruments which have lower spatial resolution.

Further work is in progress as part of which HeII Zanstra temperatures are being computed for comparison with the above quoted temperatures.

Table 1.

Name (NGC)	m_V (reddened)	m_V (reddened) (others)	Ref	Notes
2346 (a)	14.7 +/- 0.1			a
(b)	13.1 +/- 0.1			b
2438	18.4 +/- 0.1	17.74 +/- 0.20	5	
2440	18.9 +/- 0.2	14.3 +0.9/-0.2	1	
2452	17.9 +/- 0.1	18:	6	
2818	19.5 +/- 0.2	18.52 +/- 0.13	2	
2867	16.5 +/- 0.1	14.4	6	
3132	10.2 +/- 0.1	10.06	6	c
3211	19.5 +/- 0.2	16.2:	6	
3918	16.7 +/- 0.2	14.6	7	
5315	13.3 +/- 0.1	14.63	3	
6153	16.2 +/- 0.1	16.1 +/- 0.5	4	
6302	no detection			
6309	16.5 +/- 0.1	13.74 +0.17/-0.15	1	
6439	no detection			
IC 2165	17.9 +/- 0.1	> 16.4	1	
IC 2448	14.5 +/- 0.1	14.5	6	
IC 4776	13.7 +/- 0.1	> 14.6	1	
J900	17.8 +/- 0.4	16.26 +0.81/-0.52	1	
A40	19.7 +/- 0.2	19.2	8	d
HE2-120	21.2 +/- 0.3			
HE2-177	19.1 +/- 0.2			

References

1. Shaw R A, Kaler J B, 1985, Astrophys.J.,295, 537-546.
2. Kohoutek L, Roth-Hoppner M L, Lausten S, 1986, Astron.Astrophys., vol 162, 232-234.
3. de Freitas Pacheco J A, Codina S J, Viadana L, 1986, M.N.R.A.S., 220, 107-117.
4. Reay N K, Pottasch S R, Atherton P D, Taylor K, 1984, Astron.Astrophys., 137, 113-116.
5. Kaler J B, 1983, Astrophys.J., 271, 188-220.
6. Pottasch S R, 1984, Planetary Nebulae, Reidel, Dordrecht.
7. Clegg R E S, Harrington J P, Barlow M J, 1984, Proc. 4th European IUE Conf., ESA SP-128 p337
8. Abell G O, 1966, Astrophys.J., 144, 259-279.

Notes

a. This observation was taken on 15-03-85
b. This observation was taken on 16-03-85, 24.5 hrs after a. NGC 2346 has a cool A5V central star which is eclipsed by a small hot companion having a period of some 16 days
c. The central star of NGC 3132 has a spectral type A2V which is too late to late to account for the ionization of the nebulae. No hot companion was observed.
d. Photographic magnitude with error between 0.2 and 0.3 magnitudes.

Table 2.

Name	F_{vis} (ergs s^{-1} cm^{-2} A^{-1})	F(Hβ) (ergs s^{-1} cm^{-2} A^{-1})	Ref	Temp (K)	Temp corr. (K)
NGC 2438	1.6×10^{-16}	1.1×10^{-11}	2	1.7×10^{5}	
NGC 2440	1.0×10^{-16}	3.4×10^{-11}	1	3.9×10^{5}	3.5×10^{5}
NGC 2452	2.6×10^{-16}	3.2×10^{-12}	1	8.9×10^{4}	
NGC 2818	6.0×10^{-17}	4.0×10^{-12}	2	1.7×10^{5}	
NGC 2867	8.9×10^{-16}	2.6×10^{-11}	2	1.2×10^{5}	
NGC 3211	6.6×10^{-17}	9.5×10^{-12}	1	2.6×10^{5}	2.2×10^{5}
NGC 3918	7.2×10^{-16}	9.5×10^{-11}	1	2.4×10^{5}	2.1×10^{5}
NGC 5315	1.8×10^{-14}	3.9×10^{-11}	1	4.9×10^{4}	
NGC 6153	1.2×10^{-15}	1.4×10^{-11}	2	9.1×10^{4}	
NGC 6309	9.1×10^{-16}	5.6×10^{-12}	2	7.0×10^{4}	
IC 2165	2.4×10^{-16}	1.3×10^{-11}	2	1.7×10^{5}	
IC 2448	5.7×10^{-15}	1.4×10^{-11}	2	4.9×10^{4}	
IC 4776	1.3×10^{-14}	2.0×10^{-11}	2	4.3×10^{4}	
J 900	2.7×10^{-16}	5.4×10^{-12}	2	1.1×10^{5}	
A 40	4.9×10^{-17}	1.3×10^{-12}	3	1.0×10^{5}	
HE2-120	1.2×10^{-17}				
HE2-177	7.9×10^{-16}	4.0×10^{-12}	4	1.5×10^{5}	

References

1. From the compilation of Gathier, 1983, Thesis, Univ. of Groningen.
2. From the compilation of Pottasch, 1984, Planetary Nebulae.
3. This is an un-reddened flux derived from unpublished 5GHz radio flux data obtained by Milne, D. K. 1986
4. Perek, L. 1971, Bull. Astron. Inst. Czech. vol 22, 103-107.

Acknowledgements

We thank PATT for the allocation of telescope time and the staff of the AAT for their support. NAW thanks the SERC for financial support.

6. REFERENCES

1. Stasinska G, Tylenda R, 1986, Astron.Astrophys. vol 155, 137-144.
2. Atherton P D, Reay N K, Pottasch S R, 1986 Nature, vol 320, 423-424.
3. Shaw R A, Kaler J B, 1985, Astrophys.J.,vol 295 537-546.
4. Clegg R E S, Harrington L P, Barlow M J, 1894, Proc 4th ESA IUE Conf. ESA SP-128, 337.
5. Pottasch S R, 1984, Planetary Nebulae, Reidel, Dordrecht.
6. Reay N K, Pottasch S R, Atherton P D, Taylor K, 1984, Astron. Astrophys., vol 137, 113-116.
7. Landolt A U, 1983, Astr.J., vol 88, 439-460
8. Gathier R, Pottasch S R, Pel J W, 1986, Astron. Astrophys., vol 157, 171-190.
9. Abell G O, 1966, Astrophys.J., vol 144 259-279
10. Webster B L, 1969, MNRAS, vol 143, 79-95.
11. Wamsteker W. 1981, Astron.Astrophys. vol 97 329-333.
12. Harman R J, Seaton M J, 1966 MNRAS, vol 132 15-33
13. Maciel W J, Pottasch S R, 1980, Astron. Astrophys., vol 88, 1-7
14. Maciel W J, 1981, Astron.Astrophys. Suppl. Ser. vol 44, 123-125
15. Pacynski B, 1971, Acta.Astr., vol 21, 417-435.

THE INTRINSIC COLOURS OF THE WOLF-RAYET STARS

G. Ford and D. J. Stickland

Rutherford Appleton Laboratory

ABSTRACT

Ignoring rumours that the extinction law might be anomalous for some Wolf-Rayet stars, we have used dearchived IUE data to deduce the reddening of all the Galactic WR stars in the catalogue of van der Hucht et al. for which there existed narrow-band photometry and low-resolution spectra from both IUE spectrographs. The observed colours have thus been transformed into intrinsic colours for comparison with previous estimates: the agreement is good, suggesting that, ***in general***, the reddening of such stars is ***not*** peculiar.

As a further exercise in naïvity, the dereddened energy distributions were approximated by Planck curves and UV colour temperatures derived. These generally fell in the region of 50,000 - 100,000 K, giving a measure of support (of dubious pedigree) to some recent estimates of WR "core" temperatures.

Keywords: Stars, Wolf-Rayet; stars, colours; reddening.

1. INTRODUCTION

A subject of considerable debate in recent years has been that of the temperatures of the Wolf-Rayet stars. Not so long ago, temperatures in the region of 30000 K were *de rigeur* while values in excess of 50000 K, long championed by the Russian workers, have recently received a boost from studies of the binary stars CQ Cephei (Ref. 1) and V444 Cygni (Ref. 2). This continuing uncertainty means that the intrinsic energy distributions of WR stars, already cut up by strong emission lines which themselves can be regarded as strong cooling agents, are not at all well defined.

van der Hucht et al. (Ref. 3) have provided a synthesis of the narrow-band $(b-v)_o$ colours in their Table XV based on optical studies of WR stars in clusters. These provide a baseline for comparison but we thought it a worthwhile 'student exercise' to take a fresh look at the question of the intrinsic colours of the WR stars utilising the IUE data archived at RAL.

1. PROCEDURE

Our scheme was quite simple: we compiled a list of all the apparently single (ie, not obviously binary) stars in the Sixth Catalogue (Ref. 3) with observed $(b-v)$ colours for which there were low resolution IUE spectra from both spectrographs. These spectra were then interactively manipulated using the versatile DIPSO program running on the STARLINK system. All the spectra of a given star (or at least an adequate number up to about 5) were first merged together. Then where a dip was apparent at λ2200Å, dereddening was progressively applied until the resulting energy distribution was smooth and could be approximated, where not too broken up by emission features, by a black-body curve.

The form of the dereddening law used is that due to Seaton (Ref. 4). Herein lies the first contentious issue! We know already that the mean Galactic extinction law does not hold for the nearby and chemically different systems, the LMC and SMC, and that there are also anomalous regions within the Galaxy. Furthermore, there is some evidence that the reddening along sightlines to certain WRs themselves may be strongly atypical in terms of the strength of the λ2200Å feature (Ref. 5). If these worries are justified we shall expect to see not only considerable scatter in the results for different members of the same subclasses but some divergence with the results given in Ref. 3.

On the practical side, there is the difficulty occasioned by the low sensitivity of the LW cameras at the shorter wavelengths and the understandable tendency of the observers to optimise the exposures of their spectra for more productive regions. This makes for considerable noise in the vicinity of λ2200Å in most spectra and we feel that, at best, the reddening can be deduced to 0.05 mag. in $E(B-V)$. Figure 1 shows the 'before and after' spectra for some stars from the sample.

In Table 1 we list the stars investigated grouped into their subclasses. The observed colours were adopted from the Sixth Catalogue and the colour excess $E(B-V)$ found as outlined above. These values were converted to $E(b-v)$ through the formula

$$E(B-V) = 1.23\ E(b-v)$$

and the intrinsic colours $(b-v)_o$ deduced. These can be no more accurate than the reddening measures,

New Insights in Astrophysics, Proc. Joint NASA/ESA/SERC Conference, University College London, 14–16 July 1986, ESA SP-263 (September 1986)

REFERENCES

References

Abell G O, 1966, Astrophys. J., **144**, 259.

Acker A, 1978, Astron. Astrophys. Suppl., **33**, 367.

Allen C W, 1973, Astrophysical Quantities 3rd ed., London, The Athlone Press, University of London.

Aller L H, 1983, in D R Flower (ed.), "Planetary Nebulae, IAU Symposium No 103", Dordrecht, Reidel, p1.

Aller L H, Czyzak S J, 1979, Astrophys. Space Sci., **62**, 397.

Aller L H, Epps H W, 1975, Astrophys. J., **197**, 175.

Aller L H, Faulkner D J, 1964, in IAU Symp. **20**, p.45.

Atherton P D, Reay N K, Pottasch S R, 1986, Nature, **320**, 423.

Atherton P D, Hicks T R, Reay N K, Worswick S P, Smith W H, 1978, Astron. Astrophys., **66**, 297.

Atherton P D, Hicks T R, Reay N K, Robinson G J, Worswick S P, Phillips J P, 1979, Astrophys. J., **232**, 786.

Beckwith S, Persson S E, Gatley I, 1978, Astrophys. J., **219**, L33.

Berman L, 1937, Lick. Obs. Bull., **17**, 73.

Bevington P R, 1969, In "Data Reduction and Error Analysis for the Physical Sciences", McGraw-Hill, New York, p60.

Blackwell D E, Petford D, Booth A, 1986, (Private Communication).

Bless R C, Savage B D, 1972, Astrophys. J., **171**, 293.

Bohlin R C, Harrington J P, Stecher T P, 1982, Astrophys. J., **252**, 635.

Boksenberg A, 1972, Auxilary Instrumentation for Large Telescopes, Proc of ESO/CERN Conf. Geneva, p205.

Brocklehurst M, 1971, Mon. Not. R. astr. Soc., **153**, 471.

Brown R L, Mathews W G, 1970, Astrophys. J., **160**, 939.

Cahn J H, 1976, Astron. J., **81**, 407.

Cahn J H, Kaler J B, 1971, Astrophys. J. Suppl. Ser., **22**, 319.

Capriotti E R, 1973, Astrophys. J., **179**, 495.

Capriotti E R, Daub C T, 1960, Astrophys. J., **132**, 677.

Carrasco L, Serano A, Costero R, 1983, Rev.Mex.Astron.Astrofis. **8**, 187.

Clegg R E S, Harrington J P, Barlow M J, Walsh J R, 1986, Astrophys. J., Anglo-Australian Observatory Preprint.

Curtis H D, 1918, Univ. Calif. Publs. Lick. Obs. **13**, 57.

Czyzak S J, Aller L H, 1979, Mon. Not. R. astr. Soc., **188**, 229.

Daub C T, 1982, Astrophys. J., **260**, 612.

Drilling J S, Landolt A U, 1979, Astron. J., **84**, 783.

Dufour R J, 1984, Astrophys. J. **287**, 341.

Gathier R, 1984, Ph.D. Thesis, University of Groningen.

Gathier R, 1985, Astron. Astrophys. Suppl. Ser., **60**, 399.

Gathier R, 1986, (Private Communication).

Gathier R, Pottasch S R, Pel J W, 1986, Astron. Astrophys., **157**, 171.

Gathier R, Pottasch S R, Goss W M, 1986b, Astron. Astrophys., **157**, 191.

Grewing M, Bianchi L, Cerrato S, 1986, New Insights in Astrophysics, ESA SP-263, 373.

Harlan E A, Miller J S, 1979, Publ. Astron. Soc. Pac., **91**, 168.

Harman R J, Seaton M J, 1966, Mon. Not. R. astr. Soc. **132**, 15.

Harrington J P, Friebelman W A, 1983, Astrophys. J., **265**, 258.

Harrington J P, Seaton M J, Adams S, Lutz J H, 1982, Mon. Not. R. astr. Soc., **199**, 517.

Hazard C, Terlevich R, Morton D C, Sargent W L, Ferland G, 1980, Nature, **285**, 463.

Helfer H L, Herter T, Lacasse M G, Savedoff M P, Van Horn H M, 1981, Astron. Astrophys., **94**, 109.

Henry R B C, Shipman H L, 1986, Astrophys. J., **311**, 774.

Hollenbach D J, Shull J M, 1977, Astrophys. J., **216**, 419.

Howarth I D, Maslen D M, 1984, Starlink User Note 50.

Hua C-T, Grundseth B, 1985, Astron. J., **90**, 2055.

Hummer D G, Mihalas D, 1970a, JILA report No. 101, Uni. of Colorado.

Hummer D G, Mihalas D, 1970b, Mon. Not, R. astr. Soc., **147**, 339.

Iben I, 1982, Astrophys. J., **259**, 244.

Iben I, 1984, Astrophys. J., **277**, 333.

Iben I, Renzini A, 1983, Ann. Rev. Astron. Astrophys., **21**, 271.

Isaacman R, 1984, Astron. Astrophys., **130**, 151.

Jacoby G H, Ford H A, 1983, Astrophys. J., **266**, 298.

Kaler J B, 1976a, Astrophys. J., **210**, 113.

Kaler J B, 1976b, Astrophys. J. Suppl. Ser., **31**, 517.

Kaler J B, 1978, Astrophys. J., **226**, 947.

Kaler J B, 1979, Astrophys. J., **228**, 163.

Kaler J B, 1983, Astrophys. J., **271**, 188.

Kaler J B, Aller L H, Czyzak S J, 1976a, Astrophys. J., **203**, 636.

Kaler J B, Aller L H, Czyzak S J, Epps H W, 1976b, Astrophys. J. Suppl. Ser., **31**, 163.

Kohoutek L, 1982, Info. Bull. Var. Stars., No. 2113.

Kohoutek L, Lausten S, 1977, Astron. Astrophys., **61**, 761.

Kohoutek L, Martin W, 1981, Astron. Astrophys. Suppl. Ser., **44**, 325.

Kohoutek L, Martin W, 1981b, Astron. Astrophys., **94**, 365.

Kohoutek L, Roth-Hoppner M L, Lausten S, 1986, Astron.Astrophys., **162**, 232

Koppen J, 1977, Astron. Astrophys., **56**, 189.

Kwan J, 1977, Astrophys. J., **216**, 713.

Landolt A U, 1973, Astron. J., **78**, 959.

Landolt A U, 1983, Astron. J., **88**, 439.

Liller W, 1955, Astrophys. J., **122**, 240.

Maciel W J, 1981, Astron. Astrophys. Suppl. Ser., **44**, 123.

Maciel W J, Pottasch S R, 1980, Astron. Astrophys., **88**, 1.

Maciel W J, Pottasch S R, 1981, Astron. Astrophys., **106**, 1.

Mackay C D, 1986, Ann. Rev. Astron. Astrophys., **24**, 255.

Martin W, 1981, Astron. Astrophys., **98**, 328.

Mendez R H, 1978, Mon. Not. R. astr. Soc., **185**, 647.

Mendez R H, Niemela V S, 1981, Astrophys. J., **250**, 240.

Mendez R H, Niemela V S, Lee P, 1978, Mon. Not. R. astr. Soc., **184**, 351

Miller J S, Mathews W G, 1972, Astrophys. J., **172**, 593.

Milne D K, 1979, Astron. Astrophys. Suppl. Ser., **36**, 227.

Milne D K, Aller L H, 1975, Astron. Astrophys., **38**, 183.

Moseley H, 1981, Astrophys. J., **238**, 892.

Mufson S L, Lyon J, Marionni P A, 1975, Astrophys. J. Lett., **201**, L85.

Natta A, Panagia N, 1981, Astrophys. J., **248**, 189.

Natta A, Pottasch S R, Preite-Martinez A, 1980, Astron. Astrophys., **84**, 284.

O'Dell C R, 1963a, Astrophys. J., **138**, 67.

O'Dell C R, 1963b, Astrophys. J., **138**, 293.

Osterbrock, D E, 1974, Astrophysics of Gaseous Nebulae, San Francisco, Freeman.

Paczynski B, 1970a, Acta. Astron., **20**, 47.

Paczynski B, 1970b, Acta. Astron., **20**, 287.

Paczynski B, 1971, Acta. Astron., **21**, 417.

Peimbert M, 1978, in Y Terzian (ed.), "Planetary Nebulae, IAU Symposium No 76", Dordrecht, Reidel, p215.

Peimbert M, Torres-Peimbert S, 1983, in D R Flower (ed),"Planetary Nebulae IAU Symposium 103", Dordrecht, Reidel, p233.

Peimbert M, 1985, Rev. Mex. Astron. Astrofis. **10**, 125.

Pena M, Torres-Peimbert S, 1985, Rev. Mex. Astron. Astrofis., **11**, 35.

Perek L, 1971, Bull. Astron. Inst. Czech., **22**, 103.

Perek L, Kohoutek L, 1967, Catalogue of Galactic Planetary Nebulae, Academia, Prague.

Perinotto M, 1983, IAU Symposium No 103, p323 (Reidel-Dordrecht).

Pottasch S R, 1980, Astron. Astrophys., **89**, 336.

Pottasch S R, 1981, Astron. Astrophys., **94**, L13.

Pottasch S R, 1984, In Planetary Nebulae, Reidel, Dordrecht.

Pottasch S R, Goss W M, Arnal E M, Gathier R, 1982, Astron. Astrophys., **106**, 229.

Pottasch S R, Wesselius P R, Wu C-C, Fieten H, van Duinen R J, 1978, Astron.Astrophys., **62**, 95.

Preite-Martinez A, Pottasch S R, 1983, Astron. Astrophys., **126**, 31.

Reay N K, Atherton P D, 1985, Mon. Not. R. astr. Soc., **215**, 233.

Reay N K, Atherton P D, Taylor K, 1984, Mon. Not. R. astr. Soc., **206**,71.

Reay N K, Pottasch S R, Atherton P D, Taylor K, 1984b, Astron. Astrophys., **137**, 113.

Renzini A, 1979, In "Stars and Star Systems", ed B E Weserlund, Vol 75, Astrophysics & Space Science Lib., Dordrecht, Reidel, p155.

Renzini A, 1981, In "Physical Processes in Red Giants", ed I Iben Jr, A Renzini, p165, Dordrecht, Reidel.

Renzini A, 1981b, In "Physical Processes in Red Giants", ed I Iben Jr,

A Renzini, p431, Dordrecht, Reidel.
Renzini A, 1983, In "Planetary Nebulae, IAU symposium 103", ed. D R Flower, Dordrecht, Reidel, p 267.
Rodriguez L F, Garcia-Barreto, Gomez Y, 1985, Rev.Mex.Astron.Astrofis. **11**
Savage B D, Mathis J S, 1979, Ann. Rev. Astron. Astrophys., **17**, 73.
Schonberner D, 1979, Astron. Astrophys., **79**, 108.
Schonberner D, 1981, Astron. Astrophys., **103**, 119.
Scott P F, 1973, Mon. Not. R. astr. Soc., **161**, 35p.
Seaton M J, 1966, Mon. Not. R. astr. Soc., **132**, 113.
Seaton M J, 1979, Mon. Not. R. astr. Soc., **187**, 73p.
Selby, M J, 1986, (Private Communication).
Shaw R A, Kaler J B, 1982, Astrophys. J., **261**, 510.
Shaw R A, Kaler J B, 1985, Astrophys. J., **295**, 537.
Shields G A, Aller L H, Keyes C D, Czyzak S J, 1981, Astrophys. J., **248**, 569.
Smith H A, Larson H, Fink U, 1981, Astrophys. J., **244**, 835.
Stasinska G, Tylenda R, 1986, Astron. Astrophys., **155**, 137.
Storey J W V, 1984, Mon. Not. R. astr. Soc., **206**, 521.
Stoy R H, 1933, Mon. Not. R. astr. Soc., **93**, 588.
Torres-Peimbert S, Peimbert M, 1977, Rev. Mex. Astron. Astrofis., 2, 181
Treffers R R, Fink U, Larson H P, Gautier T N III, 1976, Astrophys. J., **209**, 793.
Tuchman Y, Sack N, Barkat Z, 1979, Astrophys. J., **234**, 217.
Tylenda R, 1983, Astron. Astrophys., **126**, 299.
Tylenda R, 1984, Astron. Astrophys., **138**, 317.
Tylenda R, 1986, Astron. Astrophys., **156**, 217.
Van Blerksom D, Arny T T, 1972, Mon. Not. R. astr. Soc., **156**, 91.
Wade R, 1983, Proc. S.P.I.E., **445**, 47.
Wamsteker W, 1981, Astron. Astrophys., **97**, 329.
Webster B L, 1969, Mon. Not. R. astr. Soc., **143**, 79.
Weidemann V, 1977, Astron. Astrophys., **61**, L27.
Weidemann V, Koester D, 1983, Astron. Astrophys., **121**, 77.
Wesemael et al, 1980, Astrophys. J. Supp. Ser., **43**, 159.
Zanstra H, 1931, Publ. Dom. Astrophys. Obs. **4**, 209.
Zuckerman B, 1980, In "Interstellar Molecules", ed. B H Andrew,

ADDENDUM

Use of the term 'filling factor' in section 2.6.1, p53.

The term 'filling factor' is used in the sense of a geometric filling factor and is a measure of the fraction of the sky filled with the nebula as seen at the central star. It should not be confused with the more common usage of 'filling factor' which denotes the volume of the nebula actually filled with radiating material. The definition of 'geometric filling factor' is as used in Kaler (1983)

T, L and R for NGC 7027. p82-84.

Due to a numerical error in the calculations T and hence L and R have been incorrectly determined. The correct values are Tz(H)=390,000 K and Tz(HeII)=255,000 K. Using the corrections due to Stasinska and Tylenda (1986), T_{eff}=310,000 K. This leads to L=12,600 $L_{\odot}$ and R=0.039 $R_{\odot}$. This temperature agrees with that estimated by Preite-Martinez & Pottasch (1983) assuming Case III (optically thick to H and He ionising radiation).

Error estimates in the derived masses of shocked H_2. p103.

The vibrationally excited molecular hydrogen is assumed to be at a temperature of T_{vib}=2000 K for the purposes of calculating the masses presented in Table 5.1. However it is quite possible that the T_{vib} may be somewhat lower than this, Isaacman (1984) uses a value of T_{vib}=1200 K. The mass is proportional to a term $e^{(E/kT_{vib})}$ and hence errors in T_{vib} can lead to substantial errors in the mass determinations. Changing T_{vib} from 2000 K to 1500 K increases the mass by a factor of 3. Hence the masses presented should be used with care.

p2 last line: 250,000 K should read 310,000 K, see prior Addendum.

p27 Table2.1: α_B is the recombination coefficient for hydrogen summed over all levels above the ground level. (see p24)
α_B(4686) is the equivalent for He^+

p90 line 19: 19.8 should read 18.9

p98 line 24: flux should read intensity.

p99 line 6: Θ2 should read H_2